PHOTOPHYSICS AND CATALYSIS OF PORPHYRINOIDS

by

AMIT AGGARWAL

A dissertation submitted to the Graduate Faculty in Chemistry in partial fulfillment of the requirements for the degree of Doctor of Philosophy, The City University of New York.

2011

This manuscript has been read and accepted for the Graduate Faculty in Chemistry in satisfaction of the dissertation requirements for the degree of Doctor in Philosophy.

05/25/2011

Date

Prof. Charles Michael Drain

Chair of Examining Committee

05/25/2011

Date

Prof. Mahesh Kumar Lakshman

Executive Officer

Prof. John R. Lombardi

Prof. Hiroshi Matsui

Prof. Lynn C. Francesconi

(Supervisory committee)

THE CITY UNIVERSITY OF NEW YORK

ABSTRACT

PHOTOPHYSICS AND CATALYSIS OF PORPHYRINOIDS

by

Amit Aggarwal

Advisor: Professor Charles Michael Drain

Organic nanoparticles (ONP) of metalloporphyrins can be versatile catalysts for the selective oxidation of alkenes and other hydrocarbons. Herein, we report the catalytic activity of ONP of 5,10,15,20-tetrakis-[4-(1'H,1'H,2'H,2'H-heptadecafluorodecane-1-thiol)-2,3,5,6-tetrafluorophenyl] porphyrinato iron(III), Fe(III)TPPF$_{84}$, and 5,10,15,20-tetakis-(2,3,4,5,6-pentafluorophenyl) porphyrinato manganese(III), Mn(III)TPPF$_{20}$, for cyclohexene oxidation using molecular oxygen as an oxidant in water under ambient conditions. While the solvated metalloporphyrins catalytically oxidize alkenes to the corresponding epoxide in halogenated solvent with a modest turn-over numbers (TON), 10-30 nm ONP of these metalloporphyrins have enhanced catalytic activity with up to a 4-fold greater TON and yields only allylic oxidation products. These ONP catalytic systems facilitate a greener reaction since ca. 89% of the reaction medium is water, molecular oxygen is used in place of man-made oxidants, and the ambient reaction conditions require less energy. The enhanced catalytic activity of these ONP is unexpected because the metalloporphyrins in the nanoaggregates are in the close proximity and the TON should

diminish by self-oxidative degradation. The fluorous alkanes in Fe(III)TPPF$_{84}$ stabilize the ONP towards self-oxidative degradation.

Sequential dipping of indium-tin-oxide electrodes into solutions of tetra cationic porphyrins and tetra anionic polyoxometalates results in the controlled formation of nm thick films. The potential applications of these robust films on electrodes range from catalysts to sensors. This chapter focuses on the electrochemistry of the multilayered films where it is found that the oxidation and reduction potentials of each species remain largely the same as found in solution.

Photophysical properties of Porphyrinoids bearing four rigid hydrogen bonding motifs on the *meso* positions, self-assembled into a cofacial cage with four complementary bis(decyl)melamine units in dry solvents are presented here. Self-assembly was investigated by NMR spectroscopy, dynamic light scattering, and atomic force microscopy. The phototphysical properties of the cage formation involve the measurement of their absorption and emission spectra and the fluorescence life time in dry THF. The hydrocarbon chains on the bis(decyl)melamine mediate the formation of nanofilms on surfaces as the solvent slowly evaporates.

A systematic study of the photophysical properties of a series of porphyrinoids is presented. The role of the location of a heavy atom in shunting the excited state from the singlet to the triplet manifolds is compared for three cases. It is well known that Pt(II) metalloporphyrins do not fluoresce. For meso pyridyl porphyrins, the fluorescence quantum yield decreases as the number of coordinatively attached Pt(II) complexes increase from 0-4, but the tetracoordinated species retains about 30% of the fluorescence. Covalently attaching a heavy metal complex e.g.

Pt(II) complex to the macrocycle by an organometalic bond at the peripheral meso position causes greater than a 20-fold decrease in fluorescence quantum yield and may enhance some internal conversion to the ground state. For comparison, the fluorescence quantum yield decreases somewhat as the number of pyridyl groups on the meso positions increase 0-4. We also evaluate the photophysical properties of a series of porphyrins with nitro groups on the β pyrrole position and on the meso phenyl group, which also quenches the fluorescence. These studies bear on the use of metal ions to enhance the photophysical properties of these dyes as photodynamic therapeutics and for supramolecular systems, while the nitrated macrocycles have potential application in non linear optics.

The photophysical properties of non-hydrolysable tetra- thioglycosylated conjugates of chlorin ($CGlc_4$), isobacteriochlorin ($IGlc_4$) and bacteriochlorin ($BGlc_4$) and core F_{20} platforms are reported here. These studies involve the measurement of absorption and emission spectra, fluorescence quantum yield, singlet oxygen quantum yield, and singlet state life time in three different solvents: phosphate buffer saline (PBS), ethanol, and ethylacetate. Compared to the porphyrin in PBS, $CGlc_4$ has a markedly greater absorbance of red light near 650 nm and a 6-fold increase in fluorescence quantum yield; whereas $IGlc_4$ has broad Q bands and a 12-fold increase in fluorescence quantum yield. Since $IGlc_4$ $CGlc_4$ very slowly bleach, these properties may enable their use as fluorescent tags to track biological processes. $BGlc_4$ has a similar fluorescence quantum yield to $PGlc_4$, (<10%), but the lowest energy absorption/emission peaks of $BGlc_4$ are considerably red shifted to near 730 nm with a nearly 50-fold greater absorbance, which may allow this conjugate to be an effective PDT agent. The excited state life time of these conjugates ranges from 3-11 ns. The radiative time constant for $IGlc_4$ is 20 fold less while non-radiative time constant is 2 fold more than $BGlc_4$, indicates that $IGlc_4$ has greater potential to

form triplet state via inter system crossing, and so can serves as a better PDT agent. The uptake of $CGlc_4$, $IGlc_4$ and $BGlc_4$ derivatives into cells such as human breast cancer cells MDA-MB-231 and K:Molv NIH 3T3 mouse fibroblast cells can be observed at nM concentrations. Photobleaching under these conditions is minimal.

Acknowledgements

I want to express my deeply-felt thanks to my mentor Prof. Dr. Charles Michael Drain for his warm encouragement and thoughtful guidance. I greatly appreciate his timely contribution and unconditional commitment to this work. Prof. Drain I would like to say from deep core of my heart that without your help and guidance this work would not have been possible.

I owe special thanks to my dissertation committee members: Prof. John R. Lombardi from City College, Prof. Hiroshi Matsui and Prof. Lynn C. Francisconi form Hunter College for their time and input over the years. Special thanks to Prof. Klaus Grohmann, who accepted me into this Ph.D. program and gave me an opportunity to pursue my research.

I would like to thank my wife and my esteemed colleague Sunaina Singh, who is the source of my inspiration to pursue a Ph.D., and for her consistent encouragement. It is because of her belief in me that I am able to write this thesis and finish this work. I look forward to moving ahead with our lives. Many, many thanks to you Sunaina.

I would also like to thanks my best friends Gagandeep Sharma and Bhupinder Singh. They always encouraged me and gave me a lot of strength – especially during the hard times.

My deeply thanks to my friends and lab mates Dr. Gabriela Smeureanu, Dr. Ivana Radivojevic, Dr. Giorgio Bazzan, Dr. Sebastian Thompson, Dr. Diana Samaroo, Mr. Jacopo Samson, Mr. Mathew Jurow, Mr. Brian A. Hageman, Mr. Christopher Farley, and Mr. Aaron Dolor.

I would like to thank my family especially to my parents Sh. Ram Nath Aggarwal and Ms. Nirmal Aggarwal whose hard work and encouragement brings me to this level.

Last but not least, our special thanks to the funding agencies: the National Institutes of Health for infrastructure support (GM60654); and National Science Foundation CHE-0847997. Without their financial support this work would not have been possible.

I dedicate my thesis to my wife Sunaina Singh and my Parents Sh. Ram Nath Aggarwal and Ms. Nirmal Aggarwal for their encouragement and belief in me.

Table of Contents

LIST OF TABLES

List of Schemes

List of Figures

Chapter 1

Chapter 2

Chapter 2: Appendix

Chapter 3

Chapter 3: Appendix

Chapter 4

Chapter 4: Appendix

Chapter 5

Chapter 5: Appendix

Chapter 6

Chapter 6: Appendix

Abbreviations

AFM	Atomic Force Microscopy
DLS	Dynamic Light Scattering
ESI-MS	Electrospray Mass Spectrometry
GC-MS	Gas Chromatography-Mass Spectrometry
UV-vis	Ultraviolet-visible spectroscopy
NMR	Nuclear Magnetic Resonance
DOSY	Diffusion ordered spectroscopy
CV	Cyclic Voltammetry
TCSPC	Time correlation single photon counting
PDT	Photodynamic Therapy
HOMO	Highest Occupied Molecular Orbital
LUMO	Lowest Unoccupied Molecular Orbital
ROS	Reactive Oxygen Species
ONP	Organic Nanoparticles
PEG	Polyethylene glycol
IB	Isobutyraldehyde
PBS	Phosphate Buffer Saline
THF	Tetrahydrofuran
DMF	Dimethylformamide
DMEM	Dulbecco's Modified Eagle Medium
POM	Polyoxometallate
ITO	Indium Tin Oxide
LBL	Layer by Layer
$H_4SiW_{12}O_{40}$	Silicotungstic acid hydrate
$TMPyP^{+4}$	5,10,15,20-tetrakis(4-methylpyridinium)porphyrin
$TPPF_{20}$	5,10,15,20-tetrakis-(2,3,4,5,6-pentafluorophenyl)porphyrin

$Fe(III)TPPF_{20}$	5,10,15,20-tetrakis-(2,3,4,5,6-pentafluorophenyl)porphyrinato iron(III)
$Fe(III)TPPF_{84}$	5,10,15,20-tetrakis-[4-(1'H,1'H,2'H,2'H-heptadecafluorodecane-1-thiol)-2,3,5,6-tetrafluorophenyl]porphyrinato iron(III),
$Mn(III)TPPF_{20}$	5,10,15,20-tetakis-(2,3,4,5,6-pentafluorophenyl)porphyrinato manganese(III)
$PGlc_4$	Thioglycosylated Porphyrin Conjugate
$CGlc_4$	Thioglycosylated Chlorin Conjugate
$IGlc_4$	Thioglycosylated Isobacteriochlorin Conjugate
$BGlc_4$	Thioglycosylated Bacteriochlorin Conjugate
m-THPC	meso-tetrakis(3'-hydroxyphenyl) chlorin
TPP	5,10,15,20-tetraphenyl porphyrin
ZnTPP	5,10,15,20-tetraphenyl porphyrinato Zinc(II)
M*m*PyP	5-(3'-pyridyl)-10,15,20-tris(tolyl)porphyrin
D*m*PyP	5,10-bis(3'-pyridyl)-15,20-bis(tolyl)porphyrin
T*m*PyP	5,10,15,20-tetrakis(3'-pyridyl)porphyrin
T*p*PyP	5,10,15,20-tetrakis(4'-pyridyl)porphyrin
$DPP\text{-}Pd(PPh_3)_2Br$	trans-Bromo[10,20-diphenylporphyrin-5-yl]bis(triphenyl phosphine) palladium(II)
$DPP\text{-}Pt(PPh_3)_2Br$	trans-Bromo[10,20-diphenylporphyrin5-yl]bis(triphenyl phosphine) platinum(II)
MNTPP	2-Nitro-5,10,15,20-tetraphenylporphyrin
MNTPPZn	2-Nitro-5,10,15,20-tetraphenylporphyrinato Zinc(II)
PNTPPZn	2-Nitro-5,10,15,20-tetrakis(2'-nitrophenyl)porphyrinato Zinc(II)
PNTPP	2-Nitro-5,10,15,20-tetrakis(2'-nitrophenyl)porphyrin
HNTPP	2,7-Dinitro-5,10,15,20-tetrakis(2'-nitrophenyl)porphyrin

CHAPTER 1: INTRODUCTION

1.1 Porphyrinoids

Porphyrinoids are a class of heterocyclic organic compound with a tetrapyrrole macrocyclic core appended with different substituents on the periphery of the macrocycle. Porphyrinoids include porphyrins, phthalocyanines, corroles, corrolazines just to name a few. The basic structures of these porphyrinoids are shown in figure 1.1. Porphyrins are highly conjugated aromatic rings with 22π electrons delocalized over the macrocycle. The entirety of the macrocycle is aromatic in step with Hückel's (4n +2)π electron rule for aromaticity.(*1, 2*) The high degree of conjugation makes these compounds to absorb strongly in the visible region of the electromagnetic spectrum and therefore exhibit deep colors.

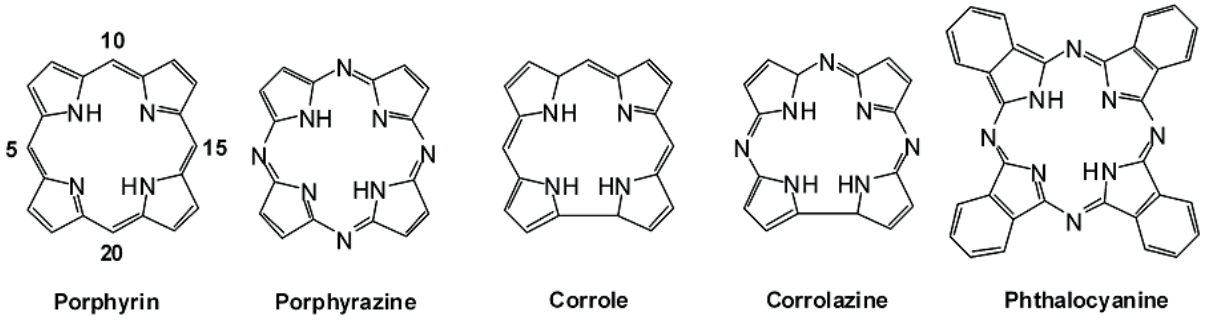

Figure 1.1: Structure of various porphyrinoids.

Free base porphyrins, those without a metal atom at the core of the macrocycle, have a strong tendency to coordinate with almost any metal atoms of the periodic table to form metalloporphyrins. Metalloporphyrins are important biological compounds. For example, hemoglobin is an iron porphyrin responsible for the red color of the blood. The green pigment of

plants, chlorophyll, is a magnesium porphyrin. Cyanocobalamin, which is the vitamin B_{12} family, is a cobalt porphyrin.

The oxidative and reductive transformation of porphyrins leads to the formation of a series of compounds with one or more pyrrolic double bonds missing, known as chlorins, isobacteriochlorins, and bacteriochlorins. These molecules exhibit strong potential for use in optical devices and are commonly observed functioning in biological systems. Chlorins, observed in plant pigments, are porphyrinoids with one pyrrolic double bond missing. Isobacteriochlorins and bacteriochlorins, found in some photosynthetic bacteria, are porphyrinoids with two missing double bonds on adjacent or opposite pyrroles, respectively. Porphyrins, chlorins, isobacteriochlorins, and bacteriochlorins all have unique photophysical properties that are heavily exploited by nature for diverse applications. These properties can be further tuned by functionalization of these chromophores through the attachment of a variety of groups at the peripheral positions.

Metalloporphyrins are being examined as potential catalysts for a variety of reactions including electrocatalytic and photocatalytic processes, but perhaps the most studied reactions are oxidation reactions. The discovery by Groves and coworkers on the use of iron porphyrins soluble in organic solvents with iodosylbenzene as a simple oxygen atom donor can mimic the oxidative catalysis observed for cytochrome P_{450} opened a new field of research on the reactivity and mechanism of this process.(*3-8*) Metalloporphyrins are also being examined as possible blood substitutes, electrocatalysts for fuel cells, and for the electrochemical generation of hydrogen peroxide. The unique optical properties of porphyrins also make them prime candidates for use in photonic devices. In addition, porphyrins have also demonstrated significant potential for use in the treatment of a wide range of diseases; one major example is

the treatment of cancer, as a photodynamic therapeutic (PDT) agent. Because of their biological relevance and diverse functions, a large number of porphyrin derivatives have been synthesized and tested on the laboratory scale. These methods and studies have allowed for extensive commercial applications of porphyrins and their chemical cousins.

Strong absorption in the visible region is the foundation for a majority of porphyrins applications. The absorption spectra of porphyrins show two types of transitions, Soret bands or B-bands and Q-bands. The Soret band for porphyrins lies in the wavelength range of 400-430 nm and is an intense band resulting from strongly allowed transitions. The Q-bands, of which there are generally four for free base porphyrins and two for metalloporphyrins, are in the range of 500-650 nm and are relatively weak. Q-bands are observed primarily because of vibronic coupling interactions between HOMO and LUMO states. The electronic spectra of porphyrinoids depend on their exocyclic modification, the nature of central metal ion or lack thereof, and the solvent. Martin Gouterman explained the absorption spectra of porphyrins based on the four orbital frontier molecular orbital theory.(*9*) Other porphyrinoids such as phthalocyanines also have a strong absorption band in the visible region, generally to the red end of the visible spectrum. Typical absorption spectra of free base and metal porphyrin derivatives and phthalocyanines are shown in figures 1.2 and 1.3.

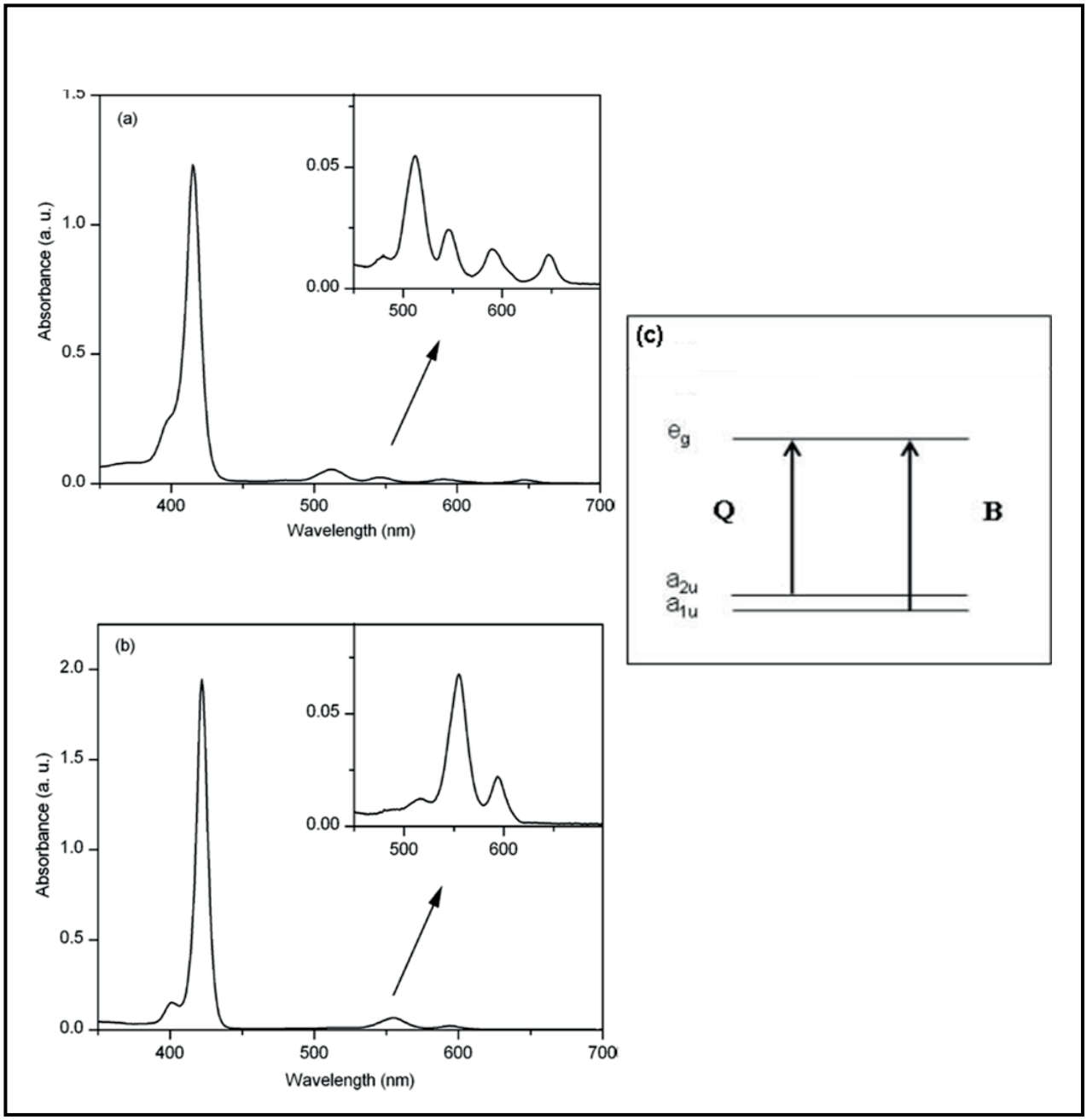

Figure 1.2: Typical UV-visible spectra of: a) Free base porphyrin b) A metalloporphyrin (c) Scheme of energy levels in metal derivatives of porphyrins with the first two π-π* transitions, the Q-and B-bands are marked. Adapted from reference (*10*).

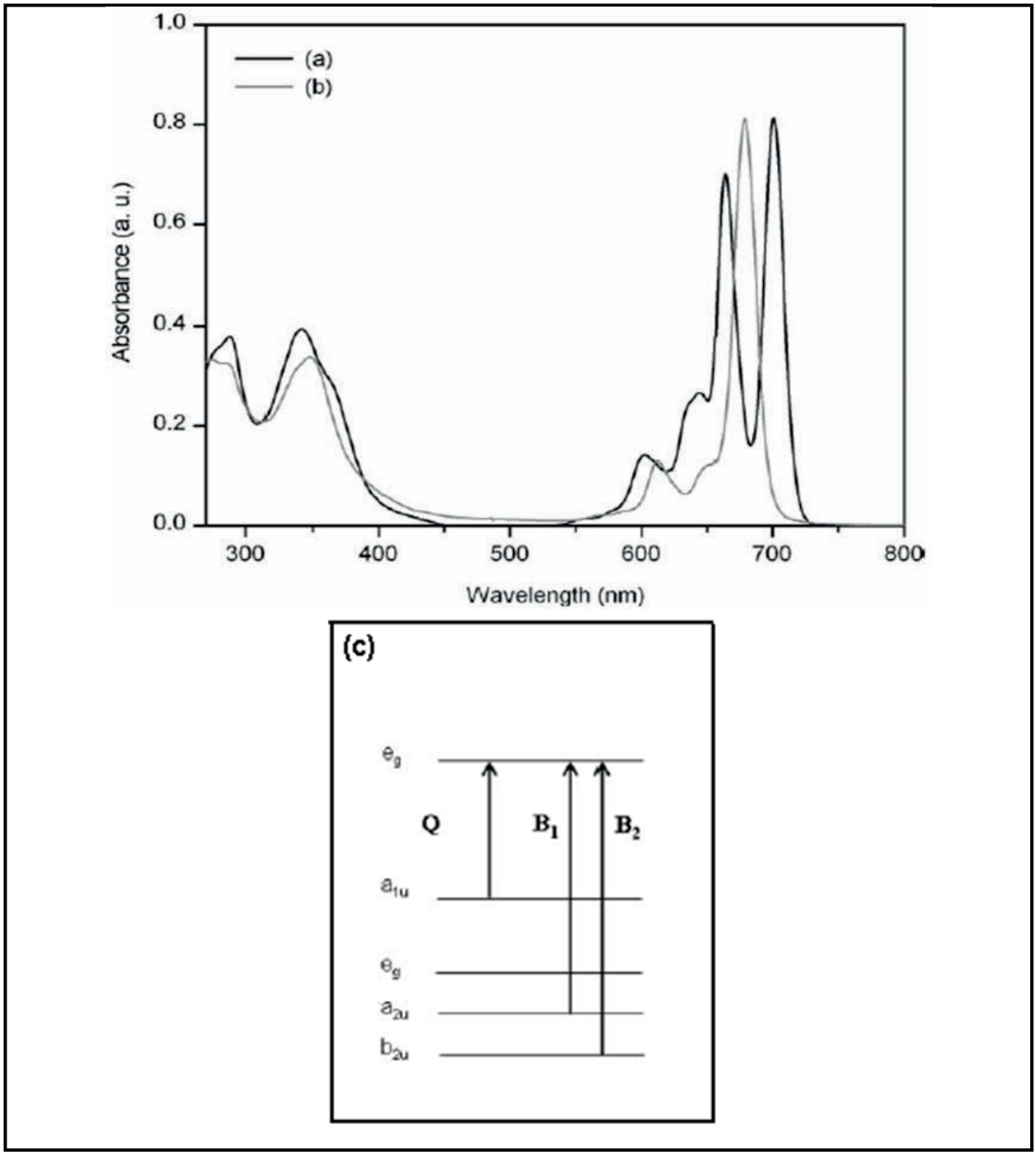

Figure 1.3: Typical UV-visible spectra of: a) Free base phthalocyanine b) A metal phthalocyanine complex. (c) Scheme of energy levels in metal derivatives of phthalocyanines with the first two π-π* transitions, the Q-and B-bands are marked. Adapted from reference (*10*).

1.2 Supramolecular Systems of Porphyrins

The decoration of porphyrinoids, at their periphery by several different groups causes change in their optical properties and solubility, allowing for a wide range of applications. Functionalization of the ring with groups which promote the formation of supramolecular systems is also one of the strongest draws of porphyrin chemistry.

Supramolecular chemistry is occasionally defined as the "chemistry beyond the molecule", a reference to spontaneous association of atoms, ions or molecules via non-covalent interactions such as electrostatic forces, van der Waals forces, H-bonding and π-π interactions. These forces play a complementary role towards the synthesis of nano materials since the formation of nano-scaled materials is rarely possible by intentional formation of covalent bonds alone. The spontaneous association of matter into well organized systems is the foundation by which life builds complex systems. These can be categorized as self-assembled and self-organized systems. Self-assembly results in the formation of an ordered supramolecular entity which is more rigid and intolerant to errors and defects. Self-organization, on the other hand results in the formation of non-discrete systems which are dynamic in nature and relatively tolerant to errors and defects.(*11-14*) Many of the unique properties of these nanoscaled materials are not observed in their component molecules. This is especially true for their electronic, optical, photonic and magnetic properties.

Porphyrinoids are ideal building blocks for supramolecular chemistry because they impart a high degree of functionality to the materials due to their extraordinary stability and their unique photophysical, chemical, and mechanical properties. They are extensively used to prepare self-assembled and self-organized systems in solutions and into/onto surfaces, for applications

such as in biosensors, molecular sieves, dyes for solar energy harvesting, drugs for PDT and catalysts.(*14*) The efficiency of electron transfer and energy transfer in organic based materials depends on both the molecules and the architecture of these molecules in the devices.(*15*) The hierarchical organization of molecules into nano-structured aggregates occasionally can have an abstruse effect on their physical, chemical, and optical properties. For example, formation of organic nanoparticles (ONP) of porphyrins and phthalocyanines have a potential to enhance or modulate their properties through quantum mechanical effects.(*16, 17*) Additionally, understanding the spontaneous formation of suspensions of molecular aggregates is becoming an important topic for the formulation of hydrophobic drugs.(*18*)

1.3 Supramolecular porphyrin system as catalyst

Metalloporphyrin catalyst: Various metalloporphyrins with Fe, Mn, Co and other metal ions have been extensively studied as catalysts in laboratory scale reactions. Using a variety of oxygen sources, these reactions can be used as model to mimic the activity of cytochrome P_{450} monooxygenation reactions.(*19-24*) Different metalloporphyrins exhibit different catalytic reactivities, which include formation of different products or product ratios.(*8, 25-30*) However their catalytic activity and stability depends on their degree of halogenations, substrate-catalyst ratio, nature of axial ligand, peripheral groups, oxidant, solvent, and other conditions. For example, the catalytic oxidation of cyclohexene by iron tetraarylporphyrin is a well investigated standard reaction and the turnover number (TON) for the catalysts in solution is only a few hundred because of the degradation of the catalyst. TON increases to ca. 350 when 5,10,15,20-tetrakis-(2,3,4,5,6-pentafluorophenyl)porphyrinato iron(III), [Fe(III)$TPPF_{20}$] is used as catalyst because the molecule may be somewhat more resistant to oxidative degradation because of the presence of the fluorine groups.

Porphyrinoids have also been studied as better candidate for the oxidative decomposition of unwanted peroxynitrite species formed in the body that cause neurological disorders. The peroxynitrite ($ONOO^-$) produced by the combination of superoxide radical anion ($O_2^{\cdot-}$) and nitric oxide (NO) in cells or tissue, is known to react with a wide variety of biomolecules; including proteins, lipids, DNA, and antioxidants. These radical species causes the apoptotic cell death in healthy body cells such as muscle cells and neural cells. Since peroxynitrite reacts very efficiently with biological metal centers, metalloporphyrins have been investigated as catalysts for their decomposition reactions. Groves et al.(*31-36*) and others (*37-41*) reported that various water soluble iron(III) and Mn(III) porphyrin can catalytically reduce peroxynitrite to nitrate.

Self-Organized metalloporphyrin catalyst: Self-organized supramolecular porphyrin nanoparticles can be a versatile catalyst for these types of oxidation reactions because of their stability and enhanced catalytic activity, which results in advantages over the homogenous and supported catalysts in terms of catalytic turnover, substrate specificity and the selective transformation of a given site on the substrate. Our group reported a simple, fast and economical way to prepare nanoparticles of ca. 30 different types of porphyrins and metalloporphyrins.(*42, 43*) Many of these nanoparticles are more efficient catalyst on a per porphyrin basis, then the individual porphyrins in solutions or individual porphyrin adsorbed on surface. We found that 10 nm ONP of Fe(III)$TPPF_{20}$ shows enhanced catalytic activity and selectively formed allylic oxidation products for cyclohexene oxidation reaction using molecular oxygen as oxidant. The results for these catalytic reactions and also with other ONP catalytic systems will be discussed in more details in chapter 2. Work by J. T. Hupp and coworkers on self-assembled metalloporphyrin catalysts show that rigid arrays can yield remarkably robust systems, but require precursor molecules which are difficult to obtain in high yields.(*30, 44, 45*)

1.4 Photophysics of Porphyrinoids

The strong absorption of porphyrinoids in the visible region- value in optical devices and their importance in biological systems, the photophysical properties of porphyrinoids have been studied extensively. The well established available synthetic methods and the ease of functionalization along their periphery allow synthetic chemists to intentionally tune the optical properties of porphyrinoids to desirable range. The photophysical properties of porphyrinoids are largely dependent on molecular geometry, nature of central metal atom/ion, nature and binding of axial ligand, nature of exocyclic groups, and the solvent polarity.

The insertion of a metal atom e.g. Zn(II) in the porphyrin core changes the symmetry of the compound. Consequently, the Q_x and Q_y absorption bands become degenerate and the absorption spectrum merely presents one B-band and two Q-bands compared to one B-band and four Q-bands in case of free base porphyrins. Based on the Gourterman four orbital frontier molecular orbital theory, the highest energy Soret or B-band, has been assigned to the $S_0 \rightarrow S_2$ transition, while the lower energy Q-bands have been assigned to the $S_0 \rightarrow S_1$ transition. The absorption of a photon of light promotes an electron from ground singlet state, S_0, to a higher excited singlet state, say S_n. From there it can follow a number of radiative and non radiative decays back to the ground singlet state. Radiative decays, non-radiative decays, internal conversion and $S_1 \rightarrow T_1$ intersystem crossing are all viable pathways. High fluorescence quantum yield indicates that the process is dominated by $S_1 \rightarrow S_0$ radiative decay whereas low fluorescence quantum yield suggests that the process is predominantly non-radiative.

The fluorescence quantum yield of a typical free base and some of their metallo derivatives (eg. Zn(II) and Mg(II)) range from ca. 1% to 15% with corresponding lifetimes

between ca. 1 and 15 ns. For these systems, free base as well as metalloporphyrins, a substantial percentage of the molecules in the excited singlet state undergo intersystem crossing to the triplet state, such that the phosphorescence quantum yield in matrices can be over 90% for Pd and Pt derivatives used in O_2 pressure sensing.(*46*) The triplet lifetime in de-aerated solutions is longer than 10μs and about 300 ns in aerated solutions. The triplet state of the chromophore interacts with the ground triplet state of molecular oxygen to produce singlet oxygen for PDT applications. The quantum yields for singlet oxygen formation can be as high as 0.67-0.93 indicating a high efficiency in the energy transfer process from the porphyrin to molecular oxygen.(*47*)

The substitution of one or more meso hydrogen atoms at the 5,10,15, or 20 positions along the periphery of the porphyrin by halogen atoms or other groups or insertion of a metal atom at the core of the porphyrin cause a decrease in the fluorescence quantum yield and consequently the fluorescence lifetime due to the heavy atom effect. Conversely, the triplet lifetime and the singlet oxygen formation quantum yield increases as a result of substitution.(*48-51*) Detailed photophysical studies of porphyrinoids is essential owing to their proposed use in photovoltaic cells for solar energy harvesting(*52*), potential use in optical devices(*53*), and their role as sensors for photoactivated biological processes, such as glucose transportation and photosensitizers for PDT treatment of cancer cells.(*54-59*) For diagnostic and PDT applications, the use of lower energy light (red – near infrared) is an important characteristics that the new generation of compounds should possess as near IR light can go deeper into the tissue to treat deep lying cancer cells.(*60*) For this reason chlorins, isobacteriochlorins, and bacteriochlorins are often synthesized due to their stronger and/or redder lowest energy absorption band.(*61*) For a

dye to be a good PDT agent: a low fluorescence quantum yield, high triplet quantum yield or high singlet oxygen formation quantum yield is necessary.

1.5 Conclusions

The enhanced optical, photophysical and chemical properties of porphyrinoids encouraged us to develop new materials. The aim of this research is to study a series of self-organized porphyrinic supramolecular systems for their catalytic applications towards oxidation reactions. We developed ONP of metalloporphyrins that exhibit enhanced catalytic activity for the oxidation of cyclohexene preferential to its component molecules in solution. These organic nanoparticles are quite stable towards self-oxidative degradation. The detailed photophysical studies of a series of porphyrinoids will be discussed in chapter 5 and 6 and will help us understand related design principles enabling formulation of new materials. The enhanced optical properties of reduced porphyrinoids and their glycosylated conjugates may make them to serve as better photosensitizers for PDT.

1.6 References

1. Kadish, K. M., Smith, K. M., and Guilard, R., (Eds.) (2000) *The Porphyrin Handbook*, Vol. 1-10, Academic Press, New York.
2. Dolphin, D., (Ed.) (1978-1979.) *The Porphyrins*, Vol. 1-7, Academic Press, New York.
3. Groves, J. T. (2006) High-valent iron in chemical and biological oxidations, *J. Inorg. Biochem. 100*, 434-447.
4. Groves, J. T., Haushalter, R. C., Nakamura, M., Nemo, T. E., and Evans, B. J. (1981) High-valent iron-porphyrin complexes related to peroxidase and cytochrome P-450, *J. Am. Chem. Soc. 103*, 2884-2886.
5. Groves, J. T., and Nemo, T. E. (1983) Epoxidation reactions catalyzed by iron porphyrins. Oxygen transfer from iodosylbenzene, *J. Am. Chem. Soc. 105*, 5786-5791.
6. Groves, J. T., Nemo, T. E., and Myers, R. S. (1979) Hydroxylation and epoxidation catalyzed by iron-porphine complexes. Oxygen transfer from iodosylbenzene, *J. Am. Chem. Soc. 101*, 1032-1033.
7. Groves, J. T., and Viski, P. (1990) Asymmetric hydroxylation, epoxidation, and sulfoxidation catalyzed by vaulted binaphthyl metalloporphyrins, *J. Org. Chem. 55*, 3628-3634.
8. Groves, J. T., and Watanabe, Y. (1986) Heterolytic and homolytic oxygen-oxygen bond cleavage reactions of acylperoxomanganese(III) porphyrins, *Inorg. Chem. 25*, 4808-4810.
9. Gouterman, M. (1978) *The Porphyrins*, Vol. 3, Academic Press, New York.
10. Rio, Y., Salome Rodriguez-Morgade, M., and Torres, T. (2008) Modulating the electronic properties of porphyrinoids: a voyage from the violet to the infrared regions of the electromagnetic spectrum, *Org. Biomol. Chem. 6*, 1877-1894.
11. Drain, C. M. (2002) Self-organization of self-assembled photonic materials into functional devices: Photo-switched conductors, *Proc. Natl. Acad. Sci. 99*, 5178-5182.
12. Drain, C. M., Batteas, J. D., Flynn, G. W., Milic, T., Chi, N., Yablon, D. G., and Sommers, H. (2002) Designing supramolecular porphyrin arrays that self-organize into nanoscale optical and magnetic materials, *Proc. Natl. Acad. Sci. 99*, 6498-6502.

13. Milic, T. N., Chi, N., Yablon, D. G., Flynn, G. W., Batteas, J. D., and Drain, C. M. (2002) Controlled Hierarchical Self-Assembly and Deposition of Nanoscale Photonic Materials *Angew Chem. Int. Ed. 41*, 2117-2119.
14. Drain, C. M., Goldberg, I., Sylvain, I., and Falber, A. (2005) Synthesis and Applications of Supramolecular Porphyrinic Materials, *Top. Curr. Chem. 245*, 55-88.
15. Drain, C. M., Batteas, J. D., Smeureanu, G., and Patel, S. (2004) Self-Assembly of Porphyrinic Materials on Surfaces, *Dekker Encyclopedia of Nanoscience and Nanotechnology*, 3481 - 3502.
16. Nitschke, C., O'Flaherty, S. M., Kröll, M., and Blau, W. J. (2004) Material Investigations and Optical Properties of Phthalocyanine Nanoparticles, *J. Phys. Chem. B 108*, 1287-1295.
17. Rangel-Rojo, R., Matsuda, H., Kasai, H., and Nakanishi, H. (2000) Irradiance dependence of the resonant nonlinearities in an organic material, *J. Opt. Soc. Am. B 17*, 1376-1382.
18. Müller, R. H., Benita, S., and Böhm, B. H. L. (1998) Emulsions and Nanosuspensions for the Formulation of Poorly Soluble Drugs, *Scientific Publishers, Stuttgart*.
19. Newcomb, M., Hollenberg, P. F., and Coon, M. J. (2003) Multiple mechanisms and multiple oxidants in P450-catalyzed hydroxylations, *Arch. Biochem. Biophys. 409*, 72-79.
20. Ortiz de Montellano, P. R. (1995) *Cytochrome P450: Structure, Mechanism, and Biochemistry*, 2nd. ed., Plenum Press, New York.
21. Chandrasena, R. E. P., Vatsis, K. P., Coon, M. J., Hollenberg, P. F., and Newcomb, M. (2004) Hydroxylation by the Hydroperoxy-Iron Species in Cytochrome P450 Enzymes, *J. Am. Chem. Soc. 126*, 115-126.
22. Meunier, B., de Visser, S. P., and Shaik, S. (2004) Mechanism of Oxidation Reactions Catalyzed by Cytochrome P450 Enzymes, *Chem. Rev. 104*, 3947-3980.
23. Silaghi-Dumitrescu, R. (2004) The nature of the high-valent complexes in the catalytic cycles of hemoproteins, *J. Biol. Inorg. Chem. 9*, 471-476.
24. Mayer, J. M. (2000) Biomimetic Oxygenations Related to Cytochrome P450: Metal-Oxo and Metal-Peroxo Intermediates, In *Biomimetic Oxidations Catalyzed by Transition Metal Complexes* (Meunier, B., Ed.), pp 1-43, Imperial College Press.

25. Dolphin, D., Traylor, T. G., and Xie, L. Y. (1997) Polyhaloporphyrins: Unusual Ligands for Metals and Metal-Catalyzed Oxidations, *Acc. Chem. Res. 30*, 251-259.
26. Mansuy, D. (1993) Activation of alkanes : the biomimetic approach, *Coord. Chem. Rev. 125*, 129-141.
27. Groves, J. T. (2000) Reactivity and mechanisms of metalloporphyrin-catalyzed oxidations, *J. Porphyrins Phthalocyanines 4*, 350-352.
28. Barloy, L., Battioni, P., and Mansuy, D. (1990) Manganese porphyrins supported on montmorillonite as hydrocarbon mono-oxygenation catalysts: particular efficacy for linear alkane hydroxylation, *J. Chem. Soc., Chem. Commun.*, 1365-1367.
29. Wang, C., Shalyaev, K. V., Bonchio, M., Carofiglio, T., and Groves, J. T. (2006) Fast Catalytic Hydroxylation of Hydrocarbons with Ruthenium Porphyrins, *Inorg. Chem. 45*, 4769-4782.
30. Merlau, M. L., Cho, S.-H., Sun, S.-S., Nguyen, S. T., and Hupp, J. T. (2005) Anthracene-Induced Turnover Enhancement in the Manganese Porphyrin-Catalyzed Epoxidation of Olefins, *Inorg. Chem. 44*, 5523-5529.
31. Groves, J. T., and Marla, S. S. (1995) Peroxynitrite-Induced DNA Strand Scission Mediated by a Manganese Porphyrin, *J. Am. Chem. Soc. 117*, 9578-9579.
32. Lee, J., Hunt, J. A., and Groves, J. T. (1998) Mechanisms of Iron Porphyrin Reactions with Peroxynitrite, *J. Am. Chem. Soc. 120*, 7493-7501.
33. Lee, J., Hunt, J. A., and Groves, J. T. (1998) Manganese Porphyrins as Redox-Coupled Peroxynitrite Reductases, *J. Am. Chem. Soc. 120*, 6053-6061.
34. Lee, J., Hunt, J. A., and Groves, J. T. (1997) Rapid decomposition of peroxynitrite by manganese porphyrin-antioxidant redox couples, *Bioorg. Med. Chem. Lett. 7*, 2913-2918.
35. Hunt, J. A., Lee, J., and Groves, J. T. (1997) Amphiphilic peroxynitrite decomposition catalysts in liposomal assemblies, *Chem. Biol. 4*, 845-858.
36. Shimanovich, R., and Groves, J. T. (2001) Mechanisms of Peroxynitrite Decomposition Catalyzed by FeTMPS, a Bioactive Sulfonated Iron Porphyrin, *Arch. Biochem. Biophys. 387*, 307-317.
37. Jensen, M. P., and Riley, D. P. (2002) Peroxynitrite Decomposition Activity of Iron Porphyrin Complexes, *Inorg. Chem. 41*, 4788-4797.

38. Crow, J. P. (2000) Peroxynitrite scavenging by metalloporphyrins and thiolates, *Free Radical Biol. Med. 28*, 1487-1494.
39. Stern, M. K., Jensen, M. P., and Kramer, K. (1996) Peroxynitrite Decomposition Catalysts, *J. Am. Chem. Soc. 118*, 8735-8736.
40. Salvemini, D., Wang, Z.-Q., Stern, M. K., Currie, M. G., and P., M. T. (1998) Peroxynitrite decomposition catalysts: Therapeutics for peroxynitrite-mediated pathology *Proc. Natl. Acad. Sci. USA 95*, 2659-2663.
41. Ferrer-Sueta, G., Vitturi, D., Batinić-Haberle, I., Fridovich, I., Goldstein, S., Czapski, G., and R., R. (2003) Reactions of Manganese Porphyrins with Peroxynitrite and Carbonate Radical Anion, *J. Biol. Chem. 278*, 27432-27438.
42. Drain, C. M., Smeureanu, G., Patel, S., X.Gong, Garno, J., and Arijeloye, J. (2006) Porphyrin nanoparticles as supramolecular systems, *New J. Chem. 30*, 1834-1843.
43. Gong, X., Milic, T., Xu, C., Batteas, J. D., and Drain, C. M. (2002) Preparation and Characterization of Porphyrin Nanoparticles, *J. Am. Chem. Soc. 124*, 14290-14291.
44. Merlau, M. L., Mejia, M. d. P., Nguyen, S. T., and Hupp, J. T. (2001) Artificial enzymes formed through directed assembly of molecular square encapsulated epoxidation catalysts, *Angew. Chem. Int. Ed. 40*, 4239-4242.
45. Lee, S. J., and Hupp, J. T. (2006) Porphyrin-containing molecular squares: Design and applications, *Coord. Chem. Rev. 250*, 1710-1723.
46. Khalil, G. E., Chang, A., Gouterman, M., Callis, J. B., dalton, L. R., Turro, N. J., and Jockusch, S. (2005) Oxygen pressure measurementusing singlet oxygen emission, *Rev. Sci. Instrum. 76*, 54101-54108.
47. Drain, C. M., Varotto, A., and Radivojevic, I. (2009) Self-Organized Porphyrinic Materials, *Chem. Rev. 109*, 1630-1658.
48. M.d'A., A., Rocha Gonsalves, Serra, A. C., and Pineiro, M. (2009) The small stones of Coimbra in the huge tetrapyrrolic chemistry building, *J. Porphyins Phthalocyanines 13*, 429-445.
49. Pineiro, M., Carvalho, A. L., Pereira, M. M., Gonsalves, A. M. d. A. R., Arnaut, L. G., and Formosinho, S. J. (1998) Photoacoustic Measurements of Porphyrin Triplet-State Quantum Yields and Singlet-Oxygen Efficiencies, *Chem. Eur. J. 4*, 2299-2307.

50. Pineiro, M., Pereira, M. M., Rocha Gonsalves, A. M. d. A., Arnaut, L. G., and Formosinho, S. J. (2001) Singlet oxygen quantum yields from halogenated chlorins: potential new photodynamic therapy agents, *J. Photochem. Photobiol. A: Chem. 138*, 147-157.

51. Azenha, E. G., Serra, A. C., Pineiro, M., Pereira, M. M., Seixas de Melo, J., Arnaut, L. G., Formosinho, S. J., and Rocha Gonsalves, A. M. d. A. (2002) Heavy-atom effects on metalloporphyrins and polyhalogenated porphyrins, *Chem. Phys. 280*, 177-190.

52. Baluschev, S., Miteva, T., Yakutkin, V., Nelles, G., Yasuda, A., and Wegner, G. (2006) Up-Conversion Fluorescence: Noncoherent Excitation by Sunlight, *Phys. Rev. Lett. 97*, 143903.

53. Mirkin, C. A., and Ratner, M. A. (1992) Molecular Electronics, *Annu. Rev. Phys. Chem. 43*, 719-754.

54. Drain, C. M., Gong, X., Ruta, V., Soll, C. E., and Chicoineau, P. F. (1999) Combinatorial Synthesis and Modification of Functional Porphyrin Libraries: Identification of New, Amphipathic Motifs for Biomolecule Binding, *J. Comb. Chem. 1*, 286-290.

55. Samaroo, D., Vinodu, M., Chen, X., and Drain, C. M. (2007) meso-Tetra(pentafluorophenyl)porphyrin as an Efficient Platform for Combinatorial Synthesis and the Selection of New Photodynamic Therapeutics using a Cancer Cell Line, *J. Comb. Chem. 9*, 998-1011.

56. Singh, S., Aggarwal, A., Thompson, S., Tom. , J. o. P. C., Zhu, X., Samaroo, D., Vinodu, M., Gao, R., and Drain, C. M. (2010) Synthesis and Photophysical Properties of Thioglycosylated Chlorins, Isobacteriochlorins, and Bacteriochlorins for Bioimaging and Diagnostics, *Bioconjugate Chem. 21*, 2136-2146.

57. Chen, X., Hui, L., Foster, D. A., and Drain, C. M. (2004) Efficient Synthesis and Photodynamic Activity of Porphyrin-Saccharide Conjugates: Targeting and Incapacitating Cancer Cells, *Biochemistry 43*, 10918-10929.

58. Thompson, S., Chen, X., Hui, L., Toschi, A., Foster, D. A., and Drain, C. M. (2008) Low concentrations of a non-hydrolysable tetra-S-glycosylated porphyrin and low light induces apoptosis in human breast cancer cells via stress of the endoplasmic reticulum, *Photochem. Photobiol. Sci. 7*, 1415-1421.

59. Chen, X., and Drain, C. M. (2004) Photodynamic Therapy using Carbohydrate Conjugated Porphyrins *Drug Des. Rev. 1*, 215-234.

60. Pushpan, S. K., Venkatraman, S., Anand, V. G., Sankar, J., Parmeswaran, D., Ganesan, S., and Chandrashekar, T. K. (2002) Porphyrins in Photodynamic Therapy - A Search for Ideal Photosensitizers *Curr. Med. Chem. - Anti-Cancer Agents 2*, 187-207.

61. Spikes, J. D. (1990) New trends in photobiology: Chlorins as photosensitizers in biology and medicine, *J. Photochem. Photobiol. B: Biol. 6*, 259-274.

CHAPTER 2: SELF-ORGANIZED METALLOPORPHYRIN NANOPARTICLES AS CATALYST FOR CYCLOHEXENE OXIDATION IN WATER USING O_2

Abstract

Organic nanoparticles (ONP) of metalloporphyrins can be versatile catalysts for the selective oxidation of alkenes and other hydrocarbons. Herein, we report the catalytic activity of ONP of two different metalloporphyrins: 5,10,15,20-tetrakis-[4-(1'H,1'H,2'H,2'H-heptadecafluorodecane-1-thiol)-2,3,5,6-tetrafluorophenyl] porphyrinato iron(III), Fe(III)$TPPF_{84}$, and 5,10,15,20-tetakis-(2,3,4,5,6-pentafluorophenyl) porphyrinato manganese(III), Mn(III)$TPPF_{20}$, for cyclohexene oxidation using molecular oxygen as an oxidant in water under ambient conditions. While the solvated metalloporphyrins catalytically oxidize alkenes to the corresponding epoxide in halogenated solvent with a modest turn-over numbers (TON), 10-30 nm ONP of Fe(III)$TPPF_{84}$ metalloporphyrins have enhanced catalytic activity with up to a 4-fold greater TON and yields only allylic oxidation products. These ONP catalytic systems facilitate a greener reaction since ca. 89% of the reaction medium is water, molecular oxygen is used in place of man-made oxidants, and the ambient reaction conditions require less energy. The enhanced catalytic activity of these ONP is unexpected because the metalloporphyrins in the nanoaggregates are in the close proximity and the TON should diminish by self-oxidative degradation. The fluorous alkanes in Fe(III)$TPPF_{84}$ stabilize the ONP towards self-oxidative degradation.

2.1 Introduction

Allylic oxidation of olefins is a key organic transformation in a variety of synthetic strategies, such as for steroids, and is often carried out using metal oxidants as reagents or as oxidation catalysts. Catalysts based on Cr(*1*), Rh(*2, 3*), Mn(*4*), Ru(*5*), Se(*6*) and other metals are reported but have different problems such as cost, scope, complete removal of the metal, and synthesis. Recently Zhao et al. reported the use of $PhI(OAc)_2$ and *t*BuOOH reagents to generate the $tBuO^{\bullet}$ radical to yield αβ-unsaturated enones in good yield and regioselectivity.(*7*) Ammonium hypoiodite catalysis is another example of metal-free oxidation.(*8*)

Metalloporphyrins have been examined extensively for these oxidation reactions and can be an effective catalyst to oxidize a variety of organic and inorganic substrates. These reactions are inspired by studies of the activity and mechanism of cytochrome P_{450} monooxygenation reactions using heme.(*9-12*) Different oxygen atom donors have been used for these oxidation reactions as they can bind effectively with the central metal atom to form oxometalloporphyrin complexes, which have very high reactivity as oxygen transfer agents. Supramolecular systems of metalloprphyrins can be a robust catalyst for these reactions because of their remarkable stability and enhaced cataltic activity on a per porphyrin basis than individual porphrin in solution or adsorbed onto support. Self-assembled metalloporphyrin catalysts relevent to the present work are inspired by the remarkably robust systems formed by Hupp and coworkers, but this system requires macrocycles that are difficult to obtain in high yields.(*13-15*) The structure of the porphyrin, type of oxidant, solvent, nature of axial ligand, temperature, pressure, and the structure of

the substrate affect the reactivity of the metalloporphyrin.

2.2 Organic Nanoparticles[a]

Inorganic nanoparticles with various capping groups or imbedded into polymers or other matrixes are widely used, or proposed, for a diverse array of catalytic applications.(*16, 17*) The inorganic cores of these conventional nanoparticles are robust and structurally static. In contrast, the structures, properties, and functions of aggregates of organic molecules organized into nanoparticles (ONP) by weak intermolecular interactions are much less understood because the organization of the molecules in the ONP can be dynamic.(*18*)

Most methods to make nanoaggregates of small organic molecules have their historical roots in the formation of colloidal dispersions of organic systems.(*19*) The methods to make nanoscaled aggregates of dyes such as porphyrinoids(*18, 20-28*) include: (a) the rapid exchange of solvent, (b) host/guest solvents whereby aggregation occurs by mixing solutions containing chromophore molecules with miscible solvents in which they are not soluble (e.g. THF/H_2O) and stabilized by surfactants or amphipathic molecules, (c) interfacial precipitation, and (d) the rapid expansion of supercritical solvents. The former two methods result in dispersions in solution and the latter two methods result in many types of nanostructures that are kinetically trapped from further aggregation by deposition on surfaces. There is considerable interest in understanding the intermolecular processes governing formation of organic colloids and ONP.(*13, 18, 20*) Hierarchical organization of molecules into nano-structured aggregates can have a

[a] Adapted from reference: Smeureanu, G., Aggarwal, A., Soll, C. E., Arijeloye, J., Malave, E., and Drain, C. M. (**2009**) Enhanced Catalytic Activity and Unexpected Products from the Oxidation of Cyclohexene by Organic Nanoparticles of 5,10,15,20-Tetrakis-(2,3,4,5,6-pentafluorophenyl)porphyrinatoiron(III) in Water by Using O_2, *Chem. Eur. J. 15*, 12133-12140.

profound effect on their photonic and catalytic properties. For example, formation of ONP of porphyrinoids and other chromophoric systems offers the potential to enhance or modulate the photonic properties of the molecules through quantum mechanical effects.(*29, 30*) Additionally, understanding the spontaneous formation of suspensions of molecular aggregates is becoming an important topic for the formulation of hydrophobic drugs.(*31*) The formation of narrowly dispersed ONP may arise from both a thermodynamic limitation due to nanoparticle surface energies, a kinetic limitation whereby the rates of formation of the individual aggregates influence the availability of material,(*20, 24, 32*) and the recent work of Van Keuren et al. indicating the importance of transient formation of unstable clusters.(*26*)

2.3 Porphyrin Catalyst[a]

The discovery by Groves and co-workers(*33-38*) on the use of commercially available iron porphyrins in organic solvents to mimic the oxidative catalysis observed for cytochrome P_{450}(*9-12, 39, 40*) using a synthetic oxygen source such as iodosylbenzene led to a huge amount of research on the reactivity and mechanism for this reaction. Different metalloporphyrins react differently to give different products or product ratios.(*38, 41-46*) Other major findings include: (a) appropriate modification of the porphyrin macrocycle alters reactivity in terms of site selectivity,(*47-50*) (b) halogenation generally makes the metalloporphyrins more efficient catalysts,(*51-65*) (c) axial ligands can alter reactivity,(*66-69*) (d) the solvent can also affect the reactivity,(*51-54*) and (e) other oxygen sources such as H_2O_2, and O_2, can be used with some systems.(*69-72*) Various metalloporphyrins are now used in laboratory scale reactions. Heterogeneous porphyrin systems include those in lipids, micelles, zeolites, or on

supports such as silica, or Montmorillonite clay.(*47, 61, 73-76*) Several reaction types are catalyzed by metalloporphyrins, but perhaps the best studied are oxidation reactions. The catalytic oxidation of cyclohexene by iron tetra arylporphyrins is a standard reaction that has been investigated thoroughly over the last few decades, and the epoxide is the major product under a range of experimental conditions. Self-oxidative degradation of metalloporphyrins is always a key issue for these oxidation reactions. Supramolecular porphyrin systems are designed to overpass this problem and also for substrate selectivity and/or regioselectivity.(*77, 78*) Different oxygen sources such as peracids, iodosylbenzene, peroxides, monopersulfates, and molecular oxygen are used for these reactions.(*79*) In many ways, activation of molecular oxygen in air is preferable because it is cheap, readily available, and a greener reagent in that there is no energy used to manufacture and store it.

5,10,15,20-tetrakis-(2,3,4,5,6-pentafluorophenyl) porphyrinato iron(III) chloride, [Fe(III)$TPPF_{20}$]Cl is found to be catalytically active for the oxidation of olefins using synthetic oxygen sources, but not with the molecular oxygen, in solution phase reactions.(*80*) Gray et al. reported significantly different oxidation chemistry for a derivative of [Fe(III)$TPPF_{20}$]Cl wherein the eight β pyrrole positions are also halogenated.(*81-83*) The difference in the catalytic oxidation of perhalogenated porphyrins arises from both distortions in the otherwise planar macrocycles and electronic effects. When the β positions of [Fe(III)$TPPF_{20}$]Cl are chlorinated the catalytic oxidation of ethylbenzene using oxygen at 100 ^{o}C is increased, but not the stability towards the oxidative degradation of the catalyst. Stability increases when the catalyst is linked to polystyrene.(*71*) The catalytic activity of the metalloporphyrin

is affected by the nature of the counter ion and the solvent in which the porphyrin is dissolved.(*84, 85*) Fe(III)TPPF$_{20}$ was reported to be inactive for olefinic epoxidation when dissolved in acetonitrile but becomes active when methanol or another alcohol is added to the aprotic solvent.(*51, 80, 85, 86*) In general the turnover number (TON) for iron porphyrin catalysts in solution is a few hundred because of the degradation of the catalyst, but this increases to ca. 350 when Fe(III)TPPF$_{20}$ is used because this is a more active catalyst and may be somewhat more resistant to oxidative degradation. There are numerous studies on the catalytic activity of this porphyrin,(*71, 87, 88*) including the recent reports by Bell et al. on the catalytic oxidation of cyclooctene by Fe(III)TPPF$_{20}$ in acetonitrile/methanol yields over 98% of the epoxide and traces of the 2-cyclooctene-1-one and the 2-cyclooctene-1-ol.(*51-54*) Under the same conditions we find similar reactivity for cyclohexene (Scheme 2.1).

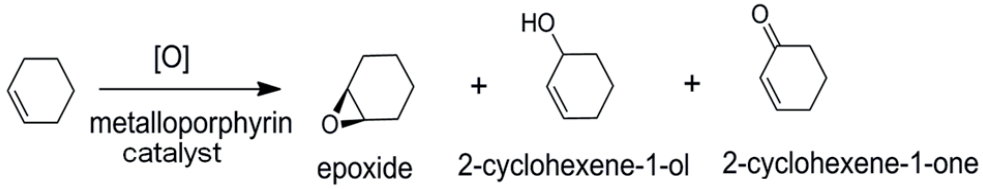

Scheme 2.1: Oxidation of cyclohexene using metalloporphyrin catalystic system.

Meso phenyl substituted Mn(III) porphyrins are catalytically active using molecular oxygen as the oxidant at elevated temperatures and pressures (120 ^{o}C, 10 atm).(*89, 90*) The catalytic activity of transition metal complexes in solution and/or adsorbed on supports can be increased with the addition of sacrificial aldehyde, such as isobutyraldehyde, under ambient conditions.(*91-95*) We found similar catalytic activity with Mn(III)TPPF$_{20}$ in dichloromethane under ambient conditions using 1:5 cyclohexene: isobutyraldehyde and molecular oxygen as oxidant. The epoxide of

cyclohexene is the major product with a TON of ca. 8885. However, we found that control reactions with isobutyraldehyde and molecular oxygen but *without metalloporphyrin* converts cyclohexene into the epoxide (45% yield). Thus, oxidation reactions with isobutyraldehyde and dioxygen may need to be reevaluated.(*91, 93, 95, 96*)

2.4 Organic Nanoparticles of Porphyrins[a]

Nanomaterials composed of inorganic materials are of great interest for a wide variety of applications,(*97, 98*) the formation and activity of organic nanoparticles (ONP) are less well developed. ONP of porphyrins and metalloporphyrins are promising components for advance materials because of their remarkable photochemical and catalytic properties, stability, and ease of preparation.(*20, 21, 99*) ONP can be considered as self-organized systems that are governed by non-covalent interactions such as van der Waals forces, H-bonding, and electrostatic interactions that depend on the structure of the porphyrin, the central metal ion, nature of the axial ligand, solvent, and the method of preparing the nanoparticles. Thus ONP are fundamentally different from inorganic nanomaterials. The formation of ONP of porphyrins is accomplished by dissolving the macrocycle in a host solvent and rapidly adding this to a miscible non-solvent with a few percent of tetraethylene glycol with vigorous mixing. In the present work the porphyrins are dissolved in THF and water serves as the guest solvent. The size and structure of porphyrinic nanoparticles formed depends on: (a) the nature and magnitude of intermolecular forces between the various components, e.g. the porphyrin, host and guest solvents, and the PEG stabilizer; (b) the ratio of the host to guest solvent, (c) the type of mixing, and (d) the nature of peripheral substituents on the porphyrin core.(*99*)

Therefore, the structure of the porphyrin and the specific metal ion influence both the size and the organization of the chromophores within the nano-aggregates. For Fe(III)TPPF$_{20}$ in THF/water as host/guest solvents, large ca. 80 nm diameter ONP are formed by magnetically stirring and are likely composed of smaller subdomains of 5-20 nm. Whereas sonication while adding the guest solvent results in ca. 10 nm ONP of this metalloporphyrin which are less prone to reorganization or disaggregation (Scheme 2.2). Since the ONP are self-organized solely by intermolecular forces, these are dynamic systems in that they can reorganize or disaggregate in response to environmental changes.(*18, 100*) These ONP are stable for weeks when placed in refrigerator at 4^{o}C. ONP of catalytically active metalloporphyrins are generally more efficient catalysts than the same system in solution.

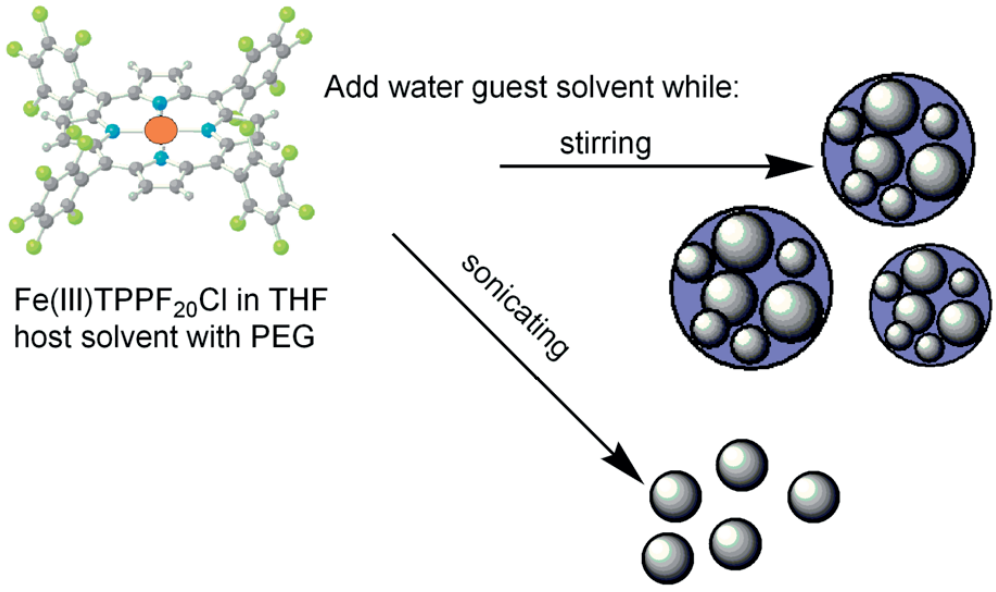

Scheme 2.2: 5.0 mL of water is added to a mixture of 0.4 mL of 1.0 mM Fe(III)TPPF$_{20}$ in THF and 0.2 mL PEG while stirring or sonicating to yield ca. 80 nm and 10 nm diameter ONP, respectively. Taken from reference 99.

2.5 ONP Fe(III)TPPF$_{20}$ Catalyst[a]

***Result and discussion*:** A solution of Fe(III)TPPF$_{20}$ in acetonitrile/methanol catalytically oxidizes cyclohexene to the epoxide using H_2O_2 with a TON of ca. 350. Previous reports using cyclooctene as a substrate parallel these results in that only the epoxide is formed and only H_2O_2 can be used.(*51-54*) In contrast, 10 nm diameter ONP of Fe(III)TPPF$_{20}$ catalytically oxidizes cyclohexene using O_2 to yield exclusively 2-cyclohexene-1-one and 2-cyclohexene-1-ol with ca. 10-fold greater TON than the completely solvated metalloporphyrin, though at a much slower rate (Table 2.1).

TON is defined as the total amount of products (3:1=ketone:alcohol) formed per porphyrin, and since the porphyrin slowly decomposes, these reactions are run until [metalloporphyrin] < 0.2 μM. This represents a greener alternative to effect these organic transformations since dioxygen is efficiently used as oxidant in place of H_2O_2 or other synthetic oxygen sources, and the reaction solvent is 89% water.

The increased TON is contrary to expectations because the metalloporphyrins are in close proximity in the ONP, which should enhance oxidative degradation of the catalyst and cause a significant *decrease* in catalytic turnovers. There have been significant efforts to isolate porphyrinoid catalysts, see above. Furthermore, the allylic oxidation products suggest a different mechanism compared to that of the corresponding solvated metalloporphyrin.(*51-54*) Control reactions in the absence of an oxygen source or metalloporphyrin result in no product formation. Adding < 5% water and the PEG to the homogeneous reaction mixture has no effect on the product ratios or TON, i.e. only the epoxide is formed with H_2O_2 and a TON of 350. The UV-visible spectra of the exhausted reaction mixtures reveals that eventually the metalloporphyrin in solution or as an ONP

decomposes(*101*) (see appendix). Unlike the solution phase reactions, the slow addition of H_2O_2 to the ONP suspension results in modest yields of the allylic products, whereas addition of a 30% solution in one aliquot degrades the porphyrin within a few minutes as observed by UV-visible spectra. These observations indicate the hierarchical organization of the metalloporphyrins in the ONP is key to the observed activity.

Table 2.1: Fe(III)TPPF$_{20}$ ONP catalysis of cyclohexene oxidation

solution[A] or ONP[B]	conditions	% oxide	% ene-1-ol	% ene-1-one	TON	Comment[D,E]
solution	CH_3CN/ CH_3OH H_2O_2	98	<1	<1	350	15 min
solution	CH_3CN/ CH_3OH H_2O_2	95 ±5	5±1	<1	not reported	cyclooctene, 15 min ref. 1-4
10 nm ONP	H_2O_2	<1	30	70	175	ca. 5 min
10 nm ONP	6.5 mL O_2	<1	26	74	500	O_2 limiting reagent
10 nm ONP	125 mL O_2	<1	28	72	3500	16 hrs
10 nm ONP	99.6% D_2O, 125 mL O_2	<1	20	80		no D in products other than the exchangeable alcohol proton
10 nm ONP	10% $H_2{}^{18}O$, 125 mL O_2	<1	34	66		^{18}O in 10% of ketone and <1% in alcohol
10 nm ONP	H_2O, 125 mL 98 % $^{18}O_2$	<1	23	76		^{18}O in <8% of ketone and >90% of alcohol
10 nm ONP	125 mL O_2 0.5 mL cyclohexene	<1	28	72	3500	16 hrs
10 nm ONP	125 mL O_2, no PEG	<1	25	75	430	8 hrs
30 nm ONP	125 mL O_2	1	29	70	3100	6 hrs
35 nm ONP[C]	H_2O/DMF C_6H_5IO	70	11	19	16,500	8 hrs
120 nm ONP[C]	H_2O/DMF C_6H_5IO	85	6	10	12,000	8 hrs

Table 2.1: [A]Solution reactions: 0.1 mM catalyst in 2.75 mL 3:1 acetonitrile:methanol; porphyrin: cyclohexene: H_2O_2 = 1:2000:3000. This is similar to the cyclooctene oxidations reported previously.(49-52) [B] ONP reactions: 2.5 mL of the ONP suspension (70 μM, 1.75 x 10^{-7} moles of porphyrin); porphyrin: substrate: H_2O_2 = 1:2000:3000, H_2O_2. Alternatively, the 2.5 mL porphyrin ONP suspension was mixed with 200 μL of cyclohexene and 125 mL O_2 at 1 atm; porphyrin:substrate:O_2 1:16,000:40,000). [C]ONP made from DMF host solvent under conditions used to obtain this size nanoparticle. (24) [D] $t_{1/2}$ for total products formed. [E]All reactions were run exhaustively. The TON = (moles products)/(moles porphyrin) has an error of + 5%. Products were extracted into CH_2Cl_2 and analyzed using an Agilent 5975 series GC-MS. Control reactions: neither H_2O_2 nor O_2 react directly with cyclohexene under these conditions (See appendix). Taken from reference 99.

2.6 New Metalloporphyrin Catalysts for Cyclohexene Oxidation

The catalytic activity and stability of the metalloporphyrins towards self-oxidative degradation is always a key concern, since most decompose rapidly under a variety of conditions. To reduce self-oxidation, electron withdrawing or bulky substituents are often appended to the porphyrin macrocycle. Metalloporphyrins bearing electron withdrawing groups such as Cl and F on the periphery of the porphyrin macrocycle and/or on meso-aryl groups generally show enhanced catalytic activity, e.g. for the selective epoxidation of alkenes(*102, 103*) and hydroxylation of alkanes(*104*) in solution phase reactions. The electron withdrawing group increases the half wave potential of the metalloporphyrin and thus protects the macrocycle ligand from oxidative self-degradation. This strategy can also prevent deactivation by formation of their μ-oxo dimers.(*102*)

Working Hypothesis: Our hypothesis was that appending fluorous alkanes to the macrocycle would increase metalloporphyrin stability and the Mn complex would increase activity. Indeed, ONP of 5,10,15,20-tetrakis-[4-(1'H,1'H,2'H,2'H-heptadecafluorodecane-1-thiol)-2,3,5,6-tetrafluorophenyl]porphyrinato iron(III) chloride, [Fe(III)TPPF$_{84}$]Cl are found to be more stable towards self-oxidative degradation for cyclohexene oxidation, but the overall yields of the αβ-unsaturated ketone and alcohol are less than ONP of [Fe(III)TPPF$_{20}$]Cl. ONP of 5,10,15,20-tetakis-(2,3,4,5,6-pentafluorophenyl) porphyrinato manganese(III), [Mn(III)TPPF$_{20}$]Cl gives the same allylic oxidation products of cyclohexene (ketone : alcohol = 4:1), but do not activate dioxygen under ambient conditions. The oxidation of cyclohexene with ONP of Mn(III)TPPF$_{20}$ becomes robust when a coreductant such as isobutyraldehyde is added,

but this is complicated by the background reaction where oxygen and isobutyraldehyde affect the oxidation too.

2.7 Experimental Details

2.7.1 Materials and Instrumentation

5,10,15,20-tetrakis-(2,3,4,5,6-pentafluorophenyl) porphyrinato iron(III) chloride, 5,10,15,20-tetrakis-(2,3,4,5,6-pentafluorophenyl) porphyrin, $TPPF_{20}$ manganese(II) acetate pentahydrate (99.99%), cyclohexeneoxide (98%), 2-cyclohexene-1-ol (95%), 2-cyclohexene-1-one (95%), tetraethylene glycol monomethyl ether (PEG_{164}), isobutyraldehyde (99.9%), tetrahydrofuran (THF, 99.9% anhydrous), methanol (99.9% anhydrous), N,N-dimethylformamide (DMF, 99.8%), and N,N-diisopropylethylamine (DIPEA, 99.5%) were purchased from Aldrich Chemical Co. while HPLC grade dichloromethane, glacial acetic acid (99.9%), 30% H_2O_2, toluene and cyclohexene were purchased from Fisher Scientific Co. HPLC grade acetonitrile was purchased from J.T baker, and 3,3,4,4,5,5,6,6,7,7,8,8,9,9,10,10-heptadecafluoro-1-decanethiol ($\geq$ 99.0%) was purchased from Fluka. Nanopure water was obtained by using Barnstead Nanopure water system. D_2O (99.6%) was obtained from Cambridge Isotope laboratories Inc. The oxidation products of cyclohexene were analyzed using an Agilent 5975 series GC-MS with a HP-5 column (HP-5MS 30 m x 0.250 mm, 0.25 micron nominal, 5% phenyl methyl siloxane). Electronic spectra were taken on Cary Bio-3 UV-visible spectrophotometer. A Precision Detector PD2000DLS Cool-Batch dynamic light scattering (DLS) instrument was used in batch mode at 25 ^{o}C to determine particle size. A Fisher SF15 sonicator was used for nanoparticle preparation.

2.7.2 Preparation of Fe(III)TPPF$_{84}$ Catalyst

Catalyst Fe(III)TPPF$_{84}$ was prepared by using a method reported previously by our group for the substitution by fluorous alkyl chain at the para position of a free base TPPF$_{20}$ porphyrin.(*105*) 27.08 mg (56.4 µmol, 6 equivalents), of 3,3,4,4,5,5,6,6,7,7,8,8,9,9,10,10-heptadecafluoro-1-decanethiol were mixed in 2 mL dimethylformamide (DMF) and 500 µL (0.37 g, 2.9 mmol) diisopropylethylamine (DIPEA) was added under a nitrogen atmosphere. The solution was stirred at room temperature for 15 min. and 10 mg (9.4 µmol) of [Fe(III)TPPF$_{20}$]Cl was added and the solution stirred at room temperature for 2 h. The product was then precipitated, filtered, and washed with distilled water and CH_2Cl_2. The precipitates were dried under vacuum, to yield 83% (22.67 mg, 7.8 µmol) of the product (Scheme 2.3). All spectral data is consistent with the structure (see appendix).

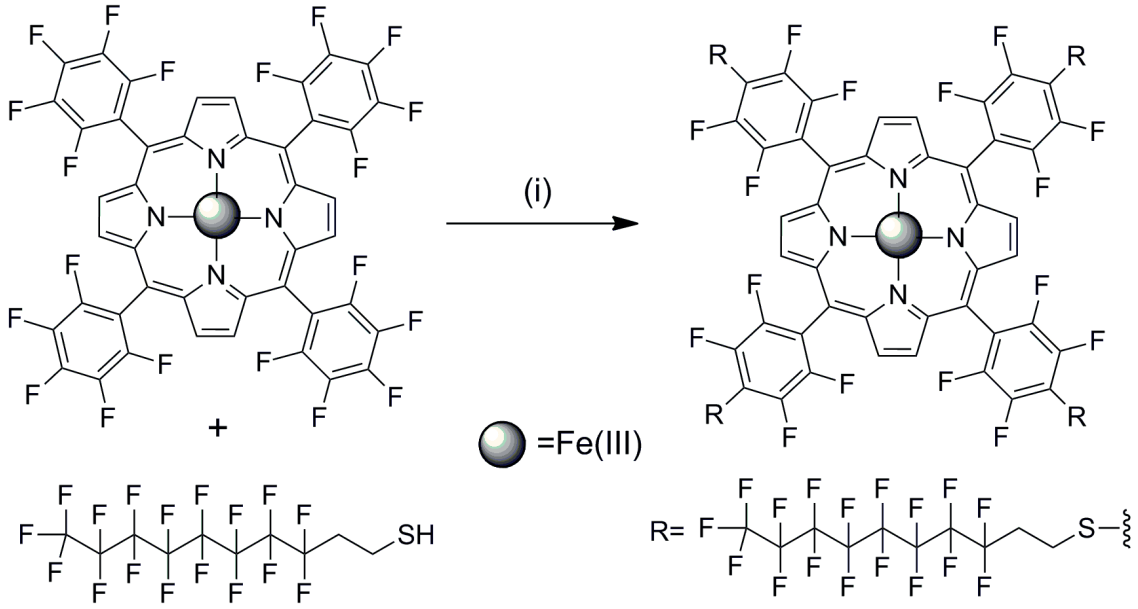

Scheme 2.3: Preparation of Fe(III)TPPF$_{84}$ catalyst: (i) DMF/DIPEA under N_2 at rt. for 2h.

2.7.3 Preparation of Mn(III)$TPPF_{20}$ Catalyst

The insertion of the manganese metal ion into the free base $TPPF_{20}$ was done as previously reported by Boucher and coworkers.(*106*) The formation of the Mn(III) porphyrin was characterized by UV-visible spectroscopy and mass spectrometry (see appendix). The 411 nm Soret band for $TPPF_{20}$ almost disappears upon metallation and a new Soret peak for the Mn(III) porphyrin appears at 463 nm, and two Q-bands appears at 565 nm and 646 nm.(*107, 108*)

2.8 Preparation of Nanoparticles

Nanoparticles of the two different metalloporphyrins were prepared by our previously reported method.(*21*) A 0.4 mL portion of 1 mM stock solution of metalloporphyrin in THF was mixed with 0.2 mL PEG in a 10.0 mL vial. 5.0 mL nanopure water was then added to this mixture while sonicating over a time period of 60 seconds and then the solution was further sonicated for another 2-3 minutes. The pH of the nanopure water was adjusted to 6.5-7.0, because the formation of the nanoaggregates, their size, stability, and their catalytic activity is highly pH dependent. The prepared nanoparticles are stable and were stored in refrigerator at ca. 4 ^{o}C. The nanoparticles were characterized by UV-visible spectroscopy and the size measured by DLS. The average diameter of the ONP of Fe(III)$TPPF_{84}$ is 12±2 nm and that of Mn(III)$TPPF_{20}$ is 25±7 nm (see appendix). However, with the addition of 1.0 mL of isobutyraldehyde to the ONP of Mn(III)$TPPF_{20}$ the average size changes to 32±4 nm. For miscible solvents, transient solvent clusters typically are observed by DLS (4-5% particle size distribution) around 350-1000 nm.

The aggregation of the metalloporphyrins in the nanoscaled particles were also confirmed by the broadening of the Soret and Q bands as discussed previously.(*20, 99*) For ONP of Mn(III)TPPF$_{20}$ the Soret band is broadened and red shifted by 20 nm and apperas at 483 nm. The two Q-bands are also shifted towards the red end of the visible spectrum. The broadening is due to edge-to-edge (J) and face-to-face (H) aggregation of the dyes in the ONP. A shoulder appears at 458 nm in the ONP spectra of Mn(III)TPPF$_{20}$. No indication of the formation of μ-oxo or μ-dioxo dimers is observed, which appear at 430-445 nm for dimers made from Mn(III)TPPF$_{20}$.(*109*)

2.9 Structure of Porphyrin ONP

The detailed structure inside the porphyrin ONP is not known because the weak intermolecular forces which hold the porphyrin moieties together are non-specific and reversible. The ONP may contain subdomains of porphyrins,(*20*) and the hierarchical organization of the porphyrins within the ONP depends on the structure of the porphyrin, nature of miscible solvents, stabilizer, and the method of mixing. Thus, ONP in solution are dynamic in nature. Our previous reports on the characterization of ONP using AFM and XRD for a group of porphyrins on surfaces does not show same size and organization for the ONP as they have in solutions.(*20, 21*). Analysis of all reaction mixtures for nanoparticles, e.g. by light scattering, should be routine.

2.10 Reaction Procedure

Oxidation of cyclohexene by air/H_2O_2/Pure O_2

Solution phase catalysis: A 1 mM stock solution of Fe(III)TPPF$_{84}$ was prepared in THF. For reactions using the O_2 in air or with H_2O_2 as oxidant, 9 mL screw capped

vials were used. 400 μL (0.4 μmol) of the porphyrin solution were mixed with 2.5 mL of methanol: acetonitrile (1:3) to make the final concentration of 0.14 mM. 25 μL of cyclohexene was added, the vial capped, and the reaction mixture stirred for 24 h. Here the 6 mL air in the vial contains ca. 1.3 mL O_2 or 53 μmol. The same conditions were used for the reactions using H_2O_2 oxidant, but 40 μL (10.7 μmol) of 30 % H_2O_2 was added. The ratio of the porphyrin: substrate: H_2O_2 = 1:600:1000 equivalents. For the reaction using O_2 as oxidant, 400 μL (0.4 μmol) of porphyrin solution were mixed with 2.5 mL of methanol: acetonitrile (1:3) and 200 μL of cyclohexene in a 25 mL pear-shaped flask fitted to a 125 mL separatory funnel filled with O_2 at 1 atm (filled by flushing the vessel three times with O_2, 5.3 mmol), and then O_2 was added by opening the stopcock. The reactions were run for ca. 24 h. The ratio of the porphyrin : substrate : O_2 = 1 : 4800 : 13000 equivalents. For oxygen reactions, the pear shaped flask was cooled in an ice bath for about 30 minutes with the stopcock to the separatory funnel open, and the separatory funnel heated with hot air to condense all volatile organic species. 20 μL (1.88 x 10^{-4} moles) of toluene was then added to the condensate as an internal standard, and 4.0 μL of this solution was then diluted with 1 mL CH_2Cl_2. 2.0 μL of this diluted sample was then injected into the GC-MS for the analysis of the oxidation products of cyclohexene. All reactions were stirred using a magnetic stirring bar and were run a minimum of four times and the reported data represents the average of these reactions.

Nanoparticle catalysis: For reactions in air with H_2O_2 as oxidant, 2.5 mL of the porphyrin ONP stock solution (70 μM, 1.75 x 10^{-7} moles of porphyrin) were mixed in a 9 mL screw caped vial (ca. 6.5 mL air) with 25 μL of cyclohexene. 40 μL (10.7 μmol) of 30% H_2O_2 was added slowly to the reaction mixture over the course of 40 min. The ratio

of the porphyrin: substrate: H_2O_2 = 1: 1400: 2200 equivalents. The reaction mixture was then stirred for ca. 24 h. After the reaction the vials were cooled in an ice bath for 30 min to condense the volatile species. The 2.6 mL reaction mixture was then extracted thoroughly once with 2.8 mL CH_2Cl_2 and the layers were allowed to separate. The water fraction and some of the organic fraction was then removed to leave a total volume of 2.0 mL (assures the same volume for every assay). 20 μL of toluene (1.88×10^{-4} moles) was then added to the 2.0 mL extraction as an internal standard, whereupon 4.0 μL of this solution was diluted into 1.0 mL CH_2Cl_2 and 2.0 μL of this solution was then injected into the GC-MS for the analysis. The same reaction conditions described above were used for the reactions using O_2 as oxidant. The ratio of porphyrin: substrate: O_2 = 1 : 11300 : 29000 equivalents. The 2.7 mL reaction volume was then extracted once with 8.0 mL CH_2Cl_2 and the layers were allowed to separate. The water fraction and some of the organic fraction was then removed to leave a final volume of 6.0 mL (assures the same volume for every assay). 20 μL of toluene was then added to this extraction as an internal standard, and 4.0 μL of this solution was then diluted with 1 mL CH_2Cl_2. 2.0 μL of this diluted sample was then injected into GC-MS for analysis. For the reactions using Mn(III)$TPPF_{20}$ ONP 1.0 mL isobutyraldehyde was also added to the reaction mixture.

2.11 Results and Discussion

The preparation and use of metalloporphyrin ONP catalysts has several advantages: ease of preparation, the reaction does not use hazardous chemicals such as halogenated solvents, and runs at ambient temperature and pressure.

Cyclohexene is widely used as a standard substrate to study the catalytic activity of various metalloporphyrins using a variety of oxidizing agents and

conditions.(*94, 110-112*) The formation of different products or product ratio depends on the catalytic system. The oxidation of cyclohexene can yield several products, including the cyclohexenoxide, 2-cyclohexene-1-ol, and 2-cyclohexene-1-one (Scheme 2.1). The catalytic activity of ONP of Fe(III)$TPPF_{84}$ and Mn(III)$TPPF_{20}$ using pure oxygen, H_2O_2, and the ca. 21% O_2 in air as oxidizing agents is discussed. The ONP of Mn(III)$TPPF_{20}$ are active only in the presence of isobutyraldehyde which is a coreductant, but this reaction does not need elevated conditions. The highly fluorinated alkyl groups on the para-positions of the meso tetrafluorophenyl groups in Fe(III)$TPPF_{84}$ increases the stability of the porphyrin towards self-oxidative degradation but render the system less catalytically active.

2.11.1 Fe(III)$TPPF_{84}$ Catalyst

Solution phase catalysis: The Fe(III)$TPPF_{84}$ catalyst activates O_2 for the oxidation of cyclohexene in 1:3 CH_3OH: CH_3CN to yield all three products, epoxide: enol: enone = 1:1.5:3 (Table 2.2). Light scattering indicates a small percentage (~ 5%) of large sized particles around 1100 nm but this is not obvious by UV-visible spectroscoy in this mixture solvent. This activity is in contrast to Fe(III)$TPPF_{20}$, which requires H_2O_2 and does not activate O_2.(*80*) The rate of the former reaction is slow compared to the later. UV-visible analysis of the reaction mixture after the reaction was over shows that ca. 36 % porphyrin remains (see appendix). An increased concentration of cyclohexene increases the TON (Figure 2.1). Thus the highly fluorinated alkanes on the para position of the tetrafluorophenyl moiety dramatically effect the catalytic activity and the stability towards self-oxidation.

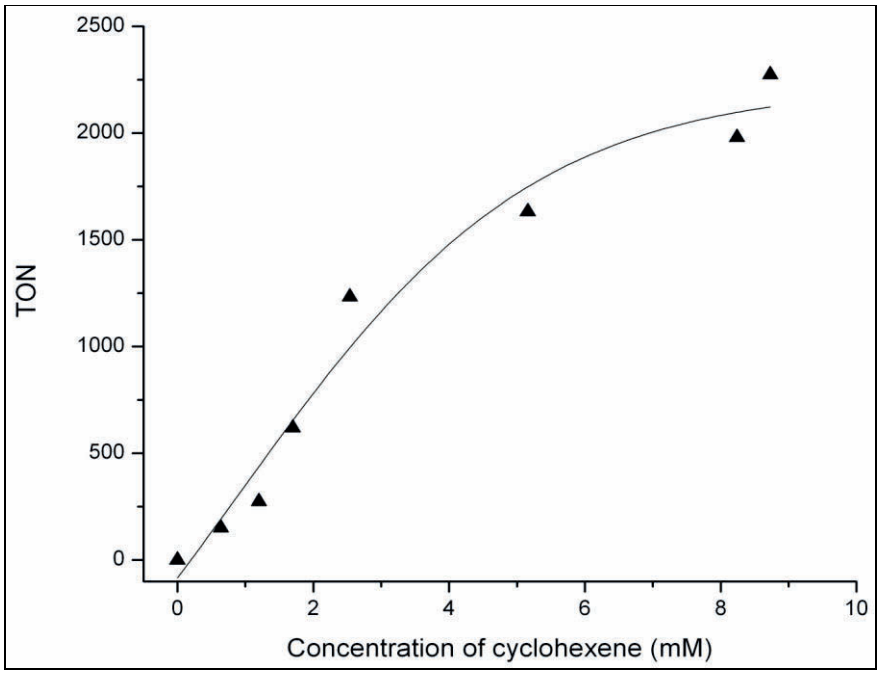

Figure 2.1: A plot of concentration of cyclohexene vs TON for the catalytic activity of ONP of Fe(III)TPPF$_{84}$ for cyclohexene oxidation reaction.

The reduced activity of this catalyst may arise from the long fluorinated alkyl chains folding back over the metalloporphyrin faces, driven by hydrophobic effects and intermolecular interactions amongst the fluorous groups. The shielding of the reactive face decreases access of the hydrocarbon substrate and concomitantly protects the macrocycle from oxidation. Oxygen is more soluble in fluorous phases so this may also contribute to the observed reactivity. Reactions run for up to 72 h have the same ratio of products, but the porphyrin is completely decomposed. Recharging the reaction after 24 h by providing more oxygen is no more efficacious than the 72 h reaction. Reactions run under elevated temperature and pressure for 24 h result in complete decomposition of the porphyrin, and similar oxidation product ratios but with reduced TON (Table 2.2). The increased rate of catalyst decomposition and decreased TON may be because the elevated

temperature increases the dynamics of the fluorinated alkyl chains to expose the macrocycle to approach of another Fe(III)TPPF$_{84}$ (see appendix). Changing the reaction solvent to ethanol/toluene (1:3) quenches the reaction when using O_2. Addition of anthracene to the reaction mixture is known to increase the catalytic activity of metalloporphyrins in terms of TON for the epoxidation of styrene,(*45*) but did not affect the Fe(III)TPPF$_{84}$ reaction system. No cyclohexene oxidation products were observed when the reactions used H_2O_2, and the porphyrin rapidly decomposes (Table 2.2). Note that the non-fluorinated analogue, the dodecanethiol adduct of Fe(III)TPPF$_{16}$, yields no cyclohexene oxidation products and no porphyrin decomposition was observed so does not activate O_2.

Table 2.2 Oxidation of cyclohexene by Fe(III)TPPF$_{84}$ in 1:3 CH_3OH/CH_3CN

Conditions	% epoxide	% enol	% enone	TON	Comments
21 % O_2 in 6.0 mL air[a]	--	--	--	--	no reaction, almost no decomposition of porphyrin
H_2O_2[b]	--	--	--	--	porphyrin decomposes in 15-20 min
125 mL O_2	16	29	55	158	24 h, 36% porphyrin left
125 mL O_2	20	27	53	147	72 h, no porphyrin left
125 mL O_2, 1.73 atm	13	32	55	129	24 h, no porphyrin left
125 mL O_2, 40 ^oC	8	35	57	140	24 h, no porphyrin left
125 mL O_2, 50 ^oC	6	38	56	123	24 h, no porphyrin left

Table 2.2: Solution Reactions: 0.4 mL (4 x 10^{-7} mol of porphyrin) of 1 mM catalyst was mixed 2.5 mL of methanol: acetonitrile (1:3) and 0.025mL of cyclohexene to a final concentration of 0.14 mM. [a] 2.93 mL reaction mixture, porphyrin: cyclohexene: 6.5 mL O_2 in air = 1:600:1400. [b] 2.97 mL reaction mixture, porphyrin: cyclohexene: H_2O_2 = 1:600:1000. With O_2, 0.2 mL cyclohexene was used. 3.1 mL reaction mixture, porphyrin: cyclohexene: O_2 = 1:4800:13000. All reactions were run exhaustively. TON = mol $_{products}$ / mol $_{porphyrin}$ has an error of ± 5%. Products were extracted into DCM and analyzed by using an Agilent 5975 series GC-MS. Control reactions: neither H_2O_2 nor O_2 react directly with cyclohexene under these conditions.

Nanoparticles catalysis: The 12 ± 2 nm diameter ONP of Fe(III)$TPPF_{84}$ are found to be more catalytically active compared to the completely solvated metalloporphyrin. These ONP oxidize cyclohexene using O_2 to yield only the allylic oxidation products, 2-cyclohexene-1-one and 2-cyclohexene-1-ol with a trace amount of epoxide (Scheme 2.1) at ca. 4-fold greater TON (Table 2.3). UV-visible spectra of the reaction mixture after a 24 h reaction shows that ca. 26% of the porphyrin is left, eventually decomposes after longer times (see appendix). Though the allylic oxidation products for ONP of Fe(III)$TPPF_{84}$ is consistent with our previous report on Fe(III)$TPPF_{20}$ ONP,(*99*) the catalytic activity is less yet they are more robust towards self-oxidative degradation. Fe(III)$TPPF_{84}$ ONP are inactive with other oxidants such as the ca. 21% O_2 in air and H_2O_2, and ONP of the hydrocarbon analogue is inactive under the same conditions.

Table 2.3 Oxidation of cyclohexene by 12 ± 2 nm ONP of Fe(III)$TPPF_{84}$

Conditions	% epoxide	% enol	% enone	TON	Comments
125 mL O_2	<1	29	70	670	24 h, 26% porphyrin left
125 mL O_2	<1	32	67	350	72 h, no porphyrin left
125 mL O_2, 1.73 atm	<1	31	68	305	24 h, no porphyrin left
125 mL O_2, 40 ^oC	-------	-------	-------	-------	24 h, no porphyrin left
125 mL O_2, 50 ^oC	-------	-------	-------	-------	24 h, no porphyrin left

Table 2.3: ONP Reaction with O_2: ONP suspension, 2.5 mL mixed with cyclohexene (200 μL) and O_2 (125 mL); porphyrin : substrate : O_2 = 1:11300: 29000. All reactions were run exhaustively. TON = mol $_{products}$ / mol $_{porphyrin}$ has an error of ± 5%. Products were extracted into DCM and analyzed by using an Agilent 5975 series GC-MS. Control reactions: neither H_2O_2 nor O_2 react directly with cyclohexene under these conditions.

2.11.2 Mn(III)TPPF$_{20}$ Catalyst

Nanoparticles catalysis: Manganese porphyrins are catalytically active for olefinic oxidation in halogenated solvents.(*94, 95*) We find that a similar reaction using a solution of Mn(III)TPPF$_{20}$ in CH_2Cl_2 gives the cyclohexyl epoxide as the major product with a TON of ca. 8378 only when isobutyraldehyde is used to mediate oxygen transfer. However, isobutyraldehyde by itself promotes the oxidation reaction and accounts for about half of this yield under these conditions. These results are similar to the previously reported work, and suggest that reactions with isobutyraldehyde need to be reevaluated.(*91-94*)

In contrast, 32 ± 4 nm diameter ONP of Mn(III)TPPF$_{20}$ with isobutyraldehyde gives only the allylic oxidation products with a TON of ca. 8977 and a ratio of ketone: alcohol = 4:1. The reaction using ONP has a slower rate than the reaction using the solvated metalloporphyrin that yields the epoxide. Isobutyraldehyde was necessary for ONP catalytic reactions and the absence of isobutyraldehyde results no oxidation product for cyclohexene and also show complete decomposition of the porphyrin ONP (Table 2.4). There is a linear relationship between molar equivalents of isobutyraldehyde to cyclohexene used in the Mn(III)TPPF$_{20}$ ONP reaction and TON (Figure 2.2). Other aldehydes such as acetaldehyde, propionaldehyde and benzaldehyde are ineffective under the same reaction conditions (Table 2.4), but protect the Mn(III)TPPF$_{20}$ ONP from decomposition. A somewhat higher pressure of ca. 1.7 atm results in a small increase in the TON = 9237, but does not change the rate of formation of the products or the product ratios.

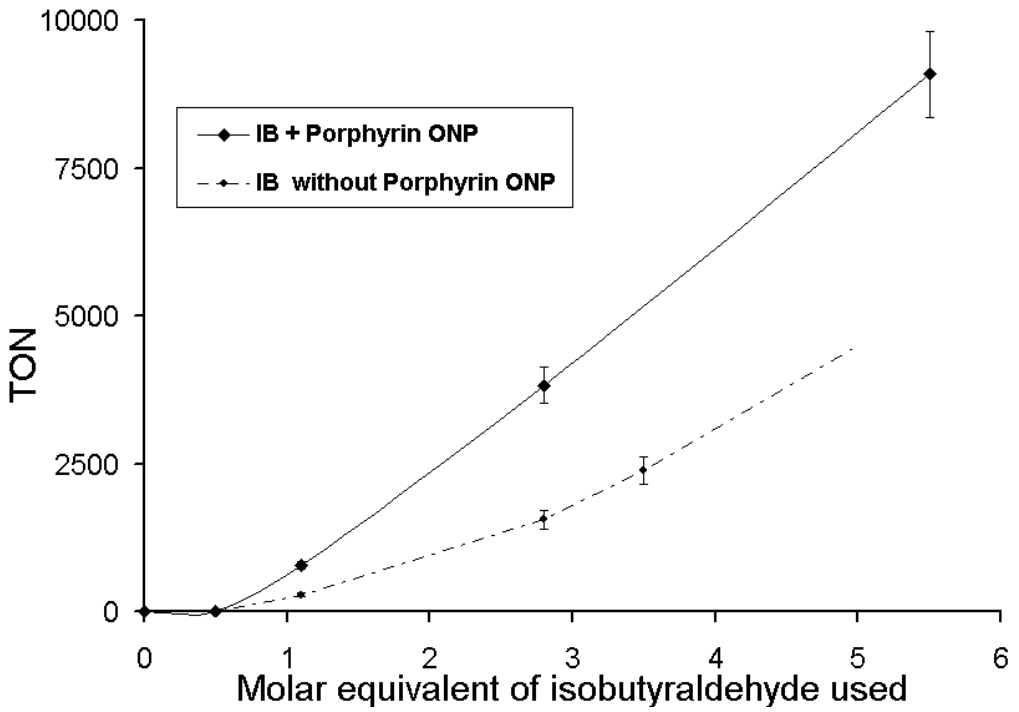

Figure 2.2: Effect of molar equivalents of isobutyraldehyde used for per mole of cyclohexene on the TON for the product formation using Mn(III)TPPF$_{20}$ ONP (solid line) as catalyst and without porphyrin ONP (dotted line). Different volumes of the isobutyraldehyde were added to the same 2.7 mL of the reaction mixture: 2.5 mL of ONP and 0.2 mL of cyclohexene.

A plot of the reaction run time vs. TON indicates that the nanoparticles have very low or almost no activity during the first few hours of the reaction. After 8-10 h of reaction time we see a noticeable conversion of cyclohexene and then saturates after about 20 h (see appendix). The TON is almost the same for the reactions run for longer times until no detectible porphyrin was left in the reaction mixture.

Table 2.4 Mn(III)TPPF$_{20}$ ONP catalysis of cyclohexene oxidation						
Reaction type (Solution[a] or ONP[b])	Conditions	Yield (% epoxide)	Yield (% ene-1-ol)	Yield (% ene-1-one)	TON	Comments
solution	CH_3OH/CH_3CN (1:3), 125 mL O_2	––	––	––	––	6 h, no reaction, no decomposition of porphyrin
solution	CH_2Cl_2, 125 mL O_2 / no **IB**	––	––	––	––	6 h, no reaction, no decomposition of porphyrin
solution	CH_2Cl_2, 125 mL O_2 / 1.0 mL **IB**	>98	<1	<1	4865	6 h, no sign of porphyrin left
solution	CH_2Cl_2, 125 mL O_2 / **IB**	> 99	––	––	––	4 h (*94*)
25 nm ONP	125 mL O_2 / no **IB**	––	––	––	––	20 h, no reaction, porphyrin ONP decomposes after 20 h reaction, and the amount of unreacted cyclohexene recovered 183 μL
32 nm ONP	125 mL O_2 / 1.0 mL **IB**	<1	21	78	8977	20 h
32 nm ONP	125 mL O_2 /1.0 mL benzaldehyde	––	––	––	––	20 h, no reaction, no decomposition of porphyrin ONP
25 nm ONP	H_2O_2 / no **IB**	––	––	––	––	no reaction, porphyrin ONP decomposes completely in few minutes ca 20-30 min
32 nm ONP	H_2O_2/ 1.0 mL **IB**	<1	19	80	378	1 h, porphyrin ONP decomposes completely
32 nm ONP	99.6% D_2O, 125 mL O_2	2	18	80		20 h, no incorporation of D in cyclohexene and products, indicates no C-D bond formation
Control reaction in H_2O + PEG	125 mL O_2 /1.0 mL **IB**	––	––	––	––	no reaction, and the amount of unreacted cyclohexene recovered 182 μL

Table 2.4: [a] Solution Reactions: 0.1 mM catalyst in DCM, porphyrin: cyclohexene: O_2 = 1:10000:25400. [b] ONP Reaction: [1] with H_2O_2: ONP suspension (2.5 mL, 70 μM, 1.75 x 10^{-7} mol of porphyrin); porphyrin: substrate: H_2O_2 = 1:1400:2200. [2] with O_2: ONP suspension, 2.5 mL mixed with cyclohexene (200 μL) and O_2 (125 mL, 1 atm); porphyrin : substrate : O_2 = 1:11300: 29000. [c] All reactions were run exhaustively. TON = mol $_{products}$ / mol $_{porphyrin}$ has an error of ± 5%. Products were extracted into DCM and analyzed by using an Agilent 5975 series GC-MS. Control reactions: neither H_2O_2 nor O_2 react directly with cyclohexene under these conditions. Also, reactions in the absence of **IB** give no oxidation products and reactions in the absence of porphyrin ONP gives no oxidation products for cyclohexene.
Note: **IB = isobutyraldehyde**

Unlike the solution phase reactions in CH_2Cl_2 where the isobutyraldehyde promotes the oxidation of the substrate in the absence of the porphyrin, control reactions using water, PEG, and isobutyraldehyde in the absence of Mn(III)$TPPF_{20}$ ONP results no oxidation products, and most of the unreacted cyclohexene was recovered. Though without the aldehyde ONP of Mn(III)$TPPF_{20}$ give no cyclohexene oxidation products, the catalyst decomposes by self-oxidation in the presence of O_2. The increase in the TON when using isobutyraldehyde and manganese (III) porphyrin together, indicate that aldehyde can serve as a mediator for the oxygen transfer to the porphyrin to form Mn(IV)=O complex.

Nanoparticles of Mn(III)$TPPF_{20}$ were also prepared in D_2O but no evicence of C-D bond formation was observed (Table 2.4). The formation of allylic oxidation epoxide products by the ONP versus the epoxide formation by the completely solvated metalloporphyrins suggests a different mechanism. The mechanism for the allylic oxidation products may involve an allylic free radical and/or the peroxide radical formation from isobutyraldehyde.(*90, 113, 114*)

2.11.3 ONP Mechanism

The fundamental chemical reactivity in terms of metalloporphyrin, substrate, solvent, temperature, and axial ligands have been studied extensively. The mechanism for the olefinic oxidation using metalloporphyrin have been well reveiwed and is believed to proceed through a H-atom abstraction.(*80, 90, 114, 115*) For our ONP catalytic reaction, the formation of different allylic oxidation products en-ol and ene-one suggest that the reaction goes through a different mechanistic pathway. One plausible explanation for the slow reactivity and increased TON for these ONP catalytic reactions may be that the

metalloporphyrins in the nanoaggregates acts like an onion in which only the outer layer (few molecules) of porphyrin is available for the oxidative process, and when these become inactive they desorb from the ONP to expose the next active layer. The onion type mechnaism was recently discussed.(*99*) The oxidation is believed to proceed through the radical mechanism combined these gives enhanced catalytic activity. Formation of keteone is the major product for these ONP catalytic reactions; likely because the initially formed alcohol gets further oxidized to ketone before it escapes the ONP/solvent cage. The roll of the aggregation of the metalloporphyrins in the in ONP may also facilitate oxo-bridge formation, slowing down the reaction, and taking up the substrate from the mostly aqueous solution. Since cyclohexene is hydrophobic and the reaction solvent is mostly water, the substrate rapidly partitions into the ONP as indicated by the chage in color of ONP and shift in UV-visible spectra peaks. Also, since nanoaggregates are dynamic in nature, the nanoarchitecture of aggregates may limit the approach of the substrate to the metal ion active sites.

2.12 Conclusion

The unique and enhanced catalytic activity displayed by the porphyrin nanoaggregates over the completely solvated molecules is similar to our previously reported work on Fe(III)TPPF$_{20}$ ONP. The nanoparticles of the Fe(III)TPPF$_{84}$ porphyrin are found to be ca. 4-fold more catalytically active for the same oxidative chemistry. The functionalization of the porphyrin with long highly fluorinated alkyl chain provides more stability to the iron(III) porphyrinato complexes towards oxidative degradation.

This application of porphyrin ONP catalysis uses molecular oxygen; a green oxidant compared to synthetic oxygen sources. In this case the slower rate of oxidation may also reduce self-oxidative degradation. New high-yield synthetic methods e.g. in solvent free reactions(*116*) may make simple metalloporphyrins attractive for use as catalysts on larger scales,(*117-119*) The system reported here represents a model for green chemistry, since most of the reaction solvent is water (89%) and we avoid using halogenated solvents. Allylic oxidations reactions are widely used in many areas of organic synthesis ranging from agricultural products to pharmaceuticals, and these ONP systems avoid use of reagents such as SeO_2 and other metal oxides.(*120, 121*)

These results illustrate that the nanoaggregates composed of porphyrins can display unique properties. These functionalities arise from the self-organized architecture inside the ONP.

2.13 Appendix

Controls for Fe(III)TPPF$_{84}$ in solution: Control experiments in the absence of porphyrin, O_2 does not react with cyclohexene. Nor does the porphyrin oxidize cyclohexene without O_2. The amount of cyclohexene recovered in these control reactions after the reaction were over was 185 μL, an average of three experiments. A variety of oxidizing agents such as organic peroxides-t-BuOOH, H_2O_2, iodosylbenzene, persulfates, $KHSO_5$ have been used in metalloporphyrin oxidation reactions.(*33, 79, 122-124*)

Controls for Fe(III)TPPF$_{84}$ ONP: Reactions under elevated temperature and pressure gives no oxidation products, because it increases porphyrin decomposition. The control experiments here also in the absence of ONP, molecular oxygen (O_2), and cyclohexene yields no oxidation products. The other control experiment with ONP (20± 6 nm) of non-fluorinated dodecanethiol iron(III) porphyrin also gives no oxidation product for cyclohexene.

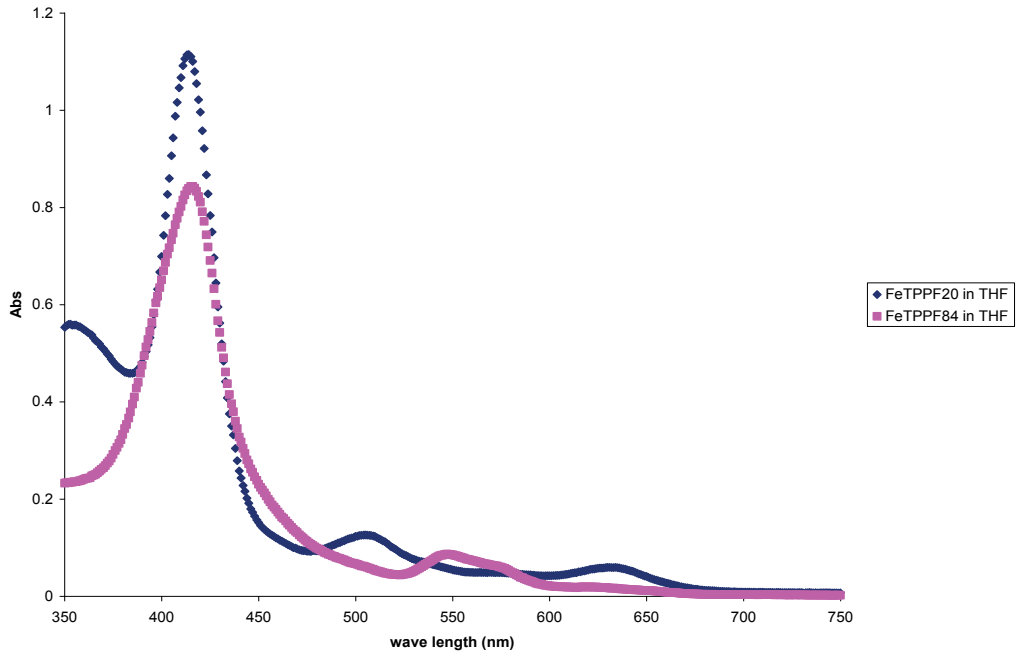

Figure A2.1: UV-visible spectra of Fe(III)TPPF$_{20}$ and Fe(III)TPPF$_{84}$ in THF. The B (Soret) bands for both Fe(III)TPPF$_{20}$ and Fe(III)TPPF$_{84}$ in THF appears at the same wavelength while the Q-bands for FeTPPF$_{84}$ are shifted towards the red, which is due to the replacement of an electron withdrawing F-atom on the para position by an electron donating S-atom. There also may be some aggregation of the highly fluorous compound in this solvent, see below.

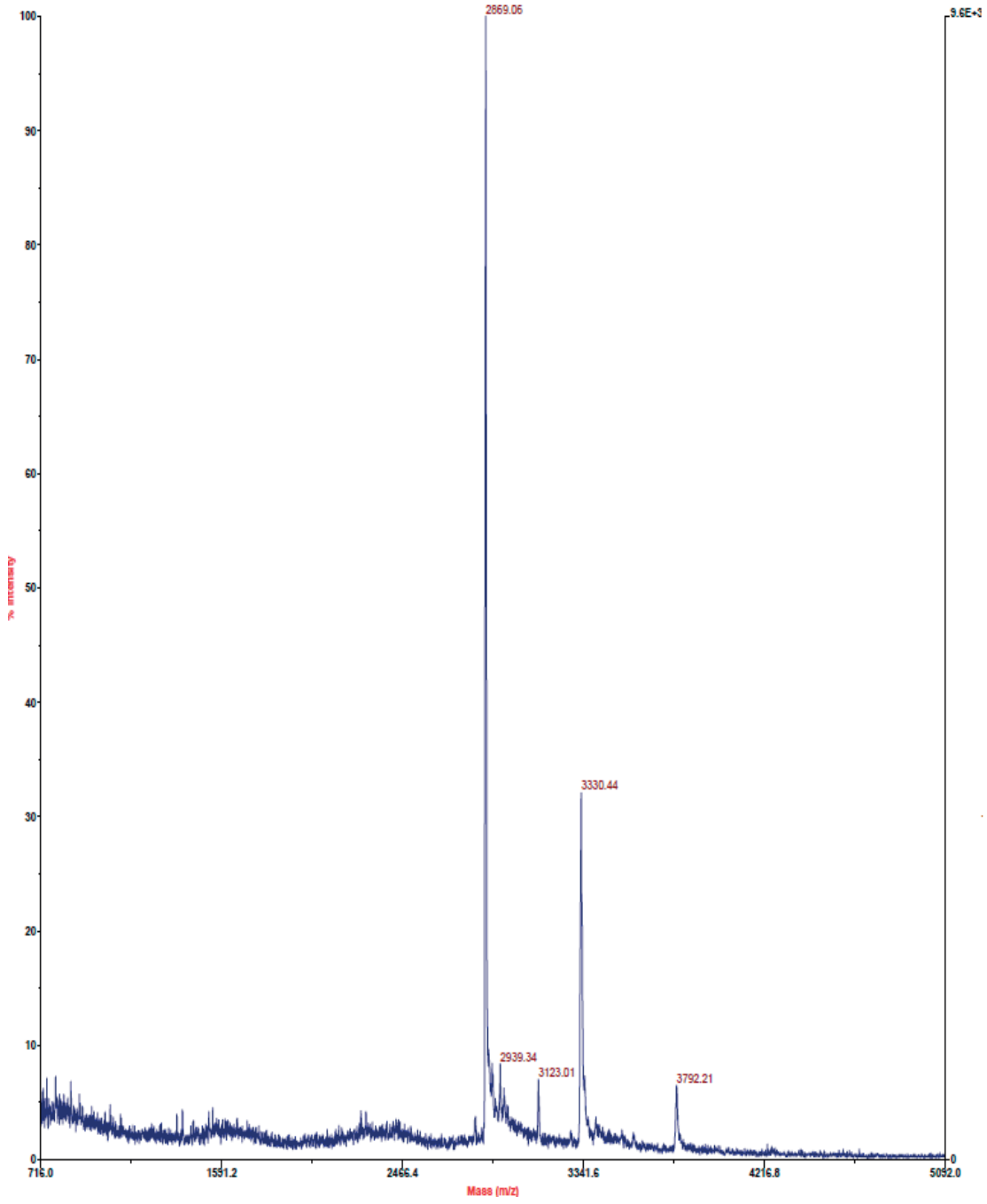

Figure A2.2: MALDI mass spec of Fe(III)TPPF$_{84}$ porphyrin. The major peak at 2869.06 corresponds to the four substitutions while the peak at 3300.44 corresponds to the five substitutions.

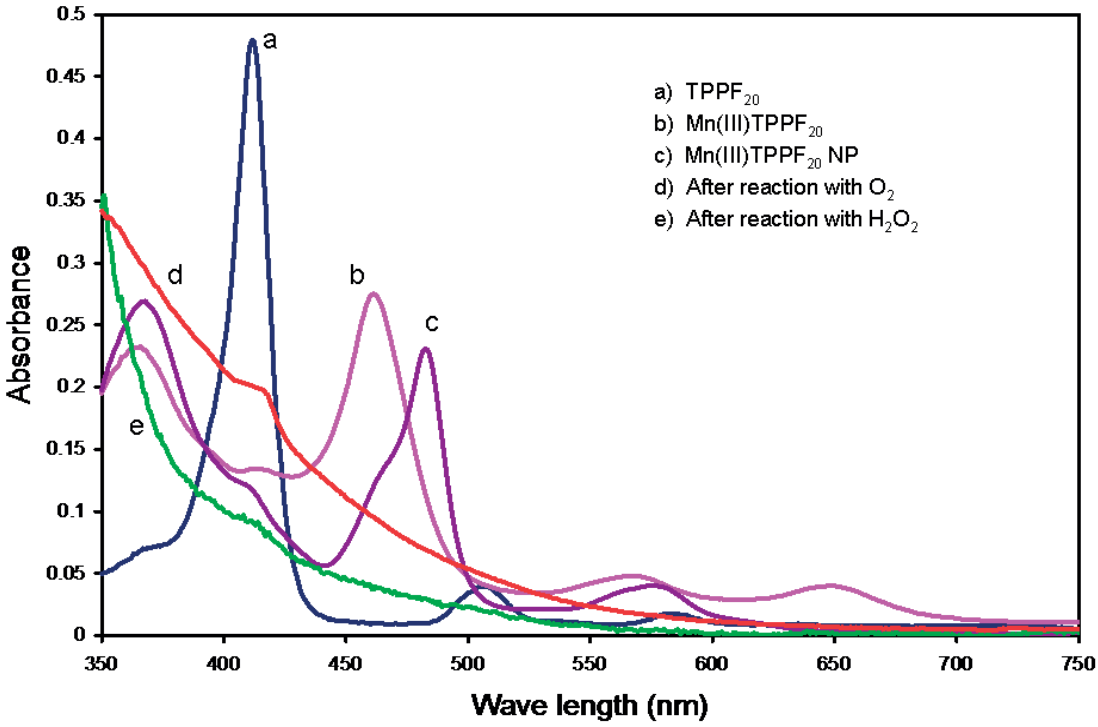

Figure A2.3: UV-visible spectra of (a) $TPPF_{20}$ and (b) $Mn(III)TPPF_{20}$ in THF. (c) $Mn(III)TPPF_{20}$ nanoparticles in THF/H_2O (d) Reaction mixture after reaction with O_2 (e) Reaction mixture after reaction with H_2O_2. The UV-visible spectra of the present ONP are similar to the case of ONP of $Fe(III)TPPF_{20}$ where an additional shoulder near the tail of the Soret band appears at 454 nm indicates J-aggregation of the porphyrin.(*99*) The Q-bands (564 nm and 644 nm) are also broadened and shifted towards the red end of the visible spectrum. Some H-aggregation, characterized by hypsochromic shift, in the electronic spectra, is observed. Generally both types of aggregation exist in the ONP.

Compound Table

Compound Label	RT	Mass	Abund	Formula	Tgt Mass	Diff (ppm)
Cpd 1: C44 H7 F20 Mn N4	0.1	1025.97176	12038	C44 H7 F20 Mn N4	1025.97318	-1.38

Compound Label	RT	Algorithm	Mass
Cpd 1: C44 H7 F20 Mn N4	0.1	Find By Formula	1025.97176

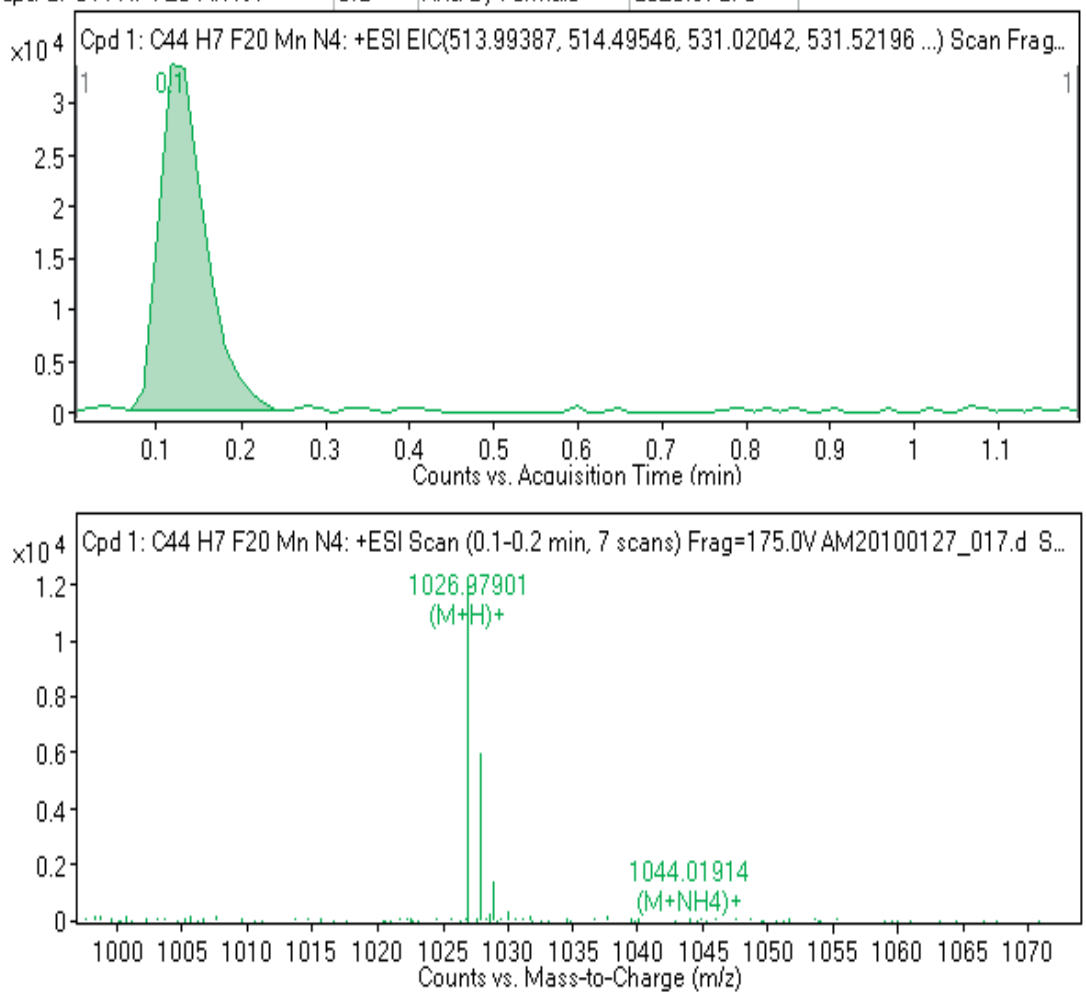

Figure A2.4: Mass spec of Mn(III)TPPF$_{20}$ porphyrin

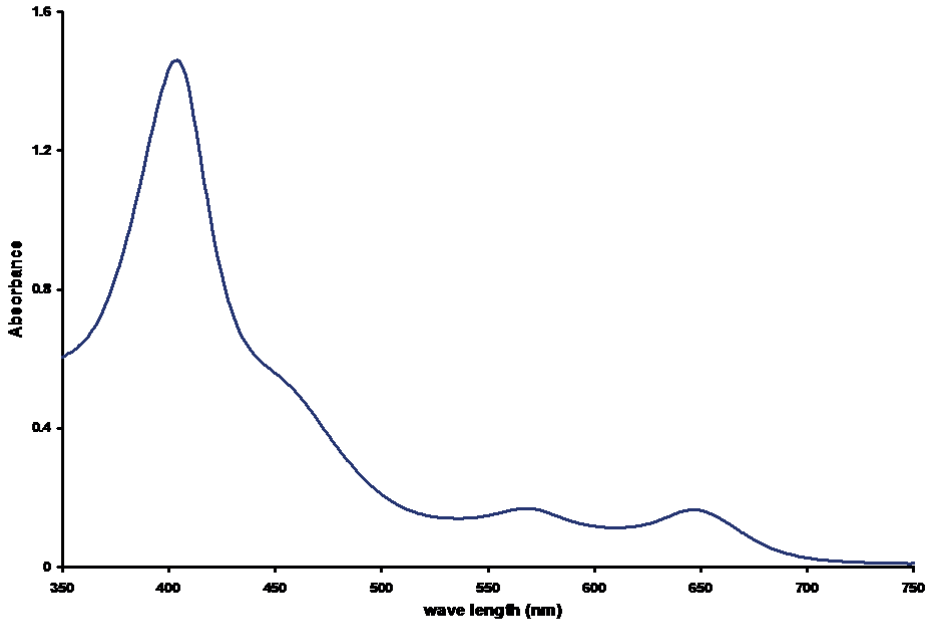

Figure A2.5: UV-visible spectra for the formation of nanoparticles of Fe(III)TPPF$_{84}$

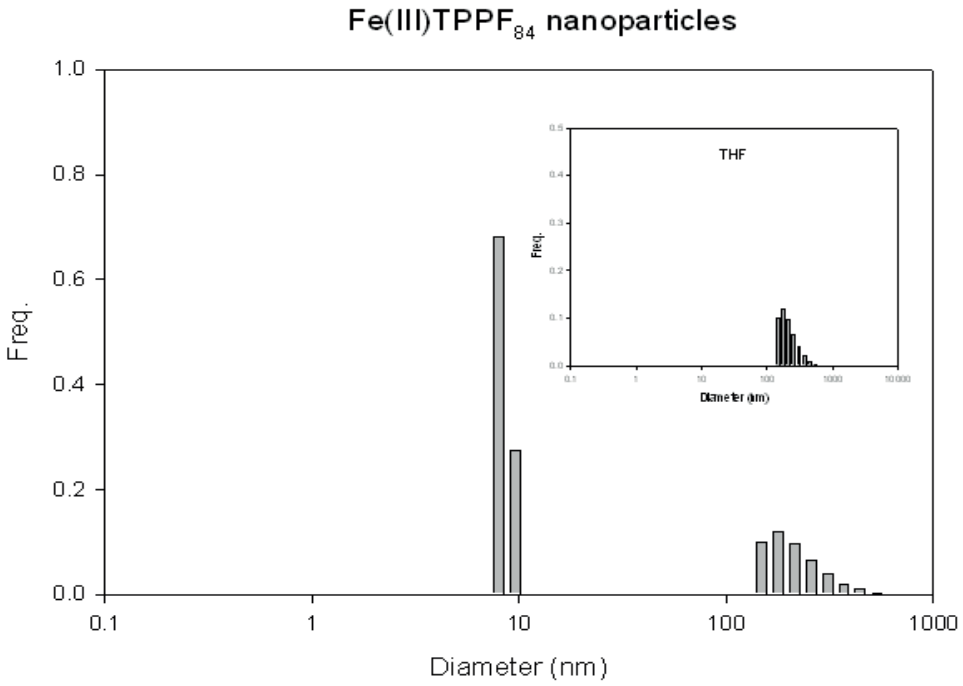

Figure A2.6: Typical dynamic light scattering data indicating the diameter of the catalytic nanoparticles, 12 ± 2 nm. The peaks at 350-750 nm (inset) are due to micelle formation from the mixture of solvents. We always observed the solvent micelles in this region even without the porphyrin in the solution.

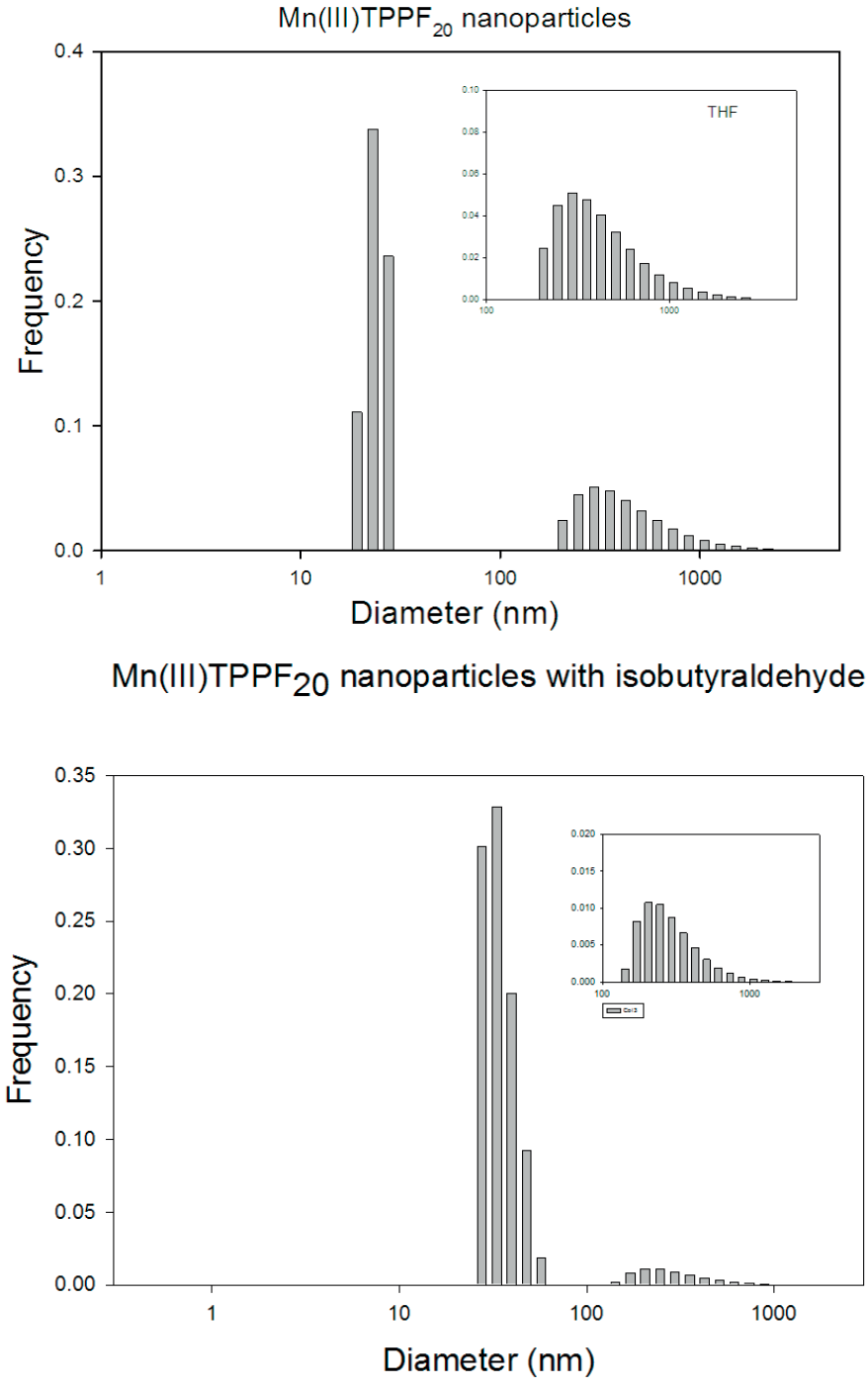

Figure A2.7: Typical dynamic light scattering data indicating the diameter of the ONP of $Mn(III)TPPF_{20}$, (a) Top: 25 ± 7 nm in the absence of isobutyraldehyde (b) bottom: 32 ± 4 nm after adding 1.0 mL of isobutyraldehyde to 2.5 mL of the ONP solution. The peaks at 350-1100 nm (inset) are due to micelles from the mixture of the solvents, which are always found to form in this region even in the absence of the porphyrin in the solution.

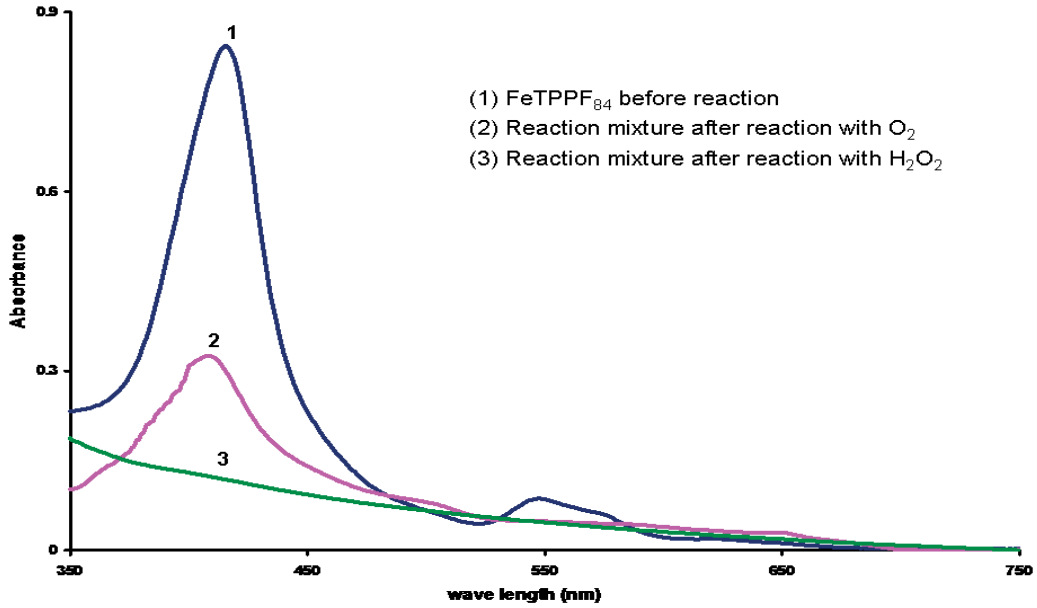

Figure A2.8: UV-visible spectra of (1) Fe(III)TPPF$_{84}$ in reaction mixture before reaction, (2) 36% left over Fe(III)TPPF$_{84}$ in reaction mixture after reaction with O_2, and (3) reaction mixture after reaction with H_2O_2 shows nearly complete decomposition of the metalloporphyrin.

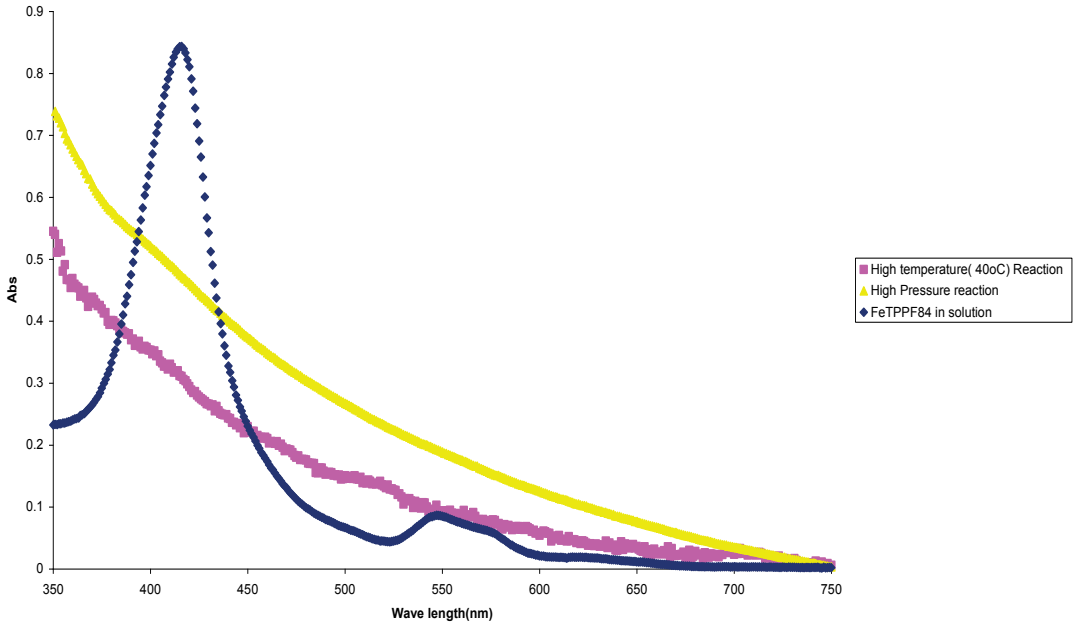

Figure A2.9: UV-visible spectra of Fe(III)TPPF$_{84}$ before reaction in blue, after reaction at elevated pressure (1.7 atm) in yellow, and after reaction at higher temperature (40 ^{o}C) in purple.

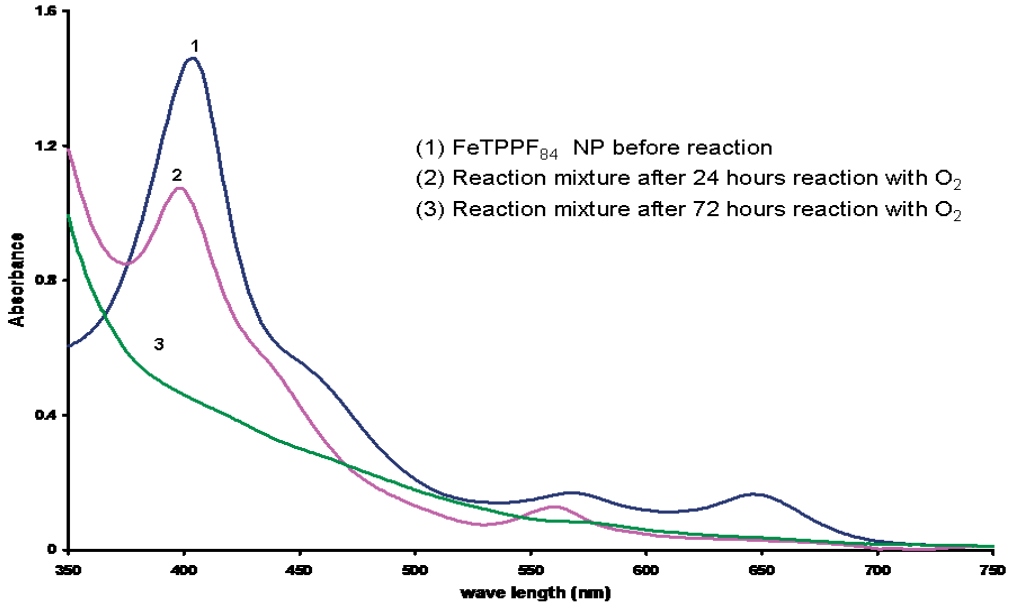

Figure A2.10: UV-visible spectra of (1) Fe(III)TPPF$_{84}$ ONP reaction mixture before reaction (2) Reaction mixture after 24 h reaction with O_2 shows ca. 26% porphyrin left, and (3) reaction mixture after 72 h reaction with O_2 shows the complete decomposition of the porphyrin in the reaction mixture.

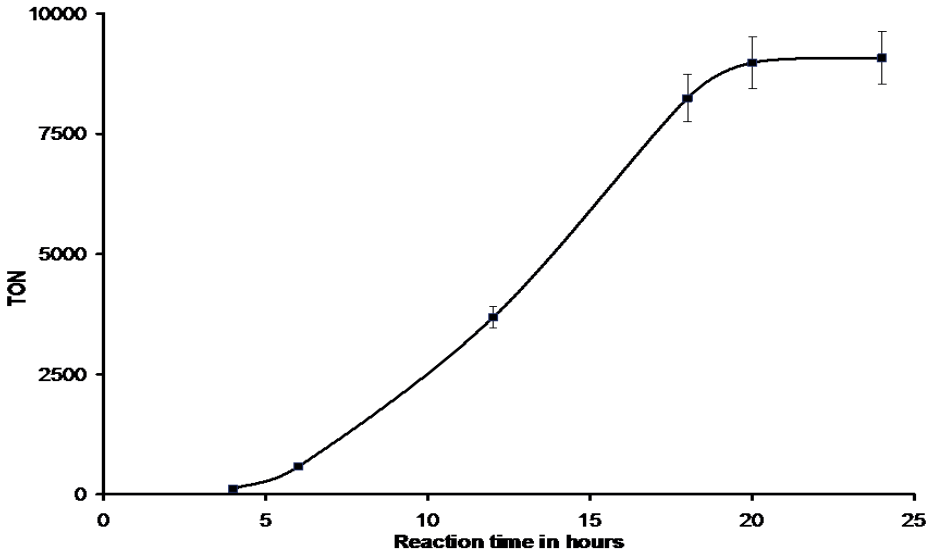

Figure A2.11: The reaction run time versus TON for Mn(III)TPPF$_{20}$ porphyrin, where the error bars represent the average of four different experiments. The half life time ($t_{1/2}$) for the product formation is ca. 14 h. Note the 4-5 h lag phase.

GC of standard mixture solution of cyclohexene, cyclohexene oxide, cyclohex-2-en-1-ol, cyclohex-2-en-1-one, and toluene.

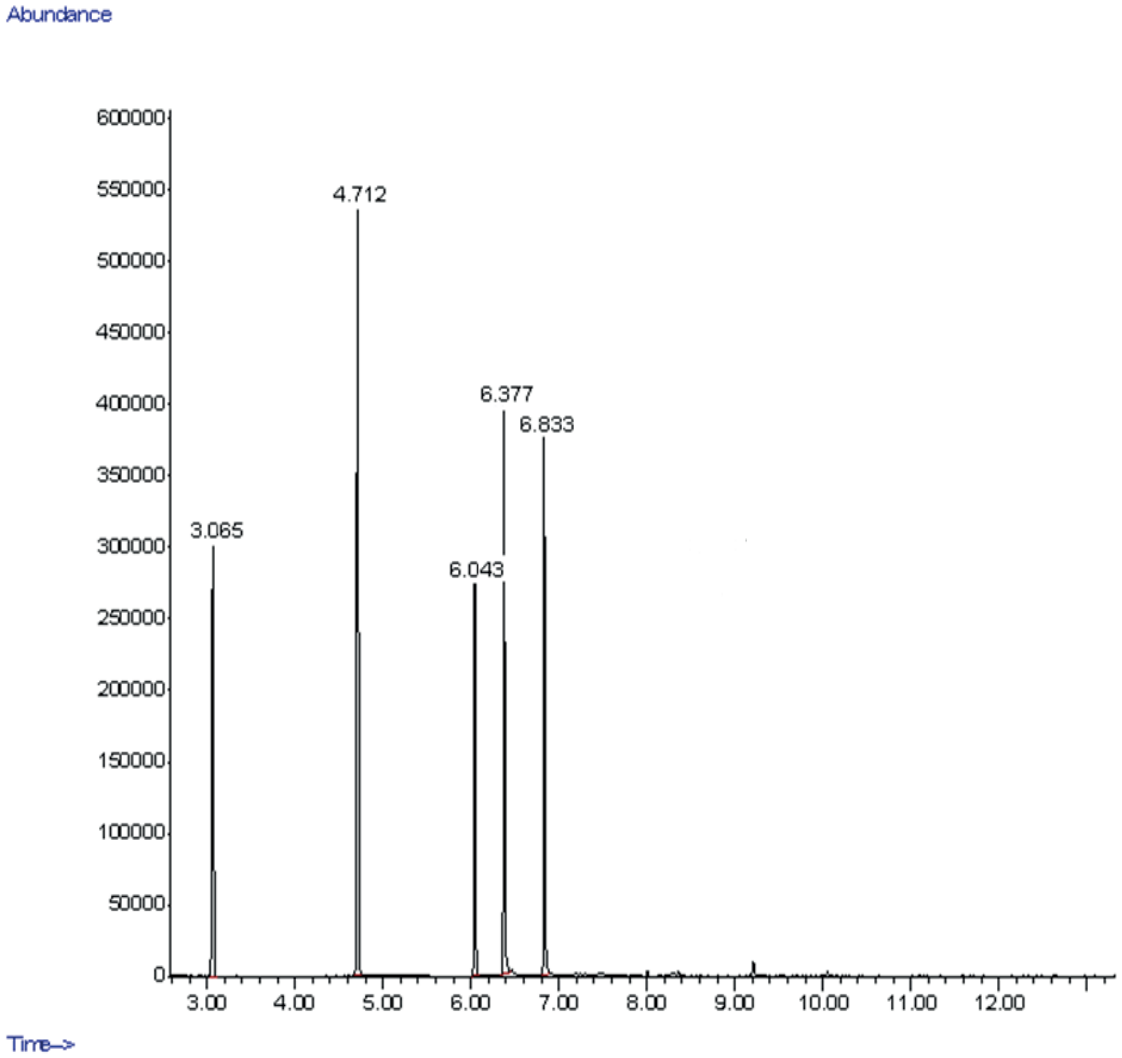

Figure A2.12: GC of standards: cyclohexene = 3.06 min, toluene = 4.71 min, cyclohexene oxide = 6.04 min, cyclohex-2-en-1-ol = 6.37 min, cyclohex-2-en-1-one = 6.83 min. Mass spectroscopy confirms the identity of each compound. The peak at 9.21 min is because of polysiloxanes from the column.

GC of Fe(III)TPPF$_{84}$ solution phase catalytic reaction using O_2 as oxidant

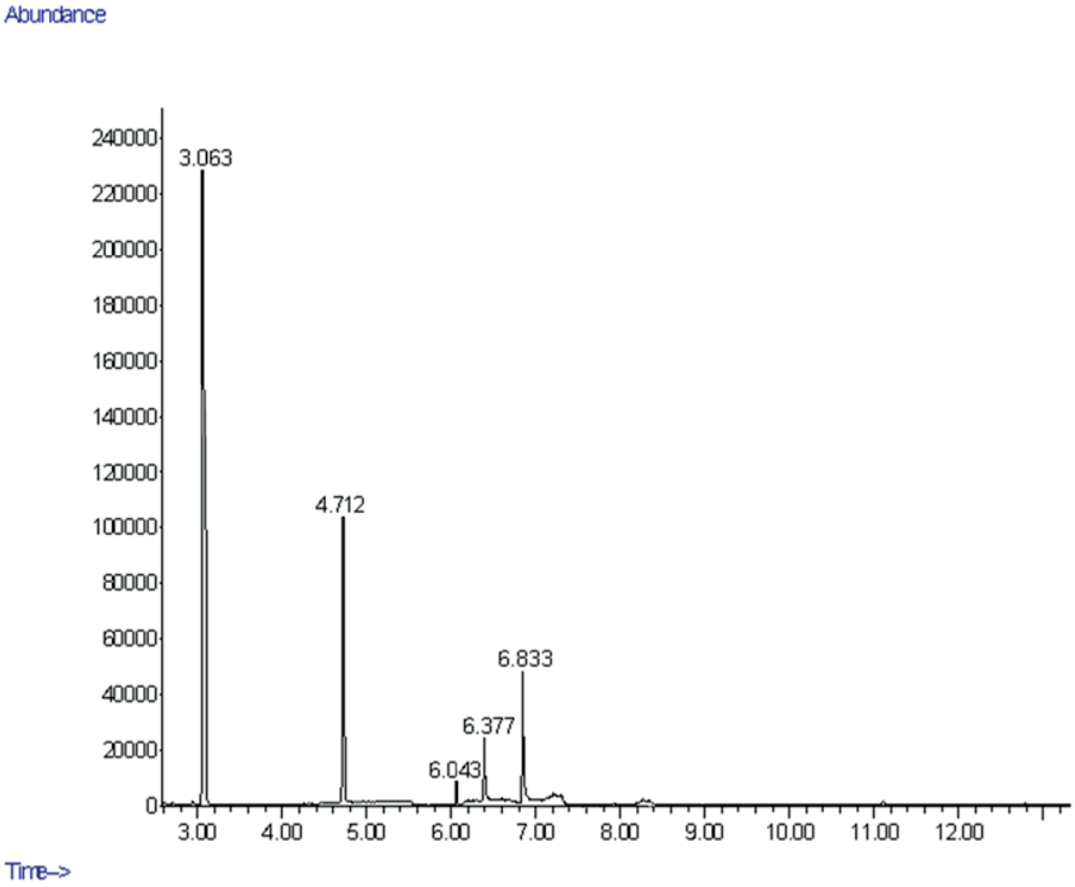

Figure A2.13: GC of a solution phase reaction using Fe(III)TPPF$_{84}$ catalyst. Retention time of cyclohexene = 3.06 min, toluene =4.71 min, cyclohexene oxide = 6.04 min, cyclohex-2-en-1-ol = 6.38 min, cyclohex-2-en-1-one = 6.83 min. Mass spectrometry confirms the identity of each compound.

GC of Fe(III)TPPF$_{84}$ ONP catalytic reaction using O_2 as oxidant

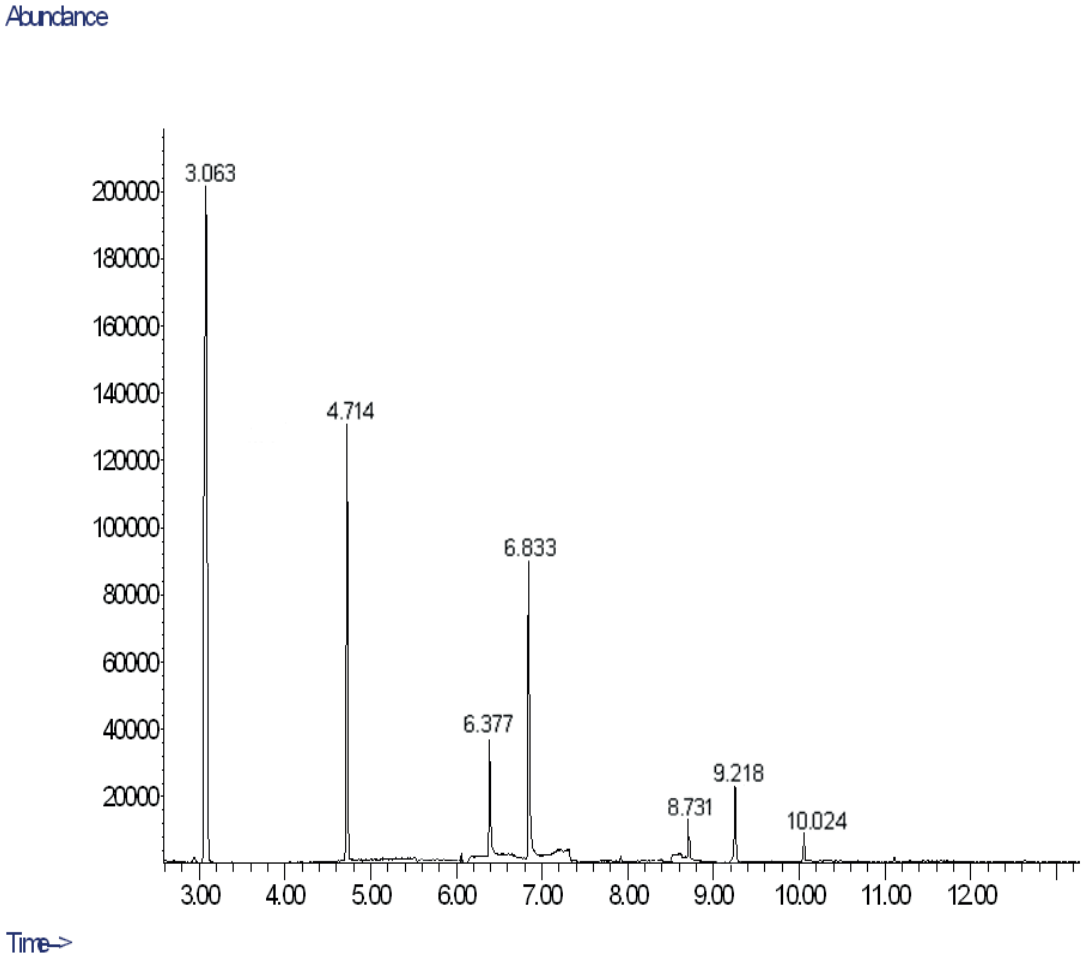

Figure A2.14: GC of a typical ONP catalytic reaction using Fe(III)TPPF$_{84}$ catalyst. Retention time of cyclohexene = 3.06 min, toluene =4.71 min, cyclohex-2-en-1-ol = 6.37 min, cyclohex-2-en-1-one = 6.83 min. Mass spectrometry confirms the identity of each compound. The peak at 8.73 min is the PEG from the ONP preparation. However the peaks at 9.21 min and 10.02 min are polysiloxane from column.

GC of Mn(III)TPPF$_{20}$ solution phase catalytic reaction using O_2 as oxidant

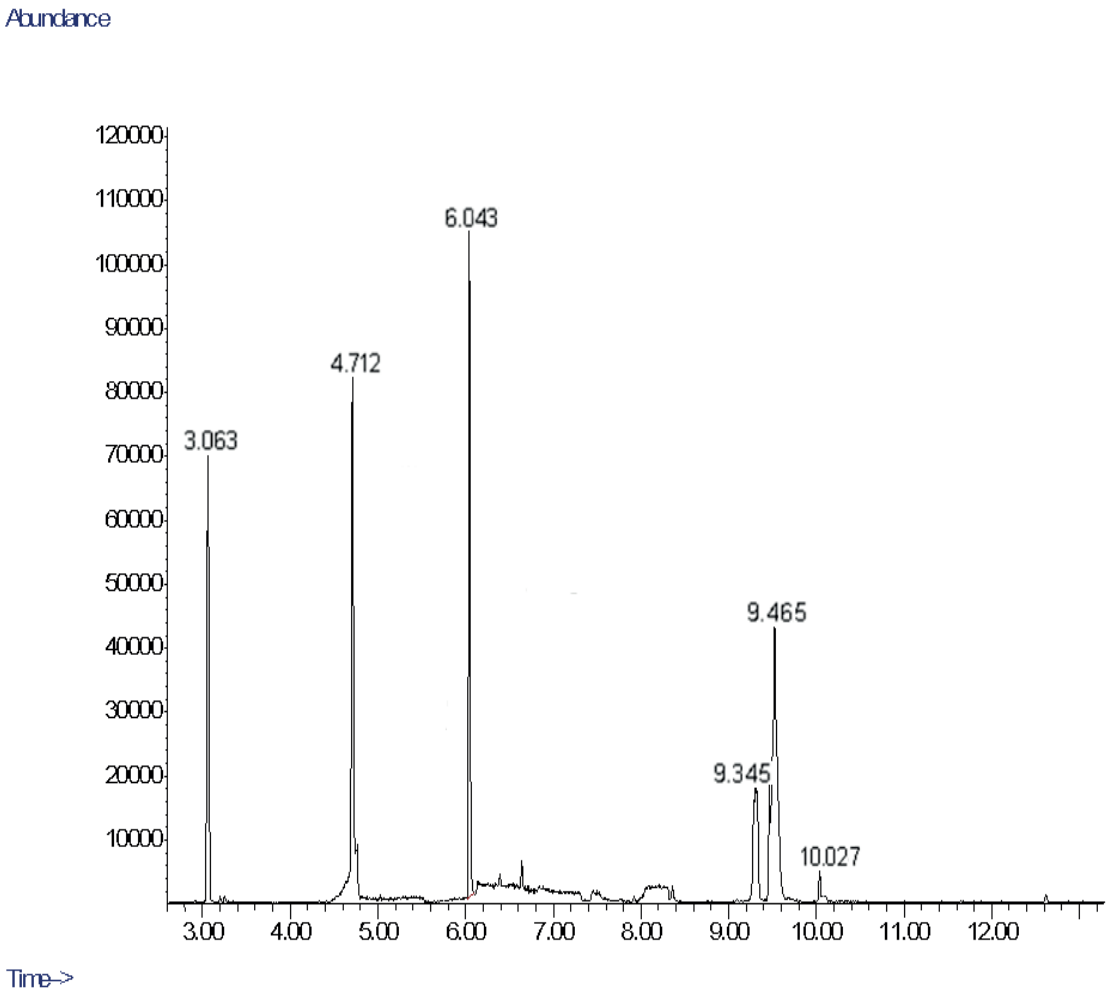

Figure A2.15: GC of a solution phase reaction using Mn(III)TPPF$_{20}$ catalyst. Retention time of cyclohexene = 3.06 min, toluene =4.71 min, cyclohexene oxide = 6.04 min. Mass spectrometry confirms the identity of each compound. The peaks at 9.34 min and 9.46 min are of isobutyric acid and at 10.02 min are polysiloxane from column.

GC of Mn(III)TPPF$_{20}$ ONP catalytic reaction using O_2 as oxidant

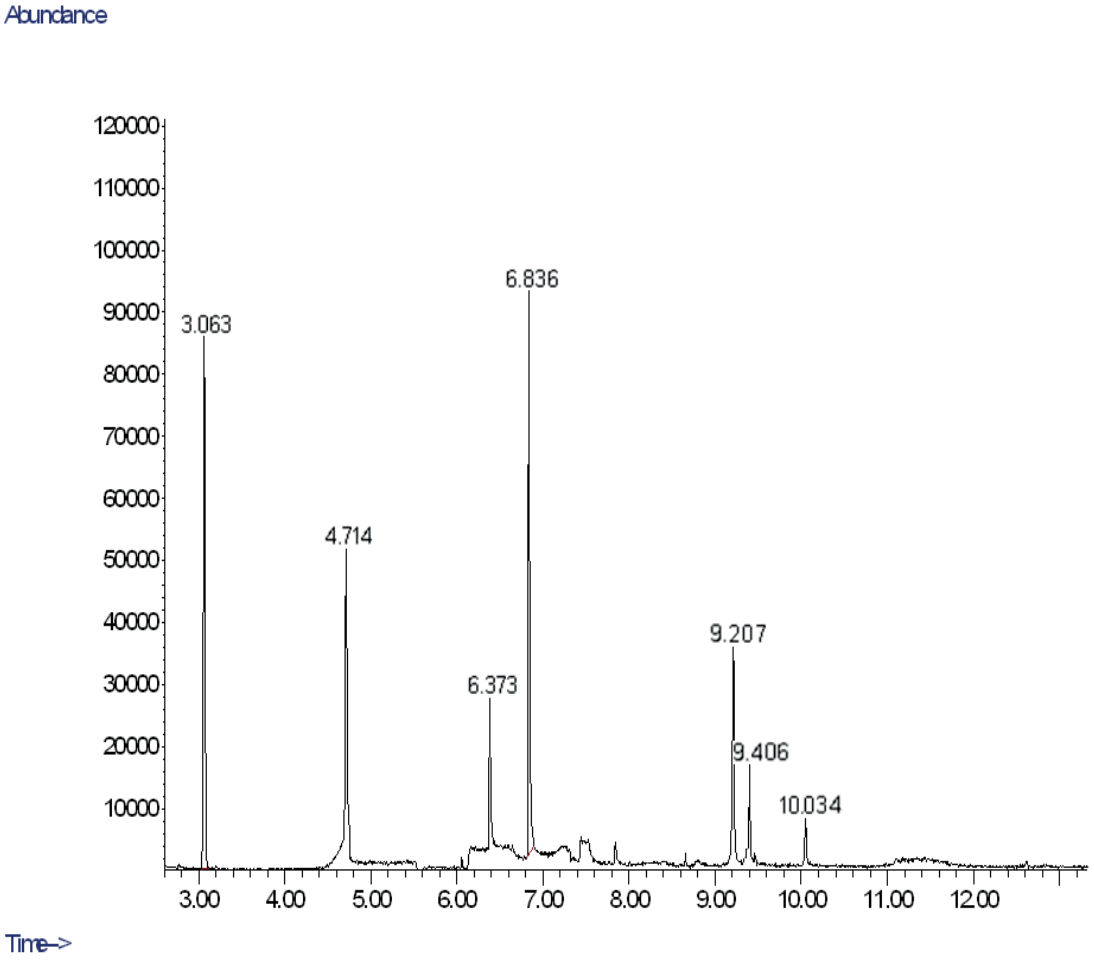

Figure A2.16: GC of a typical ONP catalytic reaction using Mn(III)TPPF$_{20}$ catalyst. Retention time of cyclohexene = 3.06 min, toluene =4.71 min, cyclohex-2-en-1-ol = 6.37 min, cyclohex-2-en-1-one = 6.83 min. Mass spectrometry confirms the identity of each compound. The peak at 9.20 min and 9.40 min are of isobutyric acid. However the peak at 10.02 min is polysiloxane from column.

The standardized response of the GC (area) for each component in CH_2Cl_2 (2.0 mL total volume) is reported in Table 1.

Table A2.1: The standard response of GC area for each component

Compounds	Response Factor	Ratio to toluene	Volume used	Corrected area	Moles injected
Cyclohexene	1.30	1.76	20 μL	4040215	7.52×10^{-10}
Toluene	2.29	1	20 μL	6782091	7.17×10^{-10}
Cyclohexene oxide	1.00	2.29	20 μL	3109662	7.54×10^{-10}
Cyclohex-2-en-1-ol	1.21	1.90	20 μL	3877485	7.77×10^{-10}
Cyclohex-2-en-1-one	1.86	1.86	20 μL	4014942	7.88×10^{-10}

A response factor of 1.90 for the combined products was used to calculate the TON for all reactions. The TON for each reaction was calculated based on the corrected area for each peak using the internal standard (toluene) and the response factor obtained in GC-MS.

For O_2 reactions:

The 2.7 mL reaction mixture volume was extracted once with 8.0 mL CH_2Cl_2 and the layers were allowed to separate. The water fraction and some of the organic fraction was removed to leave a total volume of 6.0 mL of CH_2Cl_2 (this assures the same volume for every reaction assay). To this volume was added 20 μL toluene. 4.0 μL of the extract was diluted into 1.0 mL dichloromethane and then 2.0 μL of this solution is injected into the GC-MS.

TON = moles products/moles porphyrin = $5.31 \times 10^{-4} / 1.75 \times 10^{-7} = 3037$, since the porphyrin slowly decomposes in the reaction mixture, TON is for reactions run until [porphyrin] < 0.2 μM, ca. 24 h.

2.14 References

1. Muzart, J. (1992) Chromium-catalyzed oxidations in organic synthesis, *Chem. Rev. 92*, 113-140.
2. Choi, H., and Doyle, M. P. (2007) Optimal TBHP Allylic Oxidation of Δ5-Steroids Catalyzed by Dirhodium Caprolactamate, *Org. Lett. 9*, 5349-5352.
3. Doyle, M. P. (2006) Perspective on Dirhodium Carboxamidates as Catalysts, *J. Org. Chem. 71*, 9253-9260.
4. Shing, T. K. M., Yeung, Y.-Y., and Su, P. L. (2006) Mild Manganese(III) Acetate Catalyzed Allylic Oxidation: Application to Simple and Complex Alkenes, *Org. Lett. 8*, 3149-3151.
5. Harre, M., Haufe, R., Nickisch, K., Weinig, P., Weinmann, H., Kinney, W. A., and Zhang, X. (1998) Some Reaction Safety Aspects of Ruthenium-Catalyzed Allylic Oxidations of Δ-5-Steroids in the Pilot Plant, *Org. Proc. Res. Dev. 2*, 100-104.
6. Crich, D., and Zou, Y. (2004) Catalytic Allylic Oxidation with a Recyclable, Fluorous Seleninic Acid, *Org. Lett. 6*, 775-777.
7. Zhao, Y., and Yeung, Y.-Y. (2010) An Unprecedented Method for the Generation of tert-Butylperoxy Radical Using DIB/TBHP Protocol: Solvent Effect and Application on Allylic Oxidation, *Org. Lett. 12*, 2128-2131.
8. Uyanik, M., Okamoto, H., Yasui, T., and Ishihara, K. (2010) Quaternary Ammonium (Hypo)iodite Catalysis for Enantioselective Oxidative Cycloetherification, *Science 328*, 1376-1379.
9. Silaghi-Dumitrescu, R. (2004) The nature of the high-valent complexes in the catalytic cycles of hemoproteins, *J. Biol. Inorg. Chem. 9*, 471-476.
10. Meunier, B., de Visser, S. P., and Shaik, S. (2004) Mechanism of Oxidation Reactions Catalyzed by Cytochrome P450 Enzymes, *Chem. Rev. 104*, 3947-3980.
11. Newcomb, M., Hollenberg, P. F., and Coon, M. J. (2003) Multiple mechanisms and multiple oxidants in P450-catalyzed hydroxylations, *Arch. Biochem. Biophys. 409*, 72-79.

12. Chandrasena, R. E. P., Vatsis, K. P., Coon, M. J., Hollenberg, P. F., and Newcomb, M. (2004) Hydroxylation by the Hydroperoxy-Iron Species in Cytochrome P450 Enzymes, *J. Am. Chem. Soc. 126*, 115-126.
13. Lee, S. J., and Hupp, J. T. (2006) Porphyrin-containing molecular squares: Design and applications, *Coord. Chem. Rev. 250*, 1710-1723.
14. Merlau, M. L., Mejia, M. d. P., Nguyen, S. T., and Hupp, J. T. (2001) Artificial enzymes formed through directed assembly of molecular square encapsulated epoxidation catalysts, *Angew. Chem. Int. Ed. 40*, 4239-4242.
15. Merlau, M. L., Cho, S. H., Sun, S. S., Nguyen, S. T., and Hupp, J. T. (2005) Anthracene-Induced Turnover Enhancement in the Manganese Porphyrin-Catalyzed Epoxidation of Olefins, *Inorg. Chem. 44*, 5523-5529.
16. Astruc, D., Lu, F., and Aranzaes, J. R. (2005) Nanoparticles as Recyclable Catalysts: The Frontier Between Homogeneous and Heterogeneous Catalysis, *Angew. Chem. Int. Ed. 44*, 7852-7872.
17. Scott, R. W. J., Wilson, O. M., and Crooks, R. M. (2005) Synthesis, Characterization, and Applications of Dendrimer-Encapsulated Nanoparticles, *J. Phys. Chem. B.;*, 692-704.
18. Horn, D., and Rieger, J. (2001) Organic Nanoparticles in the Aqueous Phase - Theory, Experiment, and Use, *Angew. Chem., Int. Ed. 40*, 4330-4361.
19. LaMer, V. K., and Dinegar, R. H. (1950) Theory, Production and Mechanism of Formation of Monodispersed Hydrosols, *J. Am. Chem. Soc. 72*, 4847-4854.
20. Drain, C. M., Smeureanu, G., Patel, S., X.Gong, Garno, J., and Arijeloye, J. (2006) Porphyrin nanoparticles as supramolecular systems, *New J. Chem. 30*, 1834-1843.
21. Gong, X., Milic, T., Xu, C., Batteas, J. D., and Drain, C. M. (2002) Preparation and Characterization of Porphyrin Nanoparticles, *J. Am. Chem. Soc. 124*, 14290-14291.
22. Drain, C. M., Bazzan, G., Milic, T., Vinodu, M., and Goeltz, J. C. (2005) Formation and applications of stable 10 nm to 500 nm supramolecular porphyrinic materials, *Isr. J. Chem. 45*, 255-269.

23. Drain, C. M., Goldberg, I., Sylvain, I., and Falber, A. (2005) Synthesis and Applications of Supramolecular Porphyrinic Materials, *Top. Curr. Chem. 245*, 55-88.

24. Brick, M. C., Palmer, H. J., and Whitesides, T. H. (2003) Formation of Colloidal Dispersions of Organic Materials in Aqueous Media by Solvent Shifting, *Langmuir 19*, 6367-6380.

25. Qian, D. J., Nakamura, C., Wakayama, T., and Miyake, J. (2003) Synthesis and multilayer assembly of multiporphyrin arrays at the water-chloroform interface, *J. Porphyrins Phthalocyanines 7*, 415-419.

26. Van Keuren, E., Bone, A., and Ma, C. (2008) Phthalocyanine Nanoparticle Formation in Supersaturated Solutions, *Langmuir 24*, 6079-6084.

27. Sane, A., Taylor, S., Sun, Y.-p., and Thies, M. C. (2003) RESS for the preperation of fluorinated porphyrin nanoparticles, *Chem. Commun.*, 2720-2721.

28. Sane, A., and Thies, M. C. (2005) The Formation of Fluorinated Tetraphenylporphyrin Nanoparticles via Rapid Expansion Processes: RESS vs RESOLV, *J. Phys. Chem. B 109*, 19688-19695.

29. Rangel-Rojo, R., Matsuda, H., Kasai, H., and Nakanishi, H. (2000) Irradiance dependence of the resonant nonlinearities in an organic material, *J. Opt. Soc. Am. B 17*, 1376-1382.

30. Nitschke, C., O'Flaherty, S. M., Kroll, M., and Blau, W. J. (2004) Material investigations and optical properties of phthalocyanine nanoparticles, *J. Phys. Chem. B 108*, 1287-1295.

31. Müller, R. H., Benita, S., and Böhm, B. H. L., (Eds.) (1998) *Emulsions and Nanosuspensions for the Formulation of Poorly Soluble Drugs* Scientific Publishers, Stuttgart.

32. Park, J., Privman, V., and Matijevic, E. (2001) Model of Formation of Monodispersed Colloids, *J. Phys. Chem. B 105*, 11630-11635.

33. Groves, J. T. (2006) High-valent iron in chemical and biological oxidations, *J. Inorg. Biochem. 100*, 434-447.

34. Groves, J. T., Haushalter, R. C., Nakamura, M., Nemo, T. E., and Evans, B. J. (1981) High-valent iron-porphyrin complexes related to peroxidase and cytochrome P-450, *J. Am. Chem. Soc. 103*, 2884-2886.

35. Groves, J. T., and Nemo, T. E. (1983) Epoxidation reactions catalyzed by iron porphyrins. Oxygen transfer from iodosylbenzene, *J. Am. Chem. Soc. 105*, 5786-5791.

36. Groves, J. T., Nemo, T. E., and Myers, R. S. (1979) Hydroxylation and epoxidation catalyzed by iron-porphine complexes. Oxygen transfer from iodosylbenzene, *J. Am. Chem. Soc. 101*, 1032-1033.

37. Groves, J. T., and Viski, P. (1990) Asymmetric hydroxylation, epoxidation, and sulfoxidation catalyzed by vaulted binaphthyl metalloporphyrins, *J. Org. Chem. 55*, 3628-3634.

38. Groves, J. T., and Watanabe, Y. (1986) Heterolytic and homolytic oxygen-oxygen bond cleavage reactions of acylperoxomanganese(III) porphyrins, *Inorg. Chem. 25*, 4808-4810.

39. Ortiz de Montellano, P. R. (1995) *Cytochrome P450: Structure, Mechanism, and Biochemistry*, 2nd. ed., Plenum Press, New York.

40. Mayer, J. M. (2000) Biomimetic Oxygenations Related to Cytochrome P450: Metal-Oxo and Metal-Peroxo Intermediates, In *Biomimetic Oxidations Catalyzed by Transition Metal Complexes* (Meunier, B., Ed.), pp 1-43, Imperial College Press.

41. Dolphin, D., Traylor, T. G., and Xie, L. Y. (1997) Polyhaloporphyrins: Unusual Ligands for Metals and Metal-Catalyzed Oxidations, *Acc. Chem. Res. 30*, 251-259.

42. Barloy, L., Battioni, P., and Mansuy, D. (1990) Manganese porphyrins supported on montmorillonite as hydrocarbon mono-oxygenation catalysts: particular efficacy for linear alkane hydroxylation, *J. Chem. Soc., Chem. Commun.*, 1365-1367.

43. Mansuy, D. (1993) Activation of alkanes : the biomimetic approach, *Coord. Chem. Rev. 125*, 129-141.

44. Wang, C., Shalyaev, K. V., Bonchio, M., Carofiglio, T., and Groves, J. T. (2006) Fast Catalytic Hydroxylation of Hydrocarbons with Ruthenium Porphyrins, *Inorg. Chem. 45*, 4769-4782.

45. Merlau, M. L., Cho, S.-H., Sun, S.-S., Nguyen, S. T., and Hupp, J. T. (2005) Anthracene-Induced Turnover Enhancement in the Manganese Porphyrin-Catalyzed Epoxidation of Olefins, *Inorg. Chem. 44*, 5523-5529.

46. Groves, J. T. (2000) Reactivity and mechanisms of metalloporphyrin-catalyzed oxidations, *J. Porphyrins Phthalocyanines 4*, 350-352.

47. Suslick, K. S. (2000) Shape Selective Oxidation by Metalloporphyrins, In *The Porphyrin Handbook* (Kadish, K. M., Smith, K. M., and Guilard, R., Eds.), pp 41-60, Academic Press, New York.

48. Simonneaux, G., Le Maux, P., Ferrand, Y., and Rault-Berthelot, J. (2006) Asymmetric heterogeneous catalysis by metalloporphyrins, *Coord. Chem. Rev. 250*, 2212-2221.

49. Ungashe, S. B., and Groves, J. T. (1994) Porphyrins and metalloporphyrins in synthetic bilayer membranes, *Adv. Inorg. Biochem. 9*, 317-351.

50. Groves, J. T. (2003) The bioinorganic chemistry of iron in oxygenases and supramolecular assemblies, *Proc. Natl. Acad. Sci., USA 100* 3569-3574.

51. Stephenson, N. A., and Bell, A. T. (2005) A Study of the Mechanism and Kinetics of Cyclooctene Epoxidation Catalyzed by Iron(III) Tetrakispentafluorophenyl Porphyrin, *J. Am. Chem. Soc. 127*, 8635-8643.

52. Stephenson, N. A., and Bell, A. T. (2006) Effects of Methanol on the Thermodynamics of Iron(III) [Tetrakis(pentafluorophenyl)]porphyrin Chloride Dissociation and the Creation of Catalytically Active Species for the Epoxidation of Cyclooctene, *Inorg. Chem. 45*, 5591-5599.

53. Stephenson, N. A., and Bell, A. T. (2006) Influence of Solvent Composition on the Kinetics of Cyclooctene Epoxidation by Hydrogen Peroxide Catalyzed by Iron(III) [tetrakis(pentafluorophenyl)] Porphyrin Chloride [(F_{20}TPP)FeCl], *Inorg. Chem. 45*, 2758-2766.

54. Stephenson, N. A., and Bell, A. T. (2007) Mechanistic Study of Iron(III) [Tetrakis(pentafluorophenyl)Porphyrin Triflate (F_{20}TPP)Fe(OTf) Catalyzed Cyclooctene Epoxidation by Hydrogen Peroxide, *Inorg. Chem. 46*, 2278-2285.

55. Ellis, P. E., and Lyons, J. E. (1989) Halognation substituent effects on the catalytic activity of iron porphyron complexes for the selective air oxidation of alkanes in the liquid phase, *Catal. Lett. 3*, 389-397.

56. Lyons, J. E., and Ellis, P. E. (1991) Selective low temperature oxidation of isobutane by molecular oxygen by an iron perhaloporphyrin complex, *Catal. Let. 8*, 45-51.

57. Bartoli, J. F., Brigaud, O., Battioni, P., and Mansuy, D. (1991) Hydroxylation of linear alkanes catalysed by iron porphyrins: particular efficacy and regioselectivity of perhalogenated porphyrins, *J. Chem. Commun.*, 440-442.

58. Grinstaff, M. W., Hill, M. G., Labinger, J. A., and Gray, H. B. (1994) Mechanism of catalytic oxygenation of alkanes by halogenated iron porphyrins, *Science 264*, 1311-1313.

59. Labinger, J. A. (1994) A simplified model for catalyzed isobutane autoxidation: implications for the mechanism of catalysis by halogenated porphyrin complexes, *Catal. Lett. 26*, 95-99.

60. Grinstaff, M. W., Hill, M. G., Birnbaum, E. R., Schaefer, W. P., Labinger, J. A., and Gray, H. B. (1995) Structures, Electronic Properties, and Oxidation-Reduction Reactivity of Halogenated Iron Porphyrins, *Inorg. Chem. 34*, 4896-4902.

61. Doro, F. G., Smith, J. R. L., Ferreira, A. G., and Assis, M. D. (2000) Oxidation of alkanes and alkenes by iodosylbenzene and hydrogen peroxide catalysed by halogenated manganese porphyrins in homogeneous solution and covalently bound to silica, *J. Mol. Catal. A:Chem 164*, 97-108.

62. Traylor, T. G., Kim, C., Fann, W. P., and Perrin, C. L. (1998) Reactions of hydroperoxides with iron(III) porphyrins: Heterolytic cleavage followed by hydroperoxide oxidation, *Tetrahedron 54*, 7977-7986.

63. Traylor, T. G., and Xu, F. (1990) Mechanisms of reactions of iron(III) porphyrins with hydrogen peroxide and hydroperoxides: solvent and solvent isotope effects, *J. Am. Chem. Soc. 112*, 178-186.

64. Moore, K. T., Horvath, I. T., and Therien, M. J. (2000) Mechanistic Studies of (Porphinato)Iron-Catalyzed Isobutane Oxidation. Comparative Studies of Three Classes of Electron-Deficient Porphyrin Catalysts, *Inorg. Chem. 39*, 3125-3139.

65. Nam, W., Han, H. J., Oh, S.-Y., Lee, Y. J., Choi, M.-H., Han, S.-Y., Kim, C., Woo, S. K., and Shin, W. (2000) New Insights into the Mechanisms of O−O Bond Cleavage of Hydrogen Peroxide and tert-Alkyl Hydroperoxides by Iron(III) Porphyrin Complexes, *J. Am. Chem. Soc. 122*, 8677-8684.

66. Battioni, P., Renaud, J. P., Bartoli, J. F., Reinaartiles, M., Fort, M., and Mansuy, D. (1988) Monooxygenase-Like Oxidation of Hydrocarbons by H_2O_2 Catalyzed by Manganese Porphyrins and Imidazole - Selection of the Best Catalytic-System and Nature of the Active Oxygen Species, *J. Am. Chem. Soc. 110*, 8462-8470.

67. Higuchi, T., Shimada, K., Maruyama, N., and Hirobe, M. (1993) Heterolytic O-O Bond-Cleavage of Peroxy Acid and Effective Alkane Hydroxylation in Hydrophobic Solvent Mediated by an Iron Porphyrin Coordinated by Thiolate Anion as a Model for Cytochrome-P-450, *J. Am. Chem. Soc. 115*, 7551-7552.

68. Traylor, T. G., and Popovitz-Biro, R. (1988) Hydrogen-Bonding to the Proximal Imidazole in Heme Protein Model Compounds - Effects Upon Oxygen Binding and Peroxidase-Activity, *J. Am. Chem. Soc. 110*, 239-243.

69. Yamaguchi, K., Watanabe, Y., and Morishima, I. (1993) Direct Observation of the Push Effect on the O-O Bond-Cleavage of Acylperoxoiron(III) Porphyrin Complexes, *J. Am. Chem. Soc. 115*, 4058-4065.

70. Rosenthal, J., Pistorio, B. J., Chng, L. L., and Nocera, D. G. (2005) Aerobic Catalytic Photooxidation of Olefins by an Electron-Deficient Pacman Bisiron(III)-Oxo Porphyrin, *J. Org. Chem 70*, 1885-1888.

71. Evans, S., and Smith, J. R. L. (2001) The oxidation of ethylbenzene by dioxygen catalysed by supported iron porphyrins derived from iron(III) tetrakis(pentafluorophenyl)porphyrin, *J. Chem. Soc., Perkin Trans. 2*, 174 - 180.

72. Herron, N., and Tolman, C. A. (1987) A highly selective zeolite catalyst for hydrocarbon oxidation. A completely inorganic mimic of the alkane .omega.-hydroxylases, *J. Am. Chem. Soc. 109*, 2837-2839.

73. Bedioui, F. (1995) Zeolite-encapsulated and clay-intercalated metal porphyrin, phthalocyanine and Schiff-base complexes as models for biomimetic oxidation catalysts: an overview, *Coord. Chem. Rev. 144*, 39-68.

74. Battioni, P., Lallier, J.-P., Barloy, L., and Mansuy, D. (1989) Mono-oxygenase-like oxidation of hydrocarbons using supported manganese–porpnyrin catalysts: beneficial effects of a silica support for alkane hydroxylation, *Chem. Commun.* , 1149-1151.

75. Barloy, L., Battioni, P., and Mansuy, D. (1990) Manganese porphyrins supported on montmorillonite as hydrocarbon mono-oxygenation catalysts: particular efficacy for linear alkane hydroxylation, *Chem. Commun.*, 1365-1367.

76. Benaglia, M., Danelli, T., Fabris, F., Sperandio, D., and Pozzi, G. (2002) Poly(ethyleneglycol)-supported tetrahydroxyporphryin: a convenient, recyclable catalyst for photooxidations, *Org. Lett. 4*, 4229-4232.

77. Lee, J. Y., Farha, O. K., Roberts, J., Scheidt, K. A., Nguyen, S. T., and Hupp, J. T. (2009) Metal–organic framework materials as catalysts, *Chem. Soc. Rev. 38*, 1450-1459.

78. Shultz, A. M., Farha, O. K., Hupp, J. T., and Nguyen, S. T. (2009) A Catalytically Active, Permanently Microporous MOF with Metalloporphyrin Struts, *J. Am. Chem. Soc. 131*, 4204-4205.

79. Meunier, B. (1992) Metalloporphyrins as versatile catalysts for oxidation reactions and oxidative DNA cleavage, *Chem. Rev. 92*, 1411-1456.

80. Stephenson, N. A., and Bell, A. T. (2007) Mechanistic Study of Iron(III) [Tetrakis(pentafluorophenyl)Porphyrin Triflate (F_{20}TPP)Fe(OTf) Catalyzed Cyclooctene Epoxidation by Hydrogen Peroxide, *Inorg. Chem. 46*, 2278-2285.

81. Labinger, J. A. (1994) A simplified model for catalyzed isobutane autoxidation: implications for the mechanism of catalysis by halogenated porphyrin complexes, *Catal. Lett. 26*, 95-99.

82. Grinstaff, M. W., Hill, M. G., Birnbaum, E. R., Schaefer, W. P., Labinger, J. A., and Gray, H. B. (1995) Structures, Electronic Properties, and Oxidation-Reduction Reactivity of Halogenated Iron Porphyrins, *Inorg. Chem. 34*, 4896-4902.

83. Grinstaff, M. W., Hill, M. G., Labinger, J. A., and Gray, H. B. (1994) Mechanism of Catalytic Oxygenation of Alkanes by Halogenated Iron Porphyrins, *Science 264*, 1311-1313.

84. Nam, W., Oh, S.-Y., Sun, Y. J., Kim, J., Kim, W.-K., Woo, S. K., and Shin, W. (2003) Factors Affecting the Catalytic Epoxidation of Olefins by Iron Porphyrin Complexes and H_2O_2 in Protic Solvents, *J. Org. Chem. 68*, 7903-7906.

85. Stephenson, N. A., and Bell, A. T. (2006) Influence of Solvent Composition on the Kinetics of Cyclooctene Epoxidation by Hydrogen Peroxide Catalyzed by Iron(III) [tetrakis(pentafluorophenyl)] Porphyrin Chloride [(F_{20}TPP)FeCl], *Inorg. Chem. 45*, 2758-2766.

86. Stephenson, N. A., and Bell, A. T. (2006) Effects of Methanol on the Thermodynamics of Iron(III) [Tetrakis(pentafluorophenyl)]porphyrin Chloride Dissociation and the Creation of Catalytically Active Species for the Epoxidation of Cyclooctene, *Inorg. Chem. 45*, 5591-5599.

87. Kokubo, Y., Wu, X.-W., Oshima, Y., and Koda, S. (2004) Aerobic oxidation of cyclohexene catalyzed by Fe(III)(5,10,15,20-tetrakis(pentafluorophenyl) porphyrin)Cl in supercritical CO_2, *J. of Supercritical Fluids 30*, 225-235.

88. Moore, K. T., Fletcher, J. T., and Therien, M. J. (1999) Syntheses, NMR and EPR spectroscopy, electrochemical properties, and structural studies of [5,10,15,20 - Tetrakis (perfluoroalkyl) porphinato] iron (II) and - iron (III) complexes, *J. Am. Chem. Soc. 121*, 5196-5209.

89. Haber, J., Matachowski, L., Pamin, K., and Poltowicz, J. (2000) Manganese porphyrins as catalysts for oxidation of cyclooctane in Lyons system, *J. Mol. Catal. A: Chem. 162*, 105-109.

90. Haber, J., Matachowski, L., Pamin, K., and Poltowicz, J. (2003) The effect of peripheral substituents in metalloporphyrins on their catalytic activity in Lyons system, *J. Mol. Catal. A: Chem. 198*, 215-221.

91. Haber, J., Klosowski, M., and Poltowicz, J. (2003) Co-oxidation of styrene and iso-butyraldehyde in the presence of polyaniline-supported metalloporphyrins, *J. Mol. Catal. A: Chem. 201*, 167-178.

92. Krishnan, R., and Vancheesan, S. (2002) Polynuclear manganese complexes catalyzed epoxidation of olefins with molecular oxygen, *J. Mol. Catal. A: Chem. 185*, 87-95.

93. Jian-Ying, Q., Yue-Ming, L., Zhong-Yuan, Z., Chi-Ming, C., Chi-Hung, Y., and Albert , S. C. C. (2005) Novel Manganese Complex as an Efficient Catalyst for the Isobutyraldehyde-Mediated Epoxidation of Cyclic Alkenes with Dioxygen, *Adv. Synth. Catal. 347*, 45-49.

94. Zhou, X., and Ji, H. (2010) Biomimetic kinetics and mechanism of cyclohexene epoxidation catalyzed by metalloporphyrins, *Chem. Eng. J. 156*, 411-417.

95. Lim, S. Y., Kang, M., Kim, J. M., and Lee, I.-M. (2005) Epoxidation of Simple Alkenes with O2 and Isobutyraldehyde Catalyzed by Ni Catalysts Deposited on Nanoporous Carbon, *Bull. Korean Chem. Soc. 26*, 887-891.

96. Nam, W., Kim, H. J., Kim, S. H., Ho, R. Y. N., and Valentine, J. S. (1996) Metal Complex-Catalyzed Epoxidation of Olefins by Dioxygen with Co-Oxidation of Aldehydes. A Mechanistic Study, *Inorg. Chem. 35*, 1045-1049.

97. Bao, J., Chen, W., Liu, T., Zhu, Y., Jin, P., Wang, L., Liu, J., Wei, Y., and Li, Y. (2007) Bifunctional Au-Fe_3O_4 Nanoparticles for Protein Separation, *ACS Nano 1*, 293-298.

98. Huang, Y., Ma, W., Li, J., Cheng, M., Zhao, J., Wan, L., and Yu, J. C. (2003) A Novel β-CD-Hemin Complex Photocatalyst for Efficient Degradation of Organic Pollutants at Neutral pHs under Visible Irradiation, *J. Phys. Chem. B 107*, 9409-9414.

99. Smeureanu, G., Aggarwal, A., Soll, C. E., Arijeloye, J., Malave, E., and Drain, C. M. (2009) Enhanced Catalytic Activity and Unexpected Products from the Oxidation of Cyclohexene by Organic Nanoparticles of 5,10,15,20-Tetrakis-(2,3,4,5,6-pentafluorophenyl)porphyrinatoiron(III) in Water by Using O_2, *Chem. Eur. J. 15*, 12133-12140.

100. Drain, C. M., Smeureanu, G., Patel, S., Gong, X., Garno, J., and Arijeloye, J. (2006) Porphyrin Nanoparticles as Supramolecular Systems, *New J. Chem. 30*, 1834-1843.

101. Prakash, P., and Franciscamary, L. J. (2005) Reaction of a sterically hindered iron(III) porphyrin with peroxyacetic acid: degradation kinetics, *J. Serb. Chem. Soc. 70* 1105-1111

102. Poltowicz, J., Pamin, K., and Haber, J. (2006) Influence of manganese tetraarylporphyrins substituents on the selectivity of cycloalkanes oxidation with magnesium monoperoxyphthalate, *J. Mol. Catal. A: Chem. 257*, 154-157.

103. Arasasingham, R. D., He, G. X., and Bruice, T. C. (1993) Mechanism of manganese porphyrin-catalyzed oxidation of alkenes. Role of manganese(IV)-oxo species, *J. Am. Chem. Soc. 115*, 7985-7991.

104. Ellis Jr., P. E., and Lyons, J. E. (1990) Selective air oxidation of light alkanes catalyzed by activated metalloporphyrins - the search for a suprabiotic system, *Coord. Chem. Rev. 105*, 181-193.

105. Varotto, A., Todaro, L., Vinodu, M., Koehne, J., Liu, G.-y., and Drain, C. M. (2008) Self-organization of a new fluorous porphyrin and C60 films on indium-tin-oxide electrode, *Chem. Commun*, 4921-4923.

106. Boucher, L. J. (1968) Manganese porphyrin complexes. I. Synthesis and spectroscopy of manganese(III) protoporphyrin IX dimethyl ester halides, *J. Am. Chem. Soc. 90*, 6640-6645.

107. Spreer, L. O., Maliyackel, A. C., Holbrook, S., Otvos, J. W., and Calvin, M. (1986) Synthesis and characterization of a manganese(III) porphyrin cation radical and its conversion to manganese(IV) by ligand metathesis, *J. Am. Chem. Soc. 108*, 1949-1953.

108. Hill, C. L., and Hollander, F. J. (1982) Structural characterization of a complex of Manganese(V) nitrido[tetrakis(p-methoxyphenyl)porphinato] manganese(V), *J. Am. Chem. Soc. 104*, 7318-7319.

109. Song, W. J., Seo, M. S., George, S. D., Ohta, T., Song, R., Kang, M.-J., Tosha, T., Kitagawa, T., Solomon, E. I., and Nam, W. (2007) Synthesis, Characterization,

and Reactivities of Manganese(V)−Oxo Porphyrin Complexes, *J. Am. Chem. Soc. 129*, 1268-1277.

110. Kameyama, H., Narumi, F., Hattori, T., and Kameyama, H. (2006) Oxidation of cyclohexene with molecular oxygen catalyzed by cobalt porphyrin complexes immobilized on montmorillonite, *J. Mol. Catal. A: Chem. 258*, 172-177.
111. Zhou, X.-T., Tang, Q.-H., and Ji, H.-B. (2009) Remarkable enhancement of aerobic epoxidation reactivity for olefins catalyzed by [mu]-oxo-bisiron(III) porphyrins under ambient conditions, *Tetrahedron Lett. 50*, 6601-6605.
112. Gharnati, L., Doring, M., and Arnold, U. (2009) Catalytic Oxidation with Hydrogen Peroxide in Ionic Liquids, *Curr. Org. Syn. 6*, 342-361.
113. Maraval, V., Ancel, J.-E., and Meunier, B. (2002) Manganese(III) Porphyrin Catalysts for the Oxidation of Terpene Derivatives: A Comparative Study, *J. Catal. 206*, 349-357.
114. Chellaiah, A., Yong-Min, L., Jung Yoon, L., Shunichi, F., and Wonwoo, N. (2009) Hydrogen-Atom Abstraction Reactions by Manganese(V)- and Manganese(IV)-Oxo Porphyrin Complexes in Aqueous Solution, *Chem. Eur. J. 15*, 11482-11489.
115. Lyons, J. E., Ellis, P. E., and Myers, H. K. (1995) Halogenated Metalloporphyrin Complexes as Catalysts for Selective Reactions of Acyclic Alkanes with Molecular Oxygen, *J. Catal. 155*, 59-73.
116. Nia, S., Gong, X., Drain, C. M., Jurow, M., Rizvi, W., and Qureshy, M. (2010) Solvent-free synthesis of meso tetraarylporphyrins in air: product diversity and yield optimization, *J. Porphyrins Phthalocyanines 14*, 621-629.
117. Drain, C. M., and Gong, X. (1997) Synthesis of meso substituted porphyrins in air without solvents or catalysts, *Chem. Commun.*, 2117 - 2118.
118. Drain, C. M., and Singh, S. (2010) Combinatorial Libraries of Porphyrins: Chemistry and Applications, In *The Handbook of Porphyrin Science with Applications to Chemistry, Physics, Materials Science, Engineering, Biology and Medicine* (Kadish, K., Smith, K. M., and Guilard, R., Eds.), pp 485-537, World Scientific Publisher, Singapore.

119. Cavaleiro, J. A. S., Tomé, A. C., and Neves, M. G. P. M. S. (2010) meso-Tetraarylporphyrin Derivatives: New Synthetic Methodologies, In *The Handbook of Porphyrin Science with Applications to Chemistry, Physics, Materials Science, Engineering, Biology and Medicine* (Kadish, K., Smith, K. M., and Guilard, R., Eds.), pp 193-294, World Scientific Publisher, Singapore.

120. Andrus, M. B., and Lashley, J. C. (2002) Copper catalyzed allylic oxidation with peresters, *Tetrahedron 58*, 845-866.

121. Crich, D., and Zou, Y. (2005) Catalytic Oxidation Adjacent to Carbonyl Groups and at Benzylic Positions with a Fluorous Seleninic Acid in the Presence of Iodoxybenzene, *J. Org. Chem. 70*, 3309-3311.

122. Mansuy, D., Bartoli, J. F., Battioni, P., Lyon, D. K., and Finke, R. G. (1991) Highly oxidation resistant inorganic-porphyrin analog polyoxometalate oxidation catalysts. 2. Catalysis of olefin epoxidation and aliphatic and aromatic hydroxylations starting from α_2-$P_2W_{17}O_{61}(M^{n+}..Br)^{(n-11)}$ (M^{n+} = Mn^{3+}, Fe^{3+}, Co^{2+}, Ni^{2+}, Cu^{2+}), including quantitative comparisons to metalloporphyrin catalysts, *J. Am. Chem. Soc. 113*, 7222-7226.

123. Traylor, T. G., Fann, W. P., and Bandyopadhyay, D. (1989) A common heterolytic mechanism for reactions of iodosobenzenes, peracids, hydroperoxides, and hydrogen peroxide with iron(III) porphyrins, *J. Am. Chem. Soc. 111*, 8009-8010.

124. Yang, S. J., and Nam, W. (1998) Water-Soluble Iron Porphyrin Complex-Catalyzed Epoxidation of Olefins with Hydrogen Peroxide and tert-Butyl Hydroperoxide in Aqueous Solution, *Inorg. Chem. 37*, 606-607.

CHAPTER 3: ELECTROCHEMICAL STUDIES OF SELF-ORGANIZED PORPHYRIN-POLYOXOMETALLATES FILMS ON ITO[a]

Abstract

Sequential dipping of indium-tin oxide electrodes into solutions of tetra cationic porphyrins and tetra anionic polyoxometalates results in the controlled formation of nm thick films. The potential applications of these robust films on electrodes range from catalysts to sensors. This chapter focuses on the electrochemistry of the multilayered films where it is found that the oxidation and reduction potentials of each species remain largely the same as found in solution.

[a] This chapter is adapted from the reference 1. Bazzan, G., Aggarwal, A., and Drain Charles, M. (**2011**) Electrochemical Studies of Self-Organized Porphyrin-Polyoxometalate Films on ITO, In *Interfaces and Interphases in Analytical Chemistry* (Helburn, R., and Vitha, M. F., Eds.), pp 167-184, American Chemical Society, Washington, DC. (**Note**: Bazzan and Aggarwal contributed equally to this work.)

3.1 Introduction

Organic-inorganic hybrid materials are of great interest in the field of material chemistry as these materials can exhibit synergetic, electrical, optical, and catalytic properties.(*2*) *Polyoxometalates* (POM) are a large class of inorganic oxide clusters with a wide range of chemical and oxidation/reduction properties that are used in both laboratory and commercial materials, as models of oxide surfaces, and as models of inorganic matrixes.(*3*) They are used as catalysts, and POM with defects can bind a plethora of metal ions, which alter their physical chemical properties in precise and predictable ways. Electrodes modified with POM have recently attracted increasing attention because of their good stability, wide ranging chemistry, and catalytic activity.(*3*) For example, POM-containing multilayer films can be more efficient in heterogeneous catalysis because they have unique advantages over other chemically modified electrodes, e.g. three-dimensional layered architecture of electrocatalysts and the amount of absorbed electrocatalyst can be precisely controlled.(*4-6*)

Typical methods to prepare chemically modified electrodes have been addressed in a review of the electrochemical properties of POM.(*7*) The three main methods commonly used to immobilize POM onto the electrode surface are: (1) adsorption on electrode surface by dip coating,(*8*) (2) immobilization of POM as dopant in a conductive polymer matrix,(*9*) (3) electrochemical deposition directly on the electrode via application of a potential.(*10*) Each of these methods has advantages and disadvantages. Typically, dip coated films are less robust but use the POM more efficiently because most are exposed to solvent, while the electrodeposited films are more robust but access to the catalytic sites inside the granules may be limited because of higher packing density. The chemistry and characterization on a molecular scale of the hybrid polymer/POM films are difficult, but the performance can be satisfactory.

Layer-by-layer (LBL) deposition involves the sequential dipping of a substrate, such as an electrode, into solutions containing molecules or polymers with complementary intermolecular interactions. Most LBL films are organized electrostatically by sequentially dipping the substrate into solutions containing oppositely charged species – usually polyelectrolytes.(*11-13*) Recently, layer-by-layer strategy has been successfully used to modify electrode surfaces based on electrostatic interaction between anionic POM and cationic compounds or polymers.(*14-17*)

Porphyrins are robust conjugated tetrapyrrole macrocycles that can complex a wide range of metal ions, and they possess an equally wide range of photophysical properties that arise from the complexed metal ion, exocyclic motifs, and the environment. Many porphyrinoid materials have been investigated over the last decades.(*18-26*) The macrocycle and the metallocomplexes also typically have several reversible oxidations and/or reductions.(*27*) Thus, porphyrins are used in photonic materials for sensor, catalytic, nonlinear optical, therapeutic and many other applications.

In terms of *catalysts, sensors, and analytical applications*, there are a couple of reports on the deposition of cationic porphyrins and anionic POM on modified glassy carbon electrode.(*15, 28*) These electrodes display electrocatalytic activity for the reduction of O_2 to peroxide and for hydrogen evolution from acidic water, but for their preparation the glassy carbon electrode needed to be functionalized with 4-aminobenzoic acid, and the material was deposited by cyclic potential sweeps of the electrode in a solution of the ions to be deposited.

The demonstrated electrocatalytic activity of these porphyrin/POM films, and the formation of other photonic materials with diverse potential applications prompted us to examine the structure and mechanism of electrostatically organized films on a variety of substrates.(*21*)

We recently demonstrated that porphyrin/POM modified surfaces such as quartz, glass, and indium-tin oxide (ITO) electrodes can be easily prepared by sequentially dipping these supports into solutions containing a tetracationic 5,10,15,20-tetrakis(4-methylpyridinium)porphyrin ($TMPyP^{4+}$) as the tetratosylate salt, and silicotungstic acid hydrate ($SiW_{12}O_{40}^{4-}$) (Scheme 3.1). Notably, sequential dipping of these substrates into solutions of the oppositely charged materials does not require previous preparation of the electrode surface. Since these are lower energy surfaces than those with greater charge density, the amount of either compound deposited on any given deposition is significantly less than a complete (mono) layer (Scheme 3.2). Several key points from this previous work are germane to the electrochemistry. (1) Estimates of the surface density after one deposition of the porphyrin are ca. 1 per 20 nm^2 and the porphyrin is ca. 1.5 nm^2. Thus, the surface energetics of the substrate dictates how many deposition sequences are needed to completely cover the substrate (about four rounds of dipping for all three substrates) and to form a robust film (ca. eight).

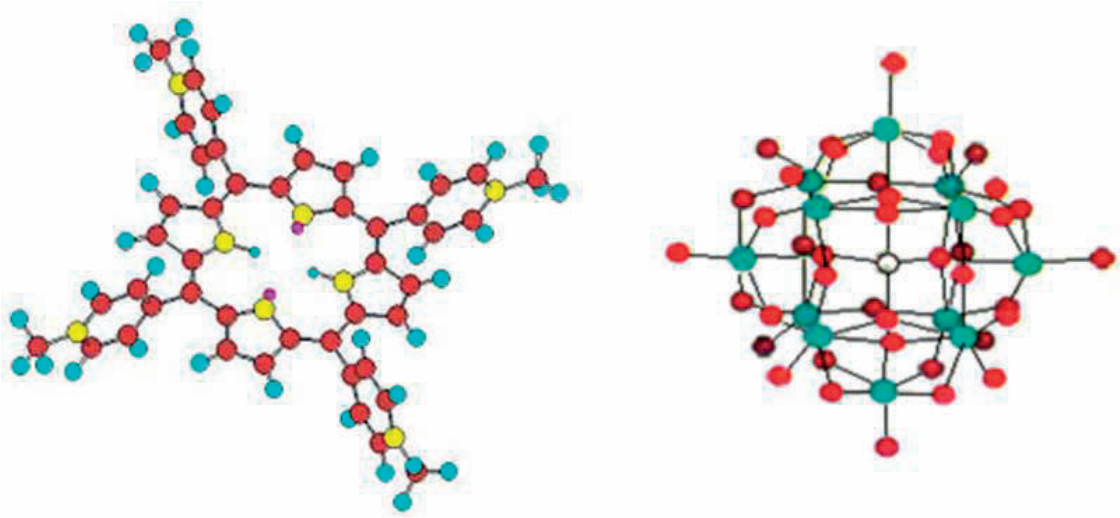

Scheme3.1: Left 5,10,15,20-tetrakis(4-methylpyridinium)porphyrin ($TMPyP^{4+}$) is used as the tosylate salt. (H = light blue, N = yellow, C = redbrown), and right: polyoxometalate (POM) $H_4SiW_{12}O_{40}$ (O = red, W = blue, Si = gray) where the counter ions are left out for clarity. Taken from reference 1.

(2) There is a linear increase in the porphyrin UV-visible absorbance spectra, e.g. the B (Soret) band, with the number of deposition cycles, which correlates to a linear increase in the amount of material deposited up to about 100 cycles, where we stopped the experiment. (3) After ca. eight layers, the films are stable to sonication in water, 1 M NaCl, and toluene. (4) Patterns of these films can be formed on ITO lithographed with lines of 600 nm wide by 20 nm high polycarbonate, and reside only on the bare surface (not on the polymer). We present herein a detailed analysis of the cyclic voltamographic properties of these films, created by sequential dipping, to correlate the structure-function relationships.

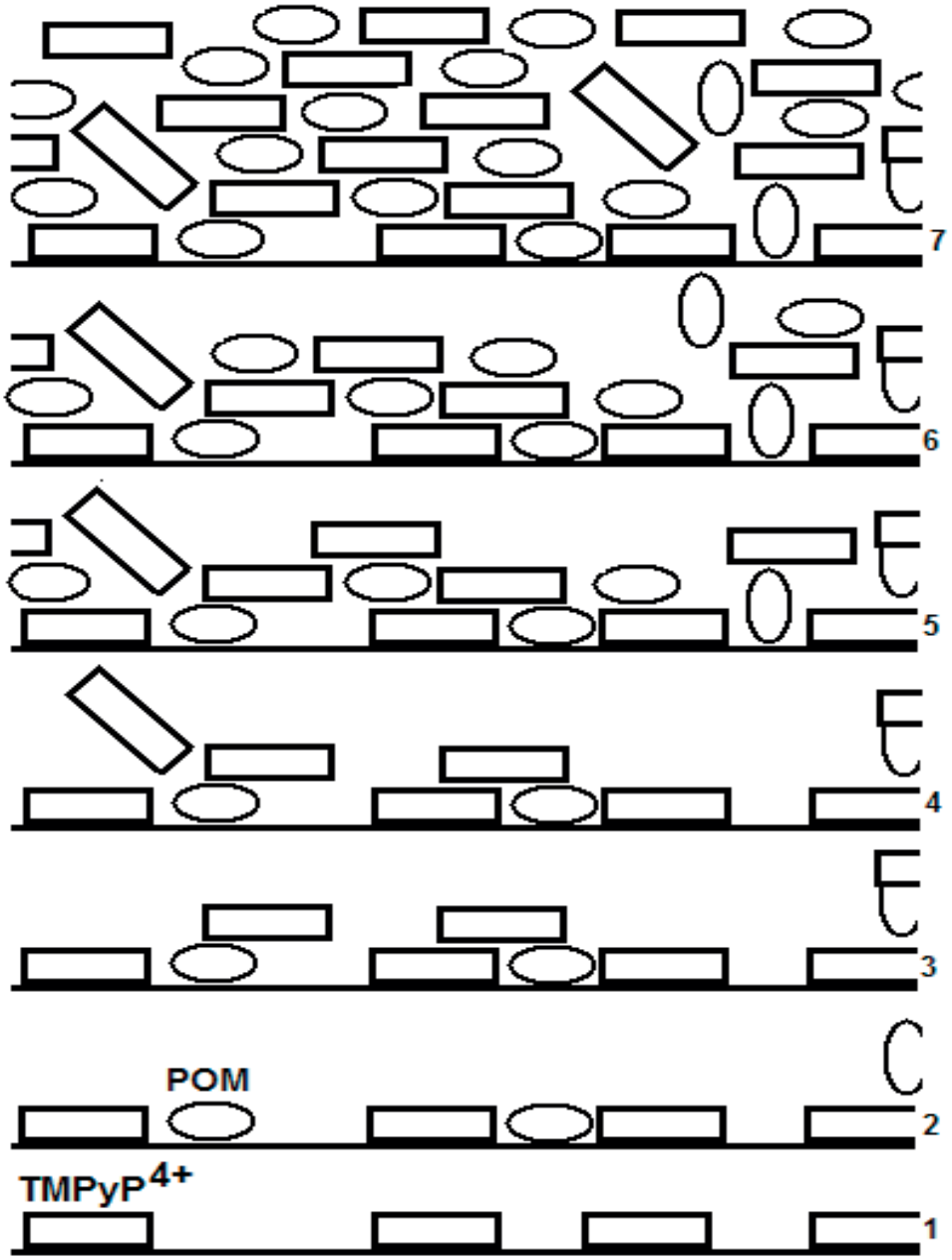

Scheme 3.2: Sequential dipping of the ITO substrate into solutions of the $TMPyP^{4+}$ and the POM results in formation of thin films. It takes ca. four sequences to form a complete layer, and eight to form a robust film. Taken from reference 1.

3.2 Experimental Details

Materials: All reagents and solvents were of analytical grade and used without further purification. The water was passed through a Barnstead NANOPure Water Purification System. The $TMPyP^{4+}$ and silicotungstic acid hydrate ($SiW_{12}O_{40}^{4-}$) were purchased from Aldrich.

Cyclic voltammetry was performed with a BAS-CV-50W in a conventional three-electrode electrochemical cell, using an ITO (0.6 cm^2) as the working electrode, a platinum wire as the auxiliary electrode, and Ag/AgCl/KCl (3 mol/L) as the reference electrode. All experiments were performed using the same area of the electrode. NaCl 0.1 M in ultrapure water was used as electrolyte with two different pH values, pH=3 (adjust by addition of 0.5 M H_2SO_4), and compared to pH=4 acetate buffer (0.1 mol/L). The scan rate was 0.1 V/s. All the solutions were degassed thoroughly with pure nitrogen and kept under a positive pressure of this gas during experimentation.

The ITO substrate was cleaned using a homemade UV/ozone cleaning system, rinsed with ultrapure water, sonicated in ethanol for 10 min., and dried by blowing a stream of nitrogen gas across the surface. Films were prepared at room temperature by soaking the ITO substrate in a 0.5 mM aqueous solution of porphyrin for 1 min, followed by dipping the substrate three times in unbuffered NANOPure water to remove the excess, non-bound porphyrin solution from the substrate. Subsequently, a layer of polyoxometalates was added by soaking the substrate for 1 minute in a 0.5 mM aqueous solution of polyoxometalates, rinsed three times by dipping in NANOPure water. The procedure was repeated until the desired film thickness was obtained. The films on the glass side of the ITO substrates were left in place.

3.3 Results and Discussion

3.3.1 Solution Analysis

The electrochemical properties of $TMPyP^{4+}$ have been reported in detail, using both Hg and ITO electrodes.(*29*) The reduction chemistry in acidic solution is pH dependent and involves six electrons overall. Between pH=2 and pH=6 two peaks are observed (Figure 3.1). The first is a quasi reversible reduction (-104 mV) step that involves the reduction of the porphyrin free base to the chlorin free base (Figure 3.1). The pH dependence is given by the equation below.

$$P(0)H_2 + 2e^- + 2H^+ \rightleftharpoons P(-II)H_4 \qquad \text{pH dependence (60 mV/pH)}$$

At potentials more negative than -0.65 V vs Ag/AgCl a complicated, irreversible four electron reduction occurs (-605 mV) which generates unstable porphyrinogen cations.

The electrochemical response of the $H_4SiW_{12}O_{40}$ in aqueous medium has been extensively studied. Sadakane et al. report that in acid solution using a glassy carbon working electrode the CV shows five reduction waves with an approximate electron ratio of 1:1:2:8:12. The first three reductions are reversible while the last two are irreversible and accompanied by chemical reactions of the complex.(*7*)

$$SiW_{12}O_{40}^{4-} + e^- \rightleftharpoons SiW_{12}O_{40}^{5-}$$

$$SiW_{12}O_{40}^{5-} + e^- \rightleftharpoons SiW_{12}O_{40}^{6-}$$

$$SiW_{12}O_{40}^{6-} + 2e^- + 2H^+ \rightleftharpoons H_2SiW_{12}O_{40}^{6-}$$

In the potential window suitable for the porphyrin (-0.6 V / +0.6 V) there are two reversible reductions for the POM (-215 mV and -490 mV) that are essentially unaltered for

1 < pH < 5 (Figure 3.2). Prior to the electrochemical study of the layer-by-layer deposition process, we analyzed the behavior in aqueous solutions (pH=3) of $TMPyP^{4+}$ and $SiW_{12}O_{40}^{4-}$ using ITO as working electrode (Figure 3.1 and 3.2). The CV curves at pH=3 confirm the above reductions and indicate that the ITO surface has a small effect on the potential measured. However, the two POM reduction peaks in solution are observed to broaden on the ITO electrode.(*15*) Accordingly, we have set the scan limit of our cyclic voltammetry to -0.55 V vs. Ag/AgCl

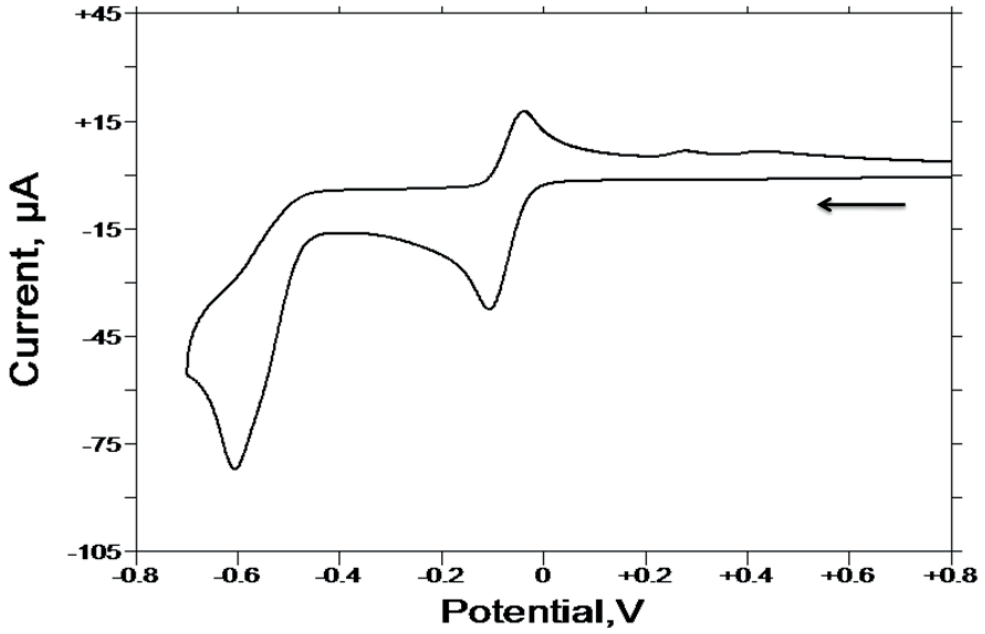

Figure 3.1: Cyclic voltammogram of a $TMPyP^{4+}$ solution using an ITO working electrode (0.6 cm^2), platinum wire counter electrode and Ag/AgCl/KCl (3 mol/L) reference electrode. Unbuffered NaCl (0.1 mol/L) in ultrapure water, pH=3 (adjusted by addition of 0.5 M H_2SO_4) was used and the scan rate was 0.1 V/s. Reduction peaks:-104 mV, and -605 mV; Oxidation peak: -37 mV vs. Ag/AgCl. Taken from reference 1.

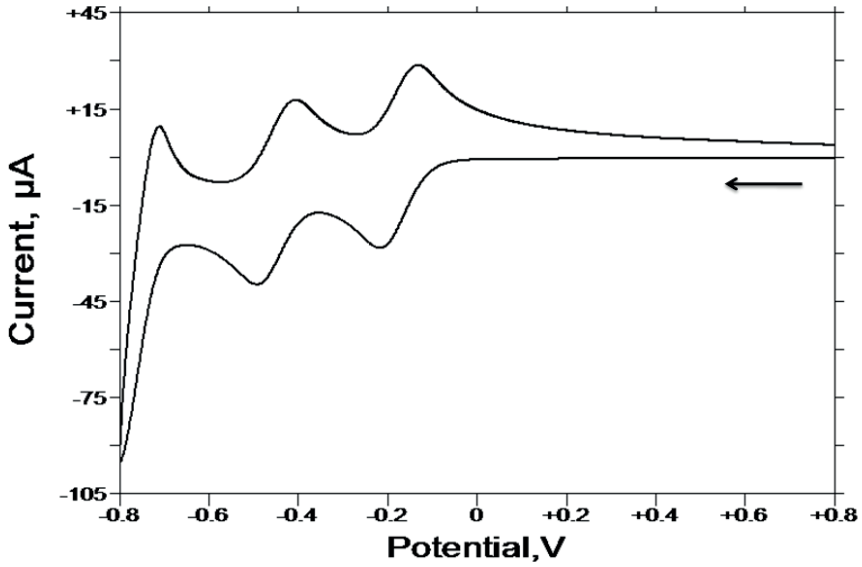

Figure 3.2: Cyclic voltammogram of a $SiW_{12}O_{40}^{4-}$ solution using an ITO (0.6 cm^2) working electrode, platinum wire counter electrode, and Ag/AgCl/KCl (3 mol/L) reference electrode. Unbuffered NaCl (0.1 mol/L) in ultrapure water, pH=3 (adjusted by addition of 0.5 M H_2SO_4) was used, and the scan rate was 0.1 V/s. Reduction peaks: -215 mV, -490 mV; Oxidation peaks: -710 mV, -408 mV, -135 mV vs. Ag/AgCl. Taken from reference 1.

3.3.2 Film Analysis

Cyclic voltammetry can be used to monitor the deposition process and to characterize the electrochemical behavior of the film. Compared to the solution properties, the film exhibits less well resolved redox peaks (Figure 3.3). There is a broad reduction peak at -325 mV for the porphyrin. The first two POM oxidation peaks almost merge with each other (-270 mV). This is probably due to surface-confined redox processes.(*30*) To assure identical and reproducible data, the CV curves shown in Figure 3.3 are the fifth after a preliminary set of polarization cycles as was done previously.(*5, 15, 16*) Previous reports do not show the data for the first few CV cycles, and this will be discussed below (Figures 3.5 and 3.6).

The CV curves in Figure 3.3 are recorded with the POM as outermost layer and after eight deposition cycles to assure that complete surface coverage and film robustness have been reached, *vida supra*. Since the currents represent the surface concentration of the POM and porphyrin loaded on the electrode, the currents increase gradually with the number of deposition cycles and indicate that a consistent amount of porphyrin and polyoxometalate are deposited with each deposition cycle. Similar CV curves are obtained when the porphyrin is the outermost layer (Figure 3.4) but with a slightly different electrochemical behavior and different slopes for plots of current versus number of deposition cycle. (See Figure 3.7 for the oxidation peak current at -270 mV and Figure 3.8 for the absolute value of the reduction peak current at -325 mV plotted versus deposition cycle number.)

Figures 3.5 and 3.6 shows the effect of the first four cycles of potential scans with the POM and porphyrin as the last deposited material, respectively. The cyclic voltammograms are quite different, exhibiting a significant decrease in the currents of both the oxidation peak (e.g. +23 mV porphyrin) and the reduction peak (e.g. -325 mV POM) of the films. The current stops diminishing after four potential scan cycle, likely indicating that only the external part of the porphyrinic/POM material present on the film desorbs or decomposes. This difference in the initial scans suggest that POM inhibits desorption of the porphyrin-POM films from the surface, or the interlayer electrostatic interactions between the porphyrin-POM layers is stronger when POM is the last layer. The steeper decrease in the oxidation peak at +23 mV compared to the reduction peak at -325 mV suggests either an irreversible reduction reaction of the porphyrinic material (in spite of the fact that the porphyrin in solution is stable in the potential window examined), or a desorption of some porphyrinic material from the film after the reduction process. UV-visible absorption measurements of the electrolyte solution after 16 deposition

cycles, and consequently many potential scans, indicates a small amount of the porphyrin in solution (see appendix Figure A3.1 inset), moreover the film is stable in high ionic strength solutions, e.g. sonication in 0.1 M NaCl shows that little of the porphyrin comes off of the substrates.

However, comparison of the initial UV-visible spectra of films for 16 porphyrin-POM layers on an ITO substrate to those after the CV experiment shows a small decrease in the absorption maximum in the Soret region (see appendix Figure A3.1). This indicates either desorption or decomposition of the porphyrinic material. Also, the UV-visible and fluorescence analysis of the electrolyte solution after the CV experiment shows the presence of trace quantities of the porphyrin in solution, clearly indicating that small amounts of desorption of some material from the ITO surface while the CV analysis was done (see appendix Figure A3.1 and A3.2).

Note also that the UV-visible spectra of both the film and the solution show no evidence of chlorin or other reduced or oxidized porphyrin products. Similar changes are observed when the POM is the last deposited material. Overall, these results suggest that the last deposition sequence, of no matter how many, does not form a complete, stable layer under the CV scanning conditions, perhaps leaving some porphyrin ~~–e~~xposed" even when the POM is the last material deposited. This is consistent with our model of film growth wherein each dipping does not form a layer *per se*, but switches the net surface charge density until an equilibrium is reached.(*21*)

Cyclic voltammograms performed after each sequence of deposition (8 through 18 or 21, data from the 5^{th} CV scan) were recorded both when porphyrin and when the POM was deposited last. A plot of the number of deposition sequences versus current (taken from the POM peaks in Figure 3.3 and 3.4: oxidation peak current at -270 mV and reduction peak current at -

325 mV) reveals that the magnitude of the current is ca. 3-fold less when the porphyrin is added last and the slopes of the lines depends on which compound was deposited last (Figure 3.7 and 3.8).

The currents increase because there are more redox active materials on the surface of the electrode, but there may be several explanations for why there is a marked dependence on which of the two molecules is deposited last onto the growing film.

(1) When the POM is the outermost layer, a greater amount of material is deposited each round of dipping.

(2) When the porphyrin is the last material deposited, more porphyrinic material is exposed on the surface and can undergo desorption. This means that the outermost POM prevents the porphyrinic material underneath from desorption.

(3) There may be morphological differences between the surfaces that depend on the last deposited compound such that the POM last films have a greater effective electrode surface, which would result in a greater observed current.

(4) The CV current also depends on the energetics and the electrostatics of the surfaces, and there are differences in the surface properties when the porphyrin is the last deposited material versus the POM. The fact that there is a linear growth of the films with increasing numbers of sequential depositions, indicates that the net surface charges alternate between positive for the $TMPyP^{4+}$ last films, and negative for the POM last films, though the surface charge densities may differ. There are also likely differences arising from the hydrophobic porphyrin core versus the hydrophilic POM. Considering the CV are performed in acidic solution (pH=3) the net positive charge of the electrode surface when the porphyrin is deposited last may inhibit

interfacial proton transport. This is consistent with proton coupled electron transfer with POM.(*10*)

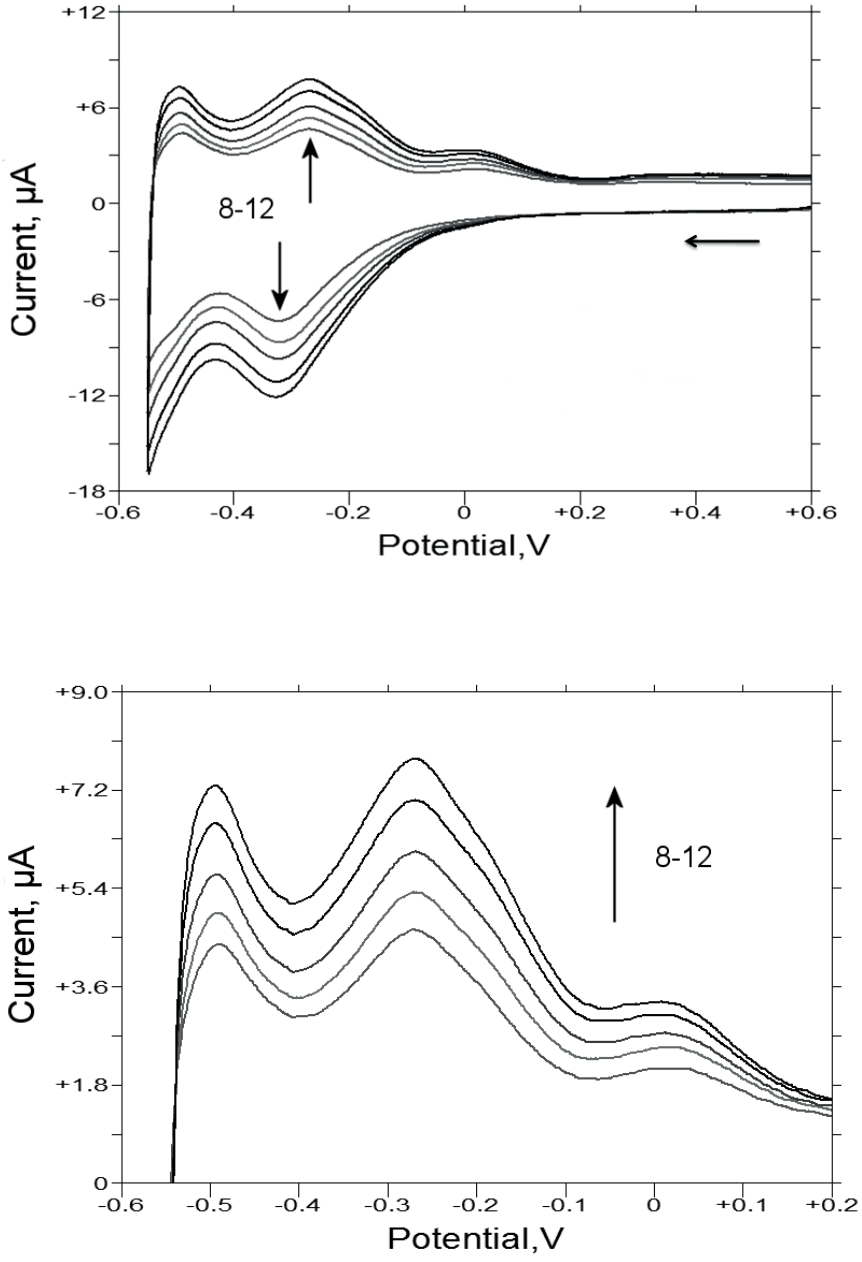

Figure 3.3: Top: Cyclic voltammogram of the films built on ITO using $TMPyP^{4+}$ and $SiW_{12}O_{40}^{4-}$ with 8 to 12 dipping cycles. Each CV was recorded with the POM as the outermost layer. Bottom**:** Details of the oxidation peaks. Reduction peak: -325 mV; Oxidation peaks: -495 mV, -270 mV, +23 mV vs. Ag/AgCl. pH=3, for the electrolytic solution

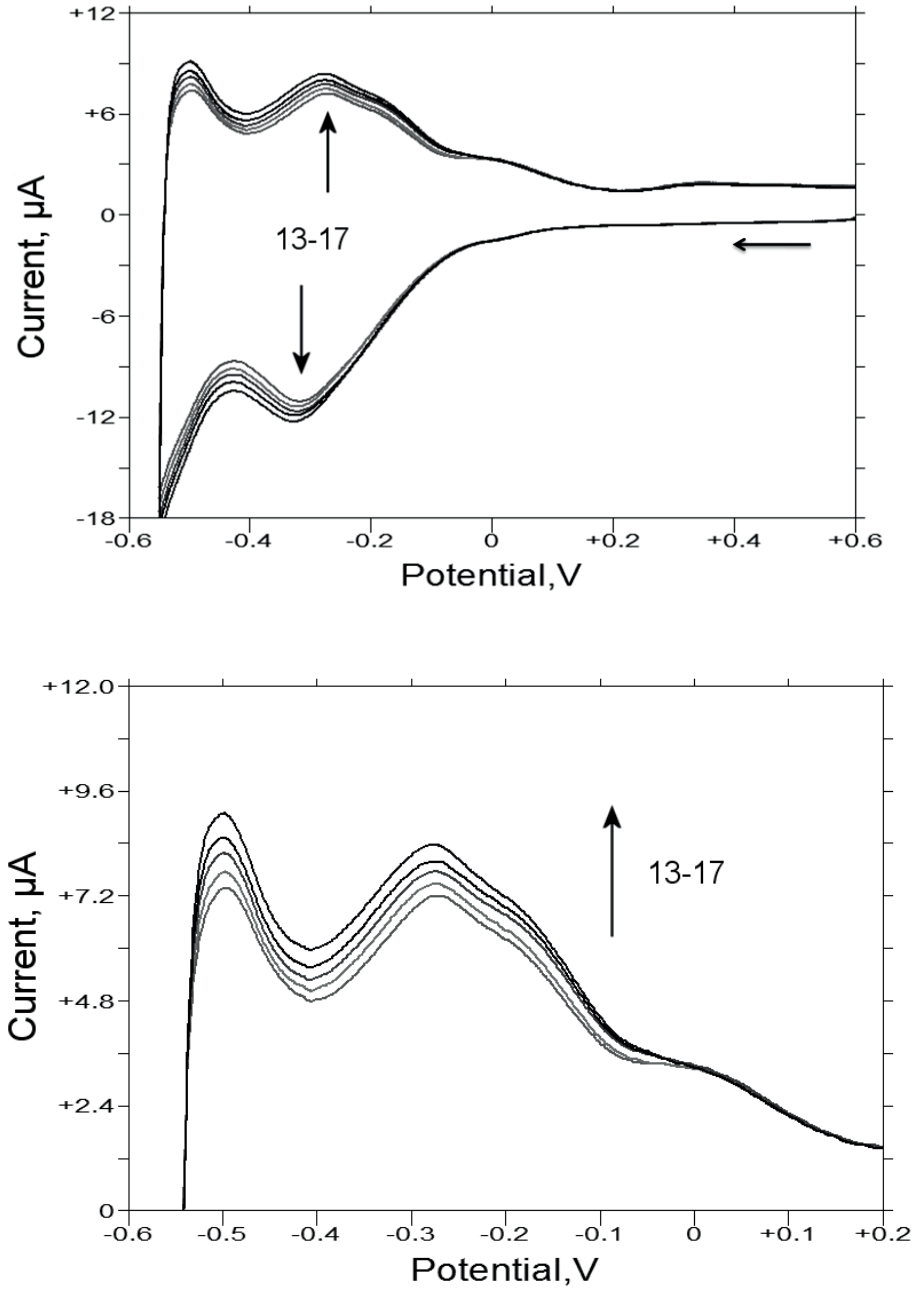

Figure 3.4: Top: Cyclic voltammogram of the films built on ITO using $TMPyP^{4+}$ and $SiW_{12}O_{40}^{4-}$ with 13 to 17 dipping cycles. Each CV was recorded with the porphyrin as the outermost layer**.** Bottom: Details of the oxidation peaks. Reduction peak: -325 mV; Oxidation peaks: -495 mV, -270 mV, +23 mV vs. Ag/AgCl. pH=3, for the electrolytic solution.

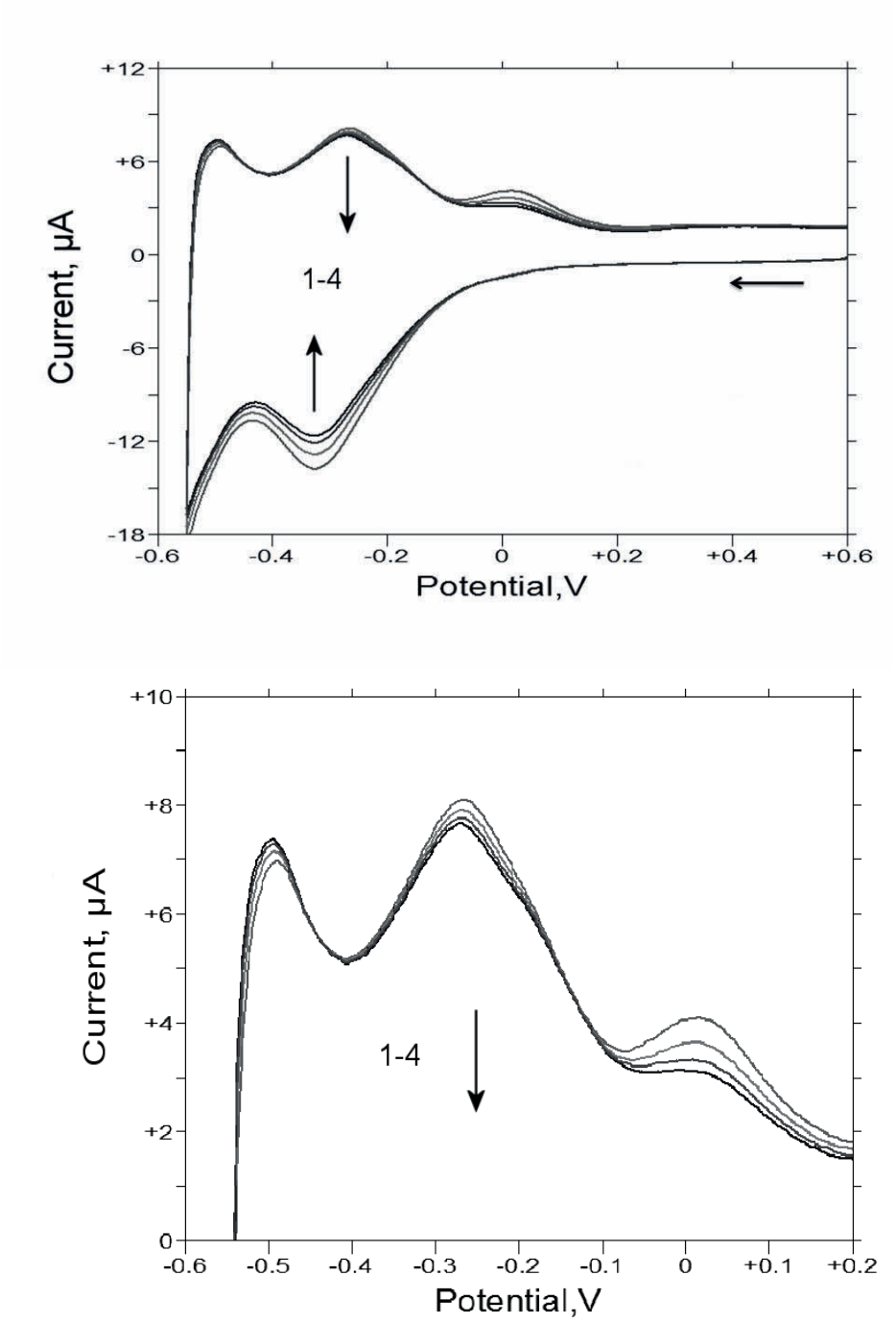

Figure 3.5: Top: The initial four potential scans of a film built on ITO after 10 deposition sequences with the POM added last shows that the current decreases. The diminishment of the peak currents stop after four CV scans with the fifth scan (see Figure 3.3) overlapping the fourth. Bottom: Details of the oxidation peaks. Reduction peak: -325 mV; Oxidation peaks: -495 mV, - 270 mV, +23 mV vs. Ag/AgCl. pH=3, for the electrolytic solution.

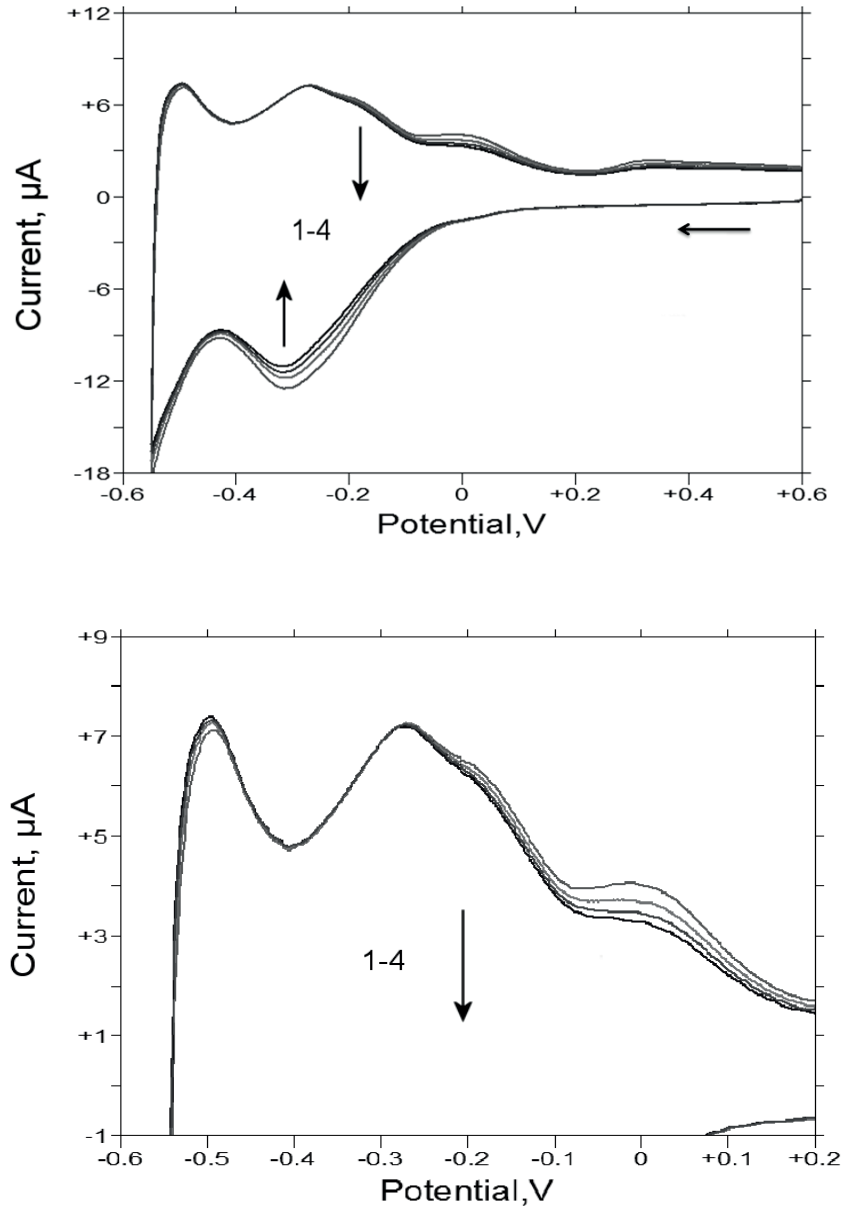

Figure 3.6: Top: The initial four potential scans on a film built on ITO after 11 deposition sequences with porphyrin added last shows that the current decreases. The diminishment of the peak currents stop after four polarization scans with the fifth scan (see Figure 3.4) overlapping the fourth. Bottom: Details of the oxidation peaks. Reduction peak: -325 mV; Oxidation peaks: -495 mV, -270 mV, +23 mV vs. Ag/AgCl. pH=3, for the electrolytic solution.

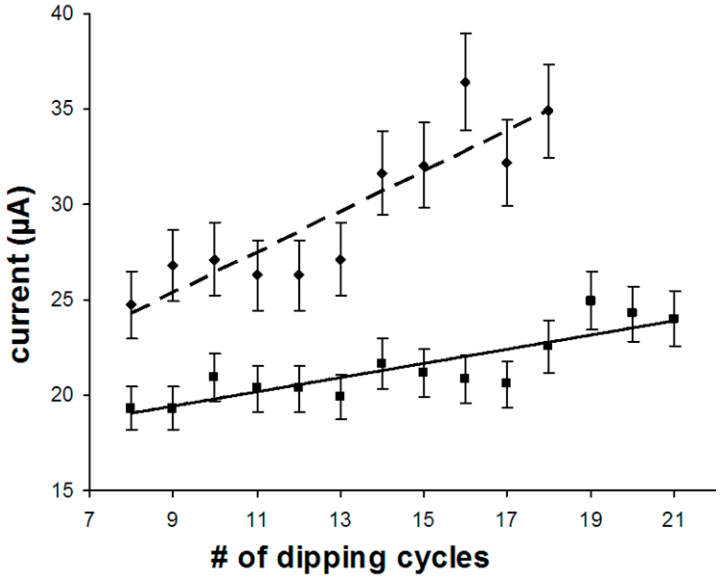

Figure 3.7: Oxidation peak current at -270 mV when (----) POM is the last material deposited (slope = 1.07), and (—) when the porphyrin is the last material deposited (slope = 0.37). These Plots are from CV data similar to what is shown in Figures 3.3 and 3.4. Error bars represent the average of four experiments. Data are recorded on the 5th CV scan. Taken from reference 1.

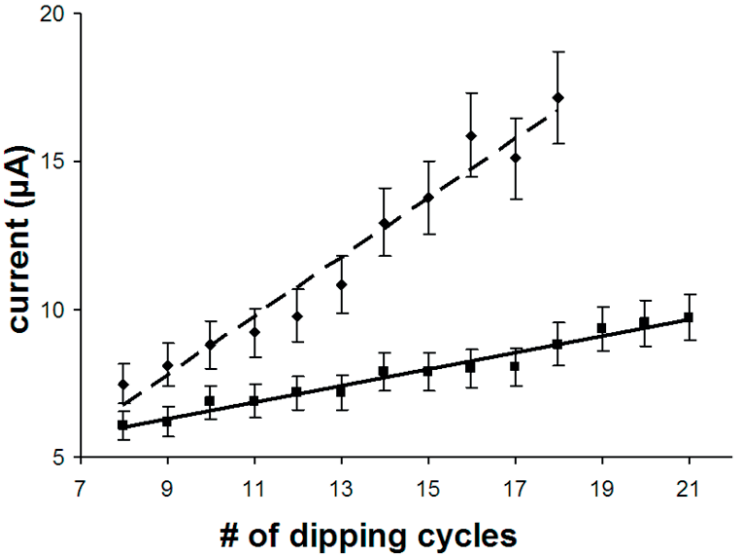

Figure 3.8: Absolute value of the reduction peak current at -325 mV when (-----) POM is the last material deposited (slope = 0.97), and (—) when the porphyrin is the last material deposited (slope = 0.28). These Plots are from CV data similar to what is shown in Figures 3.3 and 3.4. Error bars represent the average of four experiments. Data are recorded on the 5th CV scan. Taken from reference 1.

For the solution phase CV the pH of both the POM and the porphyrin solutions were adjusted to pH=3. CV experiments on the films were done when the electrolyte solutions were adjusted to pH=4 and pH=5. No resolved peak currents were observed at either of these pH values using a working potential window of -550 mV to +800 mV. At pH=4, two irreversible oxidation peaks start to appear when the POM is added last to the film. (See appendix Figures A3.3 and A3.4)

3.4 Conclusion

We have avoided the use of the word "layer" to describe the $TMPyP^{4+}$ /POM films because any given dipping of the substrate into either the POM or porphyrin solution does not form a complete layer. The CV peaks for both the porphyrin and the POM indicates that both species have access to the electrode surface. Nonetheless the sequential dipping deposition processes, which are analogous to the layer-by-layer fabrication of films, can be successfully adopted for the formation of chemically modified electrodes, without any previous preparation of the electrode surface and using two electroactive small molecules. There is no *a priori* need for either cyclic potential scans or polymeric materials (e.g. polycationic or polyanionic) to affect the deposition of thin films consisting of porphyrins and POM.

The electrochemical responses of the film correspond to the sum of the individual components – the porphyrin and the POM. After the first few deposition cycles necessary to reach a complete coverage of the electrode surface, there is no influence of the film thickness on the electrochemical potentials of the components on the modified electrode. Small increases in the currents are observed for each deposition cycle. This indicates that the electron transfer is still possible in the 2-30 nm films. The dielectric properties of the $TMPyP^{4+}$/POM films are

markedly different than films containing polyelectrolyte materials because there is a greater charge density. In order for the electron transfer to go from the electrode to the film surface, a possible electron-hopping mechanism may be involved where electron exchange between neighboring redox sites results in "percolation" of electrons through the material under the influence of a chemical potential.(*31*) Though the $TMPyP^{4+}$ has an irreversible reduction at -605 mV (versus Ag/AgCl), this is not observed in the porphyrin/POM films, thus the films confer some stability to the macrocycle. Similarly formed porphyrin/POM films have demonstrated catalytic activity,(*7, 25, 32-34*) and can serve as electrochemical sensors.(*13, 20, 35*) Small changes in the electrolyte pH (e.g. 2.5 versus 3.0) shift the observed electrochemical oxidation and reduction potentials such that this may be exploited for these applications.

Porphyrins are used as photosensitizers, therefore stimulating catalytic processes by visible light irradiation could change the electrochemical behavior of the film. Catalytic studies on a composite organic/inorganic material formed by association of metalloporphyrins and POM showed that this material has more efficient catalytic properties than the corresponding metalloporphyrins alone, and that the POM contributed to the stabilization of the metalloporphyrin against deactivation during the catalytic cycles.(*34*) Hence, the sequential dipping method using porphyrins and polyoxometalates can be a very simple and economic technique to fabricate supported catalysts (with the advantages of heterogeneous catalysis) and sensors.

The $[Fe(III)TMPyP]^{5+}$ also can be used in the above sequential dipping fabrication process as indicated by the linear increase in the UV-visible absorption of the films with increasing rounds of deposition. Since metalloporphyrins are good catalysts and these films are robust to immersion in organic solvents, perhaps these films can be exploited for a diverse array

of organic transformations or for assays of organic species in water, such that the oxidative or reducing equivalents come from the electrode rather than a stoichiometric chemical reagent. Also, the large extinction coefficients of porphyrinoids may facilitate photocatalysis by either the POM or the stabilized porphyrin.

3.5 Appendix

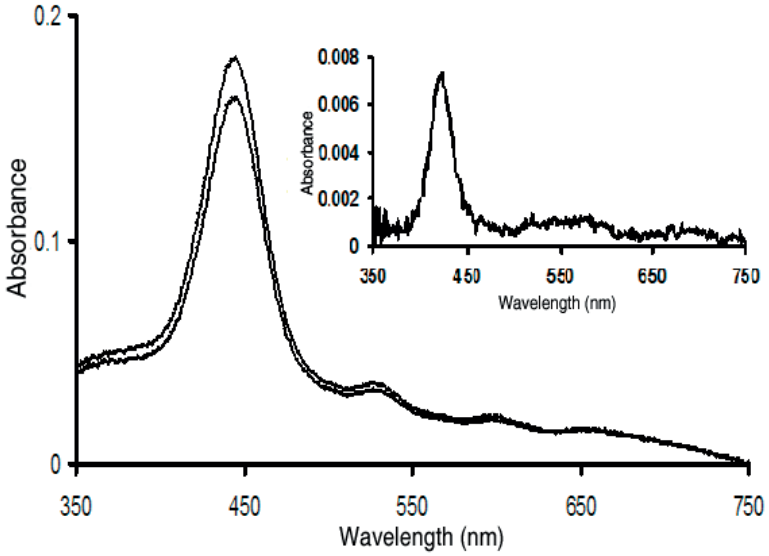

Figure A3.1: UV-visible studies of films fabricated from 16 porphyrin/POM dipping sequences on ITO before (—) and after (---) CV studies shows that ca. 9% of the porphyrin is removed and no obvious porphyrin decomposition products such as chlorins or dipyrromethanes. Inset: UV-visible spectra of the electrolyte solution (0.1 mol/L NaCl) after 16 CV scans. Taken from reference 1.

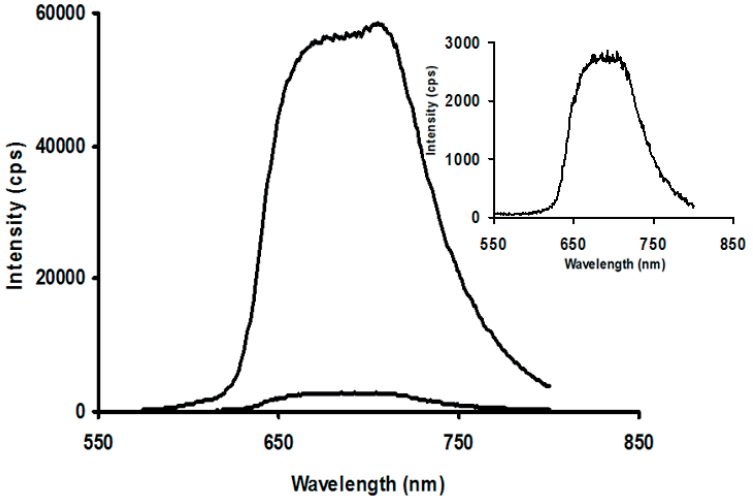

Figure A3.*2:* Fluorescence spectra of the ITO surface with 16 alternating depositions of porphyrin and POM and of the electrolyte solution after the CV analysis was done. The large emission peak is for the porphyrin on ITO surface and the small emission peak is for the porphyrin in the electrolyte solution, where the inset is an expanded plot of electrolyte solution emission peak. Taken from reference 1.

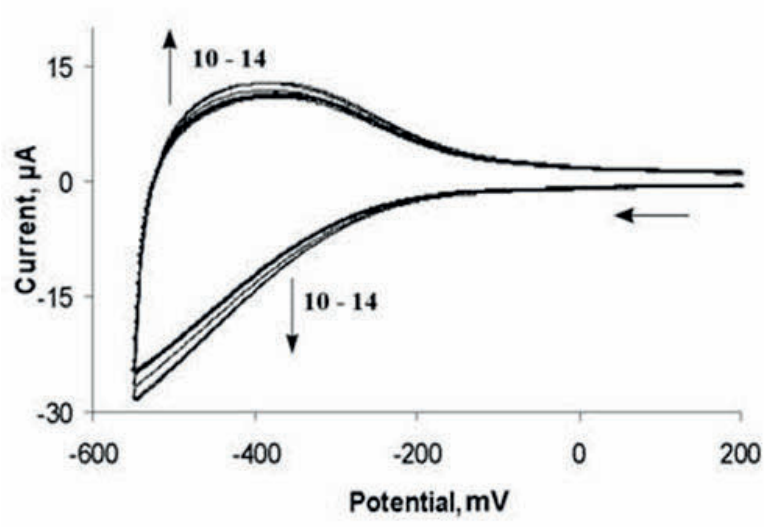

Figure A3.3: Cyclic voltammogram of films built on ITO using $TMPyP^{4+}$ and $SiW_{12}O_{40}^{4-}$ with 10-14 dipping cycles. Each CV was recorded with POM as the outermost layer. CV data was recorded when the electrolyte solution has a pH=5, keeping the other experimental parameters same. Taken from reference 1.

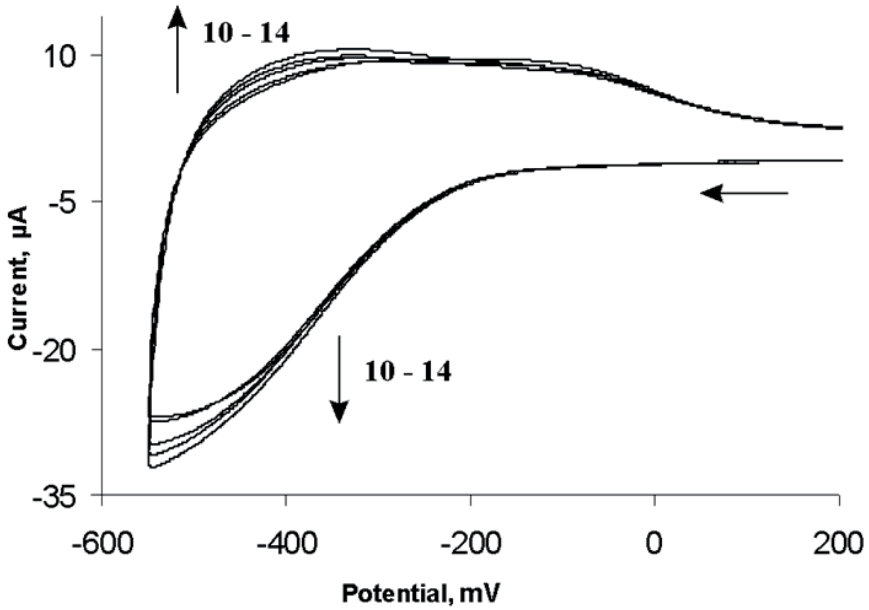

Figure A3.4: Cyclic voltammogram of films built on ITO using $TMPyP^{4+}$ and $SiW_{12}O_{40}^{4-}$ with 10-14 dipping cycles. Each CV was recorded with POM as the outermost layer. CV data was recorded when the electrolyte solution has a pH =4, keeping the other experimental parameters same. Taken from reference 1.

3.6 References

1. Bazzan, G., Aggarwal, A., and Drain Charles, M. (2011) Electrochemical Studies of Self-Organized Porphyrin-Polyoxometalate Films on ITO, In *Interfaces and Interphases in Analytical Chemistry* (Helburn, R., and Vitha, M. F., Eds.), pp 167-184, American Chemical Society, Washington, DC.
2. Mitzi, D. B. (2001) Thin-Film Deposition of Organic-Inorganic Hybrid Materials, *Chem. Mater. 13*, 3283-3298.
3. Katsoulis, D. E. (1998) A Survey of Applications of Polyoxometalates, *Chem. Rev. 98*, 359-388.
4. Cheng, Z., Cheng, L., Gao, Q., Dong, S., and Yang, X. (2002) Characterization of organic-inorganic multilayer films by cyclic voltammetry, UV-Vis spectrometry, X-ray photoelectron spectroscopy, small-angle X-ray diffraction and electrochemical impedance spectroscopy, *J. Mater. Chem. 12*, 1724-1729.
5. Martel, D., and Gross, M. (2007) Electrochemical study of multilayer films built on glassy carbon electrode with polyoxometalate anions and two multi-charged molecular cationic species, *J. Solid State Electrochem. 11*, 421-429.
6. Moriguchi, I., and Fendler, J. H. (1998) Characterization and Electrochromic Properties of Ultrathin Films Self-Assembled from Poly(diallyldimethylammonium) Chloride and Sodium Decatungstate, *Chem. Mater. 10*, 2205-2211.
7. Sadakane, M., and Steckhan, E. (1998) Electrochemical Properties of Polyoxometalates as Electrocatalysts, *Chem. Rev. 98*, 219-238.
8. Dong, S., and Wang, B. (1992) *Electrochimica Acta 37*, 11-16.
9. Keita, B., and Nadjo, L. (1988) *J. Electroanal. Chem. 240*, 325-332.
10. Keita, B., and Nadjo, L. (1987) New aspects of the electrochemistry of heteropolyacids : Part II. Coupled electron and proton transfers in the reduction of silicoungstic species, *J. Electroanal. Chem. 217*, 287-304.
11. Ariga, K., Hill, J. P., and Ji, Q. (2007) Layer-by-Layer assembly as a versitale bottom-up nanofabrication technique for exploratory research and realistic application, *Phys. Chem. Chem. Phys.*, 2319-2340.

12. Lowman, G. M., Tokuhisa, H., Lutkenhaus, J. L., and Hammond, P. T. (2004) Novel Solid-State Polymer Electrolyte Consisting of a Porous Layer-by-Layer Polyelectrolyte Thin Film and Oligoethylene Glycol, *Langmuir 20*, 9791-9795.
13. Zhao, W., Xu, J.-J., and Chen, H.-Y. (2006) Electrochemical Biosensors Based on Layer-by-Layer Assemblies, *Electroanalysis 18*, 1737-1748.
14. Liu, S., Volkmer, D., and Kurth, D. G. (2003) Functional Polyoxometalate Thin Films via Electrostatic Layer-by-Layer Self-Assembly, *J. Cluster Sci. 14*, 405-419.
15. Shen, Y., Liu, J., Jiang, J., Liu, B., and Dong, S. (2002) Fabrication of Metalloporphyrin-Polyoxometalyte Hybrid Film by Layer-by-Layer Method and Its Catalysis for Dioxygen Reduction, *Electroanalysis 14*, 1557-1563.
16. Shen, Y., Liu, J., Jiang, J., Liu, B., and Dong, S. (2003) Fabrication of a Metalloporphyrin-Polyoxometalate Hybrid Film by a Layer-by-Layer Method and Its Catalysis for Hydrogen Evolution and Dioxygen Reduction, *J. Phys. Chem. B. 107*, 9744-9748.
17. Wang, Y., Wang, X., and Hu, C. (2002) Layer-by-Layer Self-Assembled Ultrathin Multilayer Films of Lanthanide Polyoxometalates and Poly(allylamine Hydrochloride) and Their Photoluminescent Properties, *J. Colloid Interface Sci. 249*, 307-315.
18. Drain, C. M., Varotto, A., and Radivojevic, I. (2009) Self-Organized Porphyrinic Materials, *Chem. Rev. 109*, 1630-1658.
19. Beletskaya, I., Tyurin, V. S., Tsivadze, A. Y., Guilard, R., and Stern, C. (2009) Supramolecular Chemistry of Metalloporphyrins, *Chem. Rev. 109*, 1659-1713.
20. Malinski, T. (2000) Porphyrin-Based Electrochemical Sensors, In *The Porphyrin Handbook* (Kadish, K. M., Smith, K. M., and Guilard, R., Eds.), Academic Press, New York.
21. Bazzan, G., Smith, W., Francesconi, L. C., and Drain, C. M. (2008) Electrostatic Self-Organization of Robust Porphyrin-Polyoxometalate Films, *Langmuir 24*, 3244-3249.
22. Drain, C. M., Batteas, J. D., Flynn, G. W., Milic, T., Chi, N., Yablon, D. G., and Sommers, H. (2002) Designing supramolecular porphyrin arrays that self-organize into nanoscale optical and magnetic materials, *Proc. Natl. Acad. Sci. U. S. A. 99*, 6498-6502.

23. Drain, C. M., Bazzan, G., Milic, T., Vinodu, M., and Goeltz, J. C. (2005) Formation and Applications of Stable 10 nm to 500 nm Supramolecular Porphyrinic Materials, *Israel J. Chem. 45*, 255-269.

24. Drain, C. M., and Chen., X. (2004) Self-Assembled Porphyrinic Nanoarchitectures, In *Encyclopedia of Nanoscience & Nanotechnology* (Nalwa, H. S., Ed.), pp 593-616, American Scientific Press, New York, NY.

25. Drain, C. M., Goldberg, I., Sylvain, I., and Falber, A. (2005) Synthesis and applications of supramolecular porphyrinic materials, *Top. Curr. Chem. 245*, 55-88.

26. Drain, C. M., Nifiatis, F., Vasenko, A., and Batteas, J. D. (1998) Porphyrin tessellation by design: Metal mediated self-assembly of large arrays and tapes, *Angew. Chem., Int. Ed. 37*, 2344-2347.

27. Kadish, K. M., Caemelbecke, E. V., and Royal, G. (2000) Electrochemistry of Metalloporphyrins in Nonaqueous Media, In *The Porphyrin Handbook* (Kadish, K. M., Smith, K. M., and Guilard, R., Eds.), Academic Press, New York.

28. Shen, Y., Liu, J., Wu, A., Jiang, J., Bi, L., Liu, B., Li, Z., and Dong, S. (2003) Preparation of Multilayer Films Containing Pt Nanoparticles on a Glassy Carbon Electrode and Application as Electrocatalyst for Dioxygen Reduction, *Langmuir 19*, 5397-5401.

29. Neri, B. P., and Wilson, G. S. (1972) Electrochemical studies of mesotetra(4-N-methylpyridyl)porphine in acid solution, *Anal. Chem. 44*, 1002-1009.

30. Laviron, E. (1983) Electroanalytical Chemistry, Vol. 12, Marcel Dekker, New York, NY.

31. Laurent, D., and Schlenoff, J. B. (1997) Multilayer assemblies of redox polyelectrolytes, *Langmuir 13*, 1552-1557.

32. Maldotti, A., Molinari, A., Argazzi, R., Amadelli, R., Battioni, P., and Mansuy, D. (1996) Redox properties of photoexcited $(nBu_4N)_3PW_{12}O_{40}/Fe^{III}$ porphyrins composite systems, *J. Mol. Catal. A: Chem. 114*, 141-150.

33. Mayer, I., Nakamura, M., Toma, H. E., and Araki, K. (2006) Multielectronic redox and electrocatalytic supramolecular films based on a tetraruthenated iron porphyrin, *Electrochim. Acta 52*, 263-271.

34. Santos, I. C. M. S., Rebelo, S. L. H., Balula, M. S. S., Martins, R. R. L., Pereira, M. M. M. S., Simoes, M. M. Q., Neves, M. G. P. M. S., Cavaleiro, J. A. S., and Cavaleiro, A. M.

V. (2005) Association of Keggin-type anions with cationic meso-substituted porphyrins: synthesis, characterization and oxidative catalytic studies, *J. Mol. Catal. A: Chem. 231*, 35-45.

35. Han, B. H., Manners, I., and Winnik, M. A. (2005) Oxygen Sensors Based on Mesoporous Silica Particles on Layer-by-Layer Self-assembled Films, *Chem. Mater. 17*, 3160-3171.

CHAPTER 4: PHOTOPHYSICAL STUDIES OF SELF-ASSEMBLED CAGES OF PORPHYRINS APPENDED WITH HYDROGEN BONDING MOTIFS[a]

Abstract

Photophysical properties of Porphyrinoids bearing four rigid hydrogen bonding motifs on the *meso* positions, self-assembled into a cofacial cage with four complementary bis(decyl)melamine units in dry solvents are presented here. Self-assembly was investigated by NMR spectroscopy, dynamic light scttering, and atomic force microscopy. The phototphysical properties of the cage formation involves the measurement of their absorption and emission spectra and the fluorescenece lifetime in dry THF. The hydrocarbon chains on the bis(decyl)melamine mediate the formation of nanofilms on surfaces as the solvent slowly evaporates.

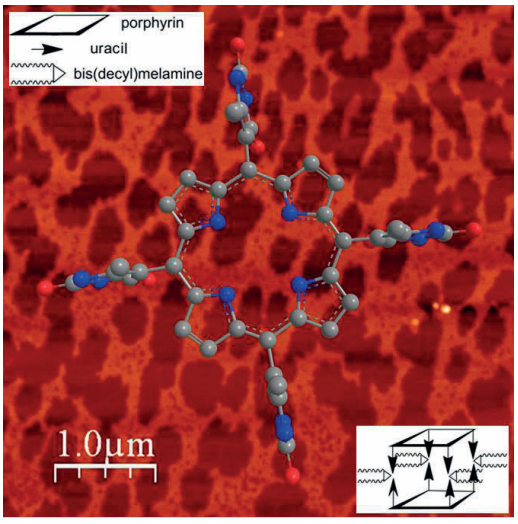

[a] This Chapter is adapted from "Hierarchical Organization of a Robust Porphyrin Cage Self-Assembled by Hydrogen Bonds", Sunaina Singh, Amit Aggarwal, Christopher Farley, Brian A. Hageman, James D. Batteas, and Charles Michael Drain, *Chem. Commun.*, **2011**, 47, 7134-7136.

4.1 Introduction

From the very beginnings of human civilization, people have been using solar energy. There are so many different ways to use solar power today: e.g. solar thermal, photovoltaic, photocatalytic. One of the most natural ways to convert solar energy is mediated by photosynthesis. Light-harvasting by pigments, such as chlorophyll, involves electron transfer in the primary step of photosynthesis and also in artificial devices for solar energy conversion, like photovoltaic cells.(*1-4*) Photosynthetic antenna complexes contain self-assembled arrays of pigments in a precise architecture, thus supramolecular porphyrin arrays are also studied as model systems for light harvesting.(*5*) Supramolecular chemistry of porphyrinic systems is extraordinarily diverse because the rigidity of the macrocycle offers a variety of topologies and their photophysical and chemical properties can be easily modulate by appending different groups on the periphery of the macrocycle. Self-assembly and self-organization of porphyrinoids(*6-8*) continue to produce functional materials with a wide range of potential applications from efficient catalysts(*9*) to optical devices.(*10*) Self-assembly into specifically designed structures involves the spontaneous association of molecules through non-covalent interactions such as electrostatic interactions, π-stacking, van der Waals forces, coordination bonding, and H-bonding.(*11, 12*) Porphyrinoids appended with H-bond motifs can assemble into diverse arrangements such as rosettes, squares, tapes, and nanoparticles for materials for solar energy harvesting, photonic devices, sensors, catalysts, and understanding biological electron transport.(*13-19*) Formation of multiple H-bonds between the complementary appended H-bonding units is widely used in the fabrication of supramolecular assemblies because of their strength,

directionality, specificity, and reversibility. Responsive H-bond materials, whereby the supramolecular structure can be modulated by environmental conditions such as temperature or solvent, can find applications as catalytic hosts for specific guests, or control of electronic communication between subunits.(*20-23*) Though porphyrins bearing hydrogen bonding motifs rigidly attached to the *meso* position can be difficult to synthesize(*13-15*), they have clear utility.(*16*) Also, the supramolecular systems can be organized differently in solution compared to surfaces because both the deposition process can play pivotal role in reorganization of the material.(*24, 25*)

The porphyrins were synthesized in one step. The synthesis and characterization of porphyrins possessing four rigid uracylic hydrogen bonding units on the four *meso* positions (Scheme 4.1) was done by Sunaina Singh. These self-assemble into robust cage structures mediated by H-bonds to four complementary 2,4-di(*n*-decylamino)-6-amino-1,3,5-triazine, bis(decyl)melamine, units. The presence of H-bonding motifs on all the four meso positions of porphyrins reduced the supramolecular dynamics compared to the supramolecular organization of porphyrins appended with two such groups because all four meso positions participate in the assembly instead of two.(*13-19*) The cage formation for both the free base and zinc complexes of two different macrocycles, one with an N-alkyl group and one without, are shown in Scheme 4.2. Formation of the cages requires interconversion of the atropisomers of the uracylporphyrins. DOSY NMR (done by Sumnaina Singh), dynamic light scattering (DLS), and photophysical measurements in solution indicate the formation of the cages, and atomic force microscopy (AFM) elucidates the self-organization of the materials cast onto mica.

4.2 Experimental Details

4.2.1 Materials and Instrumentation

UV-visible spectra of were recorded on a Varian Bio3 spectrophotometer. Steady-state fluorescence spectra and fluorescence lifetimes were measured with a Fluorolog τ3 TCSPC (time correlated single photon counting) from Jobin-SPEX Instrument S. A., (Horiba Scientific. Inc.) Dynamic light scattering (DLS) used a Precision Detector PD2000DLS Cool-Batch instrument in batch mode at 25 ^{o}C to determine size of the aggregates and cage. All reagents were obtained from commercial sources and used without purification.

4.2.2 Synthesis of Porphyrins[b]

Uracylporphyrin **1b** and *N*-alkyluracyl porphyrin **2b** are synthesized from 5-formyl-6-methyluracil and 1-ethoxymethyl-5-formyl-6-methyluracil(*17-23, 26, 27*) using Adler conditions with $Zn(OAc)_2$. *N*-alkylation of the uracil inhibits tautomerization at this position, diminishes unproductive H-bond formation, and improves solubility. Thus, we focus on these porphyrins herein. The free bases, **1a** and **2a**, are formed by demetallation reactions. The 2,4-di(*n*-decylamino)-6-amino-1,3,5-triazine: bis(decyl)melamine, was prepared similarly to literature methods(*28-30*) from 2-amino-4,6-dichloro-1,3,5-triazine, which was prepared from cyanuric chloride.(*31*)

[b] Synthesis of all compounds and NMR studies were done by Sunaina Singh.

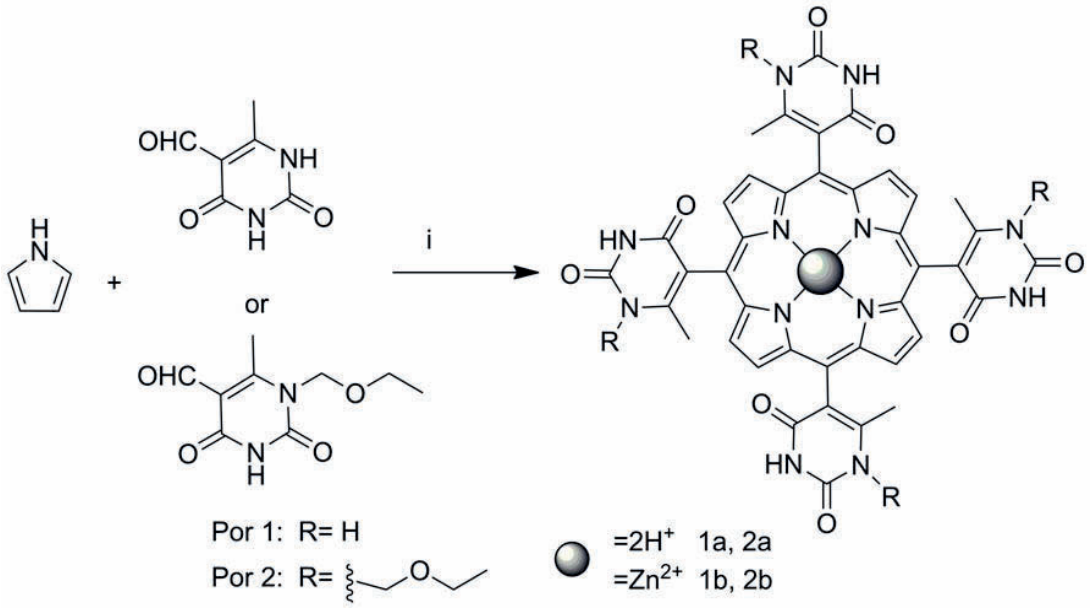

Scheme 4.1. (i) reflux 10 h in 10% nitrobenzene in acetic acid with 0.05 M $Zn(OAc)_2$. The porphyrin is prepared as a mixture of the four atropisomers (α^4, $\alpha^3\beta$, $\alpha^2\beta^2$, $\alpha\beta\alpha\beta$) since the uracyl moieties are nominally orthogonal to the macrocycle plane.

4.2.3 Atomic Force Microscopy (AFM) Studies[c]

All samples were prepared in the following manner: freshly cleaved sheets of mica, approximately 2.5 x 2.5 cm, were placed in a clean Petri dish on a flat surface. For each sample, the given solution was drawn up into a pipet, and then a single drop was drop cast onto mica square. In the voids between the samples, dry THF was deposited via pipet, taking care that the THF did not contact any of the samples. A watch glass was then placed over the Petri dish, sealing the environment so the evaporating THF could not escape. The samples were allowed to sit for 24 hrs, and then examined using an Asylum Research MFP-3D™ Stand Alone AFM. Images collected from the AFM were analyzed using a program called "WSxM 4.0 Develop 11.4", developed by Nanotec Electronica S.L.

[c] AFM studies were done by Brian A. Hageman.

4.2.4 Photophysical Studies

The porphyrinoids **1a** and **1b** are poorly soluble in dry THF, while **2a** and **2b** have better solubility in this solvent. The solutions were 38-42 μM in porphyrin. To accelerate the dissolution of **1a** and **1b** for the H-bond formation with bis(decyl)melamine, the solutions were sonicated for ca. five minutes and then transferred to a 3.5 mL quartz cuvette. N_2 gas was then purged through the mixture solution for ca. 10 minutes to make sure the complete removal of air or moisture from the solution. The 1.00 cm cuvette was then sealed with a Teflon cap and wrapped with parafilm to make sure the system is closed. The UV-visible absorption spectra, fluorescence emission spectra, and lifetime measurements were recorded at room temperature for a few days until equilibrium was observed. Time correlated single photon counting (TCSPC) fluorescence lifetime measurements used a 405 nm NanoLED laser, average power 13.6 pJ/pulse with a source pulse width <200ps to excite the molecules and ~200 ps is the instrument response. The detection monochromator was set at 405 nm with a 2 nm band-pass. The data was fit with the program available with the instrument. The decay was recorded at 651 nm. The solutions were then heated continuously for couple of hours and spectra were recorded. The UV-visible and emission spectra of all the porphyrins by themselves exhibit the aggregation but do not change after one day (see appendix).

4.3 Result and Discussion

Synthesis of Porphyrins and Atropisomerism[b]: Two zinc porphyrinic systems appended with four rigid H-bonding motifs on the meso positions: Uracylporphyrin **1b**, and N-alkyl uracylporphyrin **2b,** were synthesized. Their free base derivatives

were prepared by demetallation reaction. Characterization of these porphyrinic system were done by NMR spectroscopy and mass spectral studies. Porphyrins **1** and **2** shows atropisomerism due to the hindered rotation between the meso carbon atom of the porphyrin attached with the uracylic carbon atom. The hindered rotation arises due to interactions between 6-methyl group of uracyl molecule with β-pyrrolic H-atoms, where the rotational barrier was determined for porphyrin **2b** by doing the variable temperature NMR.(*32*) $\Delta G^{\neq}$ was found to be about 123 kJ/mol in CD_3OD for **2b**, and for $\Delta G^{\#}$ for **2a** is estimated to be about 102 kJ/mol.(*33-35*) The formation of the cage removes the α^4 atropisomer from the equilibrating solution thereby increasing the yield of the cage.(*36*) The self-assembled cage formation was characterized by the NMR chemical shifts of the uracil and melamine NH protons in the H-bonds. The mass of the cages were calculated by Diffusion ordered spectroscopy (DOSY). DOSY allows the molecular weights of the assemblies to be determined(*17-23, 37-40*) For the **1b-1b** cage the estimated mass, M_w is 3360 (calculated 3295), and for **2b-2b** cage M_w is 3820 (calculated 3717). These data are reported elsewhere.

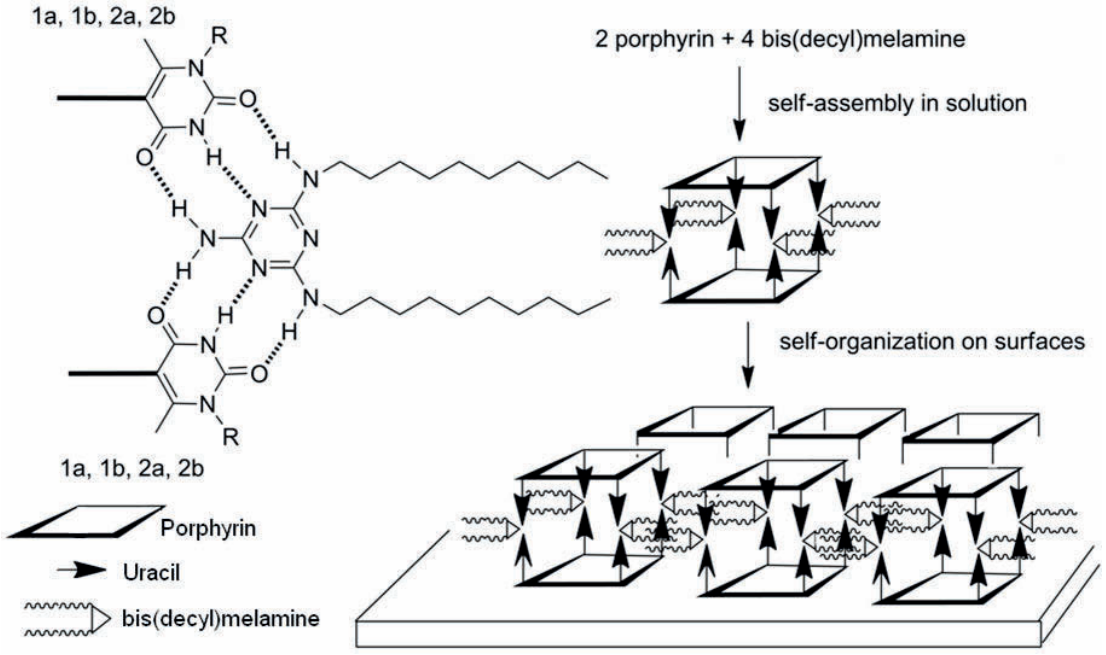

Scheme 4.2. Prolonged heating of two equivalents of one of the porphyrins in the presence of four equivalents of the H-bond complimentary bis(decyl)melamine (left) results in formation of and the α^4 atropisomer and self-assembly of the cage in solution, and the decyl groups mediate formation of monolayer films of the cage on surfaces (right).

UV-visible and Emission spectral studies: UV-visible spectra of the **2a-2a** and **2b-2b** (Figure 4.1) cages (38 μM - 42μM in porphyrin) with bis(decyl)melamine in dry THF were recorded over several days without heating. Heating at 45-47 ^{o}C for ~2 days causes an increase in the UV-visible band intensities, indicating increased solubility and a shift in the equilibrium towards formation of the α^4 atropisomer and the cages (Figure 4.1). The emission spectra of the **2a-2a** and **2b-2b** cage solutions, exciting in the Soret or Q bands, are in agreement with the UV-visible results. An initial small decrease in the fluorescence intensity due to porphyrin aggregation is followed by an increase upon formation of the more soluble cages (Figure 4.1). For the **1a-1a** and **1b-1b** the porphyrin Soret bands near 420 nm red shift by about 4 nm

with a small decrease in intensity, indicating the formation of amorphous aggregates (see appendix).

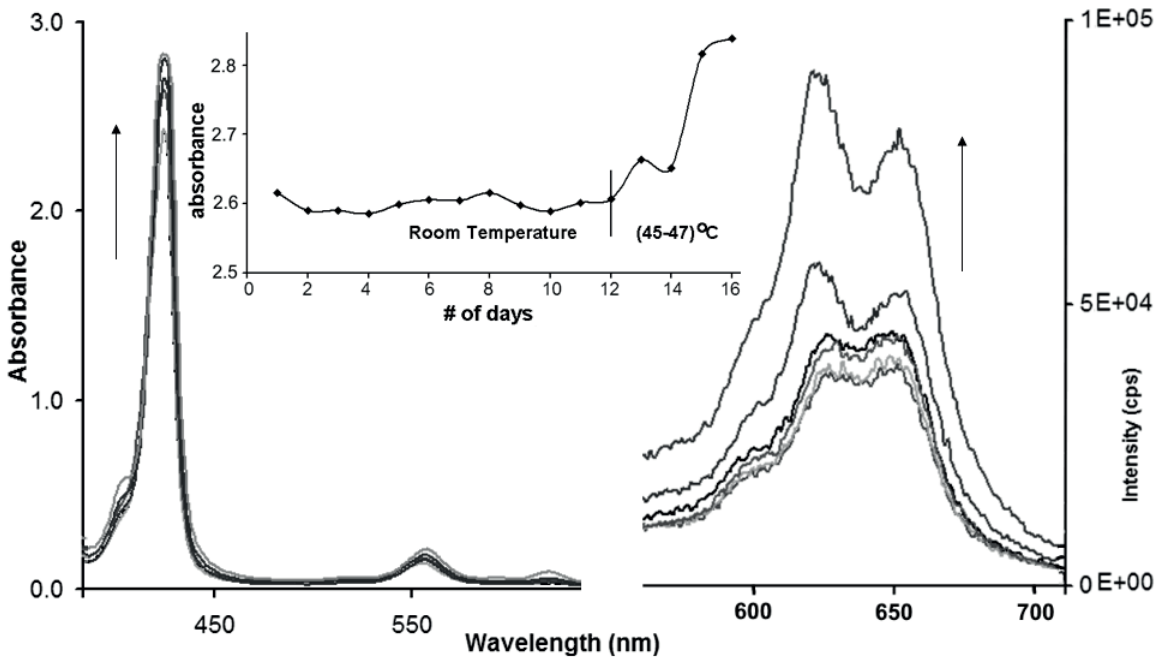

Figure 4.1. After somewhat decreasing initially due to aggregation, the intensity of the UV-visible and fluorescence spectra increase with time and heating as the amount of the self-assembled **2b-2b** cage increases. Inset: A plot of absorbance for **2b-2b** at 418 nm vs # of days.

A 1:1 mixture of free base and Zn^{2+} macrocycles, cage **2a:2b**, was also examined. At equilibrium, if the intermolecular forces that mediate the assembly are equivalent, there should be a 1:2:1 mixture of cages **2a**:**2a**, **2a**:**2b**, and **2b**:**2b**, respectively. The UV-visible spectra for this mixture shows similar trends as the above cages; the initial formation of amorphous aggregates and the more soluble cage after heating at 45-47 ^{o}C for a few days. The fluorescence spectra of cage **2a-2b** evolve in a complex manner. Initially, in the aggregation stage of the self-assembly process, some energy transfer from the metalloporphyrins to the free bases is

observed. The solution may contain more aggregates of the Zn^{2+} complexes because they are less soluble. After heating the solution, only a small amount of energy transfer is observed, which is consistent with separation of the porphyrins in the cage structure. Control experiments for **2a**, **2b**, and 1:1 mixture of **2a-2b** in dry THF without melamine shows no change in the absorption and emission spectral intensities at room temperature for few days and then upon heating at 45-47 ^{o}C for another few days.

Dynamic light scattering for size measurement: Dynamic light scattering data reveals the hydrodynamic radius of the initially formed aggregates formed for the **2a-2a, 2b-2b**, and for **2a-2b** cages to be about 42 nm, and after heating the average particle size is between 7-9 nm. There is a broad distribution of sizes for the aggregates of **1a-1a, 1b-1b,** and **1a-1b** centered at about 420 nm. The cages are found to be about 9-13 nm. Assuming extended decyl groups, an estimation of the cage dimensions from Chem 3D© is about 5.2 nm from terminal methyl to terminal methyl on opposite sides of the cage and about 2 nm perpendicular to the porphyrin planes.

Fluorescence lifetime measurement: Time correlated single photon counting experiments on these self-assembled cages were carried out in dry THF under N_2 at the same concentration used for the UV-visible studies, and 408 nm excitation (Table 4.1).

Table 4.1: Fluorescence Lifetime of Porphyrins and Cages		
Compound	τ1 (ns)	τ2 (ns)
1**a**	2.2 (19%)*	8.8 (81%)
1**b**	2.5	----------
2**a**	1.8 (5%)*	8.6 (95%)
2**b**	3.76	----------
1**a**-1**a** cage	2.8 (20%)	10.2 (80%)
1**b**-1**b** cage	2.9	----------
1**a**-1**b** cage mix	3.1 (58%)	8.6 (42%)
2**a**-2**a** cage	3.64 (11%)	9.6 (89%)
2**b**-2**b** cage	2.4	----------
2**a**-2**b** cage mix	3.5 (60%)	9.7 (40%)

*some metalloporphyrin present, 408 nm excitation, 200 ps instrument response time.

Table 4.1: Fluorescence lifetime or porphyrins and their cages were measured under N_2 using 405 nm NanoLED laser, average power 13.6 pJ/pulse with a source pulse width <200ps to excite the molecules and ~200 ps is the instrument response. The detection monochromator was set at 405 nm with a 2 nm band-pass. The data was fit with the program available with the instrument. The decay was recorded at 651 nm.

Incomplete demetalation of the Zn^{2+} complexes to form the free bases results in some of the metalloporphyrin present in the samples of **1a** and **2a**. The lifetimes for **1a**, **2a**, **1b**, **2b** are somewhat shorter than standard tetraphenylporphyrin (TPP, 11 ns) and ZnTPP (2.7 ns) under similar conditions(*41, 42*) because of some aggregation. However, the solutions with the cages, with reduced aggregation, generally display lifetimes closer to those for other meso aryl porphyrins.

AFM studies[c]*:* Self-assembled materials must interact with surfaces when incorporated into devices, we examined the self-organization of the cages into films. The supramolecular cage was drop cast from the above 30-40 μM THF solutions onto

freshly cleaved mica and imaged with AFM. The mica was placed in closed cell

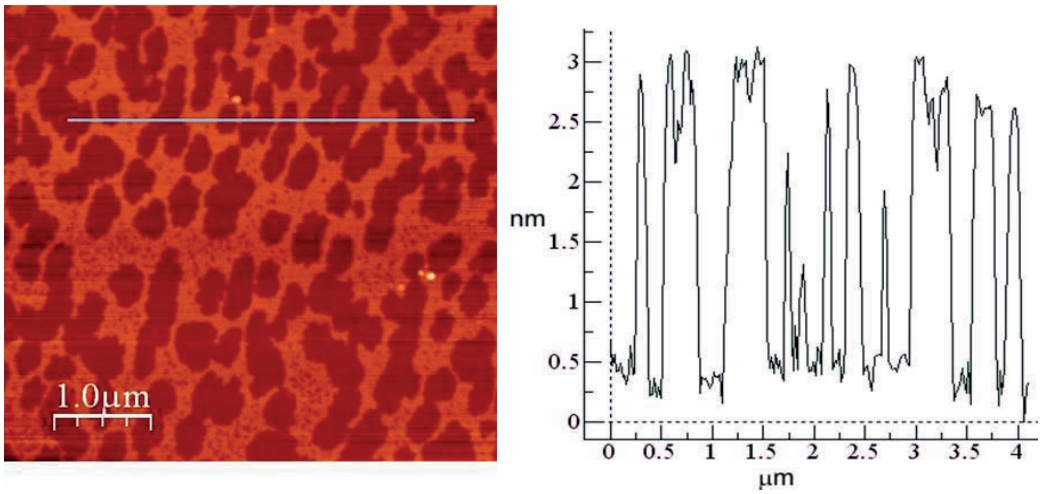

Figure 4.2. AFM of the **2a**-**2a** cage on mica (left) and height profile (right). (AFM was done by Brian A. Hageman.

culture dishes and the evaporation rate was retarded by adding the solvent to the space surrounding the sample. When the **2a**-**2a** is cast onto the mica, a film corresponding to a single layer of the cage structures is observed (Figure 4.2). In this film, the self-assembled cage is hierarchically organized by interactions between the protruding hydrocarbon chains on the four bis(decyl)melamine units.(*43*) Friction images show no indication of separation of the porphyrin and the melamine components. When the **2b**-**2b** cage is cast onto mica, somewhat thicker 12 nm films are observed, with root-mean-square roughness of about 4 nm (see appendix). The three different cages resulting from the mixture of **2a** and **2b**, yield more complex patterns on the surface. This hierarchical self-organization into films is analogous to those observed for squares of porphyrins self-assembled by coordination chemistry.(*25*)

4.4 Conclusions

The synthesis of the two presented porphyrinoids is straight forward. The two set of porphyrinoid systems appended with four rigid hydrogen bonding motifs can be used to form their supramolecular self assembled cages with four complementry bis(decyl)melamine units in solutions. The presence of bis(decyl)melamine is necessary for the cage formation as its absence results no cage formation in any case. UV-visible and emission data correlates with the NMR spectral studies. The rigid self-assembled cage formed are robust enough to allow organization on surfaces driven by the long hydrocarbon chains into nm thick films on mica. Self-assembly, in this case, turns off electronic communication between chromophores.

4.5 Appendix

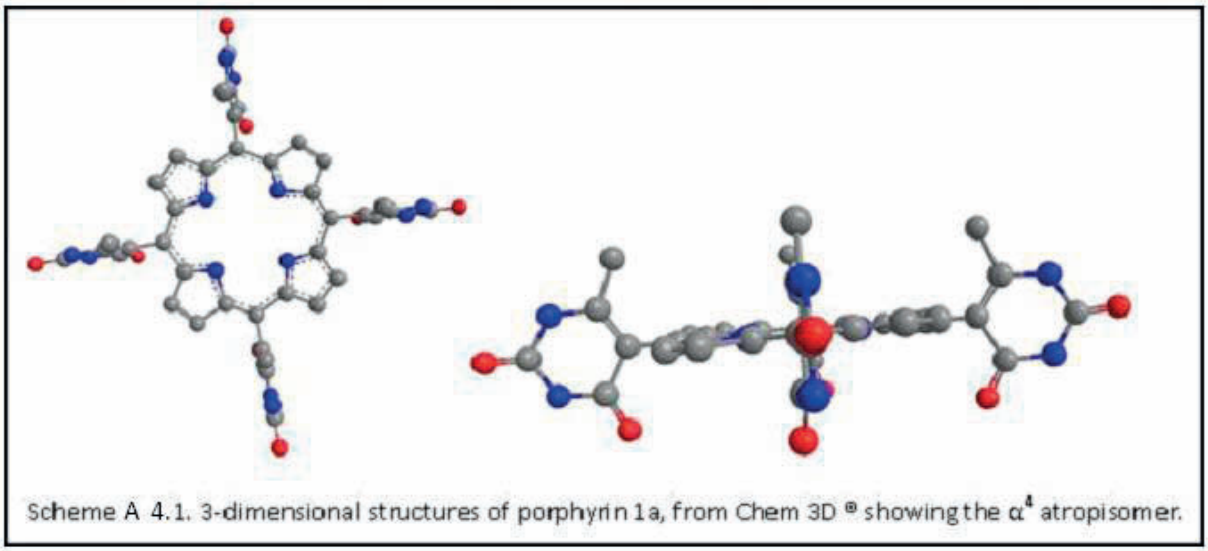

Scheme A 4.1. 3-dimensional structures of porphyrin 1a, from Chem 3D ® showing the α^4 atropisomer.

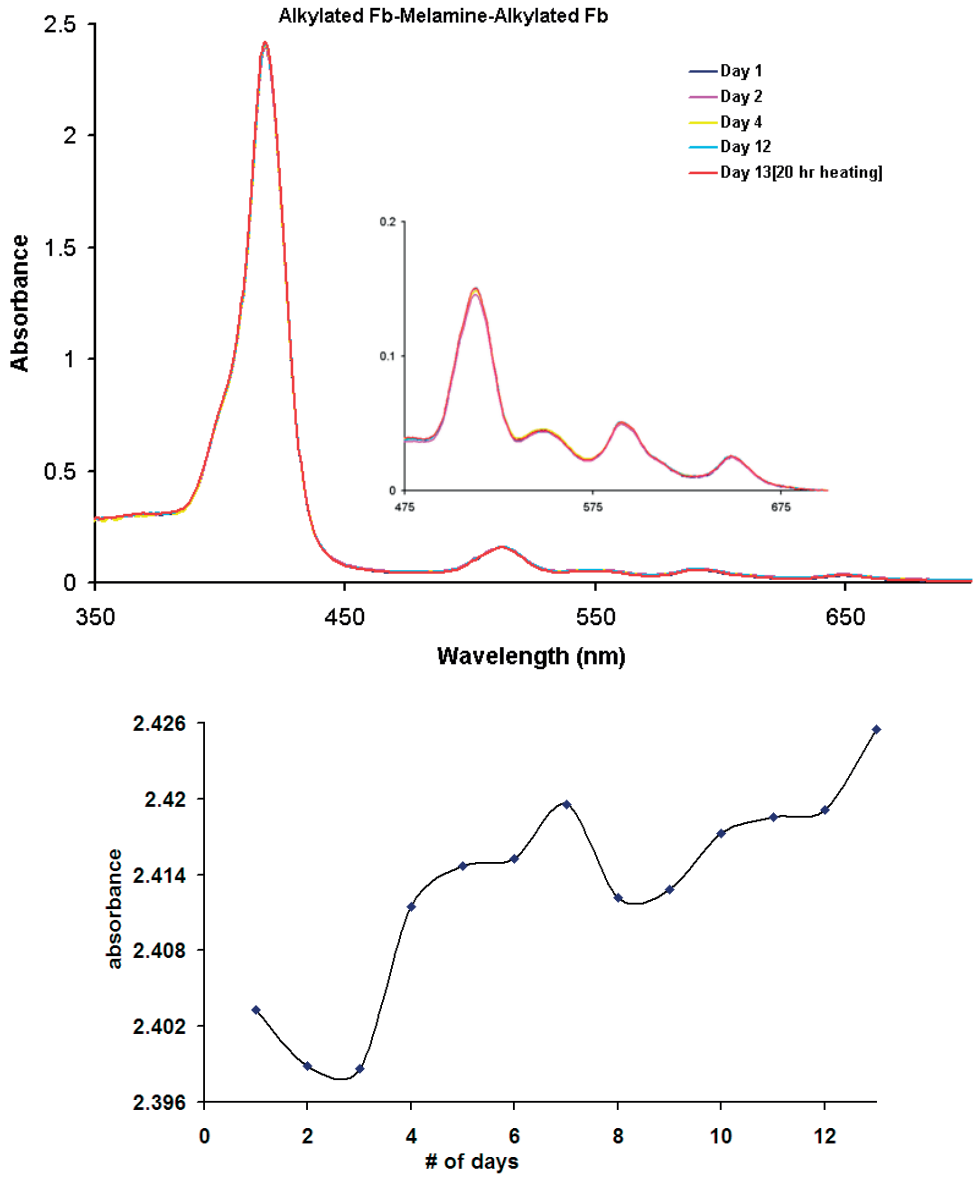

Figure A 4.1: *Top:* UV-visible absorption spectra of the cage with the alkylated free base porphyrins (**2a-2a**) with melamine in dry THF. The concentration of porphyrins in solution was 42 μM. *Bottom:* the absorption intensity decreases slightly initially, indicating the association of the porphyrin into aggregates driven by the melamine, but the after heating the sample at 45-47 ^{o}C for ~20 h, the absorption intensity increases, indicating the cage formation and increased solubility. The Soret band shifts to the red slightly for the solution containing the aggregates. In THF, the Soret band for **2a** is 422 nm and for the cage is 424 nm.

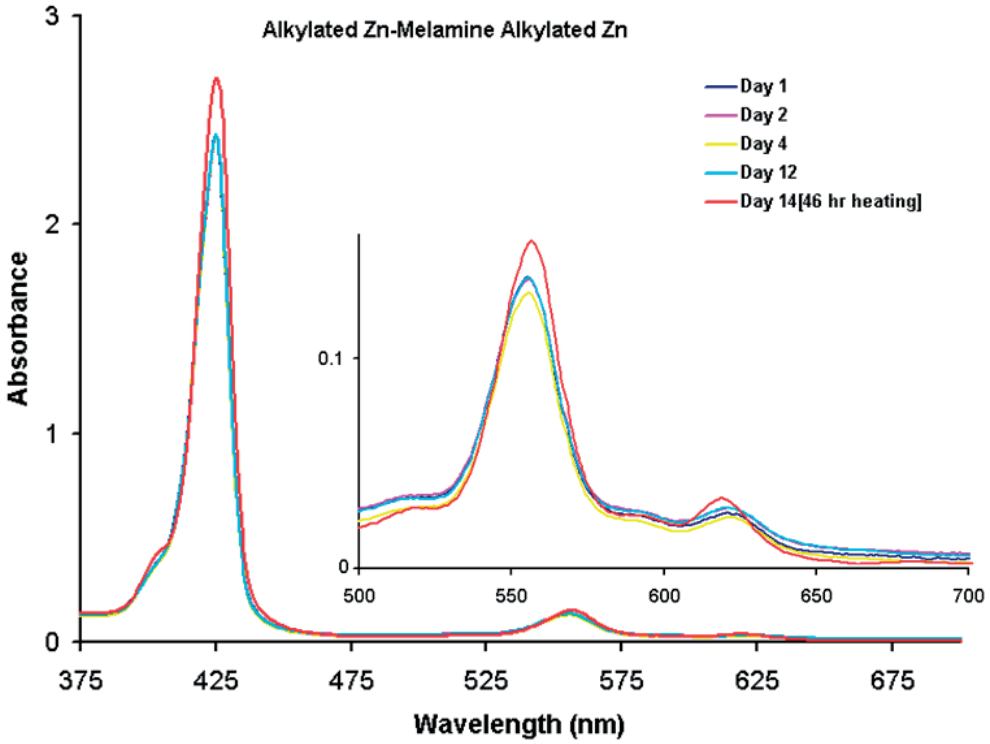

Figure A 4.2: UV-visible absorption spectra of alkylated metalloporphyrins (cage **2b-2b**) with melamine in dry THF. The concentration of the porphyrins in solution was 39 μM. The initial absorption intensity decreases because of the association on the porphyrins into aggregates driven by the melamine. After heating the sample at 45-47 ^{o}C for couple of days the absorption intensity increases, indicating increased solubility and the formation of the cage. The Soret band initially shifts to the red by 1 nm, and somewhat broadens, as expected for aggregates. The Soret band for the **2b-2b** cage is 424 nm.

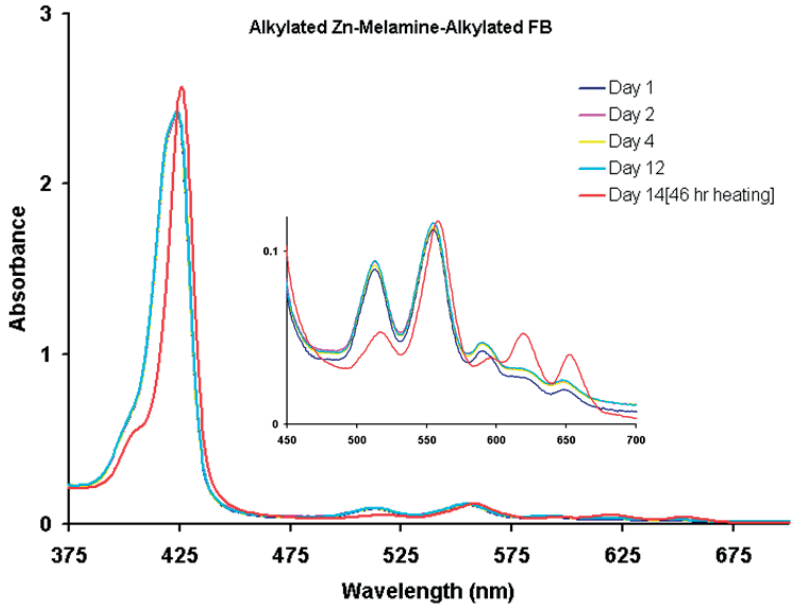

Figure A 4.3: UV-visible absorption spectra of a 1:1 mixture of the alkylated free base- and metallo- porphyrins (**2a** and **2b**) with melamine in dry THF. There is a 1:2:1 mixture of cages containing **2a-2a**, **2a-2b**, and **2b-2b**. The concentration of the porphyrins in solution was 38 μM. The absorption intensity initially decreases, indicating aggregate formation driven by the addition of the melamine. Upon heating the sample at 45-47 ^{o}C for couple of days, the absorption intensity increase, indicating increased solubility and formation of the cage. The Soret band for the mixture of supramolecular cages is at 425 nm.

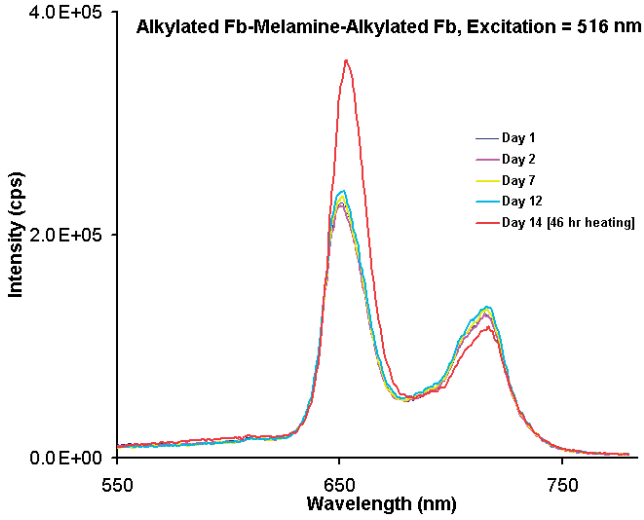

Figure A 4.4: Fluorescence emission spectra of the alkylated free base cage (**2a-2a**) with melamine in dry THF (516 nm excitation where the OD = 0.15 and band pass = 2 nm). The concentration of porphyrins in solution was 42 μM (see figure 15). The emission spectra intensity increases as the initially formed aggregates evolve into the more soluble cage structure upon heating the sample for couple of days at 45-47 ^{o}C. The emission peak shift shits to the red end by 3 nm on heating.

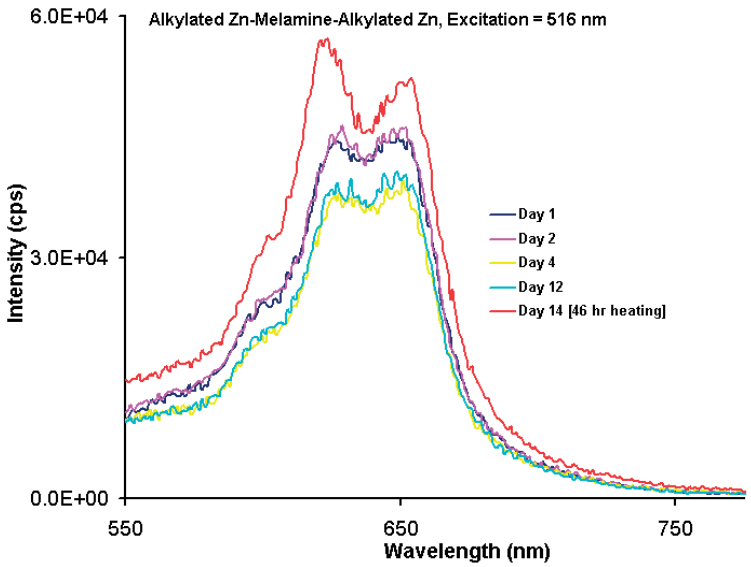

Figure A 4.5: Fluorescence emission spectra of alkylated Zn-Zn (cage **2b-2b**) with melamine in dry THF. The mixture solution was excited at 516 nm where the OD = 0.04 and band pass = 2 nm. The emission spectra intensity increases as the initially formed aggregates evolve into the more soluble cage structure upon heating the sample for couple of days at 45-47 ^{o}C.

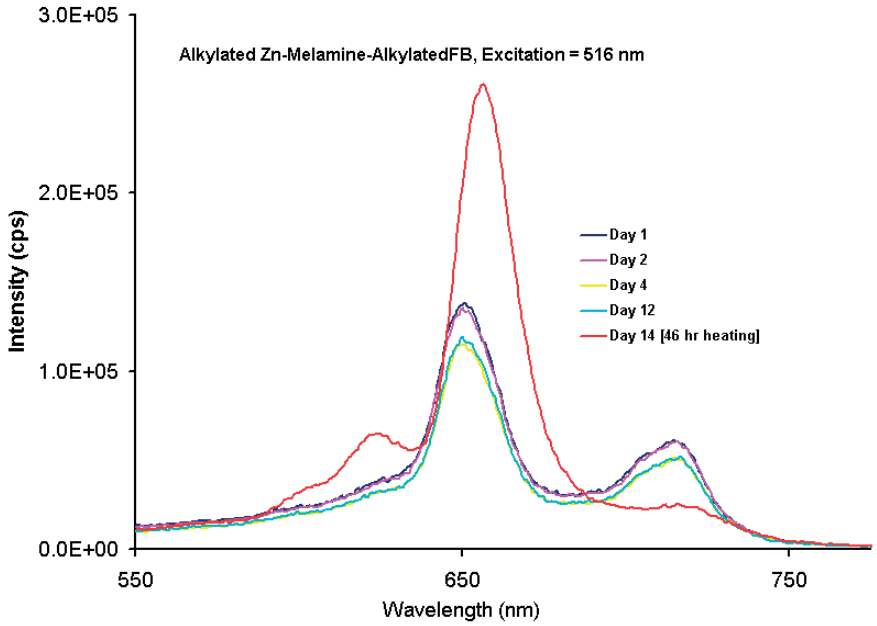

Figure A 4.6: Fluorescence emission spectra of alkylated Zn-FB (cage **2a-2b**) with melamine in dry THF. There is a 1:2:1 mixture of cages containing **2a-2a**, **2a-2b**, and **2b-2b**. The mixture solution was excited at 516 nm where the OD = 0.09 and band pass = 2 nm. At 516 nm, **2a** absorbs ~5 times more than **2b**. The emission spectra intensity increases as the initially formed aggregates evolve into the more soluble cage structure upon heating the sample for couple of days at 45-47 ^{o}C. Since **2b** is less soluble than **2a** more of **2b** is observed upon formation of the cages relative to the aggregates.

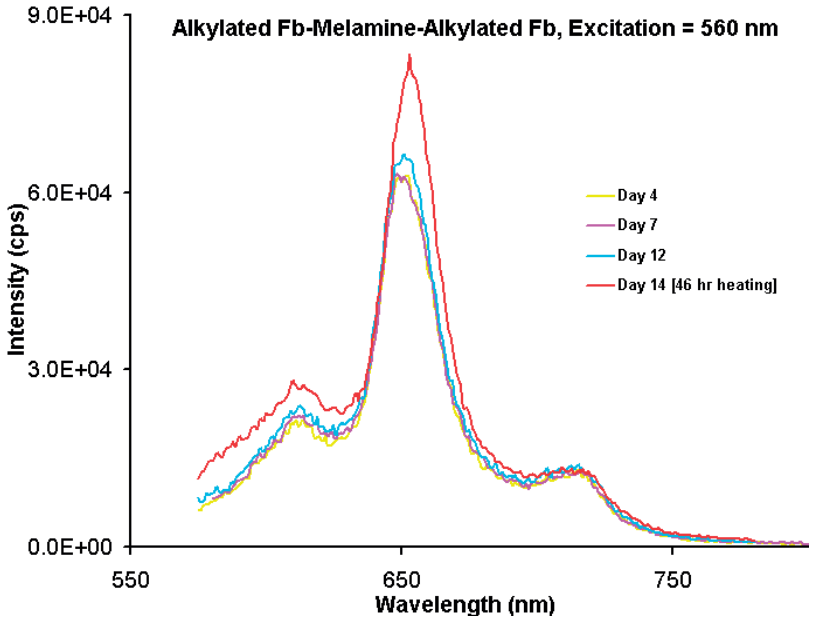

Figure A 4.7: Fluorescence emission spectra of alkylated FB-FB (cage **2a-2a**) with melamine in dry THF. The mixture solution was excited at 560 nm where the OD = 0.04 and band pass = 2 nm. The emission spectra intensity increases as the initially formed aggregates evolve into the more soluble cage structure upon heating the sample for couple of days at 45-47 ^{o}C. The emission peak shifts to the red end by 4 nm on **2a-2a** cage formation.

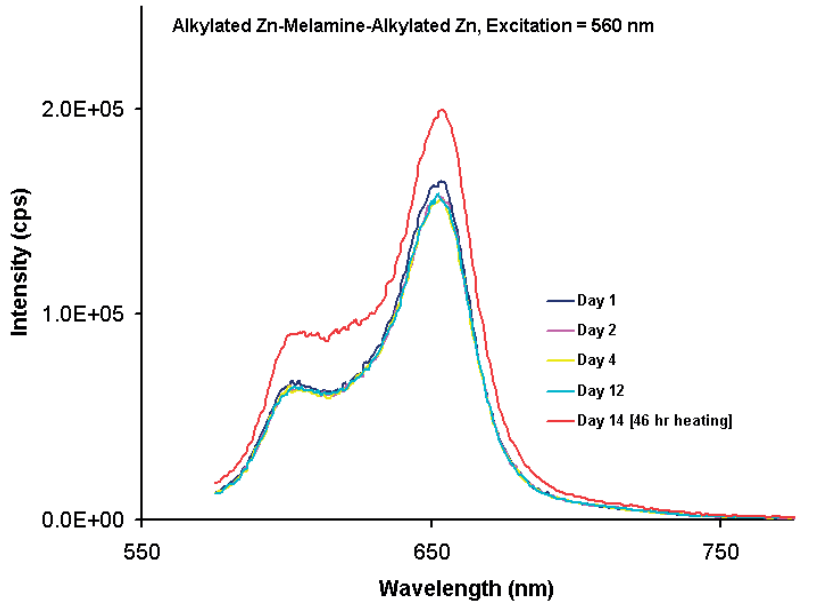

Figure A 4.8: Fluorescence emission spectra of alkylated Zn-Zn (cage **2b-2b**) with melamine in dry THF. The mixture solution was excited at 560 nm where the OD = 0.12 and band pass = 2 nm. The emission spectra intensity increases as the initially formed aggregates evolve into the more soluble cage structure upon heating the sample for couple of days at 45-47 ^{o}C.

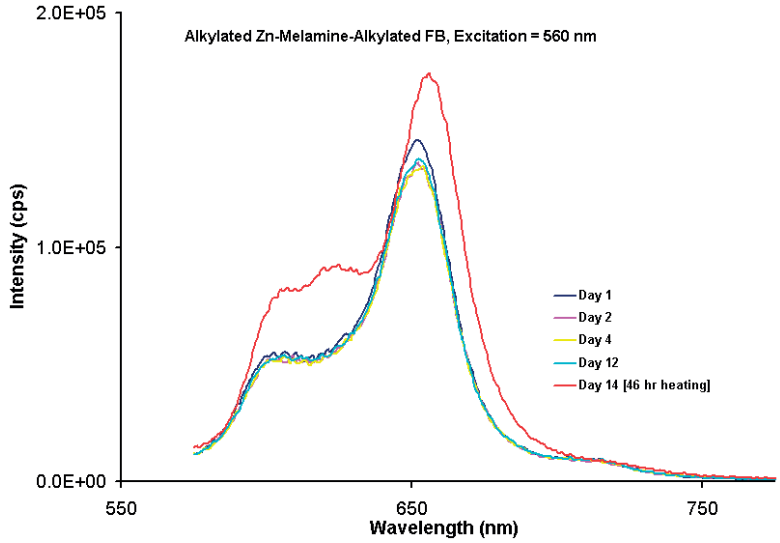

Figure A 4.9: Fluorescence emission spectra of alkylated Zn-FB (cage **2a-2b**) with melamine in dry THF. There is a 1:2:1 mixture of cages containing **2a-2a**, **2a-2b**, and **2b-2b**. Excitation is at 560 nm where the OD = 0.10 and band pass = 2 nm, and **2b** absorbs ~5 times greater than **2a**. The emission spectra intensity increases as the initially formed aggregates evolve into the more soluble cage structure upon heating the sample for couple of days at 45-47 ^{o}C. The relative increase of the zinc complex band with time indicates more of **2b** is in the cage compared to the initially formed aggregates.

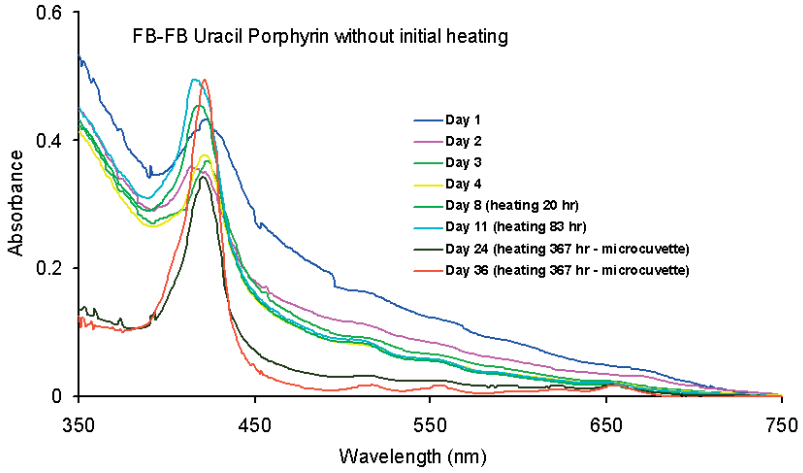

Figure A 4.10: UV-visible spectra of uracil FB-melamine-uracil FB (cage **1a-1a**) in dry THF with heating at 45-47 ^{o}C as indicated. The large background is due to the large number and size distribution of aggregates of the poorly soluble porphyrin. The absorption intensity, e.g. of the Soret band as measured from the background/baseline, increases as **1a** becomes soluble and self-assembles into the cage mediated by H-bonding with the bis(decyl)melamine.

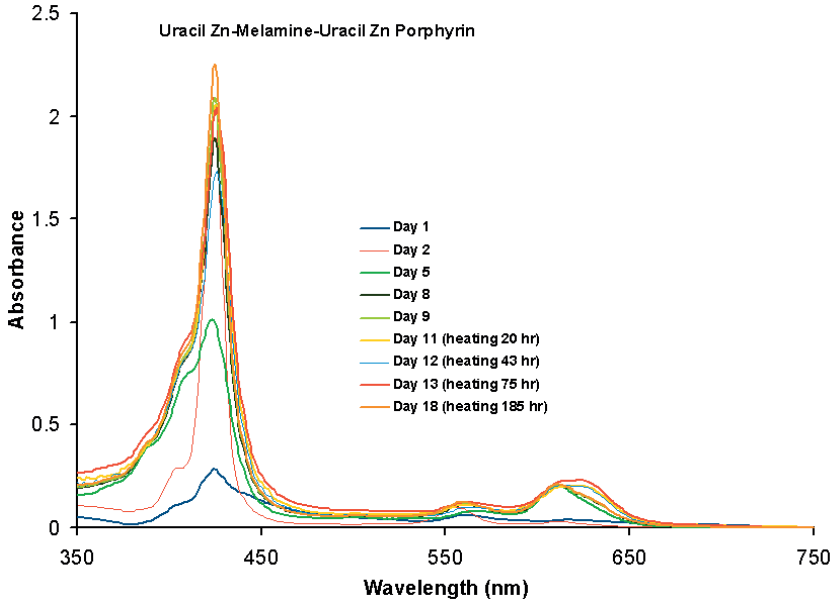

Figure A 4.11: UV-visible spectra of uracil Zn-melamine-uracil Zn (cage **1b-1b**) in dry THF with heating at 45-47 ^{o}C from day 1. The poorly soluble porphyrin is highly aggregated. The absorption intensity, e.g. of the Soret band as measured from the background/baseline, increases as **1b** becomes soluble and self-assembles into the cage mediated by H-bonding with the bis(decyl)melamine.

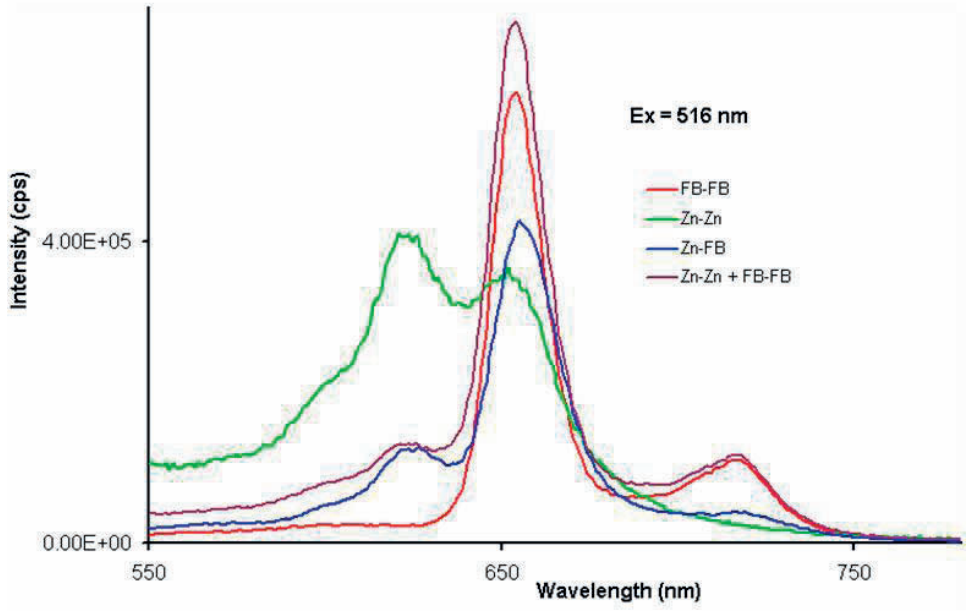

Figure A 4.12: Fluorescence emission spectra of the cages **1b-1b**, **1a-1a**, and the statistical mixture of **1a-1b** in dry THF with after heating at 45-47 ^{o}C for several days. Excitation is at 516 nm.

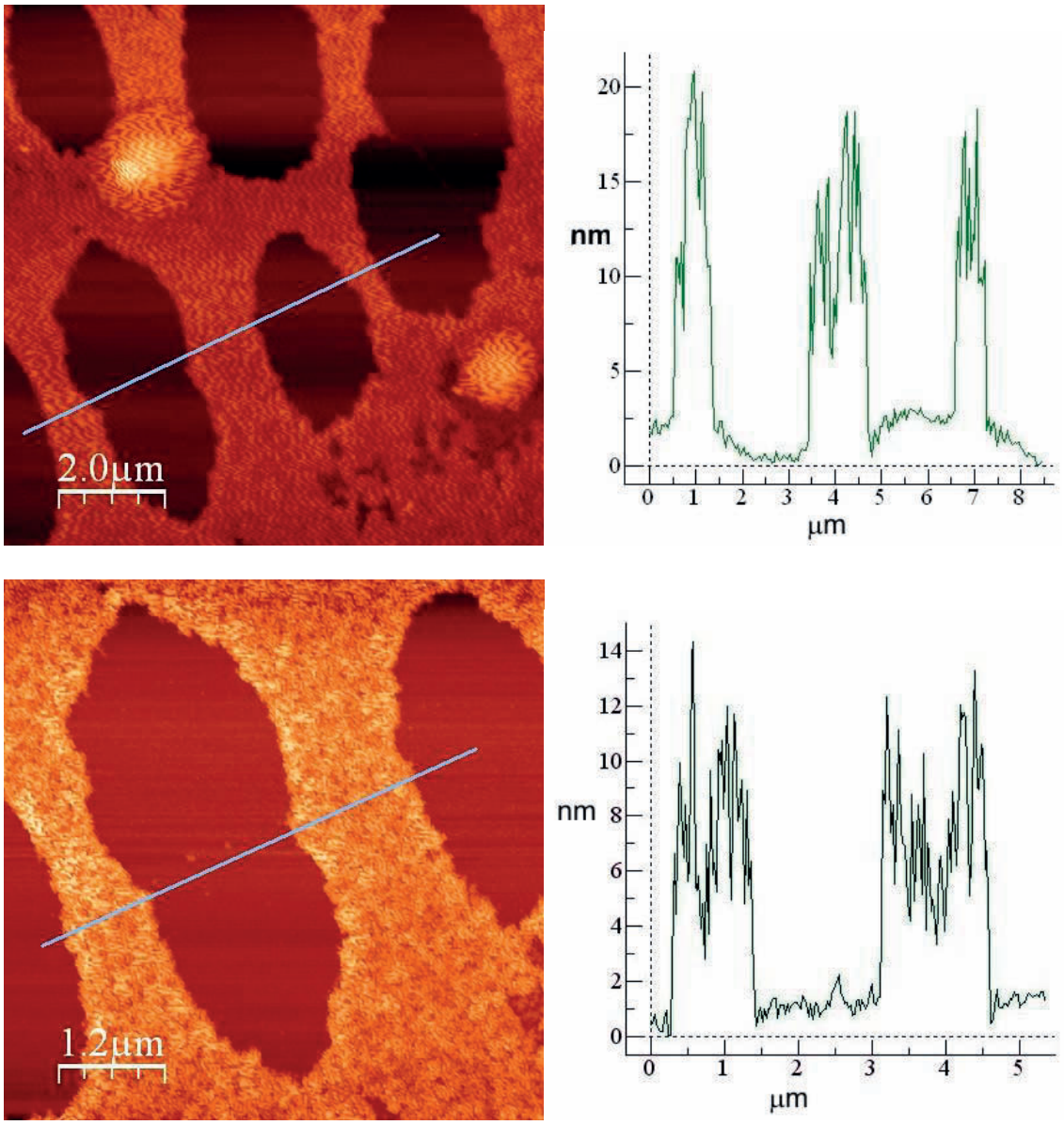

Figure A 4.13: AFM of the cage formed from **2b**.

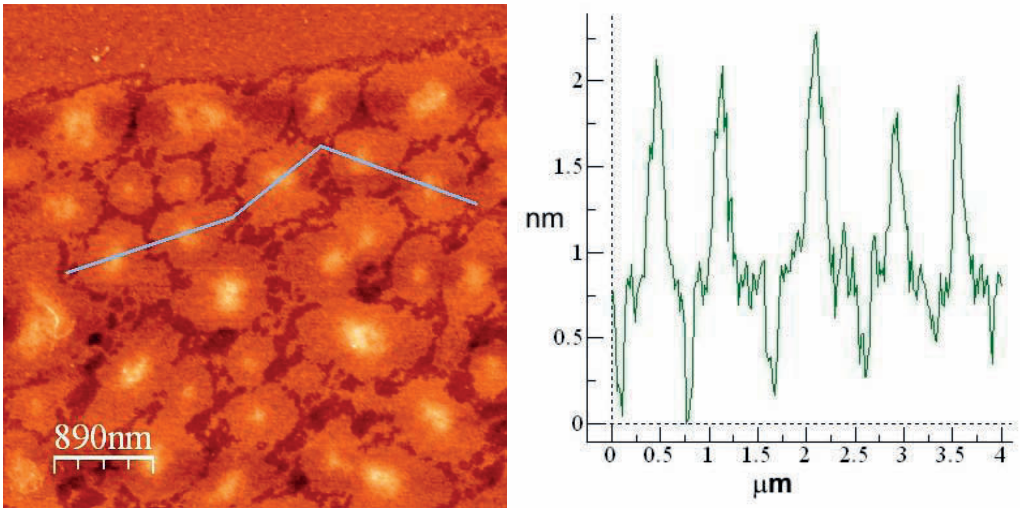

Figure A 4.14: AFM of the 1:2:1 mixture of **2a-2a**, **2a-2b**, **2b2b** cages formed from the mixture of **2a** and **2b** with the bis(decyl)melamine.

4.6 References

1. Paulo, P. M. R., Lopes, J. N. C., and Costa, S. l. M. B. (2008) Molecular Dynamics Simulations of Porphyrin−Dendrimer Systems: Toward Modeling Electron Transfer in Solution, *J. Phys. Chem. B 112*, 14779-14792.
2. Wasielewski, M. R. (1992) Photoinduced electron transfer in supramolecular systems for artificial photosynthesis, *Chem. Rev. 92*, 435-461.
3. Durrant, J. R., Haque, S. A., and Palomares, E. (2004) Towards optimisation of electron transfer processes in dye sensitised solar cells, *Coord. Chem. Rev. 248*, 1247-1257.
4. Zinth, W., and Wachtveitl, J. (2005) The First Picoseconds in Bacterial Photosynthesis—Ultrafast Electron Transfer for the Efficient Conversion of Light Energy, *ChemPhysChem 6*, 871-880.
5. Radivojevic, I., Likhtina, I., Shi, X., Singh, S., and Drain, C. M. (2010) Self-organized nanofibers and nanorods of porphyrins bearing hydrogen bonding motifs, *Chem. Commun. 46*, 1643-1645.
6. Beletskaya, I., Tyurin, V. S., Tsivadze, A. Y., Guilard, R., and Stern, C. (2009) Supramolecular Chemistry of Metalloporphyrins, *Chem. Rev. 109* 1659-1713.
7. Drain, C. M., Varotto, A., and Radivojevic, I. (2009) Self-Organized Porphyrinic Materials, *Chem. Rev. 109*, 1630-1658.
8. Jurow, M., Schuckman, A. E., Batteas, J. D., and Drain, C. M. (2010) Porphyrins as molecular electronic components of functional devices, *Coord. Chem. Rev. 254,*, 2297-2310.
9. Lee, S. J., and Hupp, J. T. (2006) Porphyrin-containing molecular squares: Design and applications, *Coord. Chem. Rev. 250*, 1710-1723.
10. Anariba, F., Tiznado, H., Diers, J. R., Schmidt, I., Muresan, A. Z., Lindsey, J. S., Zaera, F., and Bocian, D. F. (2008) Comprehensive characterization of hybrid junctions comprised of a porphyrin monolayer sandwiched between a coinage metal overlayer and a Si(100) substrate, *J. Phys. Chem. C 112*, 9474-9485.
11. Lehn, J.-M. (1994) Perspectives in supramolecular chemistry: From molecular recognition towards self-organisation, *Pure. Appl. Chem. 66*, 1961-1966.

12. Lehn, J.-M. (1990) Perspectives in Supramolecular Chemistry—From Molecular Recognition towards Molecular Information Processing and Self-Organization, *Angew. Chem. Int. Ed. 29*, 1304-1319.
13. Drain, C. M., Fischer, R., Nolen, E. G., and Lehn, J.-M. (1993) Self-assembly of a bisporphyrin supramolecular cage induced by molecular recognition between complementary hydrogen bonding sites, *J. Chem. Soc., Chem. Commun.* 243-245.
14. Drain, C. M., Shi, X., Milic, T., and Nifiatis, F. (2001) Self-assembled multiporphyrin arrays mediated by self-complementary quadruple hydrogen bond motifs, *Chem. Commun.* 287-288.
15. Shi, X., Barkigia, K. M., Fajer, J., and Drain, C. M. (2001) Design and Synthesis of Porphyrins Bearing Rigid Hydrogen Bonding Motifs: Highly Versatile Building Blocks for Self-Assembly of Polymers and Discrete Arrays, *J. Org. Chem. 66*, 6513-6522.
16. Balaban, Teodor S., Berova, N., Drain, Charles M., Hauschild, R., Huang, X., Kalt, H., Lebedkin, S., Lehn, J.-M., Nifaitis, F., Pescitelli, G., Prokhorenko, Valentyn I., Riedel, G., Smeureanu, G., and Zeller, J. (2007) Syntheses and Energy Transfer in Multiporphyrinic Arrays Self-Assembled with Hydrogen-Bonding Recognition Groups and Comparison with Covalent Steroidal Models, *Chem. - A Eur. J. 13*, 8411-8427.
17. Arai, S., Niwa, D., Nishide, H., and Takeoka, S. (2007) Atropisomers of meso-Conjugated Uracyl Porphyrin Derivatives and Their Assembling Structures, *Org. Lett. 9*, 17-20.
18. Arai, S., Okamura, T., and Takeoka, S. (2010) Synthesis and self-assembling behavior of a porphyrin bearing multiple meso-conjugated barbiturates, *Tetrahedron Lett. 51*, 5177-5180.
19. Drain, C. M., Russell, K. C., and Lehn, J.-M. (1996) Self-assembly of a multi-porphyrin supramolecular macrocycle by hydrogen-bond molecular recognition, *Chem. Commun.*, 337-338.
20. Ligthart, G. B. W. L., Ohkawa, H., Sijbesma, R. P., and Meijer, E. W. (2005) Complementary Quadruple Hydrogen Bonding in Supramolecular Copolymers, *J. Am. Chem. Soc. 127*, 810-811.

21. González-Rodríguez, D., and Schenning, A. P. H. J. (2011) Hydrogen-bonded Supramolecular π-Functional Materials, *Chem. Mater. 23*, 310-325.
22. Wessendorf, F., and Hirsch, A. (2008) Self-assembly of supramolecular oligo-phenylene-ethynylene wires consisting of double Hamilton receptor modified OPE rods and a tetraphenylporphyrin cyanurate, *Tetrahedron 64*, 11480-11489.
23. Steed, J. W. (2011) Supramolecular gel chemistry: developments over the last decade, *Chem. Commun. 47*, 1379-1383.
24. Radivojevic, I., Likhtina, I., Shi, X., Singh, S., and Drain, C. M. (2010) Self-organized nanofibers and nanorods of porphyrins bearing hydrogen bonding motifs, *Chem. Commun. 46*, 1643-1645.
25. Milic, T., Garno, J. C., Batteas, J. D., Smeureanu, G., and Drain, C. M. (2004) Self-Organization of Self-Assembled Tetrameric Porphyrin Arrays on Surfaces, *Langmuir 20*, 3974-3983.
26. Petersen, L., Pedersen, E. B., and Nielsen, C. (2001) Three Routes for the Synthesis of 6-Benzyl-1-ethoxymethyl-2,4-dioxo-1,2,3,4-tetrahydropyrimidine-5-carbaldehyde, *Synthesis*, 0559-0564.
27. Arai, S., Ohshiro, H., Nishide, H., and Takeoka, S. (2007) Synthesis of porphyrins bearing uracyl groups and their assembly induced by melamine derivatives, *Polym. Adv. Technol. 18*, 497-501.
28. Vollhardt, D., Fainerman, V. B., and Liu, F. (2005) Thermodynamic and Structural Characterization of Amphiphilic Melamine-type Monolayers, *J. Phys. Chem. B 109*, 11706-11711.
29. Fainerman, V. B., Vollhardt, D., Aksenenko, E. V., and Liu, F. (2005) Molecular Recognition Kinetics of Nonsurface Active Pyrimidine Derivatives Dissolved in the Aqueous Subphase by an Amphiphilic Melamine Type Monolayer: A Theoretical Approach, *J. Phys. Chem. B 109*, 14137-14143.
30. Kimizuka, N., Kawasaki, T., Hirata, K., and Kunitake, T. (1998) Supramolecular Membranes. Spontaneous Assembly of Aqueous Bilayer Membrane via Formation of Hydrogen Bonded Pairs of Melamine and Cyanuric Acid Derivatives, *J. Am. Chem. Soc. 120*, 4094-4104.

31. Baliani, A., Bueno, G. J., Stewart, M. L., Yardley, V., Brun, R., Barrett, M. P., and Gilbert, I. H. (2005) Design and Synthesis of a Series of Melamine-based Nitroheterocycles with Activity against Trypanosomatid Parasites, *J. Med. Chem. 48*, 5570-5579.

32. Gellman, S. H., Dado, G. P., Liang, G. B., and Adams, B. R. (1991) Conformation-directing effects of a single intramolecular amide-amide hydrogen bond: variable-temperature NMR and IR studies on a homologous diamide series, *J. Am. Chem. Soc. 113*, 1164-1173.

33. Plieger, P. G., Burrell, A. K., Jameson, G. B., and Officer, D. L. (2004) Metallation effects on the thermal interconversion of atropisomers of di(orthomethylarene)-substituted porphyrins, *Dalton Trans.*, 319-326.

34. Freitag, R. A., and Whitten, D. G. (1983) Thermal and photo-induced atropisomerization of picket-fence porphyrins, metalloporphyrins, and diacids: a means for examining porphyrin solution properties, *J. Phys. Chem. 87*, 3918-3925.

35. Kottas, G. S., Clarke, L. I., Horinek, D., and Michl, J. (2005) Artificial molecular rotors, *Chem. Rev. 105*, 1281-1376.

36. Lindsey, J. (1980) Increased Yield of A Desired Isomer by Equilibria Displacement on Binding to Silica-Gel, Applied to Meso-Tetrakis(O-Aminophenyl)Porphyrin, *J. Org. Chem. 45*, 5215-5215.

37. Ohkawa, H., Arai, S., Takeoka, S., Shibue, T., and Nishide, H. (2003) A Duplex of Tetra(2-pyridyl)porphyrin and Tetrahydroxylcalix[4]arene, *Chem. Lett. 32*, 1052-1053.

38. Ohkawa, H., Takayama, A., Nakajima, S., and Nishide, H. (2006) Cyclic Tetramer of a Metalloporphyrin Based on a Quadruple Hydrogen Bond, *Org. Lett. 8*, 2225-2228.

39. Cohen, Y., Avram, L., and Frish, L. (2005) Diffusion NMR Spectroscopy in Supramolecular and Combinatorial Chemistry: An Old Parameter—New Insights, *Angew. Chem. Int. Ed. 44*, 520-554.

40. Zhao, T., Beckham, H. W., and Gibson, H. W. (2003) Quantitative Determination of Threading in Rotaxanated Polymers by Diffusion-Ordered NMR Spectroscopy, *Macromolecules 36*, 4833-4837.

41. Tran Thi, T. H., Desforge, C., Thiec, C., and Gaspard, S. (1989) Singlet-singlet and triplet-triplet intramolecular transfer processes in a covalently linked porphyrin-phthalocyanine heterodimer, *J. Phys. Chem. 93*, 1226-1233.

42. Gouterman, M. (1978) *In The Porphyrins*, Vol. 3, Academic Press, New York.

43. Yang, Y., and Wang, C. (2009) Hierarchical construction of self-assembled low-dimensional molecular architectures observed by using scanning tunneling microscopy, *Chem. Soc. Rev. 38*, 2576-2589.

CHAPTER 5: PHOTOPHYSICAL STUDIES OF PORPHYRINOIDS

Abstract

A systematic study of the photophysical properties of a series of porphyrinoids is presented. The role of the location of a heavy atom in shunting the excited state from the singlet to the triplet manifolds is compared for three cases. It is well known that Pt(II) metalloporphyrins do not fluoresce. For meso pyridyl porphyrins, the fluorescence quantum yield decreases as the number of coordinatively attached Pt(II) complexes increase from 0-4, but the tetracoordinated species retains about 30% of the fluorescence. Covalently attaching a heavy metal complex e.g. Pt(II) complex to the macrocycle by an organometalic bond at the peripheral meso position causes greater than a 20-fold decrease in fluorescence quantum yield and may enhance some internal conversion to the ground state. For comparison, the fluorescence quantum yield decreases somewhat as the number of pyridyl groups on the meso positions increase 0-4. We also evaluate the photophysical properties of a series of porphyrins with nitro groups on the β pyrrole position and on the meso phenyl group, which also quenches the fluorescence. These studies bare on the use of metal ions to enhance the photophysical properties of these dyes as photodynamic therapeutics and for supramolecular systems, while the nitrated macrocycles have potential application in non linear optics. (to be submitted to *J. Phys. Chem.*)

5.1 Introduction

Functionalized porphyrins and their other tetra pyrrole derivatives have been studied extensively over the recent years, primarily due to their importance in biological and optical systems. Moreover their enhanced photonic and electrochemical properties and the ability to tune their properties by inserting different metal ions into their core or by grafting a variety of substituents at their peripheral positions make these molecules attractive components for advanced materials in electronic and photonic devices. Porphyrinoids find uses as photocatalysts, reduction/oxidation catalysts, sensors for electronic devices, biomarkers, photosensitizers for photodynamic therapy, and artificial solar energy harvesting devices. Due to the strong absorption in the visible region, the photophysical properties of porphyrinoids are well exploited both by the nature and in the laboratory. Significant attention has been paid to studying the photo dynamic behavior of excited electronic states of these compounds, yet these compounds present many challenges for the accurate measurement of their photophysical properties in solutions.(*1*) There are numerous reports that show aggregation of porphyrins in solution, which makes it difficult to extract the photophysical properties of monomeric species versus the aggregates. The extent of aggregation of the porphyrin depends on the nature of substituents attached to porphyrin core, the coordinated metal ion, concentration, temperature, and on the solvent.

The presence of electron withdrawing group such as nitro group(s) on the β-pyrrole position(s) or on the meso phenyl groups affect the electronic properties of the porphyrins and thus the number and position of nitro groups dictates photonic properties. Nitro groups are widely used in porphyrin chemistry as a precursor to amino group(*2*)

because the latter tend to diminish the yield of the macrocycle. The strong electron withdrawing nature of nitro group polarize the porphyrins making them potential components of non-linear optical materials(*3, 4*) and some of the photophysics of some nitroporphryins have been reported.(*5*) Nitro groups can serve to assemble supramolecular porphyrin systems by participating in H-bond formation with groups such as imidazole(*6*) to form aggregates in a variety of organic solvents.

The ease of aggregation of nitro porphyrinoids may provide an important strategy for making supramolecular porphyrin arrays via self-assembly.(*7*) Porphyrins are particularly attractive species to incorporate into supramolecular assemblies because of their rich photochemistry and ability to mediate electron and energy transfer. Self-assembly may provide efficient access to order arrays of porphyrin units by hydrogen bond molecular recognition, self-coordination of metallo derivatives, electrostatic interactions, and transition metal ion coordination.

Supramolecular assembly: As a more convenient and promising strategy, non-covalent, supramolecular assembly has emerged as an effective means for the construction of two- or three-dimensional architectures. Non-covalent strategies are inspired by the fact that natural photosynthetic systems rely on non-covalent interactions. Self-assembly by coordination chemistry, e.g. of (metallo)pyridylporphyrins(*8-10*) or (metallo)imidazolylporphryins(*11-13*) to a metal ion, has been particularly attractive because of the large association constants and favorable tendency to preserve the photoexcited state dynamics of the porphyrins.(*14, 15*) The many defined supramolecular arrangements include linear chains, squares, dendrimers, sheets and tapes, stars and rosettes.(*16, 17*) The detailed structure of component molecules and the supramolecular

architecture are important parameters that dictate functional properties, e.g. enhancing or avoiding π-staking, fixing relative conformations, and attaining optimal spacing. For the formation of supramolecular geometries, porphyrins appended with specific functional groups (such as pyridyl, imidazole, and nitro) can result in building blocks that can serve as either linear or angular components, or edges or corners, of more complex arrangement depending on the location of the functional groups. Porphyrins appended with one pyridyl group can join with another porphyrin molecule of the same or different type to form homogeneous and heterogeneous linear assemblies respectively (Figure 5.1).

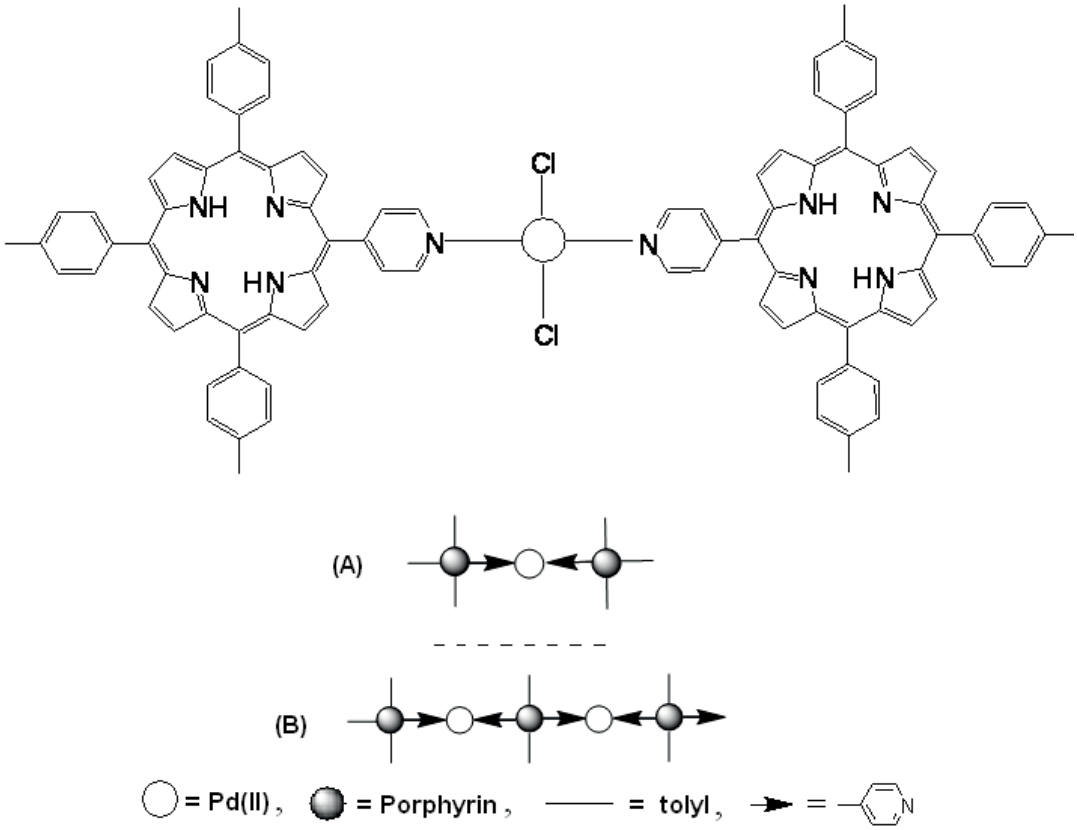

Figure 5.1: Top: Structural representation of dimer formation of 5-(4‟-pyridyl)-10,15,20-tris(4‟-tolyl)porphyrin through exocyclic coordination to $Pd(II)Cl_2$. Bottom: schematic representation of the mono pyridyl porphyrin dimer shown (A), and a liner polymer is the major component assembled from a 2:1 mixture of the mono pyridyl porphryin and 5,15-bis(4-pyridyl)-10,20-bis(4-tolyl)porphyrin.

Molecular squares of pyridylporphrins are representative of many supramolecular systems assembled by coordination chemistry.(*18, 19*) In this case porphyrins appended with pyridyl group at adjacent 5,10 or opposite 5,15- positions can easily make a supramolecular square when mixed with Pt(II) or Pd(II) complexes (Figure 5.2) (*20*). For example, two different molecular squares are formed between a corner-shaped 5,10-bis-(4‟-pyridyl)-15,20-diphenylporphyrin and 5,15-bis-(4‟-pyridyl)-10,20-diphenylporphyrin with cis Pt(II).

Figure 5.2: Schematic representation of square formation between (A) two units of each of 5,10-pyridylporphyrin and a cis Pt(II) complex (hatched circles), and (B) four units of each of 5,15- pyridylporphyrin and a cis Pt(II) complex.

Supramolecular squares formed by Pt(II) bridges tend to be more robust compared to those formed Pd(II) bridges because of reduced cis to trans isomerization. A landmark in self-assembly of porphyrins remains the 3x3 nonamer arrays prepared by mixing three different pyridyl porphyrins building blocks with „+‟, „⊥‟, and „⊤‟ topologies in correct stiochiometric ratio (1:4:4) with 9 equivalents of a trans Pd(II) complex.(*20-22*) However mixing of only „+‟ shaped porphyrin with trans Pd(II) results in the formation of a 2-dimensional polymer wherein the defect densities depend on the methods (Figure 5.3). The supramolecular structures so formed are chemically very stable for application in optical devices.

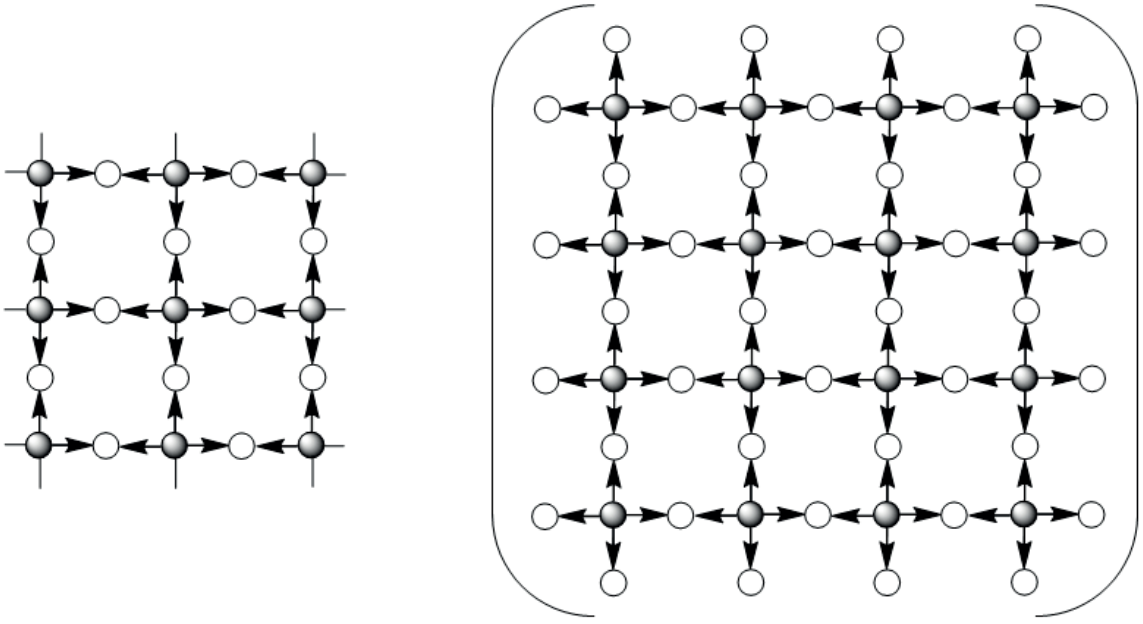

Where, ○ = Pd(II),

Figure 5.3: Schematic representation of trans Pd(II) mediated formation of a nonamer containing three different porphyrins (left), and a 2-dimensional polymer of tetrapyridylporphyrins.

These supramolecular systems have been used to examine electron and energy transfer across metal ion linkers(*23-26*), as catalyst and molecular sieves, and as a means of understanding larger self organized systems on surfaces. Supramolecular systems adsorbed onto a conducting surface, as opposed to single, non-aggregated structures, may be useful for controlling dye spacing and orientation as well as for modulating dye coverage and dye-layer porosity.(*27-29*) Energy transfer within the self-assembled porphyrin arrays generally occurs via a FRET (Förster resonance energy transfer, through space transfer) mechanism, the efficiency of which depends on the distance and orientation between donor and acceptor transition dipole moments and the overlap of

donor absorption and acceptor emission spectra. Adjustments of these parameters are achieved through modification of porphyrin units and assembly schemes.(*30*) Additionally, self-organized surface structures and surface properties, i.e. the two dimensional and three dimensional arrays, dictate the photophysical properties of the system on substrates.(*31*)

Metal-mediated porphyrin self assemblies based on meso 4-pyridyl porphyrins have been extensively studied for the last 17 years; however, there are a few reports based on metal-mediated self-assemblies of meso 3-pyridyl porphyrins. Changes in the position of the peripheral N-atoms in pyridyl group affect the architecture of the chromophore and change the electronic environment across the porphyrin, which affects their optical and chemical properties for applications. The coordination of 3-pyridyl porphyrins forms out-of-plane arrangements with exocyclic metal ions. Lengo et al. reported slipped co-facial geometry for the dimer of bis metapyridyl porphyrin with octahedral ruthenium complex and are having non-rigid geometry and form side to face arrays.(*32*)

5.2 Heavy Atom effect

The heavy atom effect presents a pathway for a "forbidden" electronic transition from an excited singlet state to an excited triplet state ($S_1 \rightarrow T_1$). "Allowed" and "forbidden" are quantum mechanical descriptions based on certain selection rules. A "forbidden" proceeds more slowly than an "allowed" transition. A "forbidden" transition takes place because of the spin-orbital coupling interactions, which leads to intersystem crossing mechanism. The spin-orbital coupling may be accelerated by the presence of heavy atom substituents appended to the dye or in the solvent.(*33*) Heavy atoms have

wide applications as a strategy to increase the triplet population. The fluorescence quantum yield can be affected by an atom or groups of atoms coordinated by the porphyrin (endocyclic position) or at the peripheral (exocyclic position) on the macrocycle.

Chelated metal ions. The photophysical properties of metalloporphyrins are well studied, including the heavy atom effect on intersystem crossing to the triplet state(*34, 35*). Some Metalloporphryins coordinated to metal ions with low energy empty d orbitals, such as Ni(II), can lose excited state energy to form metal centered d,d states or form charge transfer states as a deactivation pathway that diminishes or completely quenches fluorescence.(*36-38*) For closed shell and other metals, insertion of a metal ion into the core diminishes or quenches fluorescence by heavy atom effects that facilitate intersystem crossing to the triplet manifold. Azenha et. al reported the fluorescence quantum yields for a few diamagnetic tetraphenylporphyrin (TPP) complexes and the order is H_2TPP>MgTPP>ZnTPP>CdTPP.(*39, 40*)

Exocyclic heavy atom effect. The quenching of the fluorescence signal depends on the nature, number of atoms, and the mass of the atom(s) attached. For example, the presence of halogen atoms at the para position of peripheral phenyl groups of TPP is known to decrease the fluorescence quantum yield as the number of halogen atoms increases. For various halogens, the fluorescence signal is quenched with the increasing atomic weight of the halogen: I>Br>Cl>F.(*39*)

Organometallics. Metal complexes can be attached to a peripheral position of the porphyrin macrocycle.(*41*) Though the photophysical properties of these have generally not been studied and it part of the present work, it is reasonable to expect that metals

attached to exocyclic positions on the macrocycle will cause a decrease in the fluorescence intensity due to heavy atom effect.

It is important to note that for the molecular level systems the heavy atom effect refers to the singlet quenching mechanism, by spin-orbit coupling. But for supramolecular systems, e.g. pyridyl porphyrins with an exocyclic Ru(II) binder, two spin forbidden deactivation pathways are available to the porphyrin singlet quenching: (a) intersystem crossing within the porphyrin (k_{isc}), and (b) singlet-triplet energy transfer to the attached molecules (k_{STEn}). It is reported that both pathways can play role as a consequence of the heavy atom effect of a Ru(II) complex.(*42, 43*) The relative importance of each pathway is difficult to predict. For $k_{isc,}$the heavy atom is remote, but the process is an intracomponent one. For k_{STEn}, the heavy metal center is directly involved, and the process is an intercomponent one. Furthermore, the feasibility of k_{STEn} depends critically on the energy of the triplet state of the Ru(II) center. However, the two processes can be easily discriminated since the pyridylporphyrin triplet state population, exhibits more k_{isc} of the process than k_{STEn}.

Herein we present the self-consistent photophysical properties of a series of porphyrinoids and their zinc complexes. This includes the measurement of their absorption and emission spectra, fluorescence quantum yield, and fluorescence lifetimes in two different solvents: toluene and DMSO. The measurements were done both in air and under nitrogen (by purging the N_2 gas through the solution.)

5.3 Experimental Details

5.3.1 Materials and Instrumentation

The purity of all compounds was checked by thin layer chromatography (TLC), mass spectrometry and excitation spectra. The solvents N,N-dimethylsulfoxide and toluene are of analytical quality grade, purchased from Fisher Scientific Co. and were used without further purification. Tetra-perfluorphenylyporphyrin ($TPPF_{20}$) porphyrin was obtained from Frontier Scientific. UV-visible spectra were recorded on a Varian Bio3 spectrophotometer. Excitation spectra, steady-state fluorescence (emission) spectra, and fluorescence lifetime were measured with a Fluorolog τ3, Jobin Spex instrument S.A., Inc using a 1 cm path length cuvette at room temperature. Electrospray ionization (ESI) mass spectrometric analyses were performed at the CUNY Mass Spectrometry Facility at Hunter College using an Agilent Technologies HP-1100 LC/MSD instrument. The ESI was run in methanol, with 0.1% formic acid.

5.3.2 Synthesis of Porphyrinoids

The various Porphyrins used here were synthesized and characterized by various researchers.

a. Pyridyl porphyrinoids- Dr. Fotis Nifiatis
b. Nitro porphyrinoids- Dr. Alexander Falber
c. Exocyclic Pt and Pd porphyrins-Dr. Dennis P. Arnold

5.3.3 UV-visible, Fluorescence Spectroscopy, and Fluorescence Quantum Yield

UV-visible and fluorescence measurements were performed on dilute solutions, typically ~0.33 μM, of compounds in DMSO and toluene. For steady state fluorescence emission spectroscopy, the chromophores were excited at 414 nm, where absorbencies were ≤ 0.1. For emission spectra both the excitation and detection monochromators had a band pass of 2 nm. The excitation spectra of these compounds were also recorded by using the highest intensity emission band to check the purity. The corrected emission (for instrument response) and absorption spectra were used to calculate the fluorescence quantum yield (ϕ_F) of all compounds in air and under N_2 relative to **TPP** (ϕ_F for **TPP** = 0.11 in toluene).(*44*) The following equation used to calculate the Fluorescence quantum yield.

$$\Phi_x = \Phi_o \frac{F_x A_o n_x^2}{F_o A_x n_o^2}$$

Where Φ_x and Φ_o are the fluorescence quantum yields of the sample compound and the reference respectively. F_x and F_o are the areas of fluorescence curves integrated using the Spex software for the sample and the reference respectively. A_x and A_o represent the absorbencies of the sample and the reference respectively at the excitation wave lengths, and η_x and η_o are the refractive indices of the solvent used for the sample and the reference respectively.

5.3.4 Fluorescence Lifetime

Time correlation single photon counting (TCSPC) was used to measure the fluorescence lifetimes of porphyrinoids using a Fluorolog® spectrophotometer from Horiba Jobin Yvon in DMSO and toluene. We used a 401 nm NanoLED laser, average power 13.6 pJ/pulse with a source pulse width <200ps to excite the molecules. 200 ps is the lower limit of time measurement of our instrument. The data fitting program is available in the instrument.

5.4 Result and Discussion

Pyridylporphyrins

The absorption spectra of all compounds were measured in DMSO and toluene in air, the final concentration of each solution was ca. 0.33μM. The data for their absorption peaks and their extinction coefficients are shown in Table 5.1. The Soret band peaks for the compounds are red shifted by 1-2 nm in toluene compared to DMSO. This is because of the difference in nature and magnitude of the solute-solvent interactions. For a series of pyridyl porphyrins: **M*m*PyP**, **D*m*PyP**, **T*m*PyP**, and **T*p*PyP** a steady decrease in the fluorescence emission intensity was observed in both DMSO and toluene, and is attributed to the decreased fluorescence quantum yield, Φ_F, with the increasing numbers of pryidyl groups: the fluorescence is quenched **M*m*PyP** < **D*m*PyP** < **T*m*PyP** < **T*p*PyP**. The decrease in Φ_F value is because of the increased polarity and specific solvent-solute interactions with increased number of pyridyl groups. In addition to different polarization vectors, the reduced symmetry of the 3-pyridyl groups can also open up vibronic relaxation processes. This is consistent with the lower Φ_F value for **T*m*PyP** than for **T*p*PyP** (Table 5.1 and Table 5.2). Our Φ_F data for various pyridyl porphyrins are in

consistent with the previous reports in dichloromethane for the tetra-para-pyridylderivatives in CH_2Cl_2.(*42*)

Table 5.1: UV-visible spectra of pyridyl porphyrins in toluene.

Compound	Absorption peaks, λ_{max} nm (log ε)				
	B(0-0)	Q_y(1-0)	Q_y(0-0)	Q_x(1-0)	Q_x(0-0)
TPP	418 (5.19)	513(4.46)	547 (3.88)	592 (3.69	648 (3.71)
M*m*PyP	420 (5.72)	516 (4.29)	549 (3.97)	593 (3.66)	649 (3.71)
D*m*PyP	420 (6.08)	516 (4.68)	550 (4.27)	594 (4.21)	651 (4.12)
T*m*PyP	420 (5.70)	516 (4.14)	548 (3.43)	590 (3.36)	648 (3.26)
T*p*PyP	420 (5.58)	512 (4.24)	547 (3.26)	588 (3.78)	643 (3.44)

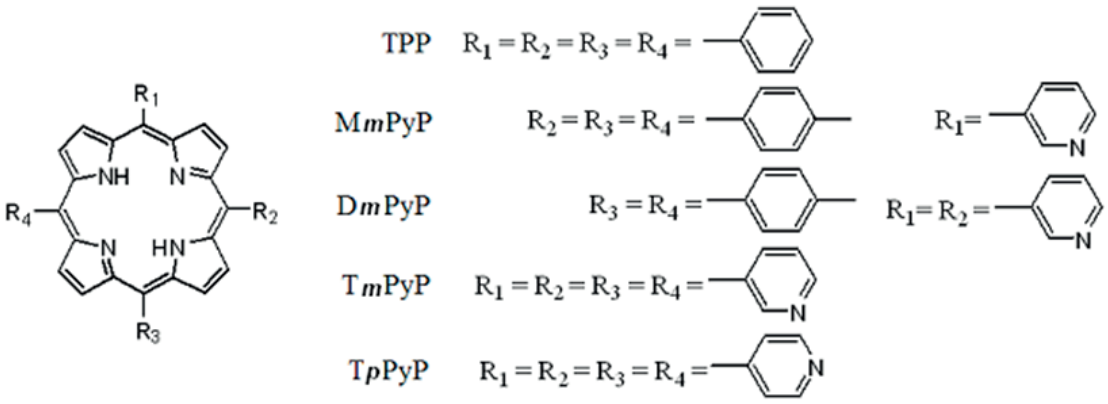

Figure 5.4: Structure of pyridyl porphyrinoids: **TPP**=5,10,15,20-tetraphenylporphyrin, **M*m*PyP** = 5-(3‟-pyridyl)-10,15,20-tris(tolyl)porphyrin, **D*m*PyP** = 5,10-bis(3‟-pyridyl)-15,20-bis(tolyl)porphyrin, **T*m*PyP** = 5,10,15,20-tetrakis(3‟-pyridyl)porphyrin, **T*p*PyP** = 5,10,15,20-tetrakis(4‟-pyridyl)porphyrin.

Table 5.2: Florescence properties of pyridylporphyrins in toluene; excitation= 414 nm, slits=2nm, emission = 550-800, slits 2 nm, absorbance at 414 nm = 0.1; for N_2 data gas was purged through the solution for ca. 10 min. Steady state excitation at 405 nm, time resolved at 651 nm.

Compound	Emission, λ_{max} nm	Quantum yield, Φ_F		Fluorescence lifetime, nsec	
		Air	N_2	Air	N_2
TPP	653, 719	0.11	0.11	9.34	11.32
M*m*PyP	654, 720	0.12	0.13	9.02	10.79
D*m*PyP	654, 719	0.10	0.11	8.64	10.67
T*m*PyP	653, 719	0.07	0.08	8.47	9.97
T*p*PyP	649, 715	0.06	0.07	9.32	11.26
M*p*PyP	in CH_2Cl_2 data from ref. 42			8.1	
D*p*PyP	in CH_2Cl_2 data from ref. 42			8.0	
Tr*p*PyP	in CH_2Cl_2 data from ref. 42			7.5	
T*p*PyP	in CH_2Cl_2 data from ref. 42			7.1	

Heavy atom effects

Solvent heavy atom effect: To study the external heavy atom effect on the photophysics of **T*p*PyP**, different amounts of methyl iodide (CH_3I) was added to 1 μM solution of porphyrin in toluene. The heavy iodine atom facilitates the intersystem crossing, making the fluorescence emission intensity decrease with increasing concentrations of CH_3I (Figure 5.5). This is typical of solvent mediated heavy atom effects. (Adapted from Dr. Fotis Nifiatis Thesis)

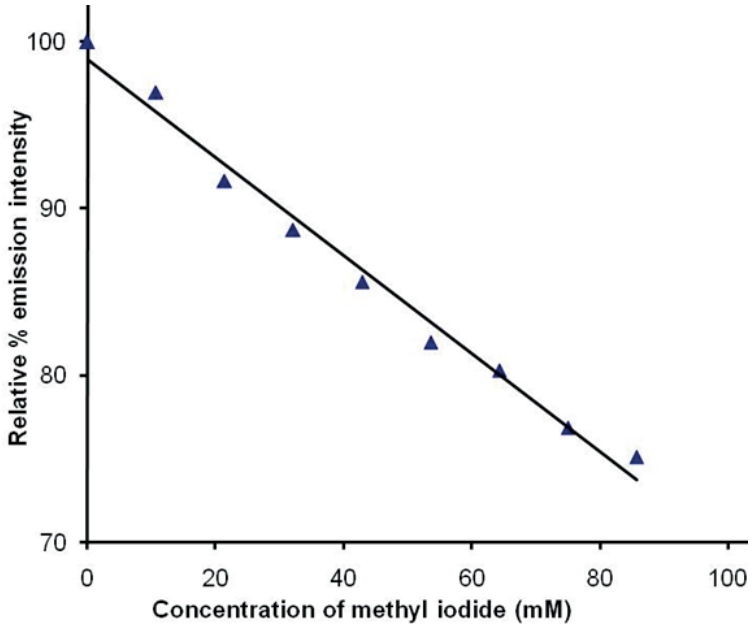

Figure 5.5: Solvent heavy atom effect shows the quenching of the **T*p*PyP** porphyrin fluorescence with the addition of methyl iodide. The dye was 1μM in toluene at room temperature.

Exocyclic heavy atom effect: The effect of the heavy Pt atoms on the photophysics of the tetra-para-pyridylporphyrin was studied. To 1 μM solutions of **T*p*PyP** in toluene, 1,2,3,and 4 eq. of $(DMSO)_2PtCl_2$ was added independently and the emission spectra was recorded (Figure 5.6). The above Pt complex gives the mono-pyridyl-Pt complex at room temperature. Coordination of the heavy Pt atom to the exocyclic pyridyl position causes quenching of the emission fluorescence spectrum that ranges from 32 to 65%.(Adapted from Dr. Fotis Nifiatis Thesis)

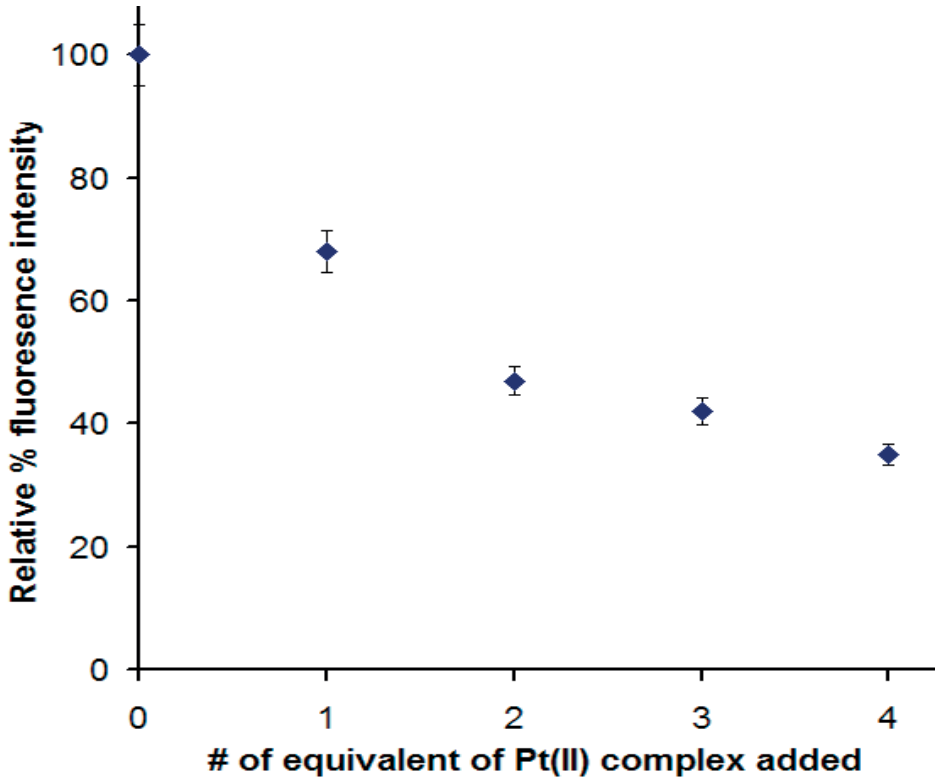

Figure 5.6: External heavy atom effect on the fluorescence emission intensity of 1 μM solution of T*p*PyP porphyrin in toluene, caused with the addition of up to four equivalents of Pt(II) complex at room temperature.

Pt(II) and Pd(II) complexes are well known to mediate the assembly of pyridylporphyrins in toluene to form supramolecular systems such as squares, tapes, and 3x3 grids.(*17, 43, 45*) UV-visible titrations that add the metal complex to appropriate pyridylporphyrin(s) show red shifts and isosbestic points. Decreases (40-90%) in the fluorescence emission spectral intensity are observed for the above titrations. The fluorescence quenching is attributed to the exocyclic heavy atom effect, electron communication that allows energy transfer between the porphyrin subunits, and π-stacking. For comparison to the coordination complexes above, exocyclic Pt or Pd complex attached covalently at one of the peripheral meso position of the porphyrin (*41, 46, 47*) were also studied (Figure 5.7). These organometallic compounds exhibit a 8-10

nm red shift in the Soret band of the porphyrin spectra compare to the Soret band at 418 nm for TPP or the 5,15-diphenylporphryin precursors. (Table 5.3 and 5.4). A red shift of the Soret band indicative of the interaction of the metal d-orbitals with π-electron system of the porphyrin ring, consequently reduces the energy gap between the HOMO and LUMO. Also, a large decrease in Φ_F for these exocyclic Pt or Pd porphyrin were observed compared to Φ_F for TPP (Table 5.7 and 5.8).

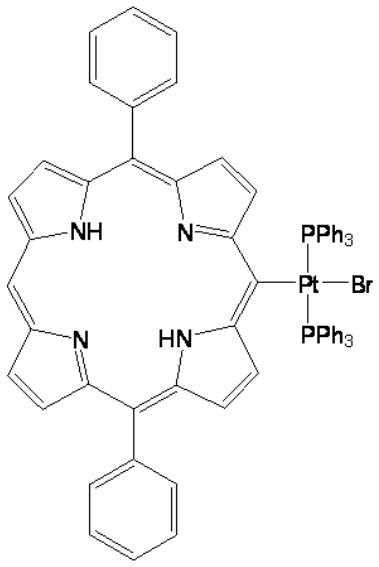

trans-Bromo[10,20-diphenylporphyrin-5-yl]bis(triphenylphosphine) platinum(II)
[DPP-Pt(PPh3)2Br]

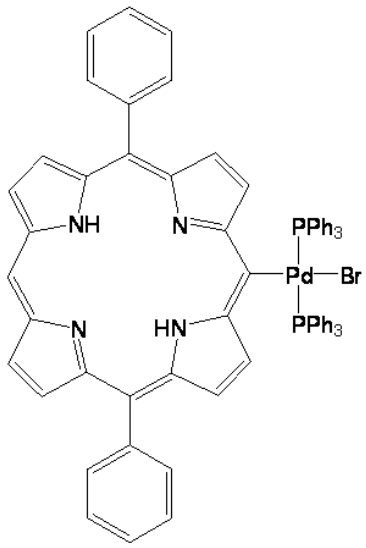

trans-Bromo[10,20-diphenylporphyrin-5-yl] bis(triphenylphosphine) palladium(II)
[DPP-Pd(PPh3)2Br]

Figure 5.7: Structure of exocyclic covalently bound Pt(II) and Pd(II) porphyrinoids: [DPP-Pt(PPh3)2Br]=trans-Bromo[10,20-diphenylporphyrin-5-yl]bis(triphenyphosphine) platinum(II) and [DPP-Pd(PPh3)2Br]=trans-Bromo[10,20-diphenylporphyrin-5-yl]bis(triphenyphosphine) palladium(II).

Table 5.3: UV-visible spectra of organometallic porphyrins in toluene.

Compounds	Absorption peaks, λ_{max} nm (log ε)				
	B(0-0)	Q_y(1-0)	Q_y(0-0)	Q_x(1-0)	Q_x(0-0)
DPP-Pd(PPh3)2Br	427 (4.89)	524 (3.29)	558 (3.42)	595 (3.10)	651 (3.22)
DPP-Pt(PPh3)2Br	429 (4.87)	526 (3.44)	561 (3.44	600 (3.21)	655 (3.41)

Table 5.4: Florescence properties of organometallic porphyrins in toluene; excitation= 414 nm, slits=2nm, emission = 550-800, slits 2 nm, absorbance at 414 nm = 0.1; for N_2 data gas was purged through the solution for ca. 10 min. Steady state excitation at 405 nm, time resolved at 656 nm.

Compounds	Emission, λmax nm	Quantum yield, Φ_F		Fluorescence lifetime, nsec	
		Air	N_2	Air	N_2
DPPPd(PPh_3)$_2$Br	656, 716	0.01	0.012	7.72	8.75
DPP-Pt(PPh_3)$_2$Br	656, 717	0.006	0.007	7.53	8.27

Nitroporphyrins

Substitution by strongly electron withdrawing nitro group(s) at the peripheral position or at the meso phenyl groups makes the porphyrins polar. Nitro groups on porphyrin macrocycle substantially perturb the energies of the HOMO and LUMO,(*48*) whereas when it is on peripheral phenyl groups, the effect is much less. The high polarizability of DMSO interacts strongly with nitro groups to further alter the energy levels, tending to causes the Soret band to move towards the red. With increasing numbers of nitro groups, the Soret band further shifts towards lower energies in the visible spectrum.(*49, 50*) This may be due to the following reasons: (a) a decrease in the energy gap between HOMO and LUMO of the porphyrin and differentiation of the frontier orbitals, (b) an increase in the π-conjugation of the nitro group with the porphyrin

ring, (c) formation of intramolecular charge separated states, (d) the degree and extent of aggregation of the porphyrin in the solvent used. The introduction of one nitro group on the meso phenyl ring causes a four-fold decrease in the fluorescence quantum yield (Φ_F) and fluorescence quantum yield, and there is a further decrease in Φ_F value up to ca. 40 fold, as the number of nitro groups increases from one to six. This is primarily due to the electron withdrawing nature of the nitro group.(*51, 52*) As pointed out by Gust and coworkers, for 2-nitro-5,10,15,20-tetra-p-tolylporphyrin and its zinc complex, the excited state conformation may twist the nitro group relative to the porphyrin, and they found good evidence for the formation of an intramolecular charge transfer state. *(5)* Herein we study three nitrated porphyrins (Figure 5.8)

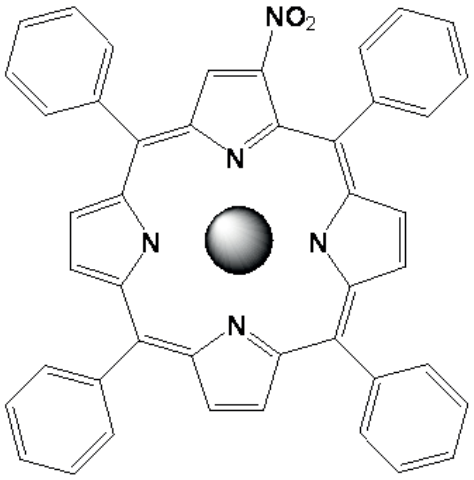

2-Nitro-5,10,15,20-tetraphenylporphyrin (MNTPP)

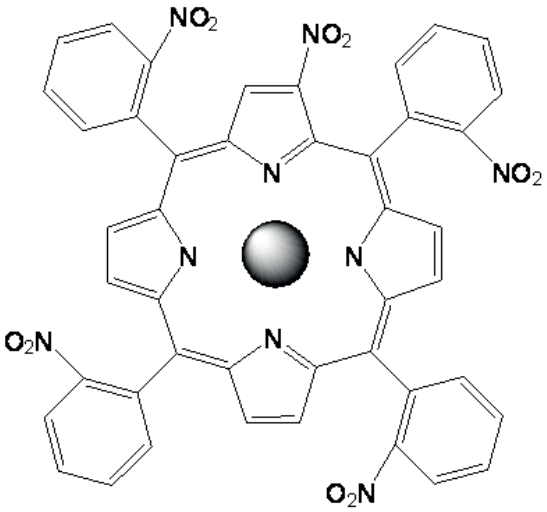

2-Nitro-5,10,15,20-tetrakis(2‟-nitro phenyl)porphyrin (PNTPP)

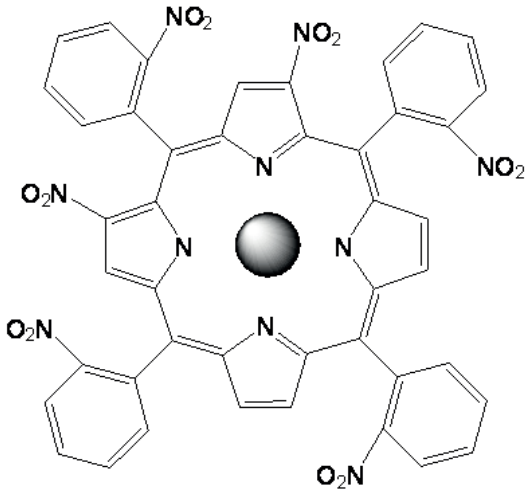

2,7-Dinitro-5,10,15,20-tetrakis(2‟-nitro phenyl)porphyrin (HNTPP)

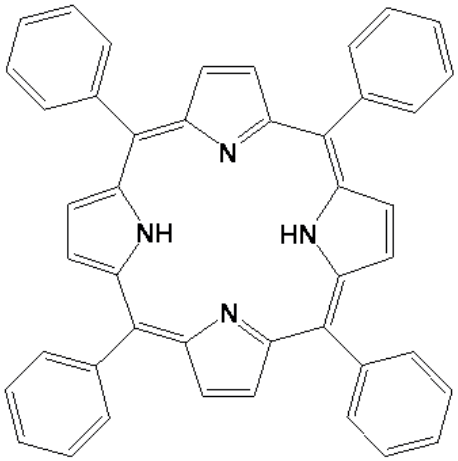

5,10,15,20-tetraphenylporphyrin (TPP)

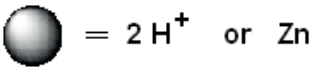

Figure 5.8: Structure of various nitro porphyrinoids: MNTPP =3-Nitro-5,10,15,20 tetraphenylporphyrin, PNTPP = 3-Nitro-5,10,15,20-tetrakis(2‟-nitrophenyl)porphyrin, HNTPP = 3,7-Dinitro-5,10,15,20-tetrakis(2‟-nitrophenyl)porphyrin.

The decrease in the quantum yield may also arise from collisional or static quenching of fluorescence.(*53*) Collisional quenching refers to the return of a molecule to the ground state upon interaction with another molecule in solution, referred to as the quencher. The static quenching involves the formation of complexes in the excited state that are not fluorescent. Though the nitro groups are known to reduce solubility and mediate intermolecular interactions, we have no evidence of aggregation under the conditions used.(*54*) The fluorescence lifetimes of nitro porphyrins are very low compare to TPP (Table 5.5 and 5.6). Consistent with earlier reports*(5)*, the 2-nitro derivative is significantly quenched relative to TPP. The decrease in the fluorescence lifetime and fluorescence quantum yield may also because of the spin orbit coupling interactions. We assume that the spin orbit coupling interactions here may arises because of the replacement of the spherical s-orbitals of the lighter H-atom by a comparatively more delocalized p-orbitals on the three (one N-atom and two O-atoms) atoms in nitro group generates comparatively heavy atom effect.(*55*)

Table 5.5. UV-visible spectra of nitro porphyrins in toluene.

Compound	Absorption peaks, λ_{max} nm (log ε)				
	B(0-0)	Q_y(1-0)	Q_y(0-0)	Q_x(1-0)	Q_x(0-0)
MNTPP Zn	432 (5.66)	--------	567 (4.71)	-------	613 (4.69)
PNTPP	429 (5.70)	527 (4.77)	564 (4.61)	610 (4.58)	667 (4.57)
PNTPP Zn	433 (5.67)	------	570 (4.72)	------	625 (4.69)
HNTPP	452 (5.33)	------	570 (4.46)	-----	627 (4.31)

Table 5.6. Florescence properties of nitro porphyrins in toluene; excitation= 414 nm, slits=2nm, emission = 550-800, slits 2 nm, absorbance at 414 nm = 0.1; for N_2 data gas was purged through the solution for ca. 10 min. Steady state excitation at 405 nm, time resolved at 651 nm.

Compounds	Emission, λmax nm	Quantum yield, Φ_F		Fluorescence lifetime, nsec	
		Air	N_2	Air	N_2
MNTPP [Ref (*56*)]	In Toluene	0.074		1.8 (0.3) 3.1 (0.7)	
MNTPP	690	0.05	0.06	3.21	3.39
MNTPP Zn [Ref (5)]	In CH_2Cl_2	2.7		2.2	
MNTPPZn	641	0.056	0.061	6.73(25%) 1.03(75%)	7.71(26%) 1.08(74%)
PNTPP	660, 698	0.043	0.048	2.87(32%) 7.72(68%)	2.96(29%) 8.22(71%)
PNTPPZn	667	0.02	0.03	3.21	3.39
HNTPP	655, 716	0.001	0.002	3.21	3.39

For comparison the *ortho*, *meta*, and *para* nitrophenyl derivative of octaethylporphyrin display lifetimes of 0.1 ns (φ_F= 0.002), 11.5 ns (φ_F= 0.05), and 10.7 ns (φ_F= 0.07) an a deoxygenated toluene methylcyclohexane solvent. Several β-pyrrole dinitro derivatives were also studied by Dahal et al. where the lifetime was found to be in the range of 1 – 2 ns in CH_2Cl_2 depending on the relative positions of the nitro groups.(*48*)

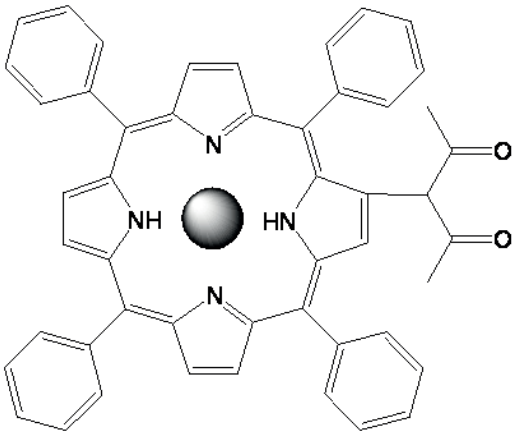

5,10,15,20-tetraphenyl-2-(1‟,1‟-diacetyl methyl)porphyrinato Zinc(II) (DATPPZn)

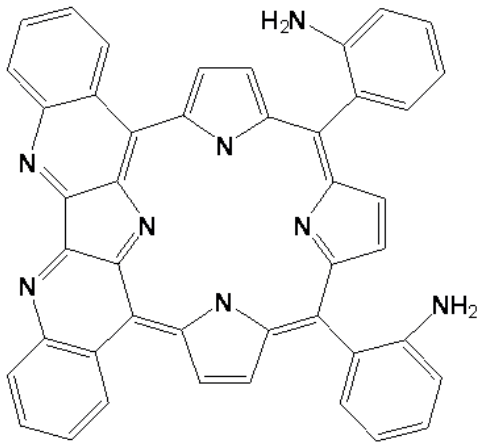

5,N-7,N-8,10-bisquinoline-15,20-bis-(2‟-aminophenyl)porphyrin

Figure 5.9: Structure of 5,10,15,20-tetraphenyl-2-(1‟,1‟-diacetylmethyl)porphyrinato Zinc(II) (DATPPZn) and N-7,N-8,10-bisquinoline-15,20-bis-(2‟-aminophenyl)porphyrin.

The absorption and fluorescence emission spectra of these two (Figure 5.9) porphyrinoids systems were recorded in DMSO and toluene. A broad Soret band for quinoline fused porphyrin was observed which indicates the aggregation of the porphyrin in the two solvents studied, consequently their low fluorescence quantum yield. However the Q-bands for this porphyrinoids gets red shifted, due to extended conjugation of the macrocycle. The red absorption and low Φ_f, is complementary of its high triplet quantum yield. This may make this compound a good candidate for PDT. The polar carbonyl group in DATPP porphyrinoid can bind with polar surfaces such as silica, ITO and so may be of interest for solar cell applications.

Table 5.7: Absorption, emission, fluorescence quantum yield and fluorescence lifetime data of porphyrinoids in toluene, Excitation= 414 nm, slits=2nm, Emission = 550-800, slits 2 nm, Absorbance at 414 nm = 0.1, For N_2 data gas was purged through the solution for ca. 10 min.

Compounds	Absorption peaks, λ_{max} nm (log ε)					Emission, λmax nm	Quantum yield, Φ_F		Fluorescence lifetime, nsec	
	B(0-0)	Q_y(1-0)	Q_y(0-0)	Q_x(1-0)	Q_x(0-0)		Air	N_2	Air	N_2
TPP	418 (5.19)	513(4.46)	547 (3.88)	592 (3.69	648 (3.71)	653, 719	0.11	0.11	9.34	11.32
M*m*PyP	420 (5.72)	516 (4.29)	549 (3.97)	593 (3.66)	649 (3.71)	654, 720	0.12	0.13	9.02	10.79
D*m*PyP	420 (6.08)	516 (4.68)	550 (4.27)	594 (4.21)	651 (4.12)	654, 719	0.10	0.11	8.64	10.67
T*m*PyP	420 (5.70)	516 (4.14)	548 (3.43)	590 (3.36)	648 (3.26)	653, 719	0.07	0.08	8.47	9.97
T*p*PyP	420 (5.58)	512 (4.24)	547 (3.26)	588 (3.78)	643 (3.44)	649, 715	0.06	0.07	9.32	11.26
MNTPP	422 (5.53)	524 (4.25)	564 (3.18)	601 (3.42)	661 (4.03)	690	0.05	0.06	3.21	3.39
MNTPP Zn	432 (5.66)	-------	567 (4.71)	-------	613 (4.69)	641	0.056	0.061	6.73(25%) 1.03(75%)	7.71(26%) 1.08(74%)
PNTPP	429 (5.70)	527 (4.77)	564 (4.61)	610 (4.58)	667 (4.57)	660, 698	0.043	0.048	2.87(32%) 7.72(68%)	2.96(29%) 8.22(71%)
PNTPP Zn	433 (5.67)	------	570 (4.72)	------	625 (4.69)	667	0.02	0.03	3.21	3.39
HNTPP	452 (5.33)	------	570 (4.46)	-----	627 (4.31)	655, 716	0.001	0.002	3.21	3.39
Zn dicarbonyl	425 (4.87)	--------	551 (3.65)	589 (3.48)	633 (3.35)	600, 646	0.04	0.06	1.87(93%) 0.28(7%)	1.95(91%) 0.28(9%)
Amino por	419 (4.71)	517 (3.12)	-----	607 (3.32)	681 (3.07)	654, 717	0.03	0.03	1.33(9%) 8.98(91%)	1.78(10% 10.4(90%)
DPP-Pd(PPh3)2Br	427 (4.89)	524 (3.29)	558 (3.42)	595 (3.10)	651 (3.22)	656, 716	0.01	0.012	7.72	8.75
DPP-Pt(PPh3)2Br	429 (4.87)	526 (3.44)	561 (3.44	600 (3.21)	655 (3.41)	656, 717	0.006	0.007	7.53	8.27

Table 5.8: Absorption, emission, fluorescence quantum yield and fluorescence lifetime data of porphyrinoids in DMSO, Excitation= 412 nm, slits=2nm, Emission = 550-800, slits 2 nm, Absorbance at 412 nm = 0.09, For N2 data gas was purged through the solution for ca. 10 min.

Compounds	Absorption peaks, λ_{max} nm (log ε)					Emission , λ_{max} nm	Quantum yield, Φ_F		Fluorescence lifetime, nsec	
	B(0-0)	Q_y(1-0)	Q_y(0-0)	Q_x(1-0)	Q_x(0-0)		Air	N_2	Air	N_2
TPP	418 (6.39)	514 (4.93)	548 (4.55)	589 (4.33)	645 (4.41)	650, 716	0.11	0.11	11.15	11.13
M*m*PyP	419 (6.36)	516 (4.88)	551 (4.56)	591 (4.32)	647 (4.41)	651, 716	0.10	0.11	10.50	10.77
D*m*PyP	419 (5.87)	515 (4.49)	551 (4.29)	591 (4.25)	648 (4.31)	651, 717	0.09	0.10	10.05	10.37
T*m*PyP	418 (5.98)	514 (4.64)	549 (4.35)	590 (4.37)	644 (4.38)	647, 715	0.07	0.08	9.49	9.79
T*p*PyP	419 (6.39)	515 (4.92)	551 (4.55)	591 (4.33)	647 (4.41)	651, 716	0.11	0.11	10.17	10.43
MNTPP	423 (6.56)	525 (4.61)	----------	607 (4.51)	663 (4.65)	649, 714	0.03	0.03	11.07	11.34
MNTPP Zn	431 (5.67)	-----	565 (4.72)	------	613 (4.71)	609, 699	0.012	0.012	2.73	3.12
PNTPP	429 (5.70)	526 (4.76)	562 (4.61)	608 (4.58)	666 (4.57)	685	0.010	0.001	3.26	3.29
PNTPP Zn	434 (5.09)	----	568 (4.47)	-------	628 (4.52)	695	0.003	0.003	0.25(35%) 6.16(65%)	0.27(21%) 7.54(79%)
HNTPP	447 (5.40)	-----	570 (4.11)	-------	622 (3.97)	648, 708	0.002	0.002	6.33	6.85
Zn dicarbonyl	430 (4.93)	-----	562 (3.73)	601 (3.53)	632 (3.41)	610, 662	0.03	0.04	1.70(84%) 0.32(16%)	1.16(73%) 2.67(27%)
Amino por	417 (4.76)	516 (3.11)	-----	604 (3.41)	688 (3.17)	654, 716	0.006	0.007	6.67(85%) 0.71(15%)	6.78(85%) 0.74(15%)
DPP-Pd(PPh3)2Br	419 (4.96)	514 (3.69)	554 (3.35)	591 (3.33)	647 (3.29)	655, 709	0.009	0.011	7.64(24%) 2.45(76%)	8.84(23%) 2.43(77%)
DPP-Pt(PPh3)2Br	428 (4.95	527 (3.56)	562 (3.52)	601 (3.26)	655 (3.46)	655	0.0008	0.001	4.70	5.60

5.5 Conclusions

The use of porphyrinoids to form self-assembled or self-organized structure to create functional, photonic materials has been cornerstone of much research because of their structural rigidity, chemical stability, and rich optical properties. The facile modulation of the photonic properties of porphyrins is accomplished both by the choice of substituents and choice of metal ion. Steric crowding and distortion of the macrocycle can alter the photonic properties of the chromophore. Pyridyl porphyrins are known to bind coordinatively with Pt(II) complex to form self-assembled structures for their applications in energy transfer or electron transfer devices. Platinum at the core of the porphyrin is known to quench the fluorescence completely. However when Pt combines coordinatively or attached covalently to porphyrins reduces their fluorescence quantum yield through exocyclic heavy atom effect. The extent of fluorescence quenching depends on the number of Pt atom attached. The nitro group on the porphyrins acts as precursor for the amino group formation also known to decrease the fluorescence quantum yield through heavy atom effect. The amount of quenching depends on the number and position of the nitro groups. The electron withdrawing nitro group attached to the peripheral position or at the *ortho* position of the *meso* phenyl group both polarizes the macrocycle thereby altering the HOMO and LUMO orbitals and providing a pathway for intramolecular charge transfer. and provides some spin-orbit coupling interactions compared to the nitro group attached at the *meta* or *para* position of the *meso* phenyl group. The low fluorescence quantum yield of both pyridyl porphyrins and nitro substituted porphyrin likely is concomitant with increased triplet quantum yield, thus may be good platforms to generate new photosensitizers for photodynamic therapy.

5.6 Appendix

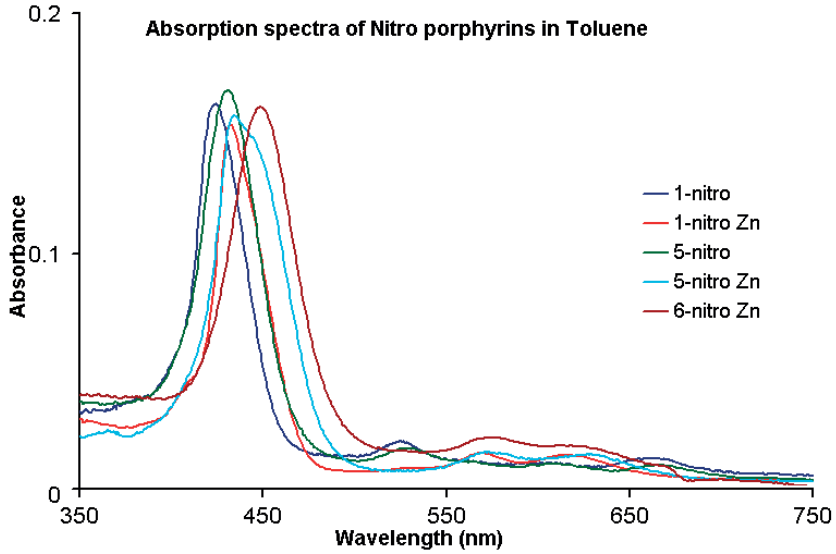

Figure A5.1: UV-visible spectra of various nitro porphyrins in toluene, concentration in each case is 0.33 μM.

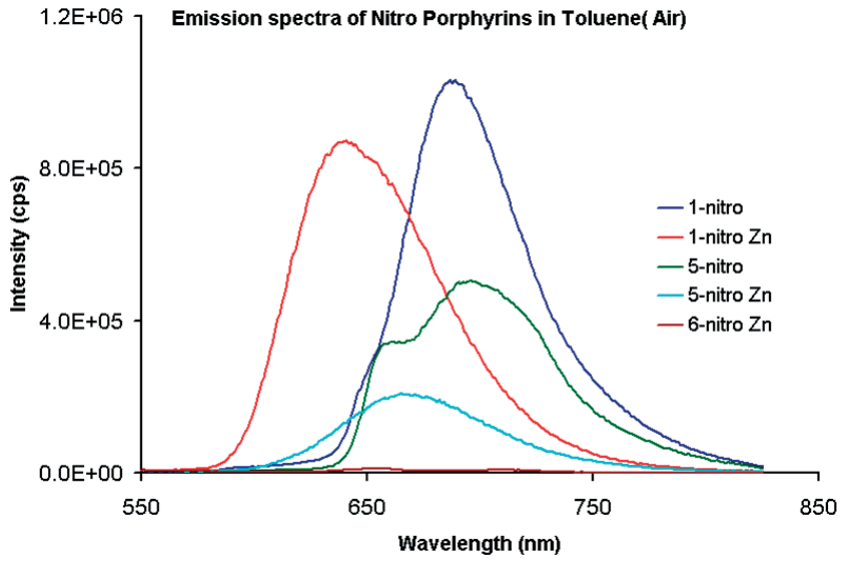

Figure A5.2: Emission spectra of various nitro porphyrins in toluene. Excitation at 414 nm, bandpass for both emission and excitation monochromator was 2 nm. Absorbencies for each compound at 414 nm ≤0.1.

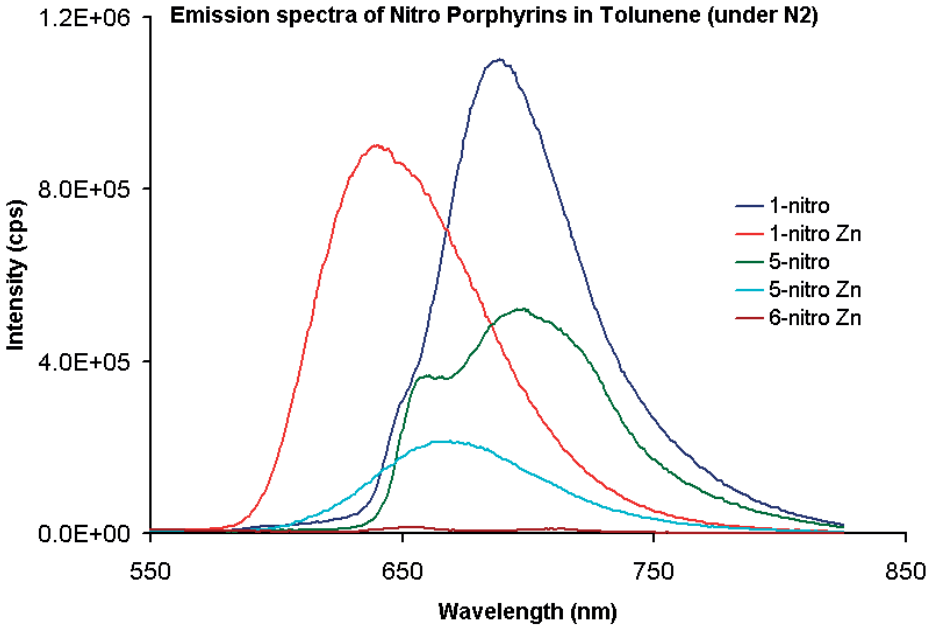

Figure A5.3: Emission spectra of various nitro porphyrins in toluene. Excitation at 414 nm, bandpass for both emission and excitation monochromator was 2 nm. Absorbencies for each compound at 414 nm ≤0.06. N_2 gas purged through the solution for ca. 10 min to deoxygenate the solution.

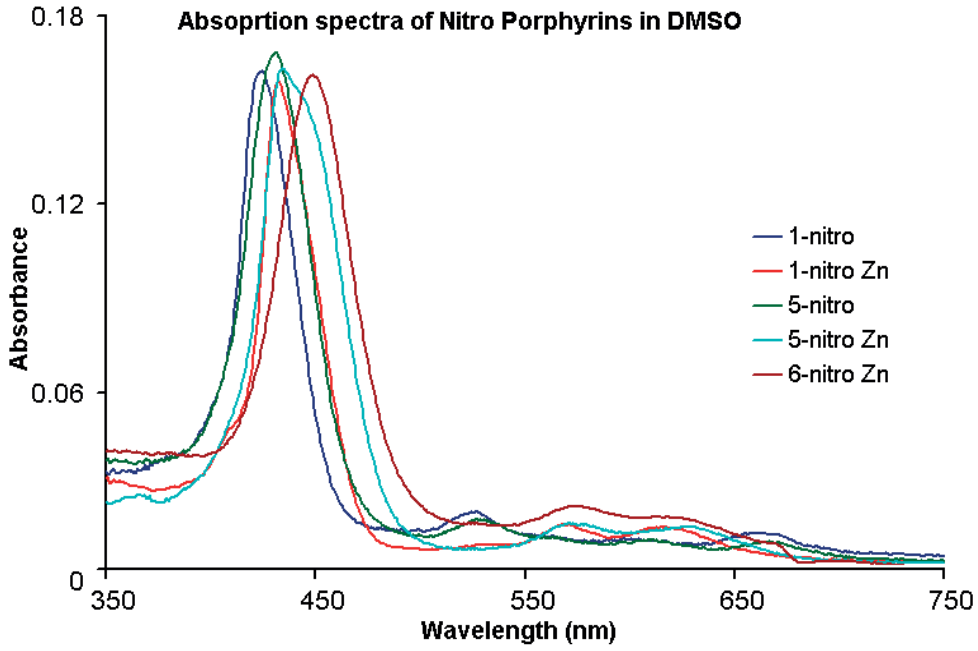

Figure A5.4: UV-visible spectra of various nitro porphyrins in DMSO, concentration in each case are 0.33 μM.

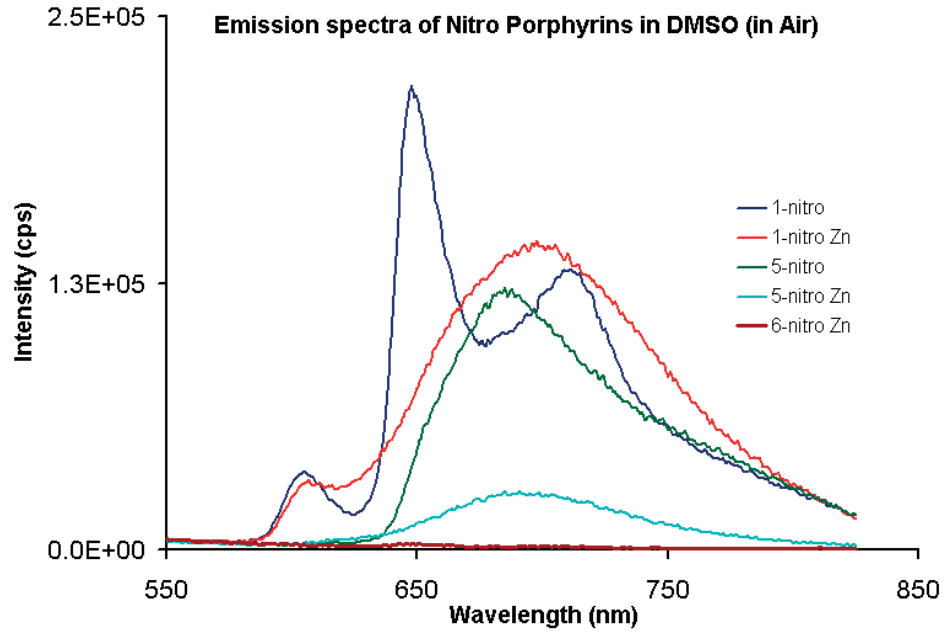

Figure A5.5: Emission spectra of various nitro porphyrins in DMSO. Excitation at 412 nm, bandpass for both emission and excitation monochromator was 2 nm. Absorbencies for each compound at 414 nm ≤0.1.

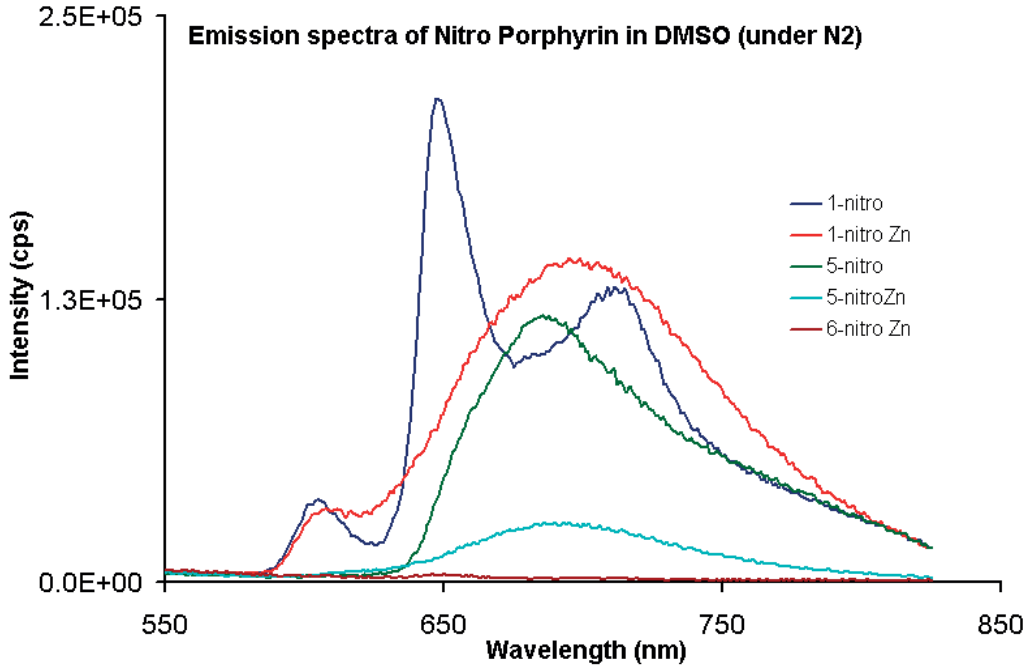

Figure A5.6: Emission spectra of various nitro porphyrins in DMSO. Excitation at 412 nm, bandpass for both emission and excitation monochromator was 2 nm. Absorbencies for each compound at 414 nm ≤0.09. N_2 gas purged through the solution for ca. 10 min to deoxygenate the solution.

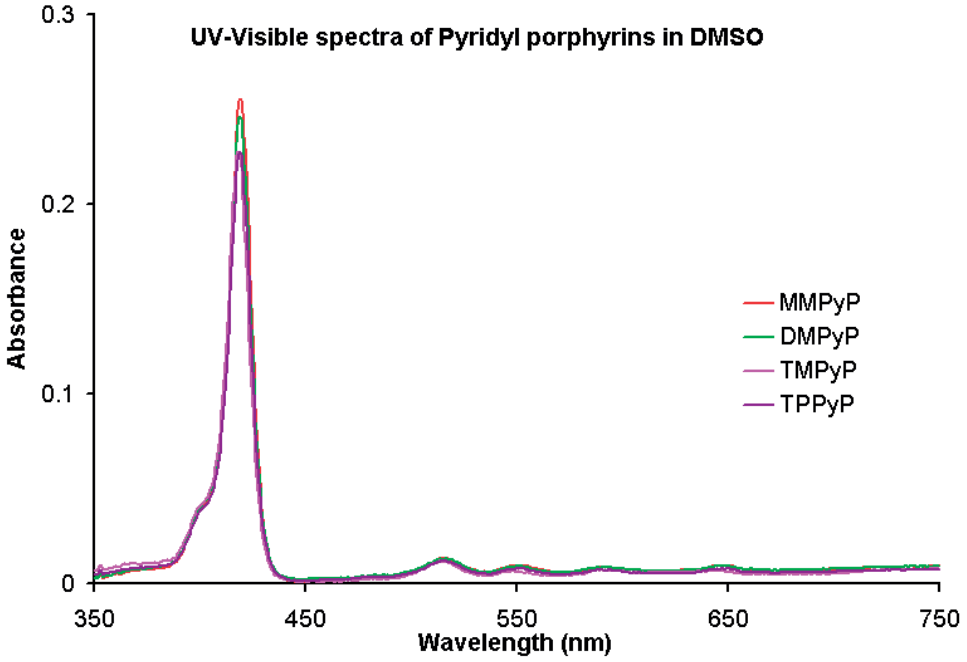

Figure A5.7: UV-visible spectra of various pyridyl porphyrins in DMSO, concentration in each case are 0.33 μM.

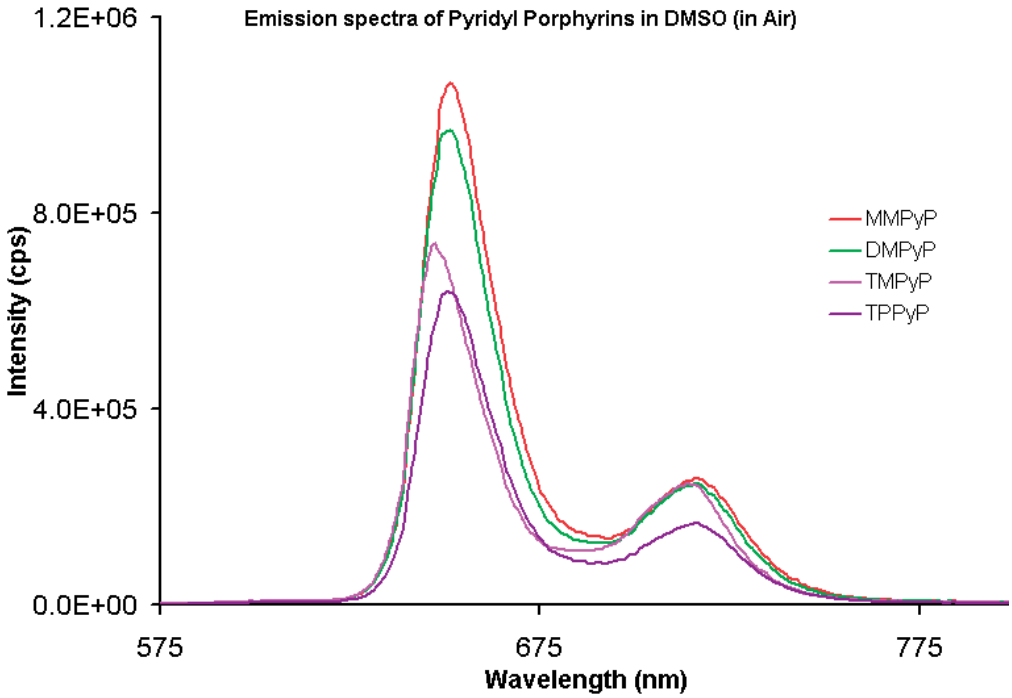

Figure A5.8: Emission spectra of various pyridyl porphyrins in DMSO. Excitation at 412 nm, bandpass for both emission and excitation monochromator was 2 nm. Absorbencies for each compound at 414 nm ≤0.09.

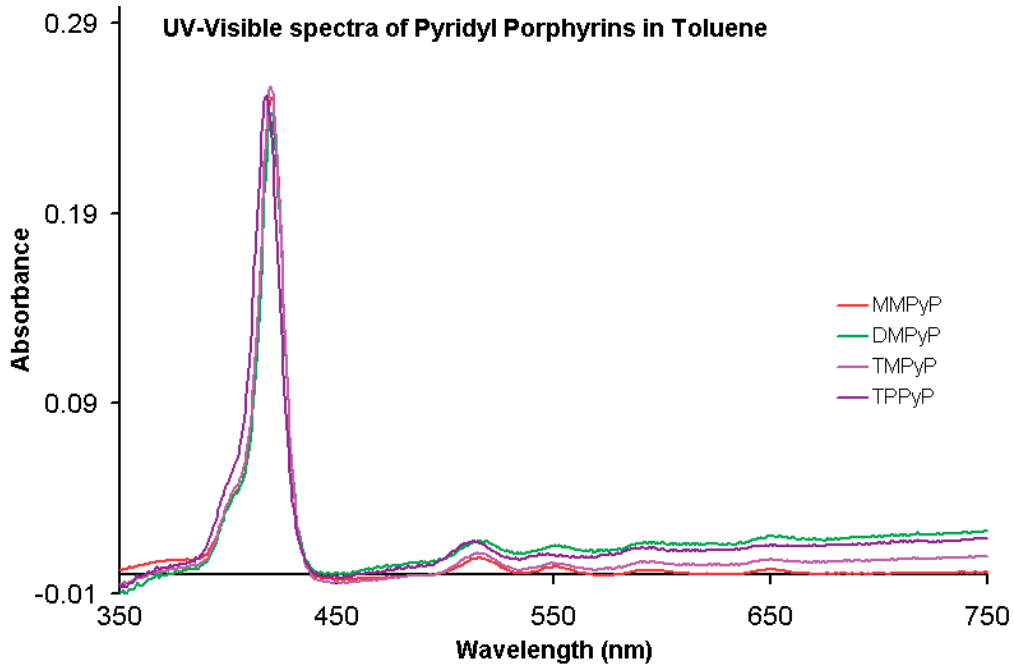

Figure A5.9: UV-visible spectra of various pyridyl porphyrins in toluene, concentration in each case are 0.33 μM.

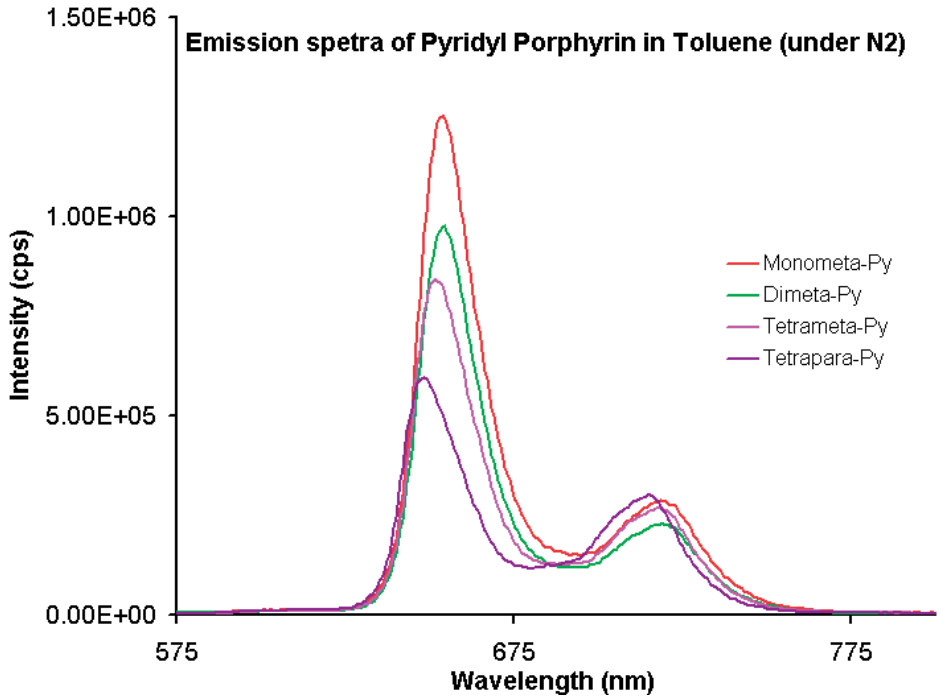

Figure A5.10: Emission spectra of various nitro porphyrins in toluene. Excitation at 414 nm, bandpass for both emission and excitation monochromator was 2 nm. Absorbencies for each compound at 414 nm ≤0.07. N_2 gas purged through the solution for ca. 10 min to deoxygenate the solution.

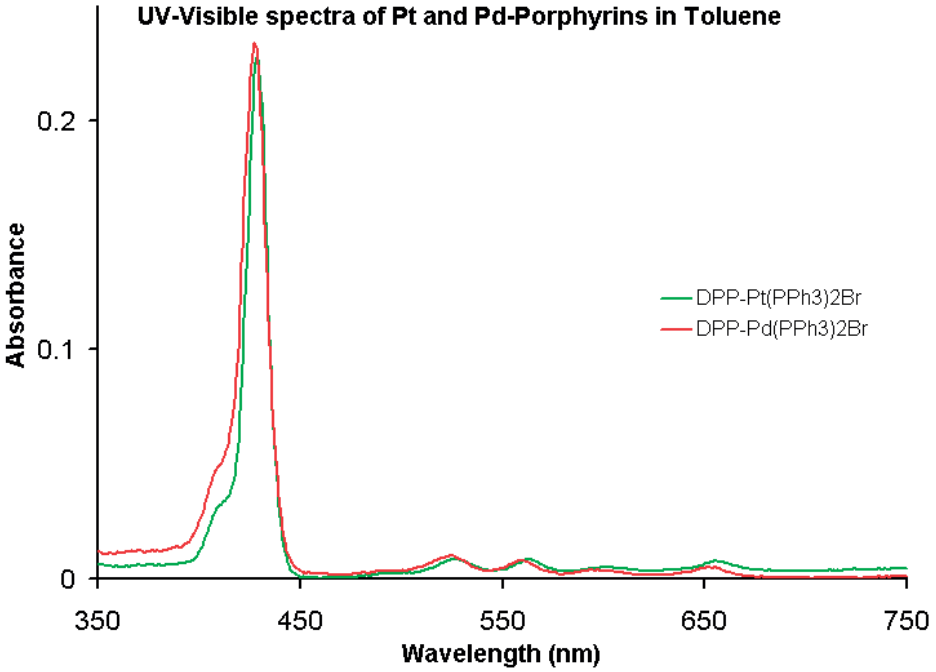

Figure A5.11: UV-visible spectra of exocyclic Pt and Pd porphyrins in toluene, concentration in each case are 0.33 μM.

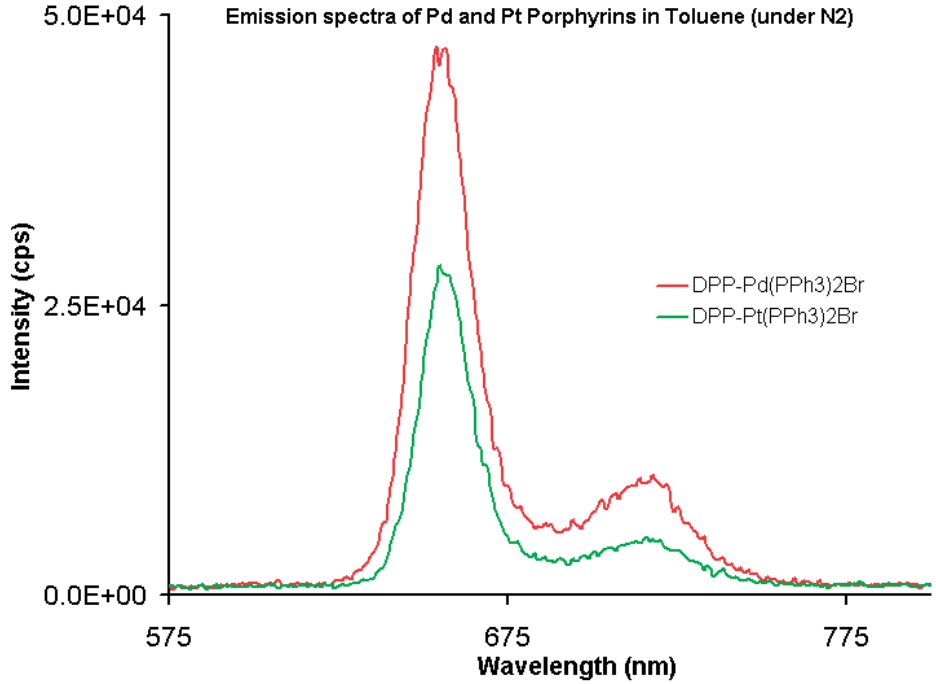

Figure A5.12: Emission spectra of various exocyclic Pt and Pd porphyrins in toluene. Excitation at 423 nm, bandpass for both emission and excitation monochromator was 2 nm. Absorbencies for each compound at 423 nm ≤0.12. N_2 gas purged through the solution for ca. 10 min to deoxygenate the solution.

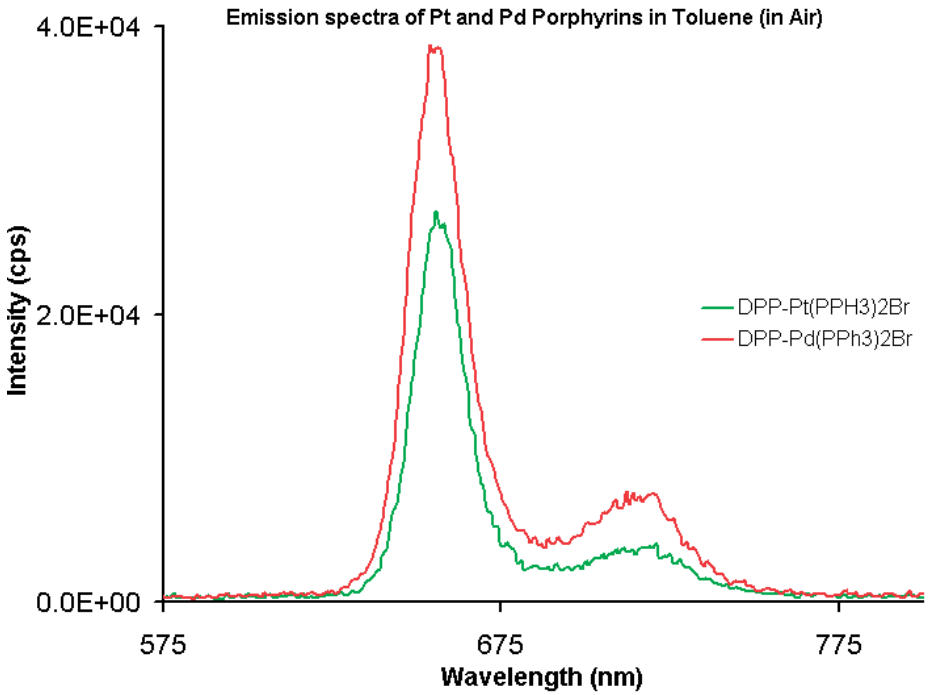

Figure A5.13: Emission spectra of various exocyclic Pt and Pd porphyrins in toluene. Excitation at 423 nm, bandpass for both emission and excitation monochromator was 2 nm. Absorbencies for each compound at 423 nm ≤0.12.

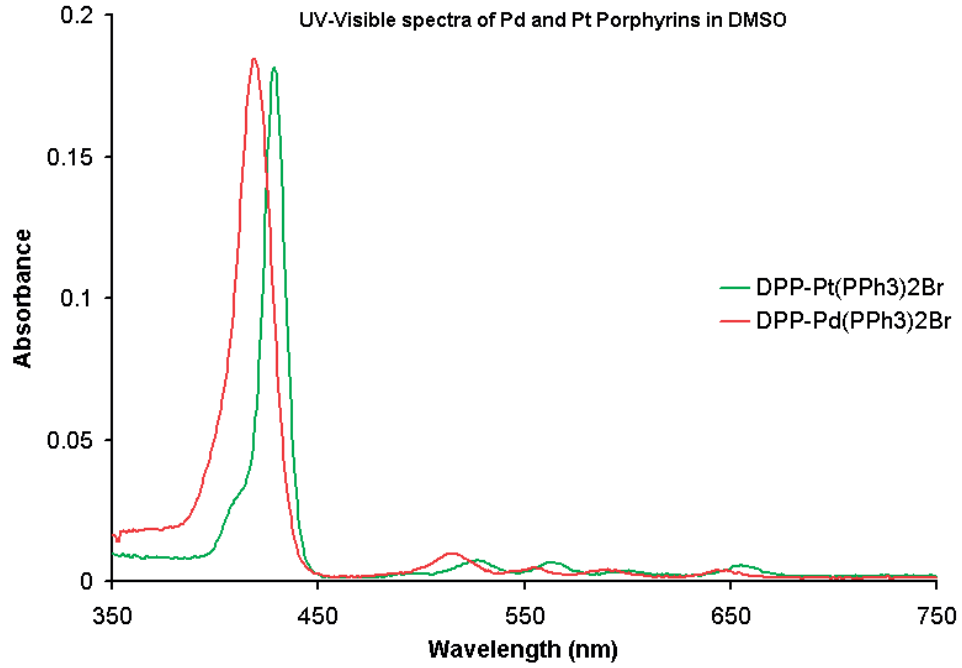

Figure A5.14: UV-visible spectra of exocyclic Pt and Pd porphyrins in DMSO, concentration in each case is 0.33 μM

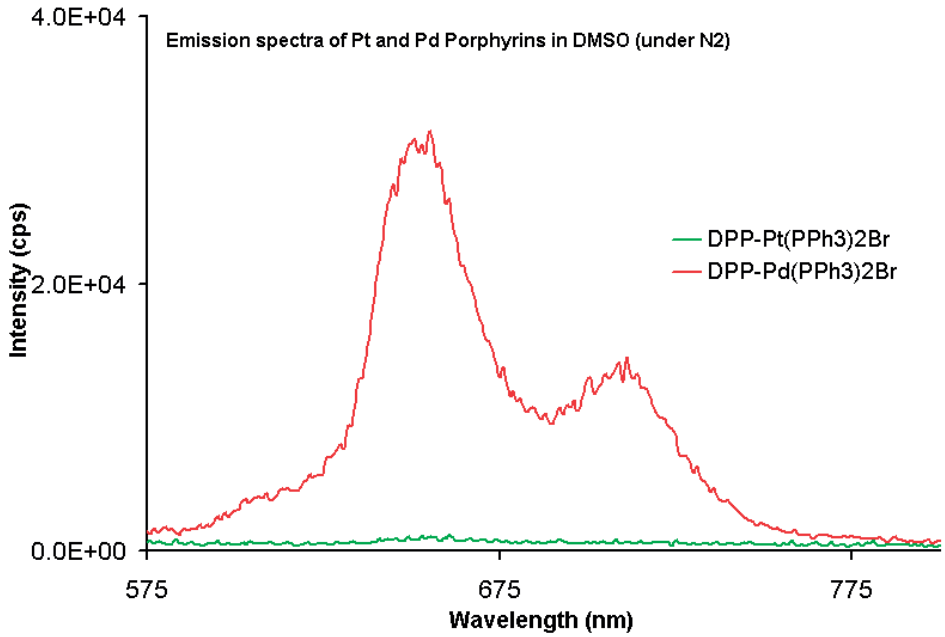

Figure A5.15: Emission spectra of various exocyclic Pt and Pd porphyrins in DMSO. Excitation at 425 nm, bandpass for both emission and excitation monochromator was 2 nm. Absorbencies for each compound at 425 nm ≤0.13. N_2 gas purged through the solution for ca. 10 min to deoxygenate the solution.

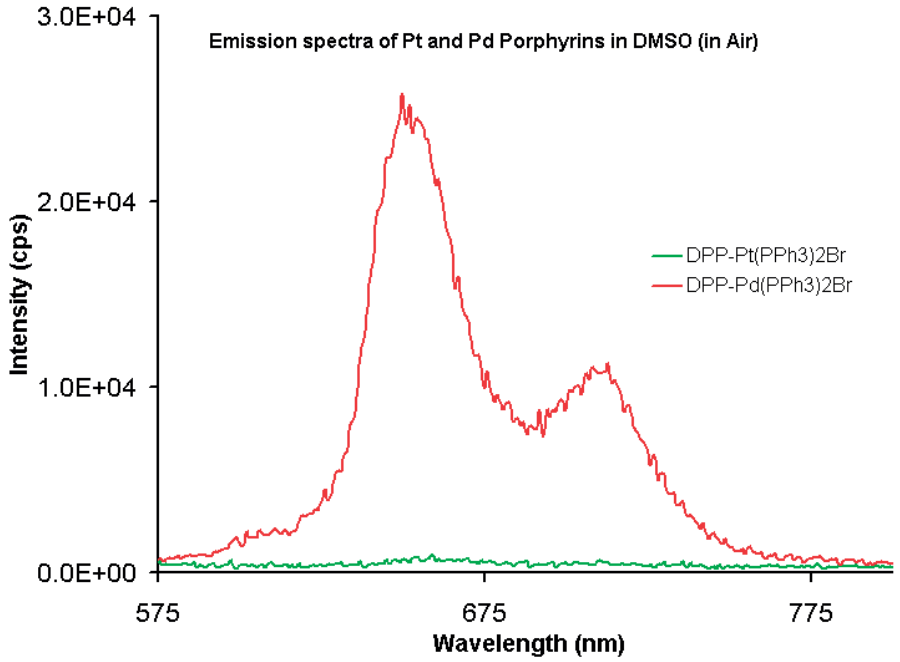

Figure A5.16: Emission spectra of various exocyclic Pt and Pd porphyrins in DMSO. Excitation at 425 nm, bandpass for both emission and excitation monochromator was 2 nm. Absorbencies for each compound at 425 nm ≤0.13.

Data File	HCMDMD23A.d	**Sample Name**	Nitroporhyrin
Sample Type	Sample	**Position**	P1-A1
Instrument Name	Instrument 1	**User Name**	
Acq Method		**Acquired Time**	5/13/2010 2:16:09 PM
IRM Calibration Status	Success	**DA Method**	HCEmpirical1.m
Comment	EM=629.2321 M=HC ESI Pos Small Molecule No HPLC.m		

Compound Table

Compound Label	RT	Mass	Abund	Formula	Tgt Mass	Diff (ppm)
Cpd 1: C44H29N5O2	0.273	659.232	4757	C44H29N5O2	659.2321	-0.24

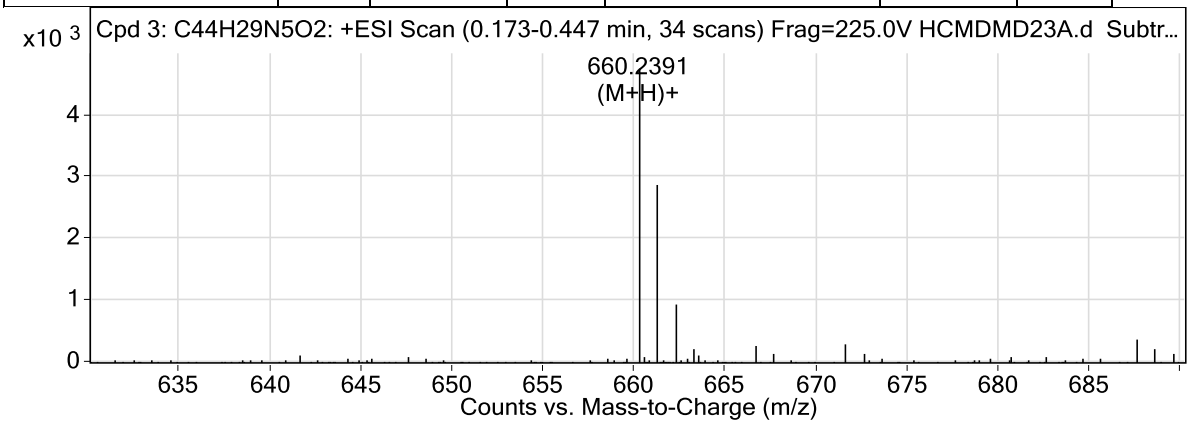

Figure A5.17: Mass spectrum of 3-Nitro-5,10,15,20-tetraphenylporphyrin (MNTPP).

Data File	HCMDAA03A.d	**Sample Name**	PNTPP
Sample Type	Sample	**Position**	P1-A1
Instrument Name	Instrument 1	**User Name**	
Acq Method		**Acquired Time**	8/9/2010 5:05:56 PM
IRM Calibration Status	Success	**DA Method**	HCEmpirical1.m
Comment	EM=839.1724 M=HC ESI Pos Small Molecule No HPLC.m		

Compound Table

Compound Label	RT	Mass	Abund	Formula	Tgt Mass	Diff (ppm)
Cpd 1: C44H25N9O10	0.282	839.1723	3784	C44H25N9O10	839.1724	-0.18

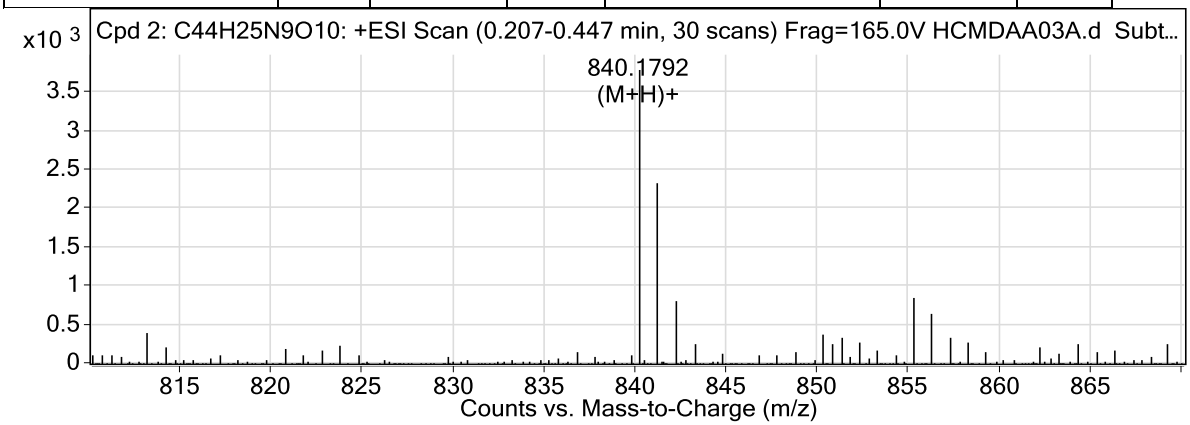

Figure A5.18: Mass spectrum of 3-Nitro-5,10,15,20-tetrakis(2‟-nitrophenyl)porphyrin (PNTPP).

Data File	HCMDAA04A.d	**Sample Name**	ZnPNTPP
Sample Type	Sample	**Position**	P1-A2
Instrument Name	Instrument 1	**User Name**	
Acq Method		**Acquired Time**	8/9/2010 5:18:01 PM
IRM Calibration Status	Success	**DA Method**	HCEmpirical1.m
Comment	EM=901.0859 M=HC ESI Pos Small Molecule No HPLC.m		

Compound Table

Compound Label	RT	Mass	Abund	Formula	Tgt Mass	Diff (ppm)
Cpd 1: C44H23N9O10Zn	0.283	901.0837	855	C44H23N9O10Zn	901.0859	-2.51

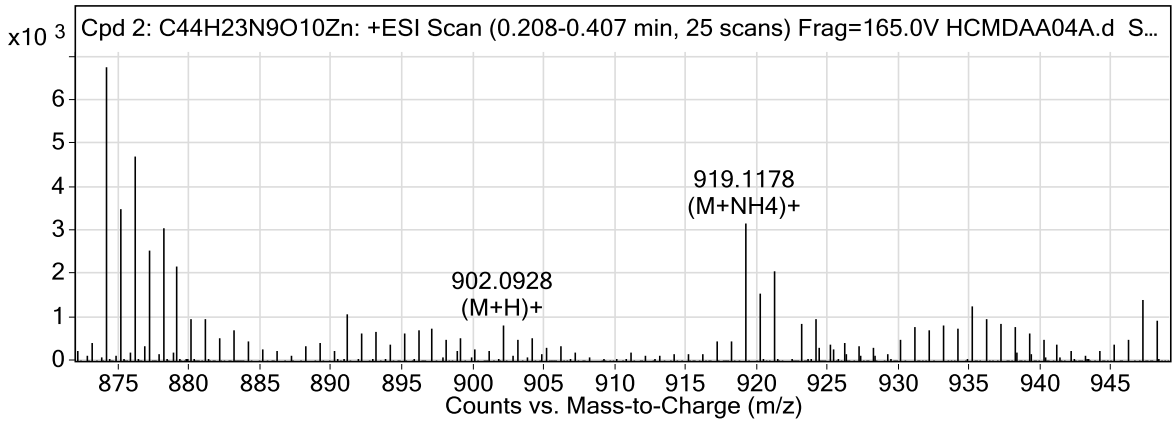

Figure A5.19: Mass spectrum of 3-Nitro-5,10,15,20-tetrakis(2‟-nitrophenyl)porphyrinato zinc(II) (PNTPPZn(II)).

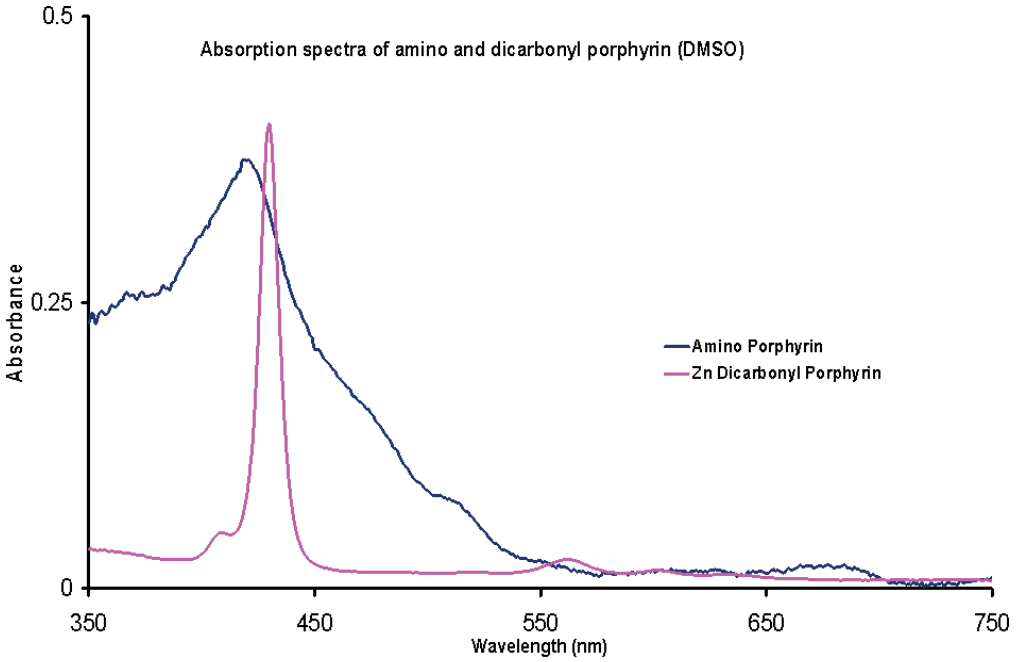

Figure A5.20: UV-visible spectra of amino porphyrin and zinc dicarbonyl porphyrin in DMSO. Concentration in each solution was 0.33 μM.

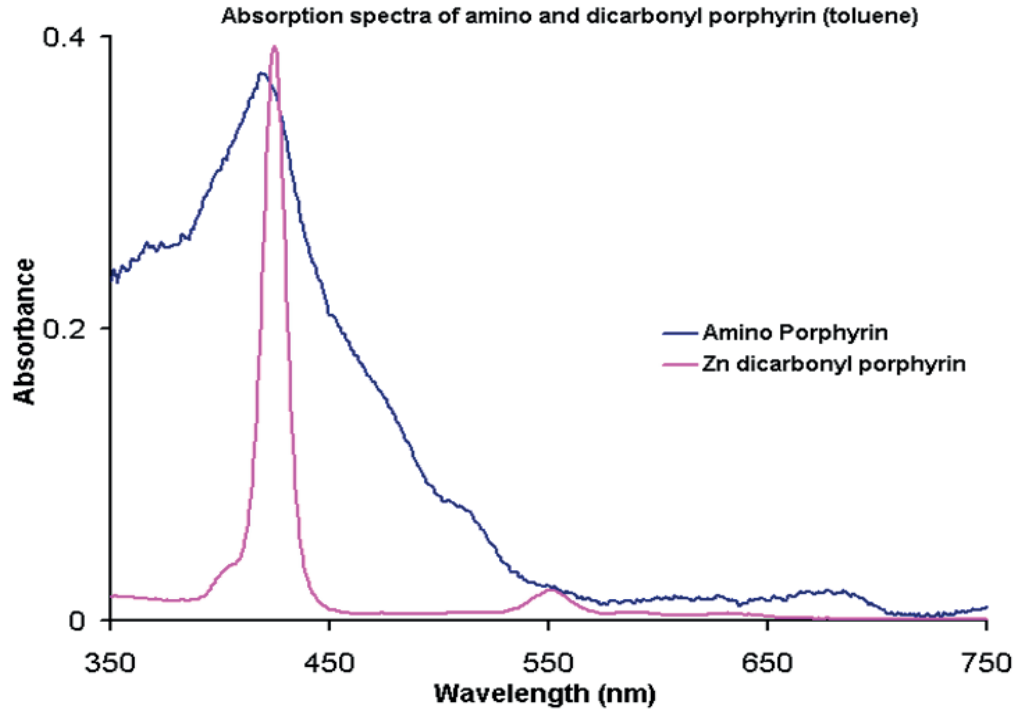

Figure A5.21: UV-visible spectra of amino porphyrin and zinc dicarbonyl porphyrin in toluene. Concentration in each solution was 0.33 μM.

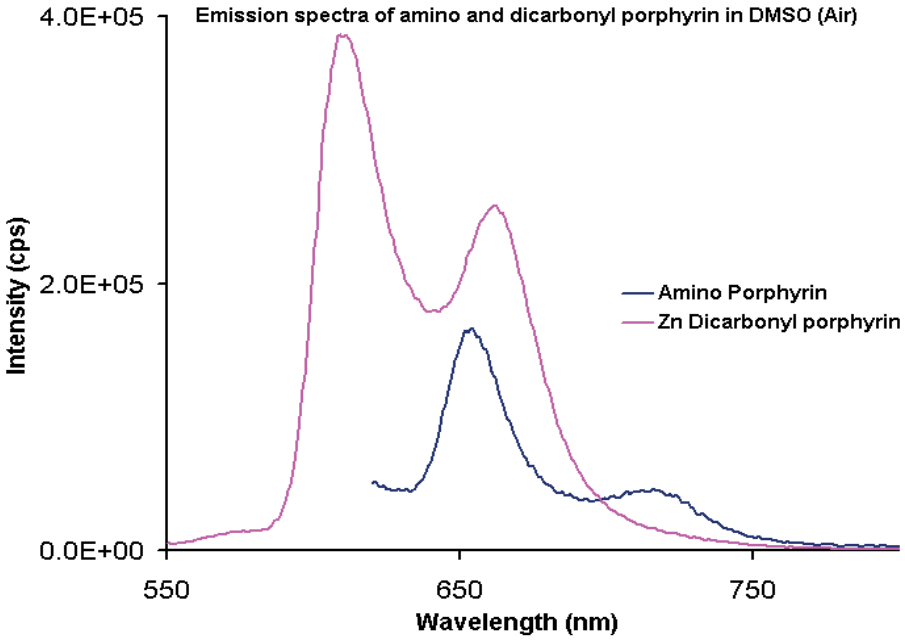

Figure A5.22: Emission spectra of amino porphyrin and zinc dicarbonyl porphyrin in DMSO (air). Excitation at 419 nm, bandpass for both emission and excitation monochromator was 2 nm. Absorbencies for each compound at 419 nm ≤0.094.

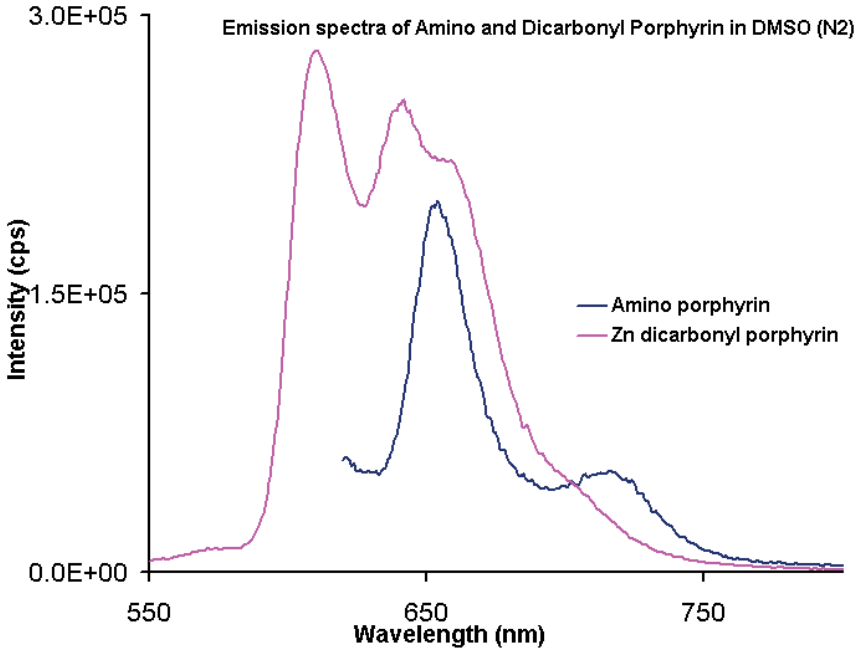

Figure A5.23: Emission spectra of amino porphyrin and zinc dicarbonyl porphyrin in DMSO (air). Excitation at 419 nm, bandpass for both emission and excitation monochromator was 2 nm. Absorbencies for each compound at 419 nm ≤0.094. N_2 gas purged through the solution for ca. 10 min to deoxygenate the solution.

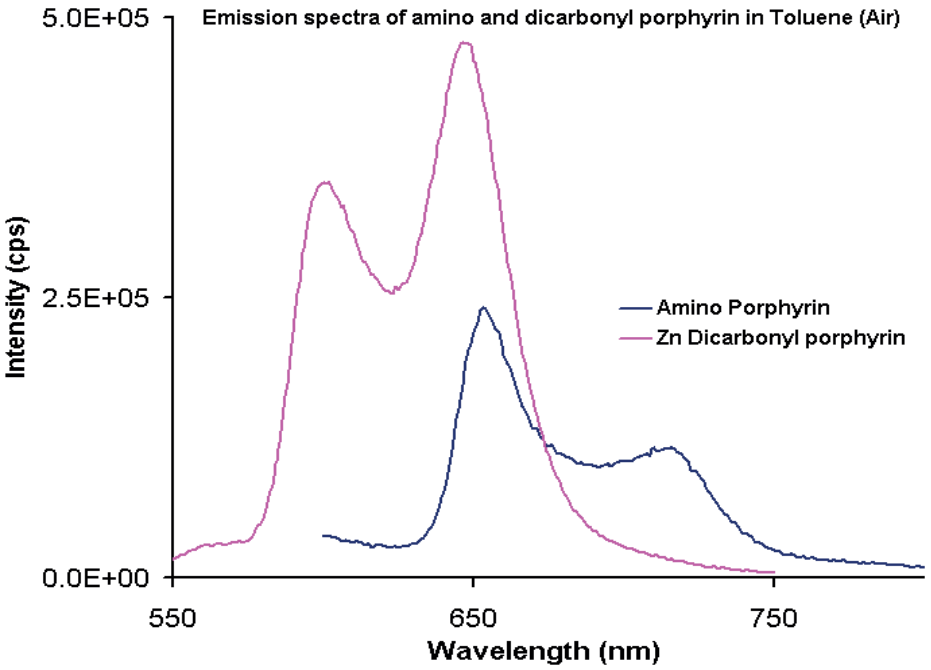

Figure A5.24: Emission spectra of amino porphyrin and zinc dicarbonyl porphyrin in toluene (air). Excitation at 409 nm, bandpass for both emission and excitation monochromator was 2 nm. Absorbencies for each compound at 409 nm ≤0.047.

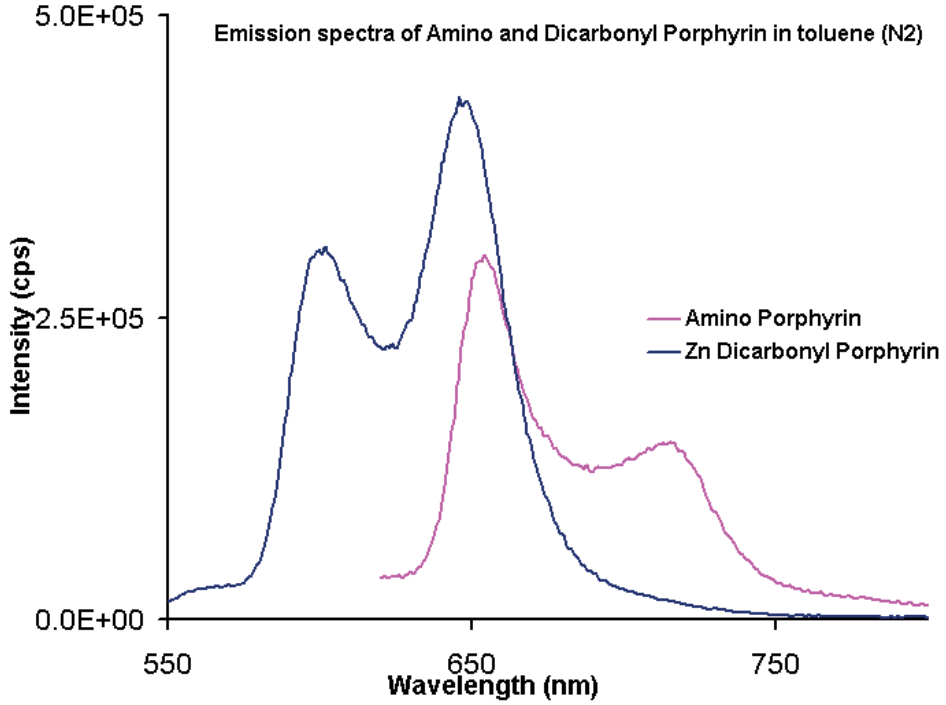

Figure A5.25: Emission spectra of amino porphyrin and zinc dicarbonyl porphyrin in DMSO (air). Excitation at 409 nm, bandpass for both emission and excitation monochromator was 2 nm. Absorbencies for each compound at 409 nm ≤0.047. N_2 gas purged through the solution for ca. 10 min to deoxygenate the solution.

5.7 References

1. Karolczak, J., Kowalska, D., Lukaszewicz, A., Maciejewski, A., and Steer, R. P. (2004) Photophysical Studies of Porphyrins and Metalloporphyrins: Accurate Measurements of Fluorescence Spectra and Fluorescence Quantum Yields for Soret Band Excitation of Zinc Tetraphenylporphyrin, *J. Phys. Chem. A 108*, 4570-4575.
2. Weimin, S., Qi, S., Yucheng, W., Lihong, L., and Jingchao, T. (2010) An alternative approach to amino porphyrins, *J. Heterocyclic chem. 47*, 1221-1224.
3. Karki, L., Vance, F. W., Hupp, J. T., LeCours, S. M., and Therien, M. J. (1998) Electronic Stark Effect Studies of a Porphyrin-Based Push−Pull Chromophore Displaying a Large First Hyperpolarizability: State-Specific Contributions to β, *J. Am. Chem. Soc. 120*, 2606-2611.
4. Suslick, K. S., Chen, C.-T., Meredith, G. R., and Cheng, L.-T. (1992) Push-Pull Porphyrins as nonlinear optical materials, *J. Am. Chem. Soc. 114*, 6928-6930.
5. Gust, D., Moore, T. A., Luttrull, D. K., Seely, G. R., Bittersmann, E., Bensasson, R. V., Rougée, M., Land, E. J., Schryver, F. C. D., and Auweraer, M. V. d. (1990) Photophysical Properties of 2-Nitro-5,10,15,20-tetra-p-tolylporphyrins, *Photochem. Photobiol. 51*, 419-426.
6. Barkigia, K. M., Renner, M. W., Senge, M. O., and Fajer, J. (2004) Interplay of Axial Ligation, Hydrogen Bonding, Self-Assembly, and Conformational Landscapes in High-Spin Ni(II) Porphyrins, *J. Phys. Chem. B 108*, 2173-2180.
7. Ono, N., Muratani, E., Fumoto, Y., Ogawa, T., and Tazima, K. (1998) Synthesis of 2,7,12,17-tetraaryl-3,8,13,18-tetranitroporphyrins; electronic effects on aggregation properties of porphyrins, *J. Chem. Soc., Perkin Trans. 1*, 3819-3824.
8. Drain, C. M., and Lehn, J.-M. (1994) Self-assembly of square multiporphyrin arrays by metal ion coordination, *J. Chem. Soc., Chem. Commun.*, 2313-2315.
9. Drain, C. M., Nifiatis, F., Vasenko, A., and Batteas, J. D. (1998) Ein Porphyrin-Mosaik nach Plan: metallvermittelte Selbstorganisation von großen Gittern und Bändern, *Angew. Chem. 110*, 2478-2481.
10. Hwang, I.-W., Kamada, T., Ahn, T. K., Ko, D. M., Nakamura, T., Tsuda, A., Osuka, A., and Kim, D. (2004) Porphyrin Boxes Constructed by Homochiral Self-

Sorting Assembly: Optical Separation, Exciton Coupling, and Efficient Excitation Energy Migration, *J. Am. Chem. Soc. 126*, 16187-16198.

11. Ogawa, K., Zhang, T., Yoshihara, K., and Kobuke, Y. (2001) Large Third-Order Optical Nonlinearity of Self-Assembled Porphyrin Oligomers, *J. Am. Chem. Soc. 124*, 22-23.
12. Takahashi, R., and Kobuke, Y. (2003) Hexameric Macroring of Gable-Porphyrins as a Light-Harvesting Antenna Mimic, *J. Am. Chem. Soc. 125*, 2372-2373.
13. Shoji, O., Okada, S., Satake, A., and Kobuke, Y. (2005) Coordination Assembled Rings of Ferrocene-Bridged Trisporphyrin with Flexible Hinge-like Motion: Selective Dimer Ring Formation, Its Transformation to Larger Rings, and Vice Versa, *J. Am. Chem. Soc. 127*, 2201-2210.
14. Hunter, C. A., Sanders, J. K. M., Beddard, G. S., and Evans, S. (1989) A new approach to the assembly of electron donor-spacer-acceptor systems, *J. Chem. Soc., Chem. Commun.*, 1765-1767.
15. Maeda, C., Kim, P., Cho, S., Park, J. K., Lim, J. M., Kim, D., Vura-Weis, J., Wasielewski, M. R., Shinokubo, H., and Osuka, A. (2010) Large Porphyrin Squares from the Self-Assembly of meso-Triazole-Appended L-Shaped meso–meso-Linked ZnII–Triporphyrins: Synthesis and Efficient Energy Transfer, *Chem. Eur. J. 16*, 5052-5061.
16. Drain, C. M., Varotto, A., and Radivojevic, I. (2009) Self-Organized Porphyrinic Materials, *Chem. Rev. 109*, 1630-1658.
17. Beletskaya, I., Tyurin, V. S., Tsivadze, A. Y., Guilard, R., and Stern, C. (2009) Supramolecular Chemistry of Metalloporphyrins, *Chem. Rev. 109* 1659-1713.
18. Chang, S. H., Chung, K.-B., Slone, R. V., and Hupp, J. T. (2001) Crown ether functionalization of a porphyrin-based "molecular square": induction of fluorescence sensitivity to alkali metal cations, *Synthetic Metals 117*, 215-217.
19. Lee, S. J., and Hupp, J. T. (2006) Porphyrin-containing molecular squares: Design and applications, *Coord. Chem. Rev. 250*, 1710-1723.
20. Drain, C. M., Hupp, J. T., Suslick, K. S., Wasielewski, M. R., and Chen, X. (2002) A perspective on four new porphyrin-based functional materials and devices, *J. Porphyrins Phthalocyanines 6*, 241-256.

21. Drain, C. M., Batteas, J. D., Flynn, G. W., Milic, T., Chi, N., Yablon, D. G., and Sommers, H. (2002) Designing supramolecular porphyrin arrays that self-organize into nanoscale optical and magnetic materials, *Proc. Natl. Acad. Sci. 99*, 6498-6502.

22. Milic, T. N., Chi, N., Yablon, D. G., Flynn, G. W., Batteas, J. D., and Drain, C. M. (2002) Controlled hierarchical self-assembly and deposition of nanoscale photonic materials, *Angew Chem. Int. Ed. 41*, 2117-2119.

23. Scandola, F., Chiorboli, C., Prodi, A., Iengo, E., and Alessio, E. (2006) Photophysical properties of metal-mediated assemblies of porphyrins, *Coord. Chem. Rev. 250*, 1471-1496.

24. Prodi, A., Chiorboli, C., Scandola, F., Iengo, E., Alessio, E., Dobrawa, R., and Würthner, F. (2005) Wavelength-Dependent Electron and Energy Transfer Pathways in a Side-to-Face Ruthenium Porphyrin/Perylene Bisimide Assembly, *J. Am. Chem. Soc. 127*, 1454-1462.

25. Drain, C. M. (2002) Supramolecular Chemistry And Self-assembly Special Feature: Self-organization of self-assembled photonic materials into functional devices: Photo-switched conductors, *Proc. Natl. Acad. Sci. 99*, 5178-5182.

26. Iengo, E., Zangrando, E., Minatel, R., and Alessio, E. (2002) Metallacycles of Porphyrins as Building Blocks in the Construction of Higher Order Assemblies through Axial Coordination of Bridging Ligands: Solution- and Solid-State Characterization of Molecular Sandwiches and Molecular Wires, *J. Am. Chem. Soc. 124*, 1003-1013.

27. Libera, J. A., Gurney, R. W., Schwartz, C., Jin, H., Lee, T.-L., Nguyen, S. T., Hupp, J. T., and Bedzyk, M. J. (2005) Comparative X-ray Standing Wave Analysis of Metal−Phosphonate Multilayer Films of Dodecane and Porphyrin Molecular Square, *J. Phys. Chem. B 109*, 1441-1450.

28. Splan, K. E., Massari, A. M., and Hupp, J. T. (2004) A Porous Multilayer Dye-Based Photoelectrochemical Cell That Unexpectedly Runs in Reverse, *J. Phys. Chem. B 108*, 4111-4115.

29. Massari, A. M., Gurney, R. W., Schwartz, C. P., Nguyen, S. T., and Hupp, J. T. (2004) Walljet Electrochemistry: Quantifying Molecular Transport through

Metallopolymeric and Zirconium Phosphonate Assembled Porphyrin Square Thin Films, *Langmuir 20*, 4422-4429.

30. Jensen, R. A., Kelley, R. F., Joong Lee, S., Wasielewski, M. R., Hupp, J. T., and Tiede, D. M. (2008) Fast energy transfer within a self-assembled cyclic porphyrin tetramer, *Chem. Commun.*, 1886-1888.
31. Milic, T., Garno, J. C., Batteas, J. D., Smeureanu, G., and Drain, C. M. (2004) Self-Organization of Self-Assembled Tetrameric Porphyrin Arrays on Surfaces, *Langmuir 20*, 3974-3983.
32. Iengo, E., Zangrando, E., Bellini, M., Alessio, E., Prodi, A., Chiorboli, C., and Scandola, F. (2005) Pyridylporphyrin Metallacycles with a Slipped Cofacial Geometry: Spectroscopic, X-ray, and Photophysical Characterization, *Inorg. Chem. 44*, 9752-9762.
33. Nifiatis, F., Athas, J. C., Gunaratne, K. D. D., Gurung, Y., Monette, K. M., and Shivokevich, P. J. (2011) Substituent Effects of Porphyrin on Singlet Oxygen Generation Quantum Yields, *The open spectroscopy journal 5*, 1-12.
34. Harriman, A. (1981) Luminescence of porphyrins and metalloporphyrins. Part 3.- Heavy-atom effects, *J. Chem. Soc., Faraday Trans. 2: Mol. Chem. Phys. 77*, 1281-1291.
35. Tripathy, U., Kowalska, D., Liu, X., Velate, S., and Steer, R. P. (2008) Photophysics of Soret-Excited Tetrapyrroles in Solution. I. Metalloporphyrins: MgTPP, ZnTPP, and CdTPP, *J. Phys. Chem. A 112*, 5824-5833.
36. Drain, C. M., Kirmaier, C., Medforth, C. J., Nurco, D. J., Smith, K. M., and Holten, D. (1996) Dynamic Photophysical Properties of Conformationally Distorted Nickel Porphyrins. 1. Nickel(II) Dodecaphenylporphyrin, *J. Phys. Chem. 100*, 11984-11993.
37. Drain, C. M., Gentemann, S., Roberts, J. A., Nelson, N. Y., Medforth, C. J., Jia, S., Simpson, M. C., Smith, K. M., Fajer, J., Shelnutt, J. A., and Holten, D. (1998) Picosecond to Microsecond Photodynamics of a Nonplanar Nickel Porphyrin: Solvent Dielectric and Temperature Effects, *J. Am. Chem. Soc. 120*, 3781-3791.
38. Retsek, J. L., Drain, C. M., Kirmaier, C., Nurco, D. J., Medforth, C. J., Smith, K. M., Sazanovich, I. V., Chirvony, V. S., Fajer, J., and Holten, D. (2003)

Photoinduced Axial Ligation and Deligation Dynamics of Nonplanar Nickel Dodecaarylporphyrins, *J. Am. Chem. Soc. 125*, 9787-9800.

39. Azenha, E. G., Serra, A. C., Pineiro, M., Pereira, M. M., Seixas de Melo, J., Arnaut, L. G., Formosinho, S. J., and Rocha Gonsalves, A. M. d. A. (2002) Heavy-atom effects on metalloporphyrins and polyhalogenated porphyrins, *Chem. Phys. 280*, 177-190.
40. António M.d'A. Rocha Gonsalves, Arménio C. Serra, and Pineiro, M. (2009) The small stones of Coimbra in the huge tetrapyrrolic chemistry building *J. Porphyrins Phthalocyanines 13*, 429-445.
41. Hartnell, R. D., and Arnold, D. P. (2004) Peripherally η^1-Platinated Organometallic Porphyrins as Building Blocks for Multiporphyrin Arrays, *Organometallics 23*, 391-399.
42. Prodi, A., Kleverlaan, C. J., Indelli, M. T., Scandola, F., Alessio, E., and Iengo, E. (2001) Photophysics of Pyridylporphyrin Ru(II) Adducts: Heavy-Atom Effects and Intramolecular Decay Pathways, *Inorg. Chem. 40*, 3498-3504.
43. Prodi, A., Indelli, M. T., Kleverlaan, C. J., Alessio, E., and Scandola, F. (2002) Energy transfer pathways in pyridylporphyrin metal adducts and side-to-face arrays, *Coord. Chem. Rev. 229*, 51-58.
44. Seybold, P. G., and Gouterman, M. (1969) Porphyrins : XIII: Fluorescence spectra and quantum yields, *J. Mol. Spectroscopy 31*, 1-13.
45. Drain, C. M., Varotto, A., and Radivojevic, I. (2009) Self-Organized Porphyrinic Materials, *Chem. Rev. 109*, 1630-1658.
46. Hartnell, R. D., and Arnold, D. P. (2004) Peripherally Metallated Porphyrins: the First Examples of meso-η^1-Palladio(II) and -Platinio(II) Complexes with Chelating Diamine Ligands, *Eur. J. Inorg. Chem.*, 1262-1269.
47. Hartnell, R. D., Edwards, A. J., and Arnold, D. P. (2002) Peripherally-metallated porphyrins: meso-η^1-porphyrinyl-platinum(II) complexes of 5,15-diaryl- and 5,10,15-triarylporphyrins, *J. Porphyrins Phthalocyanines 6*, 695-707.
48. Dahal, S., and Krishnan, V. (1997) Excited singlet state intramolecular charge transfer in di and trinitrotetraphenylporphyrins, *Chem. Phys. Lett. 274*, 390-395.

49. Karelson, M., Pihlaja, K., Tamm, T., Uri, A., and Zerner, M. C. (1995) UV-visible spectra of some nitro-substituted porphyrins, *J. Photochem. Photobiol. A: Chem. 85*, 119-126.

50. Knyukshto, V., Sagun, E., Shulʹga, A., Bachilo, S., and Zenʹkevich, É. (2000) Photoinduced electron transfer in meso-nitrophenyl-substituted porphyrins and their chemical dimers, *Opt. Spectroscopy 88*, 205-216.

51. Takahashi, K., Hase, S., Komura, T., Imanaga, H., and Ohno, O. (1992) The Fluorescence Properties of (2-Nitro-5,10,15,20- tetraphenylporphyrinato)zinc, *Bull. Chem. Soc. Jpn. 65*, 1475-1481.

52. Knyukshto, V., Zenkevich, E., Sagun, E., Shulga, A., and Bachilo, S. (1999) Pathways for photoinduced electron transfer in meso-nitro-phenyl-octaethylporphyrins and their chemical dimers, *Chem. Phys. Lett. 304*, 155-166.

53. Hirschfeld, T. (1976) Quantum efficiency independence of the time integrated emission from a fluorescent molecule, *Appl. Opt. 15*, 3135-3139.

54. Senge, M. O., Eigenbrot, C. W., Brennan, T. D., Shusta, J., Scheidt, W. R., and Smith, K. M. (1993) Aggregation properties of nitroporphyrins: comparisons between solid-state and solution structures, *Inorg. Chem. 32*, 3134-3142.

55. Serra, O. A., Neri, C. R., Iamamoto, Y., Nassar, E. J., Calefi, P. S., Cicillini, S. A., and Manso, C. M. C. P. (1999) Study of the Suppression of Porphyrin Emission upon Addition of Rare Earth Ions, *J. Incl. Phenom. Macro. Chem. 35*, 271-280.

56. Chirvony, V. S., van Hoek, A., Schaafsma, T. J., Pershukevich, P. P., Filatov, I. V., Avilov, I. V., Shishporenok, S. I., Terekhov, S. N., and Malinovskii, V. L. (1998) On the Nature of the Fluorescent State in β-Nitrotetraarylporphyrins, *J. Phys. Chem. B 102*, 9714-9724.

Chapter 6: PHOTOPHYSICAL PROPERTIES OF THIOGLYCOSYLATED DERIVATIVES OF CHLORIN, ISOBACTERIOCHLORIN, AND BACTERIOCHLORIN FOR BIOIMAGING AND DIAGNOSTICS

Abstract

The photophysical properties of non-hydrolysable tetra- thioglycosylated conjugates of chlorin ($CGlc_4$), isobacteriochlorin ($IGlc_4$) and bacteriochlorin ($BGlc_4$) and core F_{20} platforms are reported here. These studies involve the measurement of absorption and emission spectra, fluorescence quantum yield, singlet oxygen quantum yield, and singlet state lifetime in three different solvents: phosphate buffer saline (PBS), ethanol, and ethylacetate. Compared to the porphyrin in PBS, $CGlc_4$ has a markedly greater absorbance of red light near 650 nm and a 6-fold increase in fluorescence quantum yield; whereas $IGlc_4$ has broad Q bands and a 12-fold increase in fluorescence quantum yield. Since $IGlc_4$ and $CGlc_4$ very slowly bleach, these properties may enable their use as fluorescent tags to track biological processes. $BGlc_4$ has a similar fluorescence quantum yield to $PGlc_4$, (<10%), but the lowest energy absorption/emission peaks of $BGlc_4$ are considerably red shifted to near 730 nm with a nearly 50-fold greater absorbance, which may allow this conjugate to be an effective PDT agent. The excited state lifetime of these conjugates ranges from 3-11 ns. The radiative time constant for $IGlc_4$ is 20 fold less while non-radiative time constant is 2 fold more than $BGlc_4$, indicates that $IGlc_4$ has greater potential to form triplet state via inter system crossing, and so can serves as a better PDT agent. The uptake of $CGlc_4$, $IGlc_4$ and $BGlc_4$ derivatives into cells such as human breast cancer cells MDA-MB-231

and K:Molv NIH 3T3 mouse fibroblast cells can be observed at nM concentrations. Photobleaching under these conditions is minimal.

6.1 Introduction[a]

For diagnostic and photodynamic therapeutic (PDT) applications, the absorption of the lower energy light (red – near infrared) is an important characteristic that the new generation compounds should possess because these wavelengths penetrate further into tissues.(*1-5*) For this reason, porphyrinoid derivatives such as chlorins, isobacteriochlorins, and bacteriochlorins are often synthesized because of their strong and/or redder lowest energy absorption band.(*6*) Chlorins are porphyrinoids with one pyrrole double bond missing. Isobacteriochlorins and bacteriochlorins are porphyrinoids with two pyrrole double bonds missing on adjacent or opposite pyrroles, respectively. A variety of organic transformations of porphyrins can yield these chromophores. Porphyrins, chlorins, bacteriochlorins, and isobacteriochlorins each have unique photophysical properties that are exploited by nature and can be used for diverse applications.(*7, 8*) Compared to the parent tetraarylporphyrin, the intensity of the lowest energy UV-visible absorption band near 650 nm can increase by ~20 fold for chlorins, and by ~5 fold for the isobacteriochlorins. For bacteriochlorins the absorption band near 650 nm is similar to porphyrins, but an additional high intensity absorption band appears near 730 nm. The excited state lifetimes, singlet and triplet quantum yields and distortion upon metal ion binding are

[a] Part of this chapter is adapted from Singh, S., Aggarwal, A., Thompson, S., Tom. , J. P. C., Zhu, X., Samaroo, D., Vinodu, M., Gao, R., and Drain, C. M., "Synthesis and Photophysical Properties of Thioglycosylated Chlorins, Isobacteriochlorins, and Bacteriochlorins for Bioimaging and Diagnostics", *Bioconjugate Chem.,* **2010**, *21*, 2136-2146.

significantly different for these three types of macrocycles.(*9, 10*) The synthesis of these compounds is described elsewhere.

Absorption of a photon of light by a photosensitizer causes the promotion of its ground state electron from HOMO to LUMO to produce the excited state. There are several ways that the excited electron may return to the ground state: (1) by emitting a photon (fluorescence), (2) by internal conversion with energy loss as heat, (3) intersystem crossing forming the triplet state (4) bimolecular processes such as energy and electron transfer. The triplet state of the photosensitizer can interact with the triplet ground state of dioxygen and causes an energy transfer to produce reactive singlet oxygen and the dye returns to the singlet ground state – this is widely referred to as sensitization. Singlet oxygen is a highly reactive oxygen species that reacts with diffusion limited kinetics to oxidize a variety of biomolecules and with water to generate other reactive oxygen species (ROS) such as hydroxyl radicals and peroxides. Cell stress and/or death results from oxidative damage at multiple sites including: the mitochondria, endoplasmic reticulum, cell membranes, etc.

For the therapeutic use of dyes as PDT agents, high triplet quantum yields are desirable to photosensitize the formation of singlet dioxygen. Since the amount of internal conversion is expected to be reasonably consistent with a related family of dyes such as those described below, the lower the fluorescence quantum yield the greater the triplet quantum yield expected. However, the significantly greater fluorescence quantum yields of some chlorins and isobacteriochlorins make them suitable for use as fluorescent tags, trackers and contrast agents(*11*), and reasonably good triplet quantum yield still facilitates formation of singlet oxygen. Thus the chlorins and isobacteriochlorins may be dual function agents. Fluorescent dyes with targeting motifs can be used in fluorescence guided surgery.(*12*) Hematoporphyrin

oligomers, Photofrin®, are approved for many types of cancer. An example of a currently used chlorin PDT photosensitizer is meso-tetrakis(3'-hydroxyphenyl)chlorin (m-THPC) and its derivatives.(*13*) There are issues related to the clinical use of these approved photosensitizers, including: Photofrin is a mixture of compounds, inconsistent efficacy, and no targeting motifs to impart selectivity for the cancer cells over normal cells. In terms of light, the therapeutic window is about 750-900 nm. While the m-THPC is better than Photofrin, it is still not optimal. These photophyical properties make them mostly suitable for treatment of cancer cells just below the skin (few mm).

Our previous reports described simple, high-yield reactions that replace the *para* fluoro group on perfluorphenylporphryin ($TPPF_{20}$) with a wide range of substituents, thereby resulting in a diversity of cancer and bacteria targeting moieties on the core $TPPF_{20}$ (**1**) platform.(*14-16*) Having addressed the targeting, it is desirable to be able to tune the photophysical properties of the chromophore for these assorted applications, typically this is accomplished by eliminating one or two of the of double bonds in the macrocycle and by metallation.(*1, 17, 18*) The formation of the perfluorophenylchlorin ($ChlF_{20}$) (**2**), perfluorophenylisobacteriochlorin ($IbacF_{20}$) (**3**), and perfluorophenylbacteriochlorin ($BacF_{20}$) (**4**) by 1,3-dipolar additions was reported by the Cavaleiro group.(*19-23*) The advantage of this route is that it does not use toxic reagents and the products are reasonably stable chemically and to photobleaching. $ChlF_{20}$ to append carboranyl groups was reported(*24*) and as have sugars to free base and Pt derivatives of the chlorin(*25, 26*); both for potential therapeutic applications.

Previously, our group reported the synthesis of non-hydrolysable tetra thioglycosylated meso-arylporphyrins, ($PGlc_4$) (**5**), and showed that this compound is quite selective and effective PDT agent in vitro using several cell lines, such as MDA-MB-231 human breast cancer cells(*27*),

whereas the corresponding galactose derivative is much less effective.(*14*) Also, the glycosylated compounds were taken up by transformed $3Y1^{vSrc}$ cells but not taken up by normal fibroblast cells.(*14, 15*) We first reported the synthesis and ground state electronic properties of a glycosylated chlorin formed using a dipolar addition to $TPPF_{20}$ to append a fused N-methyl-pyrrolidine moiety and the same substitution chemistry to append the sugars to the perfluorphenyl moieties.(*28*) We recently reported the method for the formation of new thioglycosylated chlorin, isobacteriochlorin, and bacteriochlorin: $CGlc_4$, $IGlc_4$, and $BGlc_4$.(*29*) These compounds have strong absorption in the near the red end of the visible spectrum and are selectively taken up by human breast cancer cells such as MDA-MB 231.(*29*)

Herein we are presenting the photophysical properties of these newly formed glycosylated porphyrinoids and their non-glycosylated F_{20} analogues $ChlF_{20}$ (**2**), $IbacF_{20}$ (**3**), and $BacF_{20}$ (**4**) (scheme 6.1). The overall goal is to study the photonic properties of these new compounds for their applications such as fluorescent tags or biomarkers and therapeutics.

6.2 Experimental Details

6.2.1 Materials and Methods

UV-visible spectra were recorded on a Varian Bio3 spectrophotometer. Fluorescence spectra were measured with a Fluorolog τ3, Jobin-SPEX Instruments S.A., Inc. All reagents were obtained from commercial sources and used without further purification. $TPPF_{20}$ porphyrin was obtained from Frontier Scientific. Dulbecco's Modified Eagle Medium (DMEM), trypsin-EDTA and antimycotic for cell culture were obtained from GibcoBRL. Hanks' balanced salt solution was obtained from Cellgro (Mediatech). Bovine calf serum was obtained from HyClone.

Phosphate buffered saline (PBS) was purchased from Invitrogen. The octanol/water partition coefficients were determined by saturating 1:1 (v:v) mixtures of the solvents with the porphyrinoid, waiting 8-10 h, and measuring the Soret and first Q band intensities. This data was confirmed by saturating each solvent separately before mixing equal volumes.

6.2.2 UV-visible, Fluorescence Spectroscopy, and Fluorescence Quantum Yield

UV-visible and fluorescence measurements were performed on dilute solutions, typically ~2 μM, of compounds in ethanol, phosphate buffered saline and ethyl acetate. The UV-visible spectra were obtained from 330 nm to 800 nm using 1 cm quartz cuvettes. For steady state fluorescence spectroscopy, samples were excited at 509 nm for ethyl acetate, 512 nm for PBS and ethanol where absorbencies ≤ 0.1. For emission spectra both the excitation and detection monochromators had a band pass of 1 nm. The corrected emission (for instrument response) and absorption spectra were used to calculate the quantum yield. Fluorescence quantum yields were determined for chlorin, isobacteriochlorin, and bacteriochlorin solutions relative to TPP in toluene, which has a fluorescence quantum yield of 0.11.(*30, 31*) The quantum yields were measured indirectly using TPP, thus these values may have some systematic error. All experiments were carried out on the same day, using identical concentrations to minimize any experimental errors. These three glycosylated conjugates are quite stable towards photobleaching.

6.2.3 Quantum Yield of Singlet Oxygen Production (Φ_Δ)[b]

Φ_Δ were determined on a relative basis by using *meso*-tetra(4-sulfonatophenyl)porphine dihydrochloride (TSPP) as a reference sensitizer ($\Phi_{\Delta,TSPP}$ = 0.7 in methanol).(*32*) A time-resolved Nd:YAG laser (Polaris II, Electro Scientific Industries, Inc.) equipped with low temperature cooled Ge detector (Applied Detector Corporation) was employed as an excitation source at 532 nm. All of the experiments were carried out in deuterium methanol-d_1. The absorbances from samples and TSPP at 532 nm were controlled between 0.1-0.5. $^1O_2$ luminescence was monitored as a function of sensitizer absorbance. Slopes were analyzed from a plot of $^1O_2$ intensity via absorbance. Φ_Δ can be calculated according to following equation.

$$\Phi_{\Delta\ sample}/\Phi_{\Delta\ reference} = \text{slope}_{\ sample} / \text{slope}_{\ reference}$$

6.2.4 Fluorescence Lifetime

Time correlation single photon counting (TCSPC) fluorescence lifetime of porphyrinoids **2-8** were measured on Fluorolog® spectrophotometer from Horiba Jobin Yvon in three different solvents: ethanol, ethylacetate, and PBS. We used 401 nm NanoLED laser, average power 13.6 pJ/pulse with a source pulse width <200ps to excite the molecules. 200 ps is the lower limit of time measurement of our instrument. The fit data program is available in the instrument.

[b] Singlet oxygen production measurements were done by X. Zhu in the laboratory of Prof. R. Gao, Department of Chemistry and Biochemistry, Jackson State University.

6.2.5 Photobleaching Measurement in Sunlight

Photo stability of $IGlc_4$ and $CGlc_4$ conjugates in ethanol were measured by exposing 1μM solutions of these compounds in sun light with a power of 40-80 W/m^2 for about 3-5 hours. The absorption and emission spectra of the solutions were recorded in a timely manner. (see appendix).

6.2.6 Cell Culture

3T3 NIH cells maintained in DMEM, 10% BCS, 1% antimycotic at 37 ºC and in 5% CO_2 atmosphere were plated onto coverslips in cell culture dishes. Porphyrins, chlorins and isobacteriochlorins dissolved in methanol were added to the cultures to a final concentration of 1 or 2.5 μM such that there was never more than 0.5% methanol in the solution. After 20 h incubation, cells were washed with PBS 3 – 5 times and fixed in 4% paraformaldehyde solution for 10 min at room temperature. The cells were then washed with PBS 3 times. The cells were visualized using a Nikon Optiphot 2 fluorescence microscope. Images were captured as JPEG files at 10x magnification, with a 505 – 565 nm excitation band pass filter and a 565 – 685 nm emission band pass filter. For each set of experiments, cells were cultured and the fluorescence images were taken under identical culture and microscopic conditions. For quantitative studies, the image intensities of the cells in the fluorescence micrographs were calculated by FLim program available at: http://nathan.instras.com/projects/FLim/index.html

6.2.7 Confocal Microscopy

Cells were plated onto cover slips in cell culture dishes. $BGlc_4$ dissolved in DMSO was added to the cultures to a final concentration of 10 μM (DMSO concentrations were < 0.2%).

After incubation for 24 hours the cells were rinsed three times with PBS and incubated with a 4% paraformaldehyde solution for 15 minutes at 37 ^{0}C under cell growth conditions. Cells were then washed three times with PBS, mounted in Dako fluorescence mounting medium, and visualized using a Zeiss LSM510 laser scanning confocal microscope where images were captured with excitation at 514 nm, emission used a 710-750 nm band pass filter. Photostability of glycosylated conjugates were observed under identical cell culture conditions using K:Molv NIH 3T3 cells. The cells were exposed to the laser light and images were captured in a timely manner using an oil immersion objective lens (Leica, Fluor- 40X, NA 1.25), excitation at 552 nm, and emission band filter used was 578-700nm.

6.3 Result and Discussion

Synthesis:[c] The synthesis of the chlorin, [$ChlF_{20}$ (**2**)], isobacteriochlorin, [$IbacF_{20}$ (**3**)], and bacteriochlorin [$BacF_{20}$ (**4**)] was carried out by modifications of a reported procedure(*19, 20, 22*) and their corresponding thioglycosylated conjugates $CGlc_4$ (**6**), $IGlc_4$ (**7**), and $BGlc_4$ (**8**) were synthesized by nucleophillic substitution of thioglucose at the para position of the perfluorophenyl substituents of these porphyrinoids.(*29*) The structures of all porphyrinoids were confirmed by NMR, UV–visible, mass spectrometry and HRMS analysis.

[c] Syntheses of all compounds were done by Sunaina Singh.

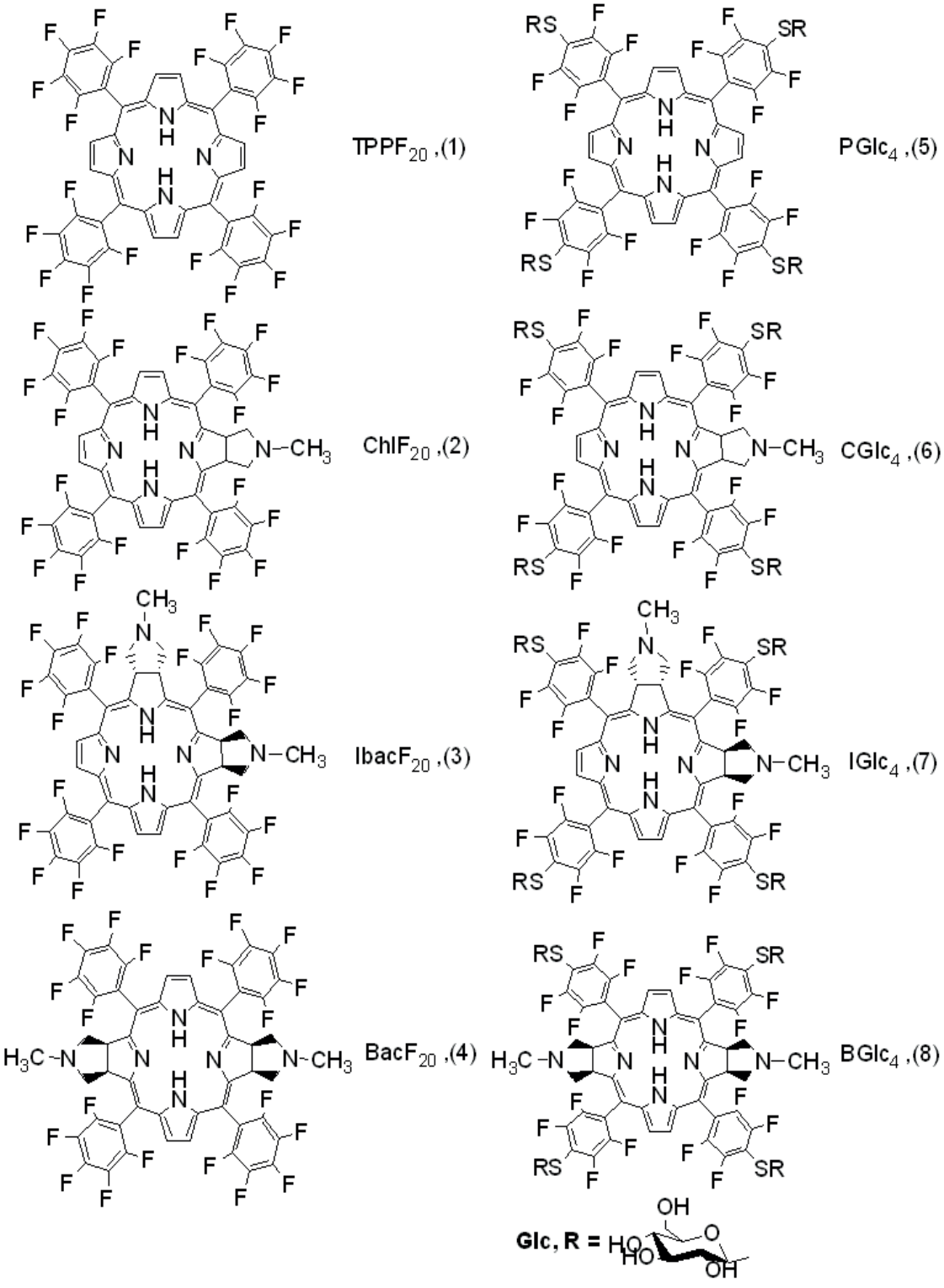

Scheme 6.1: Structure of non-glycosylated (**1-4**) and glycosylated (**5-8**) conjugates of porphyrin.

Considering the large dependence of the photophysical properties of polar chromophores on the solvent matrix and on other experimental parameters, it is important to develop a self-consistent set of data for accurate comparison of these properties and assessment of potential applications. Since the dye can partition into lipophilic, hydrophilic or amphipathic cellular structures, we have assayed the photophysical properties in three different solvents. Thus, PBS at pH = 7.4, ethanol, and ethylacetate solvents were used to probe the photophysical properties (the partition coefficients and photophysical properties are summarized in Tables 6.1 and 6.2). While the initial association with the cell is mediated by glucose receptors and the four glycosyl groups on the chromophore, some non-specific partition into the membrane is also indicated. Because of the size of the molecules, uptake is unlikely to proceed by active or passive transport, but the high local concentration around the cell increases diffusion. Thus uptake is also dependent on the relative hydrophobicity of the compounds.(*33*) The octanol/water partition coefficient and R_f for the glycoslyated compounds are listed in Table 6.1.

Table 6.1. partition coefficients

Cpd.	octanol/water	R_f[#]
$PGlc_4$	43.9 (4.8)	0.6 (5.5)
$CGlc_4$	28.5 (3.13)	0.37 (3.4)
$IGlc_4$	9.1 (1)	0.11 (1)
$BGlc_4$	12.7 (1.4)	0.13 (1.2)

[#] normalized values in parentheses. R_f data from Sunaina Singh.

UV-visible, fluorescence spectroscopy, and fluorescence quantum yield: The electronic spectra of **2**, **3**, and **4** and the glycosylated derivatives, **6-8** are significantly different from the $TPPF_{20}$ (Figure 6.1). The lowest energy Q band of chlorin, $CGlc_4$ in PBS buffer at 649 nm has about 25-fold greater intensity than corresponding Q band of porphyrin $PGlc_4$ at 645 nm. For isobacteriochlorin, $IGlc_4$ in the same buffer, the lowest energy Q band at 645 nm is 5-fold more intense than the porphyrin at the same wavelength. For $BGlc_4$ the strong lowest energy peak is located at 730 nm improving the absorption in the red region of the spectrum. The fluorescence emission spectra for the four glycosylated porphyrinoids are correspondingly different and have a strong solvent dependence (Table 6.2).

Table 6.2. Photophysical Properties of Glycosylated Porphyrinoid Derivatives.

Cpd.	Solvent	UV-visible[a]	Emission λ_{max}	Φ_F [b]	$^1O_2$ Φ_Δ
$TPPF_{20}$	DMSO	412, 504, 538, 580, 632	637, 702	--	
CF_{20}	DMSO[c]	408, 504, 536, 598, 652	656	--	
THPC	methanol[d]		653, 720	0.09	0.43
THPBC	methanol[d]		612, 653, 746	0.11	0.43
$PGlc_4$	ethanol	412, 505, 535, 586, 653	653, 702	0.05	0.85[f]
	PBS buffer	410, 510, --- 576, 646(1)[a]	646, 692	0.03	
	ethylacetate	412, 507, 450, 583, 655	649, 701	0.05	
	DMSO[c]	415, 507, 539, 581, 636	640, 705	0.06	
$CGlc_4$	ethanol	408, 507, 534, 599, 653	653, 715	0.43	0.32[f]
	PBS buffer	409, 506, 533, 597, 649(25)[a]	649, 707	0.17	
	ethylacetate	406, 504, 531, 597, 651	653, 712	0.39	
	DMSO[e]	412, 506, 537, 598, 652	652	--	0.28
$BGlc_4$	Ethanol	353, 374, 505, 732	729	0.047	--
	PBS buffer	357, 508, 730	725	0.03	
	ethylacetate	352, 379, 508, 730	730	0.055	
$IGlc_4$	ethanol	385, 513, 548, 588, 643	596, 646, 705	0.70	0.59[f]
	PBS buffer	385, 513, 548, 593, 645(5)[a]	606, 650, 711	0.36	
	ethylacetate	384, 510, 548, 589, 653	596, 646, 700	0.60	

[a]relative intensity of lowest energy Q bands, [b]fluorescence experiments done in air, [c]taken from reference(*26*), [d]mTHPC and the bacteriochlorin mTHPBC taken from reference(*11*), [e]taken from reference(*25*), [f]excited at 532 nm in methanol d_1. (adapted from the reference 28).

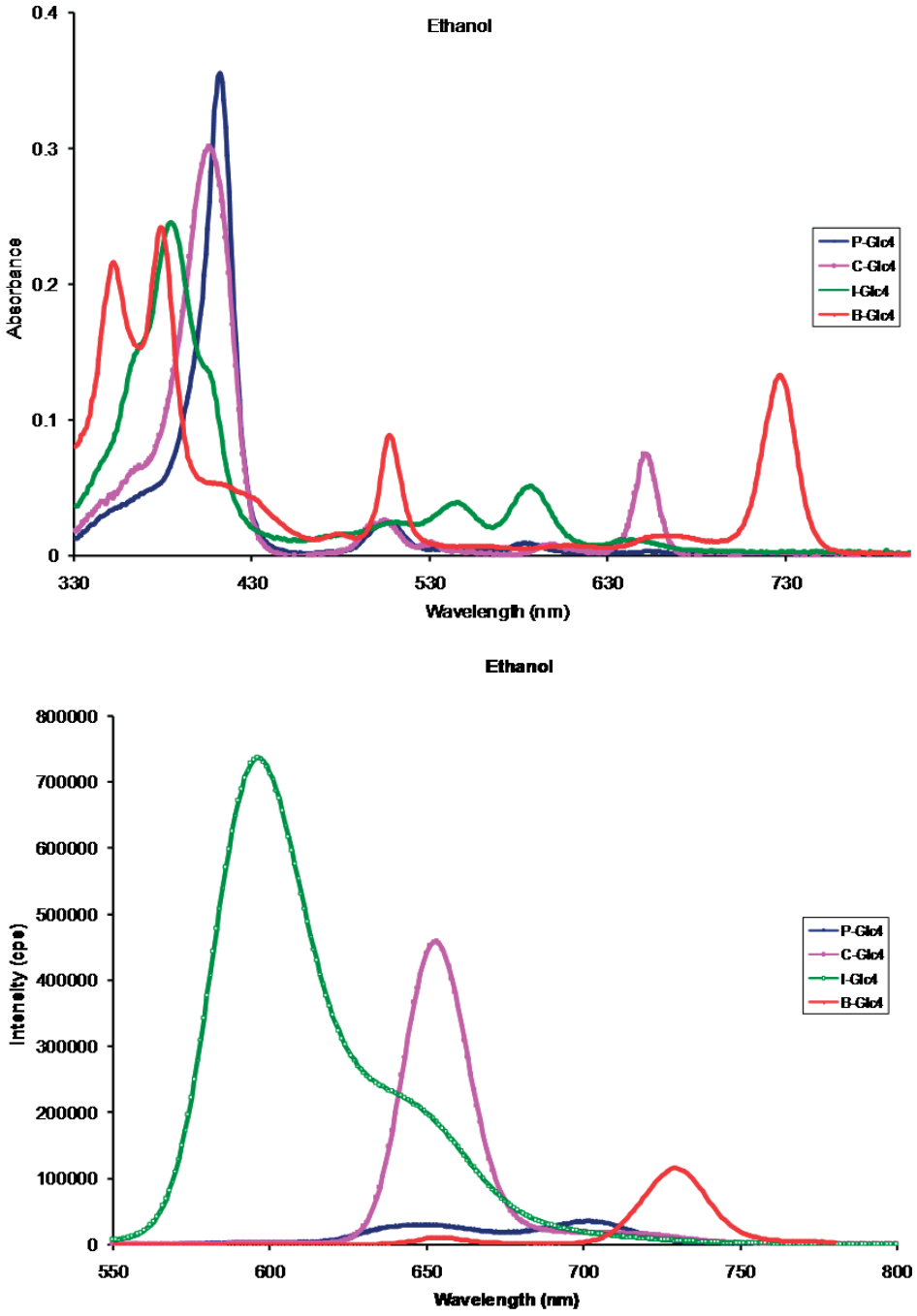

Figure 6.1. Top: UV-visible spectra of the compounds, 2 μM in ethanol. Bottom: emission spectra of the compounds in ethanol; excitation at 512 nm where the absorbance is ca. 0.05 for each compound. (Taken from reference 28)

There are negligible Stokes shifts for $PGlc_4$, $CGlc_4$ and $BGlc_4$ in the three solvents, indicating minimal specific solvent-solute interactions with the macrocycle effecting vibrational processes.(*34*) Notably, for the $IGlc_4$ in PBS, the strongest fluorescence band λ_{max} is at 606 nm with a weaker emission centered at 650 nm while for $BGlc_4$ the peak is presented at 725 nm. Excitation spectra all indicate the presence of only the given compounds. The 0.17 and 0.36 fluorescence quantum yields for $CGlc_4$ and for $IGlc_4$ in PBS are 6 times and 12 times respectively that of the porphyrin analogue $PGlc_4$ while for $BGlc_4$ is 0.03, similar to the $PGlc_4$. There is a small decrease in fluorescence quantum yield upon replacement of the para F atom by the thiocarbohydrate group due to both electronic and heavy atom effects. The greater fluorescence quantum yield of $CGlc_4$ than m-THPC(*11*) or a water soluble di-meso substituted chlorin(*35*) likely arises from the presence of the 16 F groups and relative energies of the molecular orbitals, and is consistent with the quantum yield of singlet oxygen generation by $ChlF_{20}$(*36*). However, tetraarylporphryins with a tripeptide(*37*) and other meso aryl chlorins(*38*) have similar photophysical properties to what we find. The sugars have little direct effect on the photophysics but modulate the amphipathicity and enable the observed solvent dependence.

Table 6.3: Absorption and emission spectral data of F_{20} porphyrinoids.

Compound	Solvent	UV-visible	Emission
$ChlF_{20}$	ethanol	399, 502, 528, 597, 651	654, 708
	ethylacetate	398, 501, 527, 597, 649	655, 709
$IbacF_{20}$	ethanol	381, 504, 541, 583, 635	592, 645, 707
	ethylacetate	380, 503, 541, 581, 647	594, 645, 711
$BacF_{20}$	Ethanol	348, 374, 503, 729	647, 723
	Ethylacetate	347, 373, 502, 729	651, 735

Quantum yield of singlet oxygen formation[b]*:* The quantum yields of singlet oxygen formation for three of the compounds in methanol d_1 are listed in Table 6.2. Since the porphyrin ring is the reactive site for $^1O_2$ production, the frequency of collisions that result in the formation of $^1O_2$ is related to the probability that $^3O_2$ molecule makes physical contact with the chromophore in the excited, triplet state. The additional steric effect of the pyrrolidine-fused rings on $CGlc_4$ and $IGlc_4$ could result in reduced collision frequencies and a lower Φ_Δ compared to $PGlc_4$. It is reasonable to expect that internal conversion is somewhat consistent between the compounds, so the increased fluorescence quantum yield means a decrease in the amount of triplet formed. The Φ_Δ data dovetails with the observe fluorescence yields, but the Φ_Δ for $IGlc_4$ in methanol is more consistent with the PBS buffer data.

Excited state decay properties: The decay of electron from higher excited singlet state, S_1, to the ground singlet state, S_0, follows a series of radiative and/or non radiative processes. The rate constant (k) for these decay processes relates to the fluorescence quantum yield (Φ_f) and the fluorescence lifetime (τ_f) by the following equations:

$$\tau_f = 1 / (k_f + k_{ic} + k_{isc}) \qquad (1)$$

$$\Phi_f = k_f / (k_f + k_{ic} + k_{isc}) \qquad (2)$$

Where k_f, k_{ic}, and k_{isc} are the rate constants for the radiative (spontaneous fluorescence) decay, internal conversion (from the excited singlet state to the ground singlet state), and for the intersystem crossing to the triplet excited state respectively. Equations 1 and 2 can be used to calculate the rate constant for non-radiative decay, k_{nr}, and is given by the equation:

$$k_{nr} = \tau_f^{-1} - k_f \qquad (3)$$

There is always a competition between the follwing relaxation routes: a) $S_1 \rightarrow S_0$, radiative decay b) $S_1 \rightarrow$ So, non-radiative internal conversion and c) $S_1 \rightarrow$ T, inter system crossing. High Φ_f value dictates the process predominantly via radiative $S_1 \rightarrow S_0$ decay whereas the low Φ_f suggest a non-radiative decay.(*39-41*) This is consistent with our rate constant calculations for radiative and non-radiative processes for glycosylated porphyrinoids. Comparable low Φ_f, high rate constant values for radiative decay and low rate constant for non radiative decay for $PGlc_4$ and $BGlc_4$ indicates that these conjugates may act as better fluorescent tags. On the other hand ca. 20 fold less radiative time constant value for $IGlc_4$ compare to $BGlc_4$ indicates that this compound may have better chances to create triplet state and so can act as a better PDT agent. Low Φ_f and short lifetime for bacteriochlorin conjugate suggests the deactivation of the excited singlet state predominantly via inter system crossing, which may leads to the formation of its triplet state. The distortion from the planarity of the porphyrin also causes the destabilization of the π-system exhibit significantly shorter lifetime.(*42*) This is in agreement with our our observation of ca.2-4 fold shorter lifetime for non-planar glycosylated conjugates than the planar parent $TPPF_{20}$ compound.

Table 6.4: Quantum yield and decay constant values for non-glycosylated F_{20} and thioglycosylated conjugates of porphyrinoids.							
Compound	Solvent	Φ_f	τ_f ns (χ^2)	k_f $(ns)^{-1}$	$(k_f)^{-1}$ ns	k_{nr} $(ns)^{-1}$	$(k_{nr})^{-1}$ ns
$TPPF_{20}$	EA		10.08 (1.21)				
	EtOH		11.14 (1.04)				
$ChlF_{20}$	EA	0.34	7.06 (1.21)	0.048	20.8	0.094	10.6
	EtOH	0.48	7.48 (1.37)	0.064	15.6	0.070	14.3
$IbacF_{20}$	EA	0.60	5.38 (1.25)	0.112	8.9	0.074	13.5
	EtOH	0.72	3.52 (1.19)	0.205	4.9	0.079	12.7
$BacF_{20}$	EA	0.062	6.80 (1.41)	0.009	111.1	0.138	7.3
	EtOH	0.07	6.88 (1.30)	0.010	100.0	0.135	7.4
$PGlc_4$	EA	0.052	9.88 (1.05)	0.0053	188.7	0.096	10.4
	EtOH	0.05	10.84 (1.24)	0.0046	217.4	0.088	11.4
	PBS	0.03	10.66 (1.28)	0.0028	357.1	0.091	11.0
$CGlc_4$	EA	0.39	6.91 (1.42)	0.056	17.9	0.089	11.2
	EtOH	0.43	7.21 (1.34)	0.060	16.7	0.079	12.7
	PBS	0.17	6.84 (1.24)	0.025	40.0	0.121	8.3
$IGlc_4$	EA	0.60	5.93 (1.27)	0.101	9.9	0.068	14.7
	EtOH	0.70	4.29 (1.46)	0.163	6.1	0.070	14.3
	PBS	0.36	2.98 (1.47)	0.121	8.3	0.215	4.7
$BGlc_4$	EA	0.055	7.01 (1.32)	0.0078	128.2	0.135	7.4
	EtOH	0.047	6.96 (1.39)	0.0067	149.3	0.137	7.3
	PBS	0.03	5.44 (1.33)	0.0055	181.8	0.178	5.6

Table 6.4. Quantum yield F_{20} porphyrinoid were calculated in ethanol and ethylacetate. The molecules were excited at 509 nm where the O.D = 0.02 in each case. TPP was used as reference, Φ for TPP in toluene = 0.11. The lifetime of these compounds were measured under argon, by purging argon gas through the cuvette for ca.10 min. The errors in the singlet state lifetime were ± 200 ps, which is the lower limit of time measurement of our instrument.

Cell uptake studies: K:Molv NIH 3T3 mouse fibroblasts and MDA-MB-231 breast cancer cell line were used to evaluate the cellular uptake of these glycosylated derivatives. Our initial hypothesis was that the N-methylpyrrolidine moieties used to make and stabilize the chlorin, bacteriochlorin, and isobacteriochlorin (as well as the stereo centers at the β positions), would have minimal effect on cell uptake, because these are sandwiched between the glycosylated tetrafluorophenyl groups. K:Molv NIH 3T3 cells were incubated identically with 2.5 μM concentrations of $PGlc_4$, $CGlc_4$, and $IGlc_4$, rinsed with buffer, and the relative uptake was quantified by comparison of images taken by fluorescence microscopy under identical settings (Figure 6.2). For $BGlc_4$, K:Molv NIH 3T3 cells were incubated with 10 μM concentration and confocal microscopy was used to obtain the image because the red absorption and emission are outside the range of our fluorescence microscope (Figure 6.3). The electronic spectra, fluorescence, and fluorescence microscopy studies all show that these compounds are robust to photobleaching. The remaining 16 F groups impart oxidative stability and further enhance the photonic properties.

At 2.5 μM concentration the relative integrated intensities for $PGlc_4$, $CGlc_4$ and $IGlc_4$ in the fluorescence micrographs of the K:Molv NIH 3T3 are 1:2:7, respectively (Figure 6.2). Taking into consideration both the partition coefficients and the fluorescence quantum yields, one would expect that the relative uptake of these compounds into the cells measured by fluorescence to be ca. 1:4:2 for the $PGlc_4$:$CGlc_4$:$IGlc_4$, respectively. The disparity may arise from differences in the degree of aggregation of the compounds in the PBS buffer and/or aggregation as the local concentration of the dyes around the cell increases.(*43*) The propensity of aggregation inside the cell may also vary. Also, some diastereomers may be taken up

preferentially over others. The mechanism of uptake and photodynamic effects in this and other cell lines will be reported elsewhere.

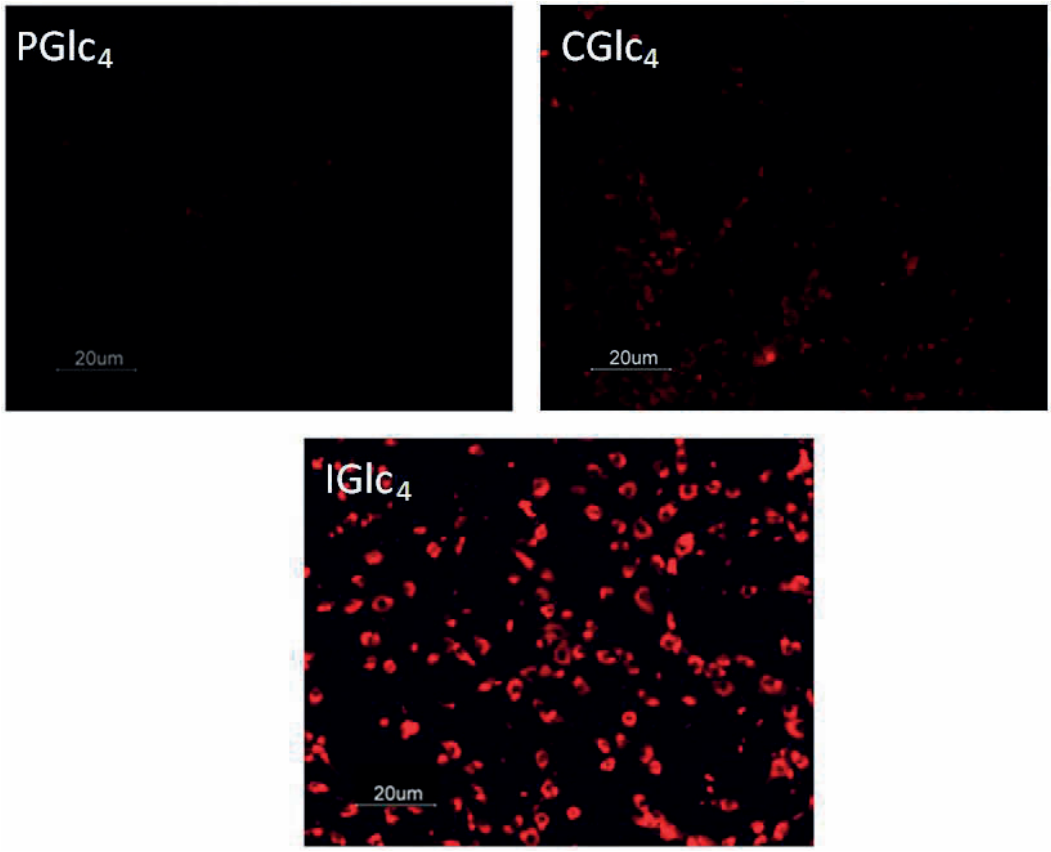

Figure 6.2. Fluorescence microscopy of 3T3 cells treated with 2.5 μM $PGlc_4$ (**1b**), $CGlc_4$ (**2b**), and $IGlc_4$ (**3b**). K:Molv NIH 3T3 cells were incubated for 20 hrs with porphyrinoid, followed by removal of unbound dye from the cell culture by repeated rinsing with PBS, and the cells were imaged under idential microscope settings and not enhanced; magnification 10X.

Though there may be differences in uptake between these compounds, our group has shown earlier that the $PGlc_4$ compound localizes in the endoplasmic reticulum because of the metabolic needs of this organelle.(*44*) The significantly greater fluorescence quantum yield of

the $IGlc_4$ system means that ca. 25 nM concentrations can be used to follow receptors and/or glycolysis processes in the cell (Figure 6.4). Thus, $IGlc_4$ it is better suited for tagging and sensor applications. For PDT applications, sensitizers with strong red absorptions are generally considered better because these wavelengths penetrate deeper into tissue.(*2, 3*) The optical cross section of $CGlc_4$ in the red region is significantly larger than the porphyrin or isobacteriochlorin analogues. Thus, if red light is used to activate the second generation dye $CGlc_4$, the increased light absorptivity more than compensates the reduced triplet quantum yield. Given the very strong 730 nm absorption, the low fluorescence quantum yield, and greater triplet quantum yield of $BGlc_4$, this may be the best photosensitizer for PDT of the compounds described herein. However, a more efficient synthesis and purification of the isomers and diastereomers needs to be developed for the bacteriochlorin compounds to be used.

Though the fluorescence of $CGlc_4$ and $IGlc_4$ is greater than the parent porphyrin, there is still sufficient triplet formation to effect cell death via necrosis and/or apoptosis. This indicates that these compounds can be used as dual function agents that both locate and treat cancerous cells.

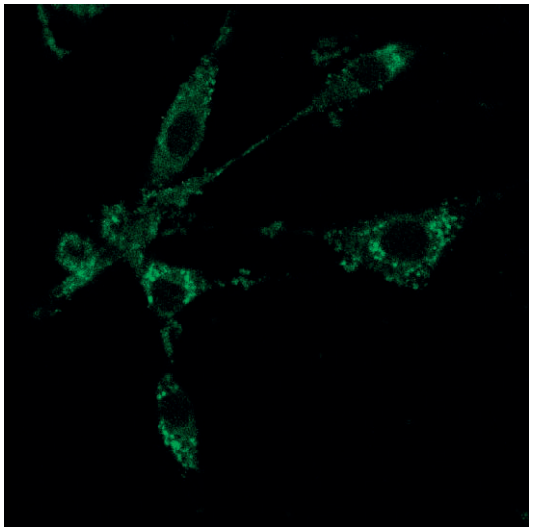

Figure 6.3. K:Molv NIH 3T3 cells were incubated with 10 μM $BGlc_4$ for 24 hours, rinsed three times with PBS buffer, and fixed with 4% paraformaldehyde solution. Confocal microscope excitation at 514 nm, emission monitored with a 710-750 band pass filter. No images are observed using a 610-650 nm emission band pass filter, so fluorescence does not arise from the one of the other dye systems. The image is not enhanced, magnification is 60x. (Image taken with Dr. Sebastian Thompson)

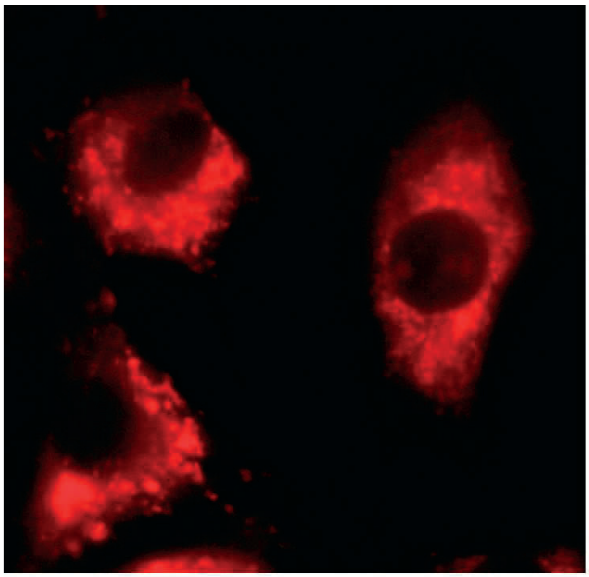

Figure 6.4. Fluorescence image of a MDA-MB-231 breast cancer cell treated with 25 nM $IGlc_4$, and rinsed three times with BPS buffer to remove unbound dye (see Supporting Information for comparisons to the other porphyrinoids). (Image taken by Dr. Sebastian Thompson)

Confocal photobleaching meausrement for $CGlc_4$: K:Molv 3T3 NIH cells were incubated with $CGlc_4$ for 24 hours to a final concentration of 0.1 μM and were prepared for confocal microscopy as described above in the experimental section. The excitation wave length was selected 552 nm and the emission band filter was 578-700 nm. The imgaes were taken shown in figure 6.5. There was almost no photobleaching was observed for this compound which indicates that this chromophore can also be a good imaging agent whereas the commercially available dyes such as mito tracker use for imaging purposes photobleaches quickly.(*45*)

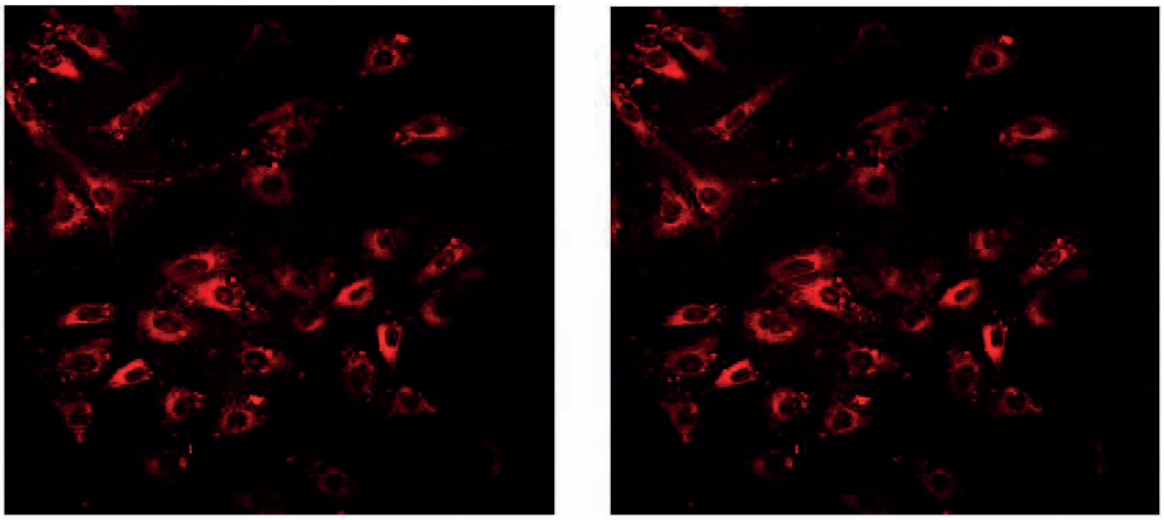

Figure 6.5. K:Molv 3T3 NIH cells plated onto cover slips were incubated with $CGlc_4$ for 24 hours, washed 3 times with PBS buffer and fixed with 4% paraformaldehyde and then again washed 3 times with PBS and mounted in Dako fluorescence mounting medium. Confocal images were taken using excitation wave length was 552 nm and emission filter was 578-700 nm. Left: image after first scan. Right: images of same sample after 25 scan. The images are not manipulated.

Photobleaching measurement in sun light: Photostability of $IGlc_4$ and $CGlc_4$ were also measured in sunlight during full sunny days. 1 μM solutions of these conjugates in ethanol were exposed to sunlight and UV-visible and emission spectra were recorded in a timely manner (see appendix). For $CGlc_4$ conjugate ca. 5% photobleaching while for $IGlc_4$ conjugate ca. 10% photobleaching was observed in sunlight.

6.4 Conclusions

In conclusion, these core platforms will enable rapid development of new multifunctional imaging, sensing, and therapeutic agents(*46*) for specific targets, and the ability to assess the effectiveness appended motifs in targeting. These platforms will also facilitate the development of effective probes for fundamental biochemical/biophysical studies.(*47, 48*) Both $CGlc_4$ and $IGlc_4$ have significantly enhanced fluorescence quantum yields compared to the $PGlc_4$, while the $BGlc_4$ derivative has a fluorescence quantum yield that is similar to the parent porphyrin. Thus $IGlc_4$ has greatest potential use as fluorescent tags, diagnostics, or imaging agents. The intermediate fluorescence of the $CGlc_4$ system may well serve as a dual purpose agent for targeting, detecting, and treating diseased tissues. The $BGlc_4$ system has near optimal properties as the PDT agent, but new synthetic strategies are needed to make these compounds. The much lower concentrations of $CGlc_4$ and $IGlc_4$ indicate that lower dose of these compounds can be used for bioimaging and diagnostic purposes. The excited state lifetime of all the compounds were measured under identical conditions and ranges from 3-11 nsec. About 20 fold less radiative time constant for $IGlc_4$ conjugate than the other analogous compounds may indicate that this compound has better chances to produce triplet state, may act as better candidate for the new generation PDT agent. Photobleaching of these compounds are minimal.

6.5 Appendix

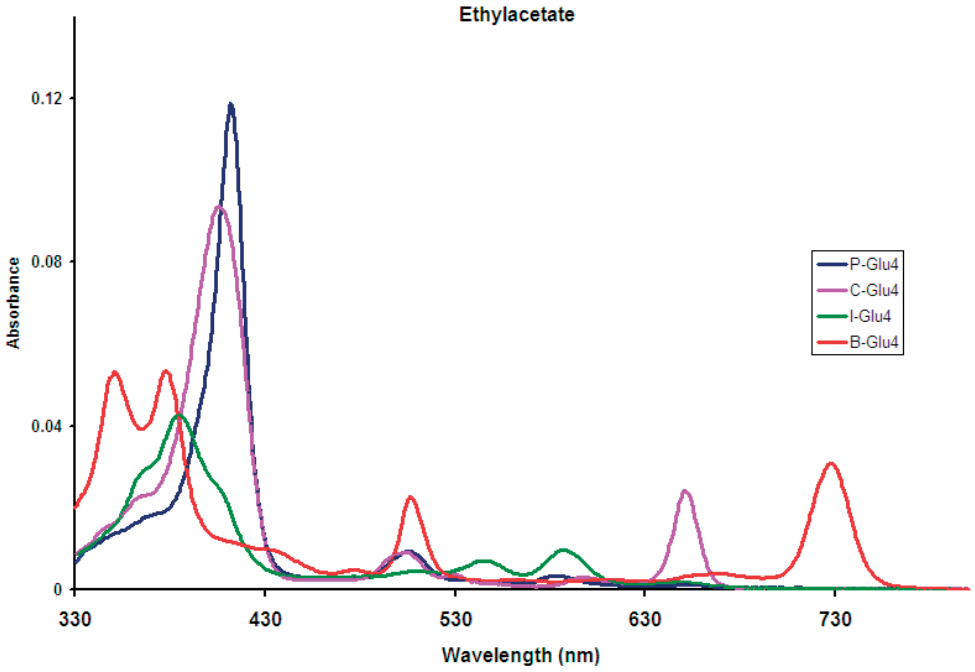

Figure A 6.1. UV-visible spectra of the compounds, 2 µM in ethylacetate**.**

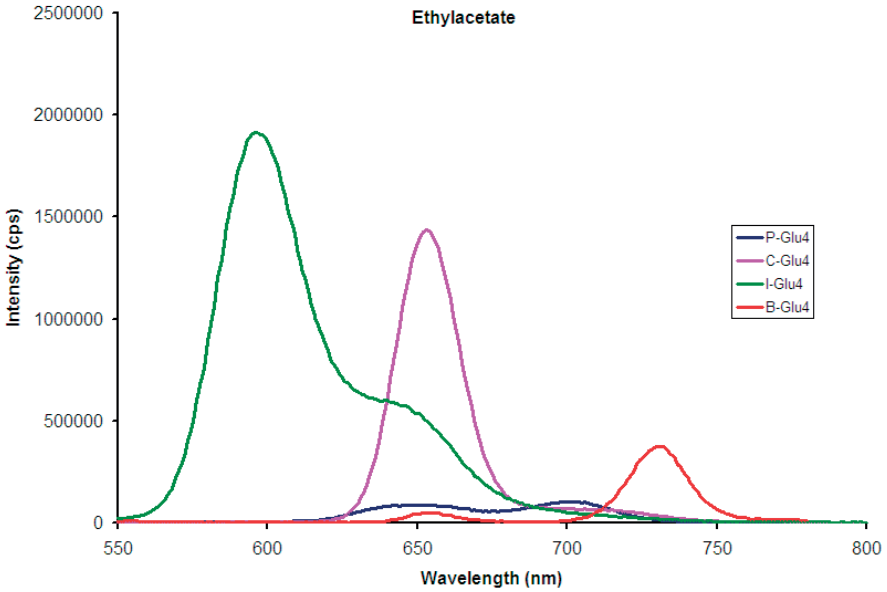

Figure A 6.2 Emission spectra of the compounds in ethylacetate; excitation at 509 nm where the O.D. was 0.098 for each compound.

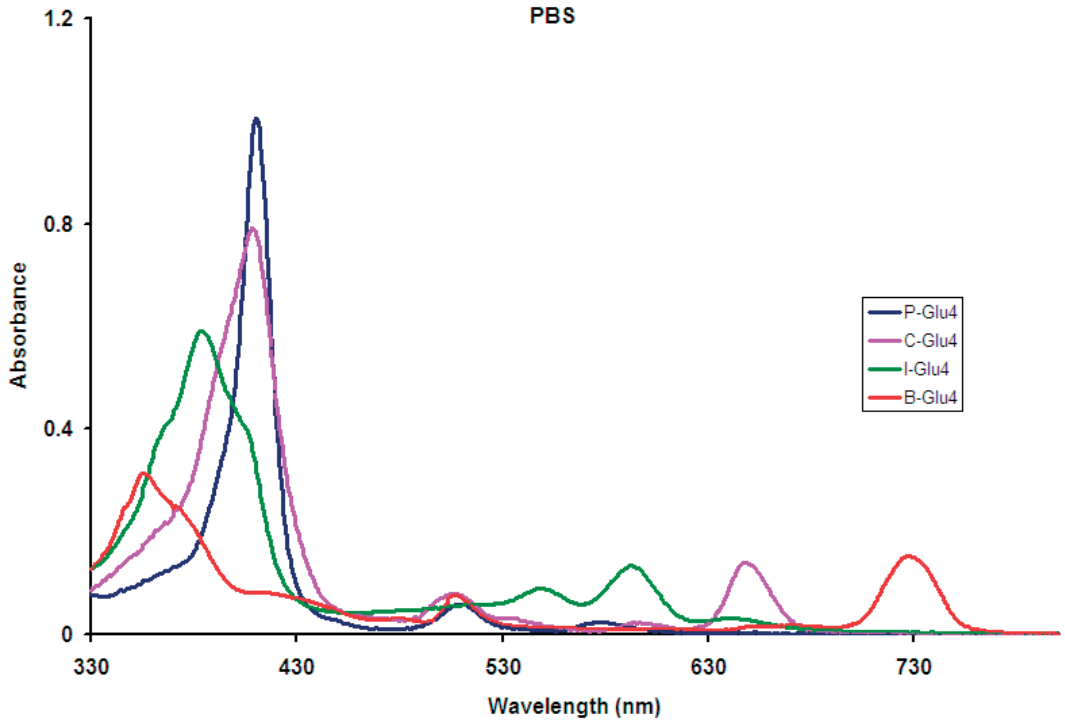

Figure A 6.3. UV-visible spectra of the compounds, 2 μM in PBS.

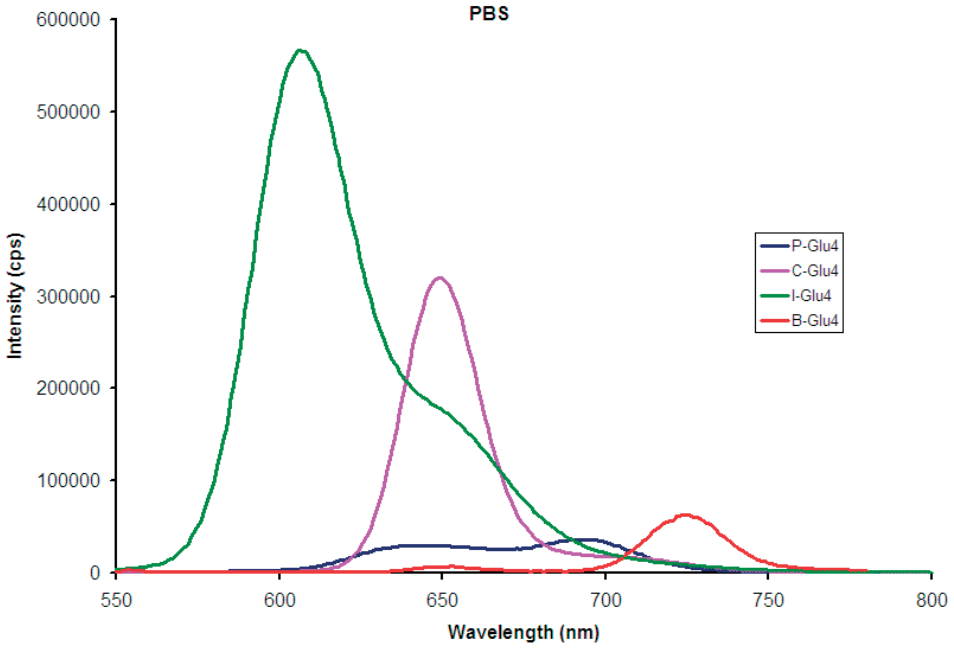

Figure A 6.4. Emission spectra of the compounds in PBS; excitation at 512 nm, where the O.D. was 0.018 for each compound.

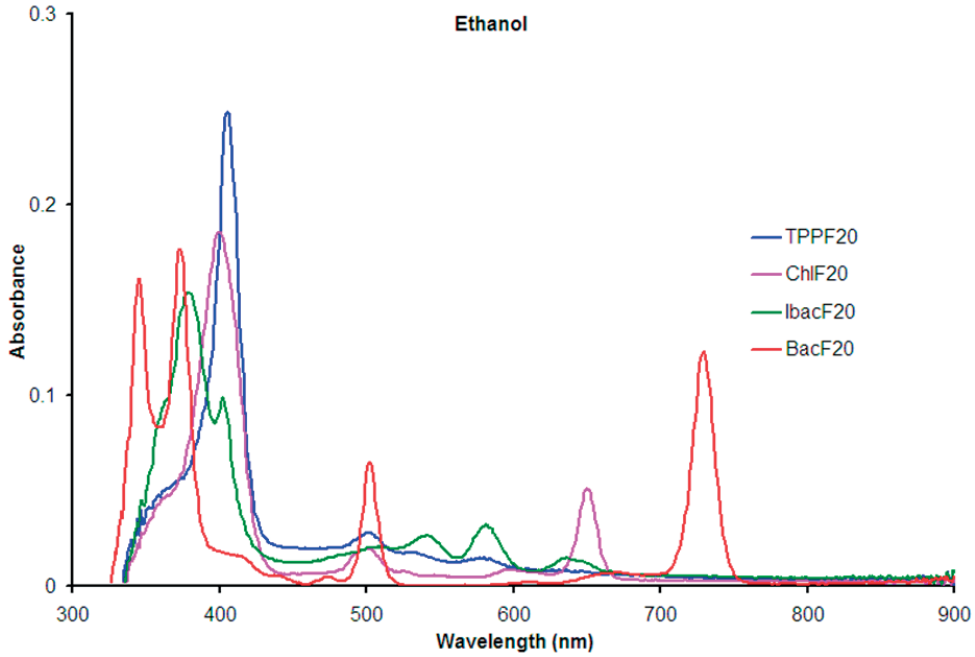

Figure A 6.5. UV-visible spectra of the compounds, 1 μM in ethanol.

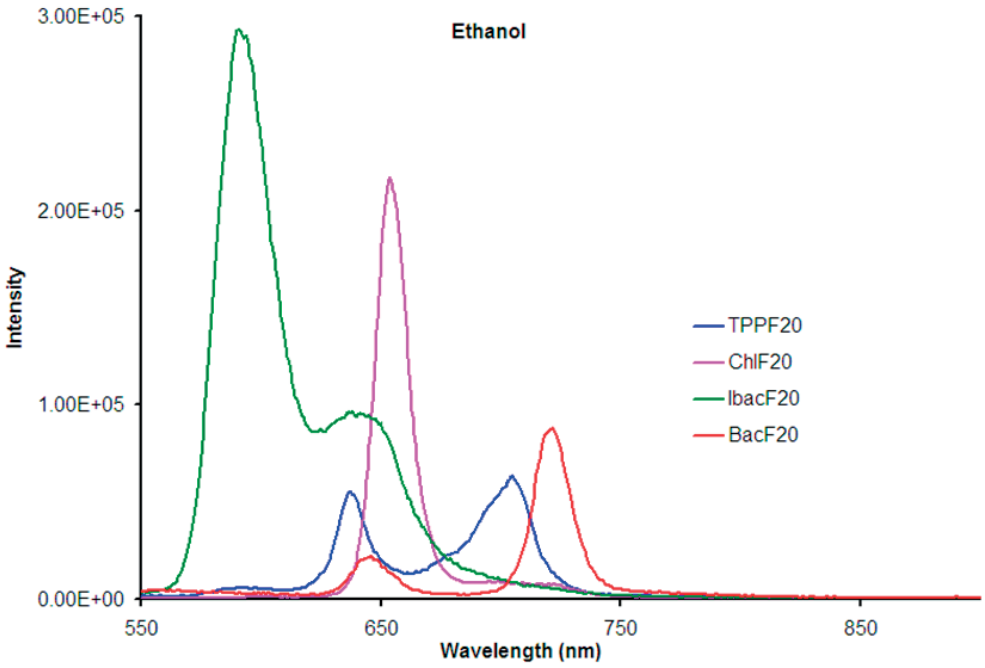

Figure A 6.6. Emission spectra of the compounds in ethanol; excitation at 509 nm where the O.D was 0.011for all the compounds.

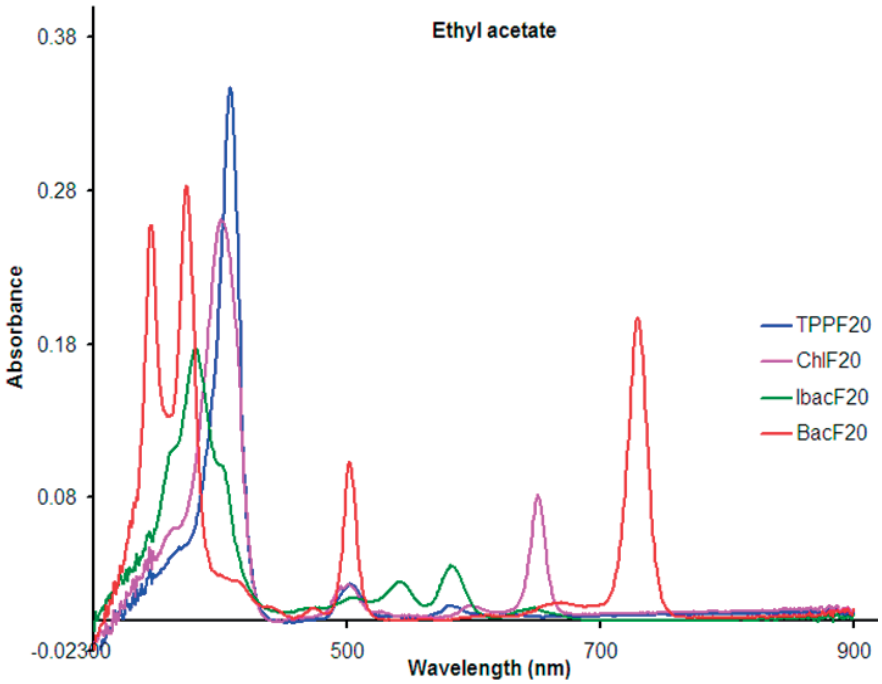

Figure A 6.7. UV-visible absorption spectra of all the compounds **1-4** in ethylacetate where the concentration of each solution was 1 µM.

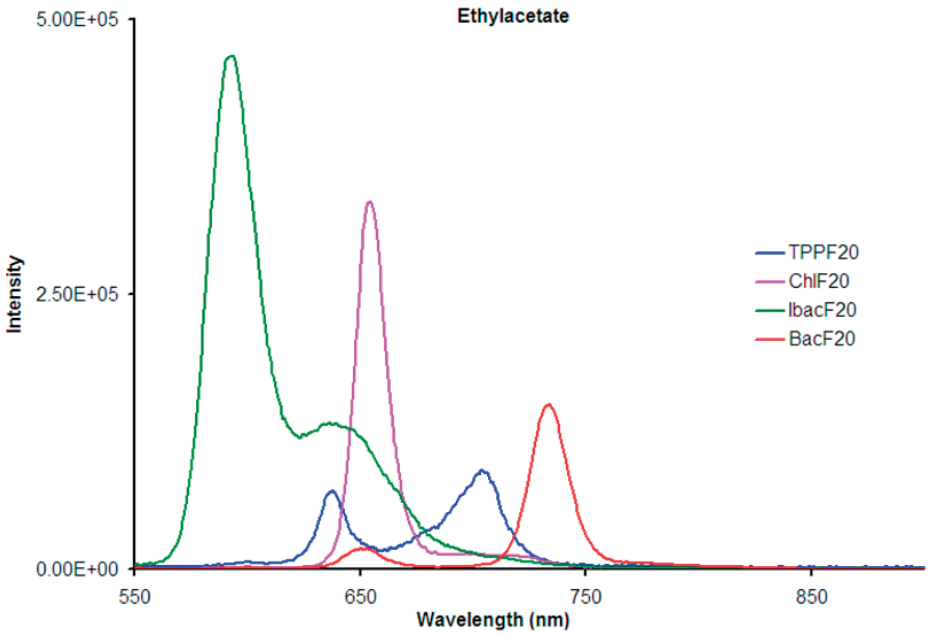

Figure A 6.8. Emission spectra of the compounds in ethylacetate; excitation at 509 nm where the O.D was 0.014 for all the compounds.

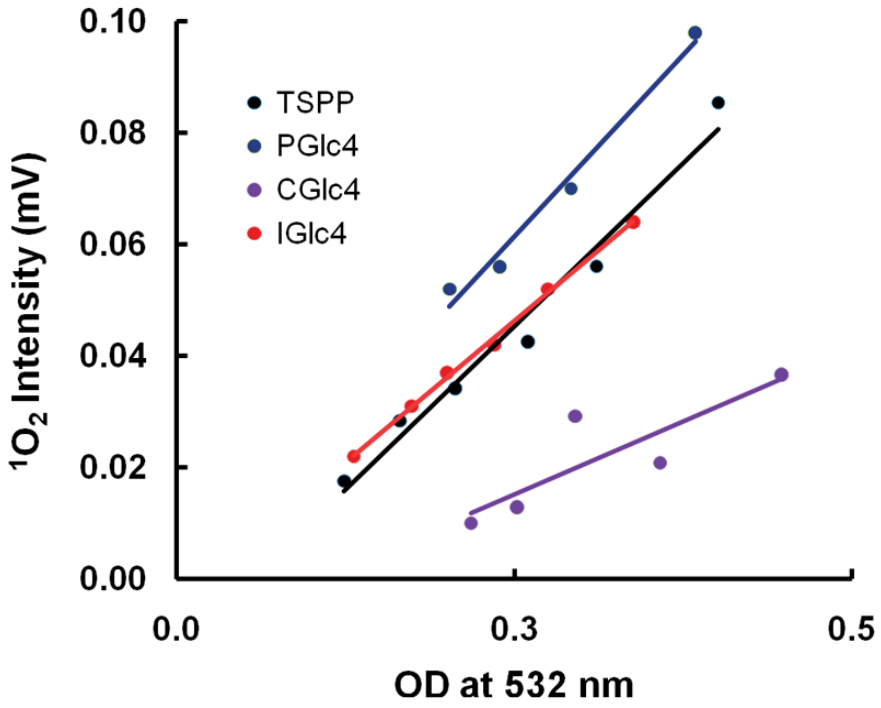

Figure A 6.9. Changes in $^1O_2$ intensity as a function of OD at 532 nm. The lower Φ_Δ from $CGlc_4$ may partially due to the inefficient light absorption at 532 nm compared to $IGlc_4$.

Ideally, all of the lines in Figure 7 should go through zero. However, in many cases the background signals from laser pulse and detector can result in a positive intercept. This is largely accounted for since the Φ_Δ were calculated by comparing the slopes to a standard.

Photo bleaching experiment of $IGlc_4$ in sunlight with time.

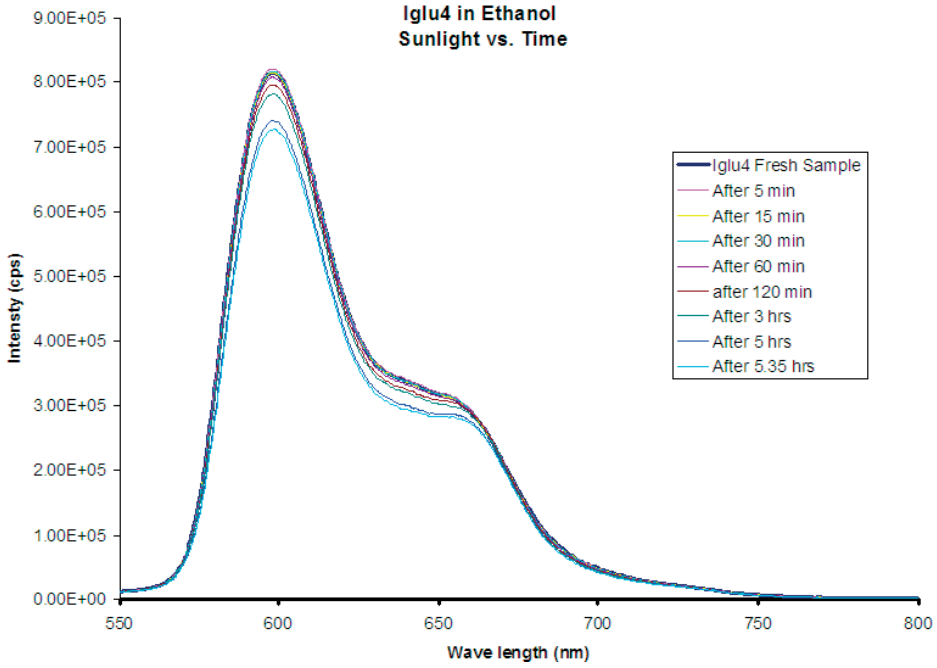

Figure A 6.10. Emission spectra of $IGlc_4$ in ethanol in air in a closed vial shows only a small degree of photobleaching of $IGlc_4$ in sun light with time.

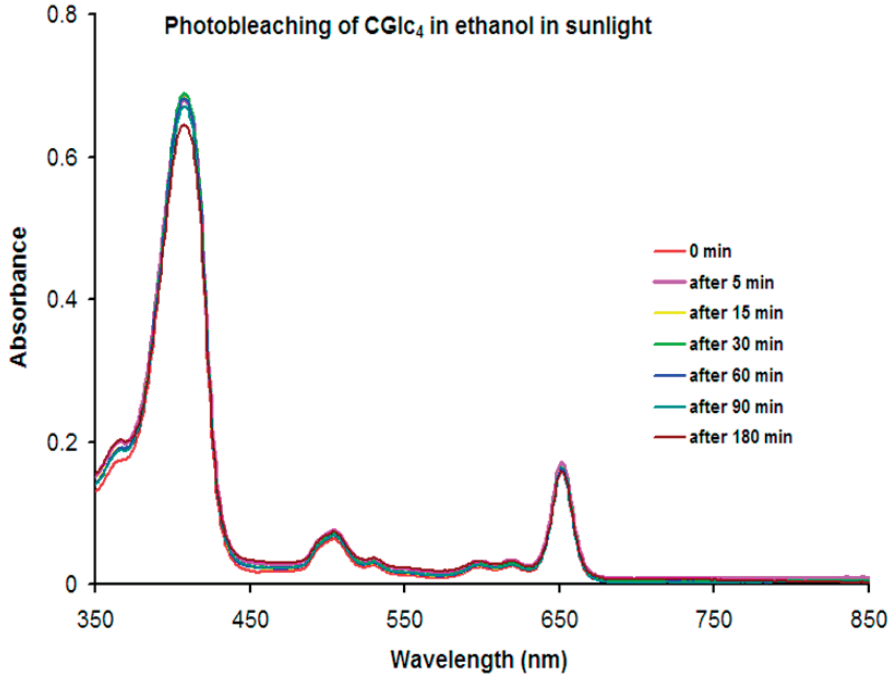

Figure A 6.11. UV-visible spectra for photobleaching of $CGlc_4$ in sunlight. 1μM solution in ethanol.

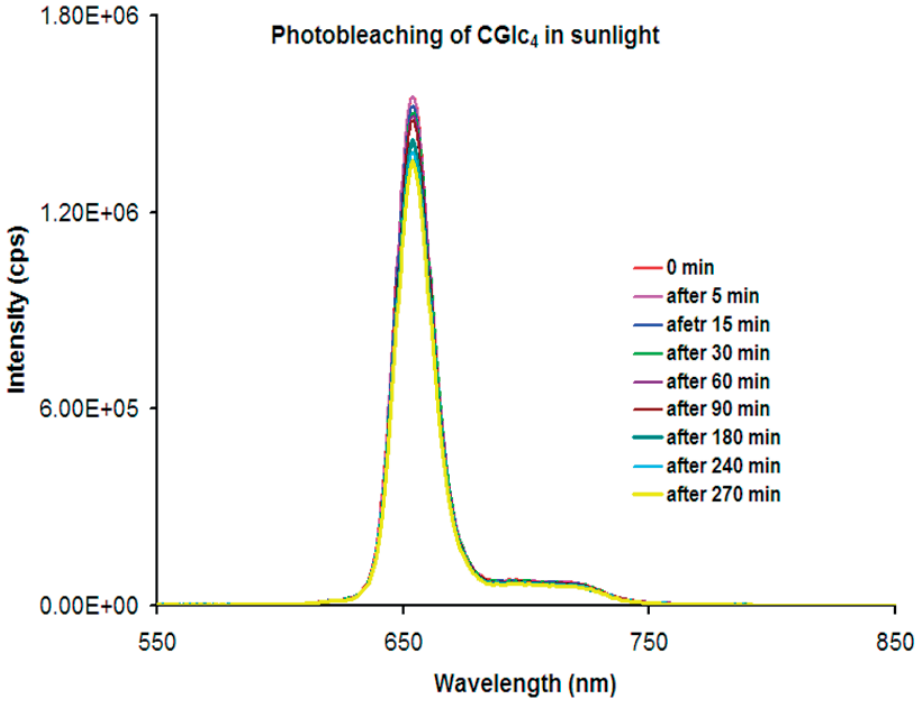

Figure A 6.12. Emission spectra for photobleaching of $CGlc_4$ in sunlight. 1 μM solution in ethanol.

Excited state decay properties:

The decay of the excited electron from higher excited singlet state, S_1 to the ground singlet state, S_0 follows a series of pathway which includes radiative and/or non radiative processes. The fluorescence quantum yield (Φf) and the fluorescence lifetime (τf) are related to their rate constants decay pathways and to also each other by the following equations:

$$\tau f = 1 / (kf + kic + kisc) \quad (1)$$

$$\Phi f = kf / (kf + kic + kisc) \quad (2)$$

Where k_f, k_{ic}, and k_{isc} are the rate constants for the radiative (spontaneous fluorescence) decay, internal conversion decay (from the excited singlet state to the ground singlet state), and for the intersystem crossing to the triplet excited state respectively.

Combining equation 1 and 2 gives the radiation rate constant via the equation:

$$kf = \Phi f / \tau f \quad (3)$$

An approximate value for k_f can be obtained for each compound in a given solvent using the measured values for Φ_f and τ_f. The inverse of k_f (units of nanoseconds) is the inherent time constant for radiative decay. It is also convenient to combine the rate constant for the two non-radiative decay routes of the lowest excited singlet state to obtain:

$$k_{nr} = k_{ic} + k_{isc} \quad (4)$$

combining equation 4 and 1 gives:

$$k_{nr} = \tau_f^{-1} - k_f \quad (5)$$

An approximate value of knr can be obtained for each compound in a given solvent using the measured values of τf and kf. The inverse of knr (units of nanoseconds) is the inherent time constant for non-radiative decay. There is always a competition between the relaxation routes of the excited electron from S1$\rightarrow$ So radiative decay with the non-radiatives S1$\rightarrow$ So internal conversion and S1$\rightarrow$ T1 inter system crossing decay pathways. The high fluorescence quantum yield dictates the process predominantly S1$\rightarrow$ So radiative decay whereas the low fluorescence quantum yield suggests the process is predominantly a non-radiative decay. (*39-41*)

6.6 References

1. Sternberg, E. D., Dolphin, D., and Brückner, C. (1998) Porphyrin-based photosensitizers for use in photodynamic therapy, *Tetrahedron 54*, 4151-4202.
2. Bonnett, R. (1995) Photosensitizers of the porphyrin the phthalocyanine series for phtodynamic therapy, *Chem. Soc. Rev. 24*, 19-33.
3. Pandey, R. K. (2000) Recent advances in photodynamic therapy, *J. Porphyrins Phthalocyanines 4*, 368-373.
4. Pandey, R. K., and Zheng, G. (2000) Porphyrins as photosensitizers in photodynamic therapy, In *The Porphyrin Handbook* (Kadish, K. M., Smith, K. M., and Guilard, R., Eds.), pp 157-230, Academic Press.
5. Pushpan, S. K., Venkatraman, S., Anand, V. G., Sankar, J., Parmeswaran, D., Ganesan, S., and Chandrashekar, T. K. (2002) Porphyrins in Photodynamic Therapy - A Search for Ideal Photosensitizers *Curr. Med. Chem. - Anti-Cancer Agents 2*, 187-207.
6. Spikes, J. D. (1990) New trends in photobiology: Chlorins as photosensitizers in biology and medicine, *J. Photochem. Photobiol. B: Biol. 6*, 259-274.
7. Kadish, K., Smith, K. M., and Guilard, R. (2000, 2003) *The Porphyrin Handbook*, Vol. 1-20, Academic Press, New York.
8. Drain, C. M., and Singh, S. (2010) Combinatorial Libraries of Porphyrins: Chemistry and Applications, In *The Handbook of Porphyrin Science with Applications to Chemistry, Physics, Materials Science, Engineering, Biology and Medicine* (Kadish, K., Smith, K. M., and Guilard, R., Eds.), pp 485-537, World Scientific Publisher, Singapore.
9. Smith, K. M. (1972) *Porphyrins and Metalloporphyrins*, Elsevier Amsterdam.
10. Dolphin, D. (1978) *The Porphyrins*, Academic Press.
11. Bonnett, R., Charlesworth, P., Djelal, B. D., Foley, S., McGarvey, D. J., and Truscott, T. G. (1999) Photophysical properties of 5,10,15,20-tetrakis(*m*-hydroxyphenyl)-porphyrin (m-THPP), 5,10,15.20-tetrakis(*m*-hydroxyphenyl)chlorin (m-THPC) and 5,10,15,20-tetrakis(*m*-hydroxyphenyl)bacteriochlorin (m-THPBC): a comparative study, *J. Chem. Soc., Perkin Trans. 2*, 325-328.
12. Nguyen, Q. T., Olson, E. S., Aguilera, T. A., Jiang, T., Scadeng, M., Ellies, L. G., and Tsien, R. Y. (2010) Surgery with molecular fluorescence imaging using activatable cell-

penetrating peptides decreases residual cancer and improves survival, *Proc. Natl. Acad. Sci., USA 107*, 4317-4322.

13. Laville, I., Figueiredo, T., Loock, B., Pigaglio, S., Maillard, P., Grierson, D. S., Carrez, D., Croisy, A., and Blais, J. (2003) Synthesis, cellular internalization and photodynamic activity of glucoconjugated derivatives of tri and tetra(meta-hydroxyphenyl)chlorins, *Bioorg. Med. Chem. 11*, 1643-1652.
14. Chen, X., Hui, L., Foster, D. A., and Drain, C. M. (2004) Efficient synthesis and photodynamic activity of porphyrin-saccharide conjugates: targeting and incapacitating cancer cells, *Biochemistry 43*, 10918-10929.
15. Pasetto, P., Chen, X., Drain, C. M., and Franck, R. W. (2001) Synthesis of hydrolytically stable porphyrin C- and S-glycoconjugates in high yields, *Chem. Commun.*, 81-82.
16. Samaroo, D., Vinodu, M., Chen, X., and Drain, C. M. (2007) meso-Tetra(pentafluorophenyl)porphyrin as an Efficient Platform for Combinatorial Synthesis and the Selection of New Photodynamic Therapeutics using a Cancer Cell Line, *J. Comb. Chem. 9*, 998-1011.
17. Mauzerall, D. C. (1998) Evolution of Porphyrins, *Clin. Dermatol. 6*, 195–201.
18. Brückner, C., McCarthy, J. R., Daniell, H. W., Pendon, Z. D., Ilagan, R. P., Francis, T. M., Ren, L., Birge, R. R., and Frank, H. A. (2003) A spectroscopic and computational study of the singlet and triplet excited states of synthetic [beta]-functionalized chlorins, *Chem. Phys. 294*, 285-303.
19. Silva, A. M. G., Tomé, A. C., Neves, M. G. P. M. S., Silva, A. M. S., and Cavaleiro, J. A. S. (1999) meso-Tetraarylporphyrins as dipolarophiles in 1,3-dipolar cycloaddition reactions, *Chem. Commun.*, 1767-1768.
20. Silva, A. M. G., Tome´, A. C., Neves, M. G. P. M. S., Silva, A. M. S., and Cavaleiro, J. A. S. (2005) 1,3-Dipolar Cycloaddition Reactions of Porphyrins with Azomethine Ylides, *J. Org. Chem. 70*, 2306-2314.
21. Cavaleiro, J. A. S., Tomé, A. C., and Neves, M. G. P. M. S. (2010) meso-Tetraarylporphyrin Derivatives: New Synthetic Methodologies, In *The Handbook of Porphyrin Science with Applications to Chemistry, Physics, Materials Science,*

Engineering, Biology and Medicine (Kadish, K., Smith, K. M., and Guilard, R., Eds.), pp 193-294, World Scientific Publisher, Singapore.

22. Jiménez-Osés, G., García, J. I., Silva, A. M. G., Santos, A. R. N., Tomé, A. C., Neves, M. G. P. M. S., and Cavaleiro, J. A. S. (2008) Mechanistic insights on the site selectivity in successive 1,3-dipolar cycloadditions to meso-tetraarylporphyrins, *Tetrahedron 64*, 7937-7943.
23. Maestrin, A. P. J., Ribeiro, A. O., Tedesco, A. C., Neri, C. R., Vinhado, F. S., Serra, O. A., Martins, P. R., Iamamoto, Y., Silva, A. M. G., Tomé, A. C., Neves, M. G. P. M. S., and Cavaleiro, J. A. S. (2004) A novel chlorin derivative of Meso-tris(pentafluorophenyl)-4-pyridylporphyrin: synthesis, photophysics and photochemical properties, *J. Braz. Chem. Soc. 15*, 923-930.
24. Hao, E., Friso, E., Miotto, G., Jori, G., Soncin, M., Fabris, C., Sibrian-Vazquez, M., and Vicente, M. G. H. (2008) Synthesis and biological investigations of tetrakis(p-carboranylthio-tetrafluorophenyl)chlorin (TPFC), *Org. Biomol. Chem. 6*, 3732-3740.
25. Hirohara, S., Obata, M., Alitomo, H., Sharyo, K., Ando, T., Tanihara, M., and Yano, S. (2009) Synthesis, photophysical properties and sugar-dependent in vitro photocytotoxicity of pyrrolidine-fused chlorins bearing S-glycosides, *J. Photochem. Photobiol. B: Biol. 97*, 22-33.
26. Hirohara, S., Obata, M., Alitomo, H., Sharyo, K., Ando, T., Yano, S., and Tanihara, M. (2009) Synthesis and Photocytotoxicity of S-Glucosylated 5,10,15,20-Tetrakis(tetrafluorophenyl)porphyrin Metal Complexes as Efficient $^1O_2$-Generating Glycoconjugates, *Bioconjugate Chem. 20*, 944-952.
27. Thompson, S., Chen, X., Hui, L., Toschi, A., Foster, D. A., and Drain, C. M. (2008) Low concentrations of a non-hydrolysable tetra-S-glycosylated porphyrin and low light induces apoptosis in human breast cancer cells via stress of the endoplasmic reticulum, *Photochem. Photobiol. Sci. 7*, 1415-1421.
28. Drain, C. M., Singh, S., Samaroo, D., Thompson, S., Vinodu, M., and Tomé, J. P. C. (2009) New Porphyrin Glyco-conjugates, *Proc. Soc. Photo-Optical Instrumentation Engineers-SPIE 7380*.

29. Singh, S., Aggarwal, A., Thompson, S., Tomé, J. o. P. C., Zhu, X., Samaroo, D., Vinodu, M., Gao, R., and Drain, C. M. (2010) Synthesis and Photophysical Properties of Thioglycosylated Chlorins, Isobacteriochlorins, and Bacteriochlorins for Bioimaging and Diagnostics, *Bioconjugate Chem. 21*, 2136-2146.
30. Bonnett, R., and Martínez, G. (2001) Photobleaching of sensitisers used in photodynamic therapy, *Tetrahedron 57*, 9513-9547.
31. Seybold, P. G., and Gouterman, M. (1969) Porphyrins XIII: Fluorescence spectra and quantum yields, *J. Mol. Spectrosc. 31*, 1-13.
32. Tanielian, C., Wolff, C., and Esch, M. (1996) Singlet Oxygen Production in Water: Aggregation and Charge-Transfer Effects, *J. Phys. Chem. 100*, 6555-6560.
33. Mishra, P. P., Patel, S., and Datta, A. (2006) Effect of Increased Hydrophobicity on the Binding of Two Model Amphiphilic Chlorin Drugs for Photodynamic Therapy with Blood Plasma and Its Components, *J. Phys. Chem. B 110*, 21238-21244.
34. Drain, C. M., Gentemann, S., Roberts, J. A., Nelson, N. Y., Medforth, C. J., Jia, S., Simpson, M. C., Smith, K. M., Fajer, J., Shelnutt, J. A., and Holten, D. (1998) Picosecond to microsecond photodynamics of a nonplanar nickel porphyrin: solvent dielectric and temperature effects, *J. Am. Chem. Soc. 120*, 3781-3791.
35. Borbas, K. E., Chandrashaker, V., Muthiah, C., Kee, H. L., Holten, D., and Lindsey, J. S. (2008) Design, Synthesis, and Photophysical Characterization of Water-Soluble Chlorins, *J. Org. Chem. 73*, 3145-3158.
36. Obata, M., Hirohara, S., Tanaka, R., Kinoshita, I., Ohkubo, K., Fukuzumi, S., Tanihara, M., and Yano, S. (2009) In Vitro Heavy-Atom Effect of Palladium(II) and Platinum(II) Complexes of Pyrrolidine-Fused Chlorin in Photodynamic Therapy, *J. Med. Chem. 52*, 2747-2753.
37. Boisbrun, M., Vanderesse, R., Engrand, P., Olié, A., Hupont, S., Regnouf-de-Vains, J.-B., and Frochot, C. (2008) Design and photophysical properties of new RGD targeted tetraphenylchlorins and porphyrins, *Tetrahedron 64*, 3494-3504.
38. Gonsalves, A. M. d. A. R., Serra, A. C., and Pineiro, M. (2009) The small stones of Coimbra in the huge tetrapyrrolic chemistry building, *J. Porphyrins Phthalocyanines 13*, 429-445.

39. Chinnasamy Muthiah, Masahiko Taniguchi, Han-Je Kim, Izabela Schmidt, Hooi Ling Kee, Dewey Holten, David F. Bocian, and Lindsey, J. S. (2007) Synthesis and Photophysical Characterization of Porphyrin, Chlorin and Bacteriochlorin Molecules Bearing Tethers for Surface Attachment, *Photochem. Photobiol. 83*, 1513-1528.

40. Huang, Y.-Y., Mroz, P., Zhiyentayev, T., Sharma, S. K., Balasubramanian, T., Ruzié, C., Krayer, M., Fan, D., Borbas, K. E., Yang, E., Kee, H. L., Kirmaier, C., Diers, J. R., Bocian, D. F., Holten, D., Lindsey, J. S., and Hamblin, M. R. (2010) In Vitro Photodynamic Therapy and Quantitative Structure−Activity Relationship Studies with Stable Synthetic Near-Infrared-Absorbing Bacteriochlorin Photosensitizers, *J. Med. Chem. 53*, 4018-4027.

41. Kee, H. L., Bhaumik, J., Diers, J. R., Mroz, P., Hamblin, M. R., Bocian, D. F., Lindsey, J. S., and Holten, D. (2008) Photophysical characterization of imidazolium-substituted Pd(II), In(III), and Zn(II) porphyrins as photosensitizers for photodynamic therapy, *J. Photochem. Photobiol. A: Chem. 200*, 346-355.

42. Gentemann, S., Medforth, C. J., Forsyth, T. P., Nurco, D. J., Smith, K. M., Fajer, J., and Holten, D. (1994) Photophysical Properties of Conformationally Distorted Metal-Free Porphyrins. Investigation into the Deactivation Mechanisms of the Lowest Excited Singlet State, *J. Am. Chem. Soc. 116*, 7363-7368.

43. Csik, G., Balog, E., Voszka, I., Tölgyesi, F., Oulmi, D., Maillard, P., and Momenteau, M. (1998) Glycosylated derivatives of tetraphenyl porphyrin: photophysical characterization, self-aggregation and membrane binding, *J. Photochem. Photobiol. B: Biol. 44*, 216-224.

44. Thompson, S., Chen, X., Hui, L., Toschi, A., Foster, D. A., and Drain, C. M. (2008) Low Concentrations of a non-hydrolysable tetra-S-glycosylated porphyrin and low light induces apoptosis in human breast cancer cells via stress of the endoplasmic reticulum, *Photochem. Photobiol. Sci. 7*, 1415-1421.

45. Cselenyák, A., Pankotai, E., Csordás, A., Kiss, L., and Lacza, Z. (2010) Live-Cell Fluorescent Imaging of Membrane or Mitochondrion Transfer between Connected Cells in Culture, *MIicroscopy Book Series 1*, 764-771.

46. Zhang, X.-a., Lovejoy, K. S., Jasanoff, A., and Lippard, S. J. (2007) Water-soluble porphyrins as a dual-function molecular imaging platform for MRI and fluorescence zinc sensing, *Proc. Natl. Acad. Sci., USA 104*, 10780-10785.

47. Morris, R. L., Azizuddin, K., Lam, M., Berlin, J., Nieminen, A.-L., Kenney, M. E., Samia, A. C. S., Burda, C., and Oleinick, N. L. (2003) Fluorescence Resonance Energy Transfer Reveals a Binding Site of a Photosensitizer for Photodynamic Therapy, *Cancer Res. 63*, 5194-5197.

48. Plaetzer, K., Kiesslich, T., Oberdanner, C. B., and Krammer, B. (2005) Apoptosis Following Photodynamic Tumor Therapy: Induction, Mechanisms and Detection, *Curr. Pharm. Des. 11*, 1151-1165.

Bibliography

Chapter 1

1. Kadish, K. M., Smith, K. M., and Guilard, R., (Eds.) (2000) *The Porphyrin Handbook*, Vol. 1-10, Academic Press, New York.
2. Dolphin, D., (Ed.) (1978-1979.) *The Porphyrins*, Vol. 1-7, Academic Press, New York.
3. Groves, J. T. (2006) High-valent iron in chemical and biological oxidations, *J. Inorg. Biochem. 100*, 434-447.
4. Groves, J. T., Haushalter, R. C., Nakamura, M., Nemo, T. E., and Evans, B. J. (1981) High-valent iron-porphyrin complexes related to peroxidase and cytochrome P-450, *J. Am. Chem. Soc. 103*, 2884-2886.
5. Groves, J. T., and Nemo, T. E. (1983) Epoxidation reactions catalyzed by iron porphyrins. Oxygen transfer from iodosylbenzene, *J. Am. Chem. Soc. 105*, 5786-5791.
6. Groves, J. T., Nemo, T. E., and Myers, R. S. (1979) Hydroxylation and epoxidation catalyzed by iron-porphine complexes. Oxygen transfer from iodosylbenzene, *J. Am. Chem. Soc. 101*, 1032-1033.
7. Groves, J. T., and Viski, P. (1990) Asymmetric hydroxylation, epoxidation, and sulfoxidation catalyzed by vaulted binaphthyl metalloporphyrins, *J. Org. Chem. 55*, 3628-3634.
8. Groves, J. T., and Watanabe, Y. (1986) Heterolytic and homolytic oxygen-oxygen bond cleavage reactions of acylperoxomanganese(III) porphyrins, *Inorg. Chem. 25*, 4808-4810.
9. Gouterman, M. (1978) *The Porphyrins*, Vol. 3, Academic Press, New York.
10. Rio, Y., Salome Rodriguez-Morgade, M., and Torres, T. (2008) Modulating the electronic properties of porphyrinoids: a voyage from the violet to the infrared regions of the electromagnetic spectrum, *Org. Biomol. Chem. 6*, 1877-1894.
11. Drain, C. M. (2002) Self-organization of self-assembled photonic materials into functional devices: Photo-switched conductors, *Proc. Natl. Acad. Sci. 99*, 5178-5182.
12. Drain, C. M., Batteas, J. D., Flynn, G. W., Milic, T., Chi, N., Yablon, D. G., and Sommers, H. (2002) Designing supramolecular porphyrin arrays that self-organize into nanoscale optical and magnetic materials, *Proc. Natl. Acad. Sci. 99*, 6498-6502.

13. Milic, T. N., Chi, N., Yablon, D. G., Flynn, G. W., Batteas, J. D., and Drain, C. M. (2002) Controlled Hierarchical Self-Assembly and Deposition of Nanoscale Photonic Materials *Angew Chem. Int. Ed. 41*, 2117-2119.
14. Drain, C. M., Goldberg, I., Sylvain, I., and Falber, A. (2005) Synthesis and Applications of Supramolecular Porphyrinic Materials, *Top. Curr. Chem. 245*, 55-88.
15. Drain, C. M., Batteas, J. D., Smeureanu, G., and Patel, S. (2004) Self-Assembly of Porphyrinic Materials on Surfaces, *Dekker Encyclopedia of Nanoscience and Nanotechnology*, 3481 - 3502.
16. Nitschke, C., O'Flaherty, S. M., Kröll, M., and Blau, W. J. (2004) Material Investigations and Optical Properties of Phthalocyanine Nanoparticles, *J. Phys. Chem. B 108*, 1287-1295.
17. Rangel-Rojo, R., Matsuda, H., Kasai, H., and Nakanishi, H. (2000) Irradiance dependence of the resonant nonlinearities in an organic material, *J. Opt. Soc. Am. B 17*, 1376-1382.
18. Müller, R. H., Benita, S., and Böhm, B. H. L. (1998) Emulsions and Nanosuspensions for the Formulation of Poorly Soluble Drugs, *Scientific Publishers, Stuttgart*.
19. Newcomb, M., Hollenberg, P. F., and Coon, M. J. (2003) Multiple mechanisms and multiple oxidants in P450-catalyzed hydroxylations, *Arch. Biochem. Biophys. 409*, 72-79.
20. Ortiz de Montellano, P. R. (1995) *Cytochrome P450: Structure, Mechanism, and Biochemistry*, 2nd. ed., Plenum Press, New York.
21. Chandrasena, R. E. P., Vatsis, K. P., Coon, M. J., Hollenberg, P. F., and Newcomb, M. (2004) Hydroxylation by the Hydroperoxy-Iron Species in Cytochrome P450 Enzymes, *J. Am. Chem. Soc. 126*, 115-126.
22. Meunier, B., de Visser, S. P., and Shaik, S. (2004) Mechanism of Oxidation Reactions Catalyzed by Cytochrome P450 Enzymes, *Chem. Rev. 104*, 3947-3980.
23. Silaghi-Dumitrescu, R. (2004) The nature of the high-valent complexes in the catalytic cycles of hemoproteins, *J. Biol. Inorg. Chem. 9*, 471-476.
24. Mayer, J. M. (2000) Biomimetic Oxygenations Related to Cytochrome P450: Metal-Oxo and Metal-Peroxo Intermediates, In *Biomimetic Oxidations Catalyzed by Transition Metal Complexes* (Meunier, B., Ed.), pp 1-43, Imperial College Press.

25. Dolphin, D., Traylor, T. G., and Xie, L. Y. (1997) Polyhaloporphyrins: Unusual Ligands for Metals and Metal-Catalyzed Oxidations, *Acc. Chem. Res. 30*, 251-259.
26. Mansuy, D. (1993) Activation of alkanes : the biomimetic approach, *Coord. Chem. Rev. 125*, 129-141.
27. Groves, J. T. (2000) Reactivity and mechanisms of metalloporphyrin-catalyzed oxidations, *J. Porphyrins Phthalocyanines 4*, 350-352.
28. Barloy, L., Battioni, P., and Mansuy, D. (1990) Manganese porphyrins supported on montmorillonite as hydrocarbon mono-oxygenation catalysts: particular efficacy for linear alkane hydroxylation, *J. Chem. Soc., Chem. Commun.*, 1365-1367.
29. Wang, C., Shalyaev, K. V., Bonchio, M., Carofiglio, T., and Groves, J. T. (2006) Fast Catalytic Hydroxylation of Hydrocarbons with Ruthenium Porphyrins, *Inorg. Chem. 45*, 4769-4782.
30. Merlau, M. L., Cho, S.-H., Sun, S.-S., Nguyen, S. T., and Hupp, J. T. (2005) Anthracene-Induced Turnover Enhancement in the Manganese Porphyrin-Catalyzed Epoxidation of Olefins, *Inorg. Chem. 44*, 5523-5529.
31. Groves, J. T., and Marla, S. S. (1995) Peroxynitrite-Induced DNA Strand Scission Mediated by a Manganese Porphyrin, *J. Am. Chem. Soc. 117*, 9578-9579.
32. Lee, J., Hunt, J. A., and Groves, J. T. (1998) Mechanisms of Iron Porphyrin Reactions with Peroxynitrite, *J. Am. Chem. Soc. 120*, 7493-7501.
33. Lee, J., Hunt, J. A., and Groves, J. T. (1998) Manganese Porphyrins as Redox-Coupled Peroxynitrite Reductases, *J. Am. Chem. Soc. 120*, 6053-6061.
34. Lee, J., Hunt, J. A., and Groves, J. T. (1997) Rapid decomposition of peroxynitrite by manganese porphyrin-antioxidant redox couples, *Bioorg. Med. Chem. Lett. 7*, 2913-2918.
35. Hunt, J. A., Lee, J., and Groves, J. T. (1997) Amphiphilic peroxynitrite decomposition catalysts in liposomal assemblies, *Chem. Biol. 4*, 845-858.
36. Shimanovich, R., and Groves, J. T. (2001) Mechanisms of Peroxynitrite Decomposition Catalyzed by FeTMPS, a Bioactive Sulfonated Iron Porphyrin, *Arch. Biochem. Biophys. 387*, 307-317.
37. Jensen, M. P., and Riley, D. P. (2002) Peroxynitrite Decomposition Activity of Iron Porphyrin Complexes, *Inorg. Chem. 41*, 4788-4797.

38. Crow, J. P. (2000) Peroxynitrite scavenging by metalloporphyrins and thiolates, *Free Radical Biol. Med. 28*, 1487-1494.

39. Stern, M. K., Jensen, M. P., and Kramer, K. (1996) Peroxynitrite Decomposition Catalysts, *J. Am. Chem. Soc. 118*, 8735-8736.

40. Salvemini, D., Wang, Z.-Q., Stern, M. K., Currie, M. G., and P., M. T. (1998) Peroxynitrite decomposition catalysts: Therapeutics for peroxynitrite-mediated pathology *Proc. Natl. Acad. Sci. USA 95*, 2659-2663.

41. Ferrer-Sueta, G., Vitturi, D., Batinić-Haberle, I., Fridovich, I., Goldstein, S., Czapski, G., and R., R. (2003) Reactions of Manganese Porphyrins with Peroxynitrite and Carbonate Radical Anion, *J. Biol. Chem. 278*, 27432-27438.

42. Drain, C. M., Smeureanu, G., Patel, S., X.Gong, Garno, J., and Arijeloye, J. (2006) Porphyrin nanoparticles as supramolecular systems, *New J. Chem. 30*, 1834-1843.

43. Gong, X., Milic, T., Xu, C., Batteas, J. D., and Drain, C. M. (2002) Preparation and Characterization of Porphyrin Nanoparticles, *J. Am. Chem. Soc. 124*, 14290-14291.

44. Merlau, M. L., Mejia, M. d. P., Nguyen, S. T., and Hupp, J. T. (2001) Artificial enzymes formed through directed assembly of molecular square encapsulated epoxidation catalysts, *Angew. Chem. Int. Ed. 40*, 4239-4242.

45. Lee, S. J., and Hupp, J. T. (2006) Porphyrin-containing molecular squares: Design and applications, *Coord. Chem. Rev. 250*, 1710-1723.

46. Khalil, G. E., Chang, A., Gouterman, M., Callis, J. B., dalton, L. R., Turro, N. J., and Jockusch, S. (2005) Oxygen pressure measurementusing singlet oxygen emission, *Rev. Sci. Instrum. 76*, 54101-54108.

47. Drain, C. M., Varotto, A., and Radivojevic, I. (2009) Self-Organized Porphyrinic Materials, *Chem. Rev. 109*, 1630-1658.

48. M.d'A., A., Rocha Gonsalves, Serra, A. C., and Pineiro, M. (2009) The small stones of Coimbra in the huge tetrapyrrolic chemistry building, *J. Porphyins Phthalocyanines 13*, 429-445.

49. Pineiro, M., Carvalho, A. L., Pereira, M. M., Gonsalves, A. M. d. A. R., Arnaut, L. G., and Formosinho, S. J. (1998) Photoacoustic Measurements of Porphyrin Triplet-State Quantum Yields and Singlet-Oxygen Efficiencies, *Chem. Eur. J. 4*, 2299-2307.

50. Pineiro, M., Pereira, M. M., Rocha Gonsalves, A. M. d. A., Arnaut, L. G., and Formosinho, S. J. (2001) Singlet oxygen quantum yields from halogenated chlorins: potential new photodynamic therapy agents, *J. Photochem. Photobiol. A: Chem. 138*, 147-157.

51. Azenha, E. G., Serra, A. C., Pineiro, M., Pereira, M. M., Seixas de Melo, J., Arnaut, L. G., Formosinho, S. J., and Rocha Gonsalves, A. M. d. A. (2002) Heavy-atom effects on metalloporphyrins and polyhalogenated porphyrins, *Chem. Phys. 280*, 177-190.

52. Baluschev, S., Miteva, T., Yakutkin, V., Nelles, G., Yasuda, A., and Wegner, G. (2006) Up-Conversion Fluorescence: Noncoherent Excitation by Sunlight, *Phys. Rev. Lett. 97*, 143903.

53. Mirkin, C. A., and Ratner, M. A. (1992) Molecular Electronics, *Annu. Rev. Phys. Chem. 43*, 719-754.

54. Drain, C. M., Gong, X., Ruta, V., Soll, C. E., and Chicoineau, P. F. (1999) Combinatorial Synthesis and Modification of Functional Porphyrin Libraries: Identification of New, Amphipathic Motifs for Biomolecule Binding, *J. Comb. Chem. 1*, 286-290.

55. Samaroo, D., Vinodu, M., Chen, X., and Drain, C. M. (2007) meso-Tetra(pentafluorophenyl)porphyrin as an Efficient Platform for Combinatorial Synthesis and the Selection of New Photodynamic Therapeutics using a Cancer Cell Line, *J. Comb. Chem. 9*, 998-1011.

56. Singh, S., Aggarwal, A., Thompson, S., Tom. , J. o. P. C., Zhu, X., Samaroo, D., Vinodu, M., Gao, R., and Drain, C. M. (2010) Synthesis and Photophysical Properties of Thioglycosylated Chlorins, Isobacteriochlorins, and Bacteriochlorins for Bioimaging and Diagnostics, *Bioconjugate Chem. 21*, 2136-2146.

57. Chen, X., Hui, L., Foster, D. A., and Drain, C. M. (2004) Efficient Synthesis and Photodynamic Activity of Porphyrin-Saccharide Conjugates: Targeting and Incapacitating Cancer Cells, *Biochemistry 43*, 10918-10929.

58. Thompson, S., Chen, X., Hui, L., Toschi, A., Foster, D. A., and Drain, C. M. (2008) Low concentrations of a non-hydrolysable tetra-S-glycosylated porphyrin and low light induces apoptosis in human breast cancer cells via stress of the endoplasmic reticulum, *Photochem. Photobiol. Sci. 7*, 1415-1421.

59. Chen, X., and Drain, C. M. (2004) Photodynamic Therapy using Carbohydrate Conjugated Porphyrins *Drug Des. Rev. 1*, 215-234.
60. Pushpan, S. K., Venkatraman, S., Anand, V. G., Sankar, J., Parmeswaran, D., Ganesan, S., and Chandrashekar, T. K. (2002) Porphyrins in Photodynamic Therapy - A Search for Ideal Photosensitizers *Curr. Med. Chem. - Anti-Cancer Agents 2*, 187-207.
61. Spikes, J. D. (1990) New trends in photobiology: Chlorins as photosensitizers in biology and medicine, *J. Photochem. Photobiol. B: Biol. 6*, 259-274.

Chapter 2

1. Muzart, J. (1992) Chromium-catalyzed oxidations in organic synthesis, *Chem. Rev. 92*, 113-140.
2. Choi, H., and Doyle, M. P. (2007) Optimal TBHP Allylic Oxidation of Δ5-Steroids Catalyzed by Dirhodium Caprolactamate, *Org. Lett. 9*, 5349-5352.
3. Doyle, M. P. (2006) Perspective on Dirhodium Carboxamidates as Catalysts, *J. Org. Chem. 71*, 9253-9260.
4. Shing, T. K. M., Yeung, Y.-Y., and Su, P. L. (2006) Mild Manganese(III) Acetate Catalyzed Allylic Oxidation: Application to Simple and Complex Alkenes, *Org. Lett. 8*, 3149-3151.
5. Harre, M., Haufe, R., Nickisch, K., Weinig, P., Weinmann, H., Kinney, W. A., and Zhang, X. (1998) Some Reaction Safety Aspects of Ruthenium-Catalyzed Allylic Oxidations of Δ-5-Steroids in the Pilot Plant, *Org. Proc. Res. Dev. 2*, 100-104.
6. Crich, D., and Zou, Y. (2004) Catalytic Allylic Oxidation with a Recyclable, Fluorous Seleninic Acid, *Org. Lett. 6*, 775-777.
7. Zhao, Y., and Yeung, Y.-Y. (2010) An Unprecedented Method for the Generation of tert-Butylperoxy Radical Using DIB/TBHP Protocol: Solvent Effect and Application on Allylic Oxidation, *Org. Lett. 12*, 2128-2131.

8. Uyanik, M., Okamoto, H., Yasui, T., and Ishihara, K. (2010) Quaternary Ammonium (Hypo)iodite Catalysis for Enantioselective Oxidative Cycloetherification, *Science 328*, 1376-1379.
9. Silaghi-Dumitrescu, R. (2004) The nature of the high-valent complexes in the catalytic cycles of hemoproteins, *J. Biol. Inorg. Chem. 9*, 471-476.
10. Meunier, B., de Visser, S. P., and Shaik, S. (2004) Mechanism of Oxidation Reactions Catalyzed by Cytochrome P450 Enzymes, *Chem. Rev. 104*, 3947-3980.
11. Newcomb, M., Hollenberg, P. F., and Coon, M. J. (2003) Multiple mechanisms and multiple oxidants in P450-catalyzed hydroxylations, *Arch. Biochem. Biophys. 409*, 72-79.
12. Chandrasena, R. E. P., Vatsis, K. P., Coon, M. J., Hollenberg, P. F., and Newcomb, M. (2004) Hydroxylation by the Hydroperoxy-Iron Species in Cytochrome P450 Enzymes, *J. Am. Chem. Soc. 126*, 115-126.
13. Lee, S. J., and Hupp, J. T. (2006) Porphyrin-containing molecular squares: Design and applications, *Coord. Chem. Rev. 250*, 1710-1723.
14. Merlau, M. L., Mejia, M. d. P., Nguyen, S. T., and Hupp, J. T. (2001) Artificial enzymes formed through directed assembly of molecular square encapsulated epoxidation catalysts, *Angew. Chem. Int. Ed. 40*, 4239-4242.
15. Merlau, M. L., Cho, S. H., Sun, S. S., Nguyen, S. T., and Hupp, J. T. (2005) Anthracene-Induced Turnover Enhancement in the Manganese Porphyrin-Catalyzed Epoxidation of Olefins, *Inorg. Chem. 44*, 5523-5529.
16. Astruc, D., Lu, F., and Aranzaes, J. R. (2005) Nanoparticles as Recyclable Catalysts: The Frontier Between Homogeneous and Heterogeneous Catalysis, *Angew. Chem. Int. Ed. 44*, 7852-7872.
17. Scott, R. W. J., Wilson, O. M., and Crooks, R. M. (2005) Synthesis, Characterization, and Applications of Dendrimer-Encapsulated Nanoparticles, *J. Phys. Chem. B.;*, 692-704.
18. Horn, D., and Rieger, J. (2001) Organic Nanoparticles in the Aqueous Phase - Theory, Experiment, and Use, *Angew. Chem. Int. Ed. 40*, 4330-4361.
19. LaMer, V. K., and Dinegar, R. H. (1950) Theory, Production and Mechanism of Formation of Monodispersed Hydrosols, *J. Am. Chem. Soc. 72*, 4847-4854.
20. Drain, C. M., Smeureanu, G., Patel, S., X.Gong, Garno, J., and Arijeloye, J. (2006) Porphyrin nanoparticles as supramolecular systems, *New J. Chem. 30*, 1834-1843.

21. Gong, X., Milic, T., Xu, C., Batteas, J. D., and Drain, C. M. (2002) Preparation and Characterization of Porphyrin Nanoparticles, *J. Am. Chem. Soc. 124*, 14290-14291.
22. Drain, C. M., Bazzan, G., Milic, T., Vinodu, M., and Goeltz, J. C. (2005) Formation and applications of stable 10 nm to 500 nm supramolecular porphyrinic materials, *Isr. J. Chem. 45*, 255-269.
23. Drain, C. M., Goldberg, I., Sylvain, I., and Falber, A. (2005) Synthesis and Applications of Supramolecular Porphyrinic Materials, *Top. Curr. Chem. 245*, 55-88.
24. Brick, M. C., Palmer, H. J., and Whitesides, T. H. (2003) Formation of Colloidal Dispersions of Organic Materials in Aqueous Media by Solvent Shifting, *Langmuir 19*, 6367-6380.
25. Qian, D. J., Nakamura, C., Wakayama, T., and Miyake, J. (2003) Synthesis and multilayer assembly of multiporphyrin arrays at the water-chloroform interface, *J. Porphyrins Phthalocyanines 7*, 415-419.
26. Van Keuren, E., Bone, A., and Ma, C. (2008) Phthalocyanine Nanoparticle Formation in Supersaturated Solutions, *Langmuir 24*, 6079-6084.
27. Sane, A., Taylor, S., Sun, Y.-p., and Thies, M. C. (2003) RESS for the preperation of fluorinated porphyrin nanoparticles, *Chem. Commun.*, 2720-2721.
28. Sane, A., and Thies, M. C. (2005) The Formation of Fluorinated Tetraphenylporphyrin Nanoparticles via Rapid Expansion Processes: RESS vs RESOLV, *J. Phys. Chem. B 109*, 19688-19695.
29. Rangel-Rojo, R., Matsuda, H., Kasai, H., and Nakanishi, H. (2000) Irradiance dependence of the resonant nonlinearities in an organic material, *J. Opt. Soc. Am. B 17*, 1376-1382.
30. Nitschke, C., O'Flaherty, S. M., Kroll, M., and Blau, W. J. (2004) Material investigations and optical properties of phthalocyanine nanoparticles, *J. Phys. Chem. B 108*, 1287-1295.
31. Müller, R. H., Benita, S., and Böhm, B. H. L., (Eds.) (1998) *Emulsions and Nanosuspensions for the Formulation of Poorly Soluble Drugs* Scientific Publishers, Stuttgart.
32. Park, J., Privman, V., and Matijevic, E. (2001) Model of Formation of Monodispersed Colloids, *J. Phys. Chem. B 105*, 11630-11635.

33. Groves, J. T. (2006) High-valent iron in chemical and biological oxidations, *J. Inorg. Biochem. 100*, 434-447.

34. Groves, J. T., Haushalter, R. C., Nakamura, M., Nemo, T. E., and Evans, B. J. (1981) High-valent iron-porphyrin complexes related to peroxidase and cytochrome P-450, *J. Am. Chem. Soc. 103*, 2884-2886.

35. Groves, J. T., and Nemo, T. E. (1983) Epoxidation reactions catalyzed by iron porphyrins. Oxygen transfer from iodosylbenzene, *J. Am. Chem. Soc. 105*, 5786-5791.

36. Groves, J. T., Nemo, T. E., and Myers, R. S. (1979) Hydroxylation and epoxidation catalyzed by iron-porphine complexes. Oxygen transfer from iodosylbenzene, *J. Am. Chem. Soc. 101*, 1032-1033.

37. Groves, J. T., and Viski, P. (1990) Asymmetric hydroxylation, epoxidation, and sulfoxidation catalyzed by vaulted binaphthyl metalloporphyrins, *J. Org. Chem. 55*, 3628-3634.

38. Groves, J. T., and Watanabe, Y. (1986) Heterolytic and homolytic oxygen-oxygen bond cleavage reactions of acylperoxomanganese(III) porphyrins, *Inorg. Chem. 25*, 4808-4810.

39. Ortiz de Montellano, P. R. (1995) *Cytochrome P450: Structure, Mechanism, and Biochemistry*, 2nd. ed., Plenum Press, New York.

40. Mayer, J. M. (2000) Biomimetic Oxygenations Related to Cytochrome P450: Metal-Oxo and Metal-Peroxo Intermediates, In *Biomimetic Oxidations Catalyzed by Transition Metal Complexes* (Meunier, B., Ed.), pp 1-43, Imperial College Press.

41. Dolphin, D., Traylor, T. G., and Xie, L. Y. (1997) Polyhaloporphyrins: Unusual Ligands for Metals and Metal-Catalyzed Oxidations, *Acc. Chem. Res. 30*, 251-259.

42. Barloy, L., Battioni, P., and Mansuy, D. (1990) Manganese porphyrins supported on montmorillonite as hydrocarbon mono-oxygenation catalysts: particular efficacy for linear alkane hydroxylation, *J. Chem. Soc., Chem. Commun.*, 1365-1367.

43. Mansuy, D. (1993) Activation of alkanes : the biomimetic approach, *Coord. Chem. Rev. 125*, 129-141.

44. Wang, C., Shalyaev, K. V., Bonchio, M., Carofiglio, T., and Groves, J. T. (2006) Fast Catalytic Hydroxylation of Hydrocarbons with Ruthenium Porphyrins, *Inorg. Chem. 45*, 4769-4782.

45. Merlau, M. L., Cho, S.-H., Sun, S.-S., Nguyen, S. T., and Hupp, J. T. (2005) Anthracene-Induced Turnover Enhancement in the Manganese Porphyrin-Catalyzed Epoxidation of Olefins, *Inorg. Chem. 44*, 5523-5529.

46. Groves, J. T. (2000) Reactivity and mechanisms of metalloporphyrin-catalyzed oxidations, *J. Porphyrins Phthalocyanines 4*, 350-352.

47. Suslick, K. S. (2000) Shape Selective Oxidation by Metalloporphyrins, In *The Porphyrin Handbook* (Kadish, K. M., Smith, K. M., and Guilard, R., Eds.), pp 41-60, Academic Press, New York.

48. Simonneaux, G., Le Maux, P., Ferrand, Y., and Rault-Berthelot, J. (2006) Asymmetric heterogeneous catalysis by metalloporphyrins, *Coord. Chem. Rev. 250*, 2212-2221.

49. Ungashe, S. B., and Groves, J. T. (1994) Porphyrins and metalloporphyrins in synthetic bilayer membranes, *Adv. Inorg. Biochem. 9*, 317-351.

50. Groves, J. T. (2003) The bioinorganic chemistry of iron in oxygenases and supramolecular assemblies, *Proc. Natl. Acad. Sci., USA 100* 3569-3574.

51. Stephenson, N. A., and Bell, A. T. (2005) A Study of the Mechanism and Kinetics of Cyclooctene Epoxidation Catalyzed by Iron(III) Tetrakispentafluorophenyl Porphyrin, *J. Am. Chem. Soc. 127*, 8635-8643.

52. Stephenson, N. A., and Bell, A. T. (2006) Effects of Methanol on the Thermodynamics of Iron(III) [Tetrakis(pentafluorophenyl)]porphyrin Chloride Dissociation and the Creation of Catalytically Active Species for the Epoxidation of Cyclooctene, *Inorg. Chem. 45*, 5591-5599.

53. Stephenson, N. A., and Bell, A. T. (2006) Influence of Solvent Composition on the Kinetics of Cyclooctene Epoxidation by Hydrogen Peroxide Catalyzed by Iron(III) [tetrakis(pentafluorophenyl)] Porphyrin Chloride [(F_{20}TPP)FeCl], *Inorg. Chem. 45*, 2758-2766.

54. Stephenson, N. A., and Bell, A. T. (2007) Mechanistic Study of Iron(III) [Tetrakis(pentafluorophenyl)Porphyrin Triflate (F_{20}TPP)Fe(OTf) Catalyzed Cyclooctene Epoxidation by Hydrogen Peroxide, *Inorg. Chem. 46*, 2278-2285.

55. Ellis, P. E., and Lyons, J. E. (1989) Halognation substituent effects on the catalytic activity of iron porphyron complexes for the selective air oxidation of alkanes in the liquid phase, *Catal. Lett. 3*, 389-397.

56. Lyons, J. E., and Ellis, P. E. (1991) Selective low temperature oxidation of isobutane by molecular oxygen by an iron perhaloporphyrin complex, *Catal. Lett. 8*, 45-51.

57. Bartoli, J. F., Brigaud, O., Battioni, P., and Mansuy, D. (1991) Hydroxylation of linear alkanes catalysed by iron porphyrins: particular efficacy and regioselectivity of perhalogenated porphyrins, *J. Chem. Commun.*, 440-442.

58. Grinstaff, M. W., Hill, M. G., Labinger, J. A., and Gray, H. B. (1994) Mechanism of catalytic oxygenation of alkanes by halogenated iron porphyrins, *Science 264*, 1311-1313.

59. Labinger, J. A. (1994) A simplified model for catalyzed isobutane autoxidation: implications for the mechanism of catalysis by halogenated porphyrin complexes, *Catal. Lett. 26*, 95-99.

60. Grinstaff, M. W., Hill, M. G., Birnbaum, E. R., Schaefer, W. P., Labinger, J. A., and Gray, H. B. (1995) Structures, Electronic Properties, and Oxidation-Reduction Reactivity of Halogenated Iron Porphyrins, *Inorg. Chem. 34*, 4896-4902.

61. Doro, F. G., Smith, J. R. L., Ferreira, A. G., and Assis, M. D. (2000) Oxidation of alkanes and alkenes by iodosylbenzene and hydrogen peroxide catalysed by halogenated manganese porphyrins in homogeneous solution and covalently bound to silica, *J. Mol. Catal. A Chem 164*, 97-108.

62. Traylor, T. G., Kim, C., Fann, W. P., and Perrin, C. L. (1998) Reactions of hydroperoxides with iron(III) porphyrins: Heterolytic cleavage followed by hydroperoxide oxidation, *Tetrahedron 54*, 7977-7986.

63. Traylor, T. G., and Xu, F. (1990) Mechanisms of reactions of iron(III) porphyrins with hydrogen peroxide and hydroperoxides: solvent and solvent isotope effects, *J. Am. Chem. Soc. 112*, 178-186.

64. Moore, K. T., Horvath, I. T., and Therien, M. J. (2000) Mechanistic Studies of (Porphinato)Iron-Catalyzed Isobutane Oxidation. Comparative Studies of Three Classes of Electron-Deficient Porphyrin Catalysts, *Inorg. Chem. 39*, 3125-3139.

65. Nam, W., Han, H. J., Oh, S.-Y., Lee, Y. J., Choi, M.-H., Han, S.-Y., Kim, C., Woo, S. K., and Shin, W. (2000) New Insights into the Mechanisms of O−O Bond Cleavage of Hydrogen Peroxide and tert-Alkyl Hydroperoxides by Iron(III) Porphyrin Complexes, *J. Am. Chem. Soc. 122*, 8677-8684.

66. Battioni, P., Renaud, J. P., Bartoli, J. F., Reinaartiles, M., Fort, M., and Mansuy, D. (1988) Monooxygenase-Like Oxidation of Hydrocarbons by H_2O_2 Catalyzed by Manganese Porphyrins and Imidazole - Selection of the Best Catalytic-System and Nature of the Active Oxygen Species, *J. Am. Chem. Soc. 110*, 8462-8470.

67. Higuchi, T., Shimada, K., Maruyama, N., and Hirobe, M. (1993) Heterolytic O-O Bond-Cleavage of Peroxy Acid and Effective Alkane Hydroxylation in Hydrophobic Solvent Mediated by an Iron Porphyrin Coordinated by Thiolate Anion as a Model for Cytochrome-P-450, *J. Am. Chem. Soc. 115*, 7551-7552.

68. Traylor, T. G., and Popovitz-Biro, R. (1988) Hydrogen-Bonding to the Proximal Imidazole in Heme Protein Model Compounds - Effects Upon Oxygen Binding and Peroxidase-Activity, *J. Am. Chem. Soc. 110*, 239-243.

69. Yamaguchi, K., Watanabe, Y., and Morishima, I. (1993) Direct Observation of the Push Effect on the O-O Bond-Cleavage of Acylperoxoiron(Iii) Porphyrin Complexes, *J. Am. Chem. Soc. 115*, 4058-4065.

70. Rosenthal, J., Pistorio, B. J., Chng, L. L., and Nocera, D. G. (2005) Aerobic Catalytic Photooxidation of Olefins by an Electron-Deficient Pacman Bisiron(III)-Oxo Porphyrin, *J. Org. Chem 70*, 1885-1888.

71. Evans, S., and Smith, J. R. L. (2001) The oxidation of ethylbenzene by dioxygen catalysed by supported iron porphyrins derived from iron(III) tetrakis(pentafluorophenyl)porphyrin, *J. Chem. Soc., Perkin Trans. 2*, 174 - 180.

72. Herron, N., and Tolman, C. A. (1987) A highly selective zeolite catalyst for hydrocarbon oxidation. A completely inorganic mimic of the alkane .omega.-hydroxylases, *J. Am. Chem. Soc. 109*, 2837-2839.

73. Bedioui, F. (1995) Zeolite-encapsulated and clay-intercalated metal porphyrin, phthalocyanine and Schiff-base complexes as models for biomimetic oxidation catalysts: an overview, *Coord. Chem. Rev. 144*, 39-68.

74. Battioni, P., Lallier, J.-P., Barloy, L., and Mansuy, D. (1989) Mono-oxygenase-like oxidation of hydrocarbons using supported manganese–porpnyrin catalysts: beneficial effects of a silica support for alkane hydroxylation, *Chem. Commun.* , 1149-1151.

75. Barloy, L., Battioni, P., and Mansuy, D. (1990) Manganese porphyrins supported on montmorillonite as hydrocarbon mono-oxygenation catalysts: particular efficacy for linear alkane hydroxylation, *Chem. Commun.*, 1365-1367.

76. Benaglia, M., Danelli, T., Fabris, F., Sperandio, D., and Pozzi, G. (2002) Poly(ethyleneglycol)-supported tetrahydroxyporphryin: a convenient, recyclable catalyst for photooxidations, *Org. Lett. 4*, 4229-4232.

77. Lee, J. Y., Farha, O. K., Roberts, J., Scheidt, K. A., Nguyen, S. T., and Hupp, J. T. (2009) Metal–organic framework materials as catalysts, *Chem. Soc. Rev. 38*, 1450-1459.

78. Shultz, A. M., Farha, O. K., Hupp, J. T., and Nguyen, S. T. (2009) A Catalytically Active, Permanently Microporous MOF with Metalloporphyrin Struts, *J. Am. Chem. Soc. 131*, 4204-4205.

79. Meunier, B. (1992) Metalloporphyrins as versatile catalysts for oxidation reactions and oxidative DNA cleavage, *Chem. Rev. 92*, 1411-1456.

80. Stephenson, N. A., and Bell, A. T. (2007) Mechanistic Study of Iron(III) [Tetrakis(pentafluorophenyl)Porphyrin Triflate (F_{20}TPP)Fe(OTf) Catalyzed Cyclooctene Epoxidation by Hydrogen Peroxide, *Inorg. Chem. 46*, 2278-2285.

81. Labinger, J. A. (1994) A simplified model for catalyzed isobutane autoxidation: implications for the mechanism of catalysis by halogenated porphyrin complexes, *Catal. Lett. 26*, 95-99.

82. Grinstaff, M. W., Hill, M. G., Birnbaum, E. R., Schaefer, W. P., Labinger, J. A., and Gray, H. B. (1995) Structures, Electronic Properties, and Oxidation-Reduction Reactivity of Halogenated Iron Porphyrins, *Inorg. Chem. 34*, 4896-4902.

83. Grinstaff, M. W., Hill, M. G., Labinger, J. A., and Gray, H. B. (1994) Mechanism of Catalytic Oxygenation of Alkanes by Halogenated Iron Porphyrins, *Science 264*, 1311-1313.

84. Nam, W., Oh, S.-Y., Sun, Y. J., Kim, J., Kim, W.-K., Woo, S. K., and Shin, W. (2003) Factors Affecting the Catalytic Epoxidation of Olefins by Iron Porphyrin Complexes and H2O2 in Protic Solvents, *J. Org. Chem. 68*, 7903-7906.

85. Stephenson, N. A., and Bell, A. T. (2006) Influence of Solvent Composition on the Kinetics of Cyclooctene Epoxidation by Hydrogen Peroxide Catalyzed by Iron(III)

[tetrakis(pentafluorophenyl)] Porphyrin Chloride [(F20TPP)FeCl], *Inorg. Chem. 45*, 2758-2766.

86. Stephenson, N. A., and Bell, A. T. (2006) Effects of Methanol on the Thermodynamics of Iron(III) [Tetrakis(pentafluorophenyl)]porphyrin Chloride Dissociation and the Creation of Catalytically Active Species for the Epoxidation of Cyclooctene, *Inorg. Chem. 45*, 5591-5599.
87. Kokubo, Y., Wu, X.-W., Oshima, Y., and Koda, S. (2004) Aerobic oxidation of cyclohexene catalyzed by Fe(III)(5,10,15,20-tetrakis(pentafluorophenyl)porphyrin)Cl in supercritical CO_2, *J. Supercritical Fluids 30*, 225-235.
88. Moore, K. T., Fletcher, J. T., and Therien, M. J. (1999) Syntheses, NMR and EPR spectroscopy, electrochemical properties, and structural studies of [5,10,15,20 - Tetrakis (perfluoroalkyl) porphinato] iron (II) and - iron (III) complexes, *J. Am. Chem. Soc. 121*, 5196-5209.
89. Haber, J., Matachowski, L., Pamin, K., and Poltowicz, J. (2000) Manganese porphyrins as catalysts for oxidation of cyclooctane in Lyons system, *J. Mol. Catal. A: Chem. 162*, 105-109.
90. Haber, J., Matachowski, L., Pamin, K., and Poltowicz, J. (2003) The effect of peripheral substituents in metalloporphyrins on their catalytic activity in Lyons system, *J. Mol. Catal. A: Chem. 198*, 215-221.
91. Haber, J., Klosowski, M., and Poltowicz, J. (2003) Co-oxidation of styrene and iso-butyraldehyde in the presence of polyaniline-supported metalloporphyrins, *J. Mol. Catal. A: Chem. 201*, 167-178.
92. Krishnan, R., and Vancheesan, S. (2002) Polynuclear manganese complexes catalyzed epoxidation of olefins with molecular oxygen, *J. Mol. Catal. A: Chem. 185*, 87-95.
93. Jian-Ying, Q., Yue-Ming, L., Zhong-Yuan, Z., Chi-Ming, C., Chi-Hung, Y., and Albert , S. C. C. (2005) Novel Manganese Complex as an Efficient Catalyst for the Isobutyraldehyde-Mediated Epoxidation of Cyclic Alkenes with Dioxygen, *Adv. Synth. Catal. 347*, 45-49.
94. Zhou, X., and Ji, H. (2010) Biomimetic kinetics and mechanism of cyclohexene epoxidation catalyzed by metalloporphyrins, *Chem. Eng. J. 156*, 411-417.

95. Lim, S. Y., Kang, M., Kim, J. M., and Lee, I.-M. (2005) Epoxidation of Simple Alkenes with O2 and Isobutyraldehyde Catalyzed by Ni Catalysts Deposited on Nanoporous Carbon, *Bull. Korean Chem. Soc. 26*, 887-891.

96. Nam, W., Kim, H. J., Kim, S. H., Ho, R. Y. N., and Valentine, J. S. (1996) Metal Complex-Catalyzed Epoxidation of Olefins by Dioxygen with Co-Oxidation of Aldehydes. A Mechanistic Study, *Inorg. Chem. 35*, 1045-1049.

97. Bao, J., Chen, W., Liu, T., Zhu, Y., Jin, P., Wang, L., Liu, J., Wei, Y., and Li, Y. (2007) Bifunctional Au-Fe3O4 Nanoparticles for Protein Separation, *ACS Nano 1*, 293-298.

98. Huang, Y., Ma, W., Li, J., Cheng, M., Zhao, J., Wan, L., and Yu, J. C. (2003) A Novel β-CD-Hemin Complex Photocatalyst for Efficient Degradation of Organic Pollutants at Neutral pHs under Visible Irradiation, *J. Phys. Chem. B 107*, 9409-9414.

99. Smeureanu, G., Aggarwal, A., Soll, C. E., Arijeloye, J., Malave, E., and Drain, C. M. (2009) Enhanced Catalytic Activity and Unexpected Products from the Oxidation of Cyclohexene by Organic Nanoparticles of 5,10,15,20-Tetrakis-(2,3,4,5,6-pentafluorophenyl)porphyrinatoiron(III) in Water by Using O_2, *Chem. Eur. J. 15*, 12133-12140.

100. Drain, C. M., Smeureanu, G., Patel, S., Gong, X., Garno, J., and Arijeloye, J. (2006) Porphyrin Nanoparticles as Supramolecular Systems, *New J. Chem. 30*, 1834-1843.

101. Prakash, P., and Franciscamary, L. J. (2005) Reaction of a sterically hindered iron(III) porphyrin with peroxyacetic acid: degradation kinetics, *J. Serb. Chem. Soc. 70* 1105-1111

102. Poltowicz, J., Pamin, K., and Haber, J. (2006) Influence of manganese tetraarylporphyrins substituents on the selectivity of cycloalkanes oxidation with magnesium monoperoxyphthalate, *J. Mol. Catal. A: Chem. 257*, 154-157.

103. Arasasingham, R. D., He, G. X., and Bruice, T. C. (1993) Mechanism of manganese porphyrin-catalyzed oxidation of alkenes. Role of manganese(IV)-oxo species, *J. Am. Chem. Soc. 115*, 7985-7991.

104. Ellis Jr., P. E., and Lyons, J. E. (1990) Selective air oxidation of light alkanes catalyzed by activated metalloporphyrins - the search for a suprabiotic system, *Coord. Chem. Rev. 105*, 181-193.

105. Varotto, A., Todaro, L., Vinodu, M., Koehne, J., Liu, G.-y., and Drain, C. M. (2008) Self-organization of a new fluorous porphyrin and C60 films on indium-tin-oxide electrode, *Chem. Commun*, 4921-4923.

106. Boucher, L. J. (1968) Manganese porphyrin complexes. I. Synthesis and spectroscopy of manganese(III) protoporphyrin IX dimethyl ester halides, *J. Am. Chem. Soc. 90*, 6640-6645.

107. Spreer, L. O., Maliyackel, A. C., Holbrook, S., Otvos, J. W., and Calvin, M. (1986) Synthesis and characterization of a manganese(III) porphyrin cation radical and its conversion to manganese(IV) by ligand metathesis, *J. Am. Chem. Soc. 108*, 1949-1953.

108. Hill, C. L., and Hollander, F. J. (1982) Structural characterization of a complex of Manganese(V) nitrido[tetrakis(p-methoxyphenyl)porphinato] manganese(V), *J. Am. Chem. Soc. 104*, 7318-7319.

109. Song, W. J., Seo, M. S., George, S. D., Ohta, T., Song, R., Kang, M.-J., Tosha, T., Kitagawa, T., Solomon, E. I., and Nam, W. (2007) Synthesis, Characterization, and Reactivities of Manganese(V)−Oxo Porphyrin Complexes, *J. Am. Chem. Soc. 129*, 1268-1277.

110. Kameyama, H., Narumi, F., Hattori, T., and Kameyama, H. (2006) Oxidation of cyclohexene with molecular oxygen catalyzed by cobalt porphyrin complexes immobilized on montmorillonite, *J. Mol. Catal. A: Chem. 258*, 172-177.

111. Zhou, X.-T., Tang, Q.-H., and Ji, H.-B. (2009) Remarkable enhancement of aerobic epoxidation reactivity for olefins catalyzed by [mu]-oxo-bisiron(III) porphyrins under ambient conditions, *Tetrahedron Lett. 50*, 6601-6605.

112. Gharnati, L., Doring, M., and Arnold, U. (2009) Catalytic Oxidation with Hydrogen Peroxide in Ionic Liquids, *Curr. Org. Syn. 6*, 342-361.

113. Maraval, V., Ancel, J.-E., and Meunier, B. (2002) Manganese(III) Porphyrin Catalysts for the Oxidation of Terpene Derivatives: A Comparative Study, *J. Catal. 206*, 349-357.

114. Chellaiah, A., Yong-Min, L., Jung Yoon, L., Shunichi, F., and Wonwoo, N. (2009) Hydrogen-Atom Abstraction Reactions by Manganese(V)- and Manganese(IV)-Oxo Porphyrin Complexes in Aqueous Solution, *Chem. Eur. J. 15*, 11482-11489.

115. Lyons, J. E., Ellis, P. E., and Myers, H. K. (1995) Halogenated Metalloporphyrin Complexes as Catalysts for Selective Reactions of Acyclic Alkanes with Molecular Oxygen, *J. Catal. 155*, 59-73.

116. Drain, C. M., and Gong, X. (1997) Synthesis of meso substituted porphyrins in air without solvents or catalysts, *Chem. Commun.*, 2117 - 2118.

117. Drain, C. M., and Singh, S. (2010) Combinatorial Libraries of Porphyrins: Chemistry and Applications, In *The Handbook of Porphyrin Science with Applications to Chemistry, Physics, Materials Science, Engineering, Biology and Medicine* (Kadish, K., Smith, K. M., and Guilard, R., Eds.), pp 485-537, World Scientific Publisher, Singapore.

118. Cavaleiro, J. A. S., Tomé, A. C., and Neves, M. G. P. M. S. (2010) meso-Tetraarylporphyrin Derivatives: New Synthetic Methodologies, In *The Handbook of Porphyrin Science with Applications to Chemistry, Physics, Materials Science, Engineering, Biology and Medicine* (Kadish, K., Smith, K. M., and Guilard, R., Eds.), pp 193-294, World Scientific Publisher, Singapore.

119. Nia, S., Gong, X., Drain, C. M., Jurow, M., Rizvi, W., and Qureshy, M. (2010) Solvent-free synthesis of meso tetraarylporphyrins in air: product diversity and yield optimization, *J. Porphyrins Phthalocyanines 14*, 621-629.

120. Andrus, M. B., and Lashley, J. C. (2002) Copper catalyzed allylic oxidation with peresters, *Tetrahedron 58*, 845-866.

121. Crich, D., and Zou, Y. (2005) Catalytic Oxidation Adjacent to Carbonyl Groups and at Benzylic Positions with a Fluorous Seleninic Acid in the Presence of Iodoxybenzene, *J. Org. Chem. 70*, 3309-3311.

122. Mansuy, D., Bartoli, J. F., Battioni, P., Lyon, D. K., and Finke, R. G. (1991) Highly oxidation resistant inorganic-porphyrin analog polyoxometalate oxidation catalysts. 2. Catalysis of olefin epoxidation and aliphatic and aromatic hydroxylations starting from α_2-$P_2W_{17}O_{61}(M^{n+}.Br)^{(n-11)}$ (M^{n+} = Mn^{3+}, Fe^{3+}, Co^{2+}, Ni^{2+}, Cu^{2+}), including quantitative comparisons to metalloporphyrin catalysts, *J. Am. Chem. Soc. 113*, 7222-7226.

123. Traylor, T. G., Fann, W. P., and Bandyopadhyay, D. (1989) A common heterolytic mechanism for reactions of iodosobenzenes, peracids, hydroperoxides, and hydrogen peroxide with iron(III) porphyrins, *J. Am. Chem. Soc. 111*, 8009-8010.

124. Yang, S. J., and Nam, W. (1998) Water-Soluble Iron Porphyrin Complex-Catalyzed Epoxidation of Olefins with Hydrogen Peroxide and tert-Butyl Hydroperoxide in Aqueous Solution, *Inorg. Chem. 37*, 606-607.

Chapter 3

1. Bazzan, G., Aggarwal, A., and Drain Charles, M. (2011) Electrochemical Studies of Self-Organized Porphyrin-Polyoxometalate Films on ITO, In *Interfaces and Interphases in Analytical Chemistry* (Helburn, R., and Vitha, M. F., Eds.), pp 167-184, American Chemical Society, Washington, DC.
2. Mitzi, D. B. (2001) Thin-Film Deposition of Organic-Inorganic Hybrid Materials, *Chem. Mater. 13*, 3283-3298.
3. Katsoulis, D. E. (1998) A Survey of Applications of Polyoxometalates, *Chem. Rev. 98*, 359-388.
4. Cheng, Z., Cheng, L., Gao, Q., Dong, S., and Yang, X. (2002) Characterization of organic-inorganic multilayer films by cyclic voltammetry, UV-Vis spectrometry, X-ray photoelectron spectroscopy, small-angle X-ray diffraction and electrochemical impedance spectroscopy, *J. Mater. Chem. 12*, 1724-1729.
5. Martel, D., and Gross, M. (2007) Electrochemical study of multilayer films built on glassy carbon electrode with polyoxometalate anions and two multi-charged molecular cationic species, *J. Solid State Electrochem. 11*, 421-429.
6. Moriguchi, I., and Fendler, J. H. (1998) Characterization and Electrochromic Properties of Ultrathin Films Self-Assembled from Poly(diallyldimethylammonium) Chloride and Sodium Decatungstate, *Chem. Mater. 10*, 2205-2211.
7. Sadakane, M., and Steckhan, E. (1998) Electrochemical Properties of Polyoxometalates as Electrocatalysts, *Chem. Rev. 98*, 219-238.
8. Dong, S., and Wang, B. (1992) *Electrochimica Acta 37*, 11-16.
9. Keita, B., and Nadjo, L. (1988) *J. Electroanal. Chem. 240*, 325-332.
10. Keita, B., and Nadjo, L. (1987) New aspects of the electrochemistry of heteropolyacids : Part II. Coupled electron and proton transfers in the reduction of silicoungstic species, *J. Electroanal. Chem. 217*, 287-304.

11. Ariga, K., Hill, J. P., and Ji, Q. (2007) Layer-by-Layer assembly as a versitale bottom-up nanofabrication technique for exploratory research and realistic application, *Phys. Chem. Chem. Phys.*, 2319-2340.
12. Lowman, G. M., Tokuhisa, H., Lutkenhaus, J. L., and Hammond, P. T. (2004) Novel Solid-State Polymer Electrolyte Consisting of a Porous Layer-by-Layer Polyelectrolyte Thin Film and Oligoethylene Glycol, *Langmuir 20*, 9791-9795.
13. Zhao, W., Xu, J.-J., and Chen, H.-Y. (2006) Electrochemical Biosensors Based on Layer-by-Layer Assemblies, *Electroanalysis 18*, 1737-1748.
14. Liu, S., Volkmer, D., and Kurth, D. G. (2003) Functional Polyoxometalate Thin Films via Electrostatic Layer-by-Layer Self-Assembly, *J. Cluster Sci. 14*, 405-419.
15. Shen, Y., Liu, J., Jiang, J., Liu, B., and Dong, S. (2002) Fabrication of Metalloporphyrin-Polyoxometalyte Hybrid Film by Layer-by-Layer Method and Its Catalysis for Dioxygen Reduction, *Electroanalysis 14*, 1557-1563.
16. Shen, Y., Liu, J., Jiang, J., Liu, B., and Dong, S. (2003) Fabrication of a Metalloporphyrin-Polyoxometalate Hybrid Film by a Layer-by-Layer Method and Its Catalysis for Hydrogen Evolution and Dioxygen Reduction, *J. Phys. Chem. B. 107*, 9744-9748.
17. Wang, Y., Wang, X., and Hu, C. (2002) Layer-by-Layer Self-Assembled Ultrathin Multilayer Films of Lanthanide Polyoxometalates and Poly(allylamine Hydrochloride) and Their Photoluminescent Properties, *J. Colloid Interface Sci. 249*, 307-315.
18. Drain, C. M., Varotto, A., and Radivojevic, I. (2009) Self-Organized Porphyrinic Materials, *Chem. Rev. 109*, 1630-1658.
19. Beletskaya, I., Tyurin, V. S., Tsivadze, A. Y., Guilard, R., and Stern, C. (2009) Supramolecular Chemistry of Metalloporphyrins, *Chem. Rev. 109*, 1659-1713.
20. Malinski, T. (2000) Porphyrin-Based Electrochemical Sensors, In *The Porphyrin Handbook* (Kadish, K. M., Smith, K. M., and Guilard, R., Eds.), Academic Press, New York.
21. Bazzan, G., Smith, W., Francesconi, L. C., and Drain, C. M. (2008) Electrostatic Self-Organization of Robust Porphyrin-Polyoxometalate Films, *Langmuir 24*, 3244-3249.

22. Drain, C. M., Batteas, J. D., Flynn, G. W., Milic, T., Chi, N., Yablon, D. G., and Sommers, H. (2002) Designing supramolecular porphyrin arrays that self-organize into nanoscale optical and magnetic materials, *Proc. Natl. Acad. Sci. U. S. A. 99*, 6498-6502.

23. Drain, C. M., Bazzan, G., Milic, T., Vinodu, M., and Goeltz, J. C. (2005) Formation and Applications of Stable 10 nm to 500 nm Supramolecular Porphyrinic Materials, *Israel J. Chem. 45*, 255-269.

24. Drain, C. M., and Chen., X. (2004) Self-Assembled Porphyrinic Nanoarchitectures, In *Encyclopedia of Nanoscience & Nanotechnology* (Nalwa, H. S., Ed.), pp 593-616, American Scientific Press, New York, NY.

25. Drain, C. M., Goldberg, I., Sylvain, I., and Falber, A. (2005) Synthesis and applications of supramolecular porphyrinic materials, *Top. Curr. Chem. 245*, 55-88.

26. Drain, C. M., Nifiatis, F., Vasenko, A., and Batteas, J. D. (1998) Porphyrin tessellation by design: Metal mediated self-assembly of large arrays and tapes, *Angew. Chem., Int. Ed. 37*, 2344-2347.

27. Kadish, K. M., Caemelbecke, E. V., and Royal, G. (2000) Electrochemistry of Metalloporphyrins in Nonaqueous Media, In *The Porphyrin Handbook* (Kadish, K. M., Smith, K. M., and Guilard, R., Eds.), Academic Press, New York.

28. Shen, Y., Liu, J., Wu, A., Jiang, J., Bi, L., Liu, B., Li, Z., and Dong, S. (2003) Preparation of Multilayer Films Containing Pt Nanoparticles on a Glassy Carbon Electrode and Application as Electrocatalyst for Dioxygen Reduction, *Langmuir 19*, 5397-5401.

29. Neri, B. P., and Wilson, G. S. (1972) Electrochemical studies of mesotetra(4-N-methylpyridyl)porphine in acid solution, *Anal. Chem. 44*, 1002-1009.

30. Laviron, E. (1983) *Electroanalytical Chemistry*, Vol. 12, Marcel Dekker, New York, NY.

31. Laurent, D., and Schlenoff, J. B. (1997) Multilayer assemblies of redox polyelectrolytes, *Langmuir 13*, 1552-1557.

32. Maldotti, A., Molinari, A., Argazzi, R., Amadelli, R., Battioni, P., and Mansuy, D. (1996) Redox properties of photoexcited (nBu4N)3PW12O40/FeIII porphyrins composite systems, *J. Mol. Catal. A: Chem. 114*, 141-150.

33. Mayer, I., Nakamura, M., Toma, H. E., and Araki, K. (2006) Multielectronic redox and electrocatalytic supramolecular films based on a tetraruthenated iron porphyrin, *Electrochim. Acta 52*, 263-271.

34. Santos, I. C. M. S., Rebelo, S. L. H., Balula, M. S. S., Martins, R. R. L., Pereira, M. M. M. S., Simoes, M. M. Q., Neves, M. G. P. M. S., Cavaleiro, J. A. S., and Cavaleiro, A. M. V. (2005) Association of Keggin-type anions with cationic meso-substituted porphyrins: synthesis, characterization and oxidative catalytic studies, *J. Mol. Catal. A: Chem. 231*, 35-45.

35. Han, B. H., Manners, I., and Winnik, M. A. (2005) Oxygen Sensors Based on Mesoporous Silica Particles on Layer-by-Layer Self-assembled Films, *Chem. Mater. 17*, 3160-3171.

Chapter 4

1. Paulo, P. M. R., Lopes, J. N. C., and Costa, S. l. M. B. (2008) Molecular Dynamics Simulations of Porphyrin−Dendrimer Systems: Toward Modeling Electron Transfer in Solution, *J. Phys. Chem. B 112*, 14779-14792.

2. Wasielewski, M. R. (1992) Photoinduced electron transfer in supramolecular systems for artificial photosynthesis, *Chem. Rev. 92*, 435-461.

3. Durrant, J. R., Haque, S. A., and Palomares, E. (2004) Towards optimisation of electron transfer processes in dye sensitised solar cells, *Coord. Chem. Rev. 248*, 1247-1257.

4. Zinth, W., and Wachtveitl, J. (2005) The First Picoseconds in Bacterial Photosynthesis—Ultrafast Electron Transfer for the Efficient Conversion of Light Energy, *ChemPhysChem 6*, 871-880.

5. Radivojevic, I., Likhtina, I., Shi, X., Singh, S., and Drain, C. M. (2010) Self-organized nanofibers and nanorods of porphyrins bearing hydrogen bonding motifs, *Chem. Commun. 46*, 1643-1645.

6. Beletskaya, I., Tyurin, V. S., Tsivadze, A. Y., Guilard, R., and Stern, C. (2009) Supramolecular Chemistry of Metalloporphyrins, *Chem. Rev. 109* 1659-1713.

7. Drain, C. M., Varotto, A., and Radivojevic, I. (2009) Self-Organized Porphyrinic Materials, *Chem. Rev. 109*, 1630-1658.

8. Jurow, M., Schuckman, A. E., Batteas, J. D., and Drain, C. M. (2010) Porphyrins as molecular electronic components of functional devices, *Coord. Chem. Rev. 254,*, 2297-2310.
9. Lee, S. J., and Hupp, J. T. (2006) Porphyrin-containing molecular squares: Design and applications, *Coord. Chem. Rev. 250*, 1710-1723.
10. Anariba, F., Tiznado, H., Diers, J. R., Schmidt, I., Muresan, A. Z., Lindsey, J. S., Zaera, F., and Bocian, D. F. (2008) Comprehensive characterization of hybrid junctions comprised of a porphyrin monolayer sandwiched between a coinage metal overlayer and a Si(100) substrate, *J. Phys. Chem. C 112*, 9474-9485.
11. Lehn, J.-M. (1994) Perspectives in supramolecular chemistry: From molecular recognition towards self-organisation, *Pure. Appl. Chem 66*, 1961-1966.
12. Lehn, J.-M. (1990) Perspectives in Supramolecular Chemistry—From Molecular Recognition towards Molecular Information Processing and Self-Organization, *Angew. Chem. Int. Ed. 29*, 1304-1319.
13. Drain, C. M., Fischer, R., Nolen, E. G., and Lehn, J.-M. (1993) Self-assembly of a bisporphyrin supramolecular cage induced by molecular recognition between complementary hydrogen bonding sites, *J. Chem. Soc., Chem. Commun.*, 243-245.
14. Drain, C. M., Shi, X., Milic, T., and Nifiatis, F. (2001) Self-assembled multiporphyrin arrays mediated by self-complementary quadruple hydrogen bond motifs, *Chem. Commun.*, 287-288.
15. Shi, X., Barkigia, K. M., Fajer, J., and Drain, C. M. (2001) Design and Synthesis of Porphyrins Bearing Rigid Hydrogen Bonding Motifs: Highly Versatile Building Blocks for Self-Assembly of Polymers and Discrete Arrays, *J. Org. Chem. 66*, 6513-6522.
16. Balaban, Teodor S., Berova, N., Drain, Charles M., Hauschild, R., Huang, X., Kalt, H., Lebedkin, S., Lehn, J.-M., Nifaitis, F., Pescitelli, G., Prokhorenko, Valentyn I., Riedel, G., Smeureanu, G., and Zeller, J. (2007) Syntheses and Energy Transfer in Multiporphyrinic Arrays Self-Assembled with Hydrogen-Bonding Recognition Groups and Comparison with Covalent Steroidal Models, *Chem. - A Eur. J. 13*, 8411-8427.
17. Arai, S., Niwa, D., Nishide, H., and Takeoka, S. (2007) Atropisomers of meso-Conjugated Uracyl Porphyrin Derivatives and Their Assembling Structures, *Org. Lett. 9*, 17-20.

18. Arai, S., Okamura, T., and Takeoka, S. (2010) Synthesis and self-assembling behavior of a porphyrin bearing multiple meso-conjugated barbiturates, *Tetrahedron Lett. 51*, 5177-5180.

19. Drain, C. M., Russell, K. C., and Lehn, J.-M. (1996) Self-assembly of a multi-porphyrin supramolecular macrocycle by hydrogen-bond molecular recognition, *Chem. Commun.*, 337-338.

20. Ligthart, G. B. W. L., Ohkawa, H., Sijbesma, R. P., and Meijer, E. W. (2005) Complementary Quadruple Hydrogen Bonding in Supramolecular Copolymers, *J. Am. Chem. Soc. 127*, 810-811.

21. González-Rodríguez, D., and Schenning, A. P. H. J. (2011) Hydrogen-bonded Supramolecular π-Functional Materials, *Chem. Mater. 23*, 310-325.

22. Wessendorf, F., and Hirsch, A. (2008) Self-assembly of supramolecular oligo-phenylene-ethynylene wires consisting of double Hamilton receptor modified OPE rods and a tetraphenylporphyrin cyanurate, *Tetrahedron 64*, 11480-11489.

23. Steed, J. W. (2011) Supramolecular gel chemistry: developments over the last decade, *Chem. Commun. 47*, 1379-1383.

24. Radivojevic, I., Likhtina, I., Shi, X., Singh, S., and Drain, C. M. (2010) Self-organized nanofibers and nanorods of porphyrins bearing hydrogen bonding motifs, *Chem. Commun. 46*, 1643-1645.

25. Milic, T., Garno, J. C., Batteas, J. D., Smeureanu, G., and Drain, C. M. (2004) Self-Organization of Self-Assembled Tetrameric Porphyrin Arrays on Surfaces, *Langmuir 20*, 3974-3983.

26. Petersen, L., Pedersen, E. B., and Nielsen, C. (2001) Three Routes for the Synthesis of 6-Benzyl-1-ethoxymethyl-2,4-dioxo-1,2,3,4-tetrahydropyrimidine-5-carbaldehyde, *Synthesis*, 0559-0564.

27. Arai, S., Ohshiro, H., Nishide, H., and Takeoka, S. (2007) Synthesis of porphyrins bearing uracyl groups and their assembly induced by melamine derivatives, *Polym. Adv. Technol. 18*, 497-501.

28. Vollhardt, D., Fainerman, V. B., and Liu, F. (2005) Thermodynamic and Structural Characterization of Amphiphilic Melamine-type Monolayers, *J. Phys. Chem. B 109*, 11706-11711.

29. Fainerman, V. B., Vollhardt, D., Aksenenko, E. V., and Liu, F. (2005) Molecular Recognition Kinetics of Nonsurface Active Pyrimidine Derivatives Dissolved in the Aqueous Subphase by an Amphiphilic Melamine Type Monolayer: A Theoretical Approach, *J. Phys. Chem. B 109*, 14137-14143.

30. Kimizuka, N., Kawasaki, T., Hirata, K., and Kunitake, T. (1998) Supramolecular Membranes. Spontaneous Assembly of Aqueous Bilayer Membrane via Formation of Hydrogen Bonded Pairs of Melamine and Cyanuric Acid Derivatives, *J. Am. Chem. Soc. 120*, 4094-4104.

31. Baliani, A., Bueno, G. J., Stewart, M. L., Yardley, V., Brun, R., Barrett, M. P., and Gilbert, I. H. (2005) Design and Synthesis of a Series of Melamine-based Nitroheterocycles with Activity against Trypanosomatid Parasites, *J. Med. Chem. 48*, 5570-5579.

32. Gellman, S. H., Dado, G. P., Liang, G. B., and Adams, B. R. (1991) Conformation-directing effects of a single intramolecular amide-amide hydrogen bond: variable-temperature NMR and IR studies on a homologous diamide series, *J. Am. Chem. Soc. 113*, 1164-1173.

33. Plieger, P. G., Burrell, A. K., Jameson, G. B., and Officer, D. L. (2004) Metallation effects on the thermal interconversion of atropisomers of di(orthomethylarene)-substituted porphyrins, *Dalton Trans.*, 319-326.

34. Freitag, R. A., and Whitten, D. G. (1983) Thermal and photo-induced atropisomerization of picket-fence porphyrins, metalloporphyrins, and diacids: a means for examining porphyrin solution properties, *J. Phys. Chem. 87*, 3918-3925.

35. Kottas, G. S., Clarke, L. I., Horinek, D., and Michl, J. (2005) Artificial molecular rotors, *Chem. Rev. 105*, 1281-1376.

36. Lindsey, J. (1980) Increased Yield of A Desired Isomer by Equilibria Displacement on Binding to Silica-Gel, Applied to Meso-Tetrakis(O-Aminophenyl)Porphyrin, *J. Org. Chem. 45*, 5215-5215.

37. Ohkawa, H., Arai, S., Takeoka, S., Shibue, T., and Nishide, H. (2003) A Duplex of Tetra(2-pyridyl)porphyrin and Tetrahydroxylcalix[4]arene, *Chem. Lett. 32*, 1052-1053.

38. Ohkawa, H., Takayama, A., Nakajima, S., and Nishide, H. (2006) Cyclic Tetramer of a Metalloporphyrin Based on a Quadruple Hydrogen Bond, *Org. Lett. 8*, 2225-2228.

39. Cohen, Y., Avram, L., and Frish, L. (2005) Diffusion NMR Spectroscopy in Supramolecular and Combinatorial Chemistry: An Old Parameter—New Insights, *Angew. Chem. Inter. Ed. 44*, 520-554.
40. Zhao, T., Beckham, H. W., and Gibson, H. W. (2003) Quantitative Determination of Threading in Rotaxanated Polymers by Diffusion-Ordered NMR Spectroscopy, *Macromolecules 36*, 4833-4837.
41. Tran Thi, T. H., Desforge, C., Thiec, C., and Gaspard, S. (1989) Singlet-singlet and triplet-triplet intramolecular transfer processes in a covalently linked porphyrin-phthalocyanine heterodimer, *J. Phys. Chem. 93*, 1226-1233.
42. Gouterman, M. (1978) *In The Porphyrins*, Vol. 3, Academic Press, New York.
43. Yang, Y., and Wang, C. (2009) Hierarchical construction of self-assembled low-dimensional molecular architectures observed by using scanning tunneling microscopy, *Chem. Soc. Rev. 38*, 2576-2589.

Chapter 5

1. Karolczak, J., Kowalska, D., Lukaszewicz, A., Maciejewski, A., and Steer, R. P. (2004) Photophysical Studies of Porphyrins and Metalloporphyrins: Accurate Measurements of Fluorescence Spectra and Fluorescence Quantum Yields for Soret Band Excitation of Zinc Tetraphenylporphyrin, *J. Phys. Chem. A 108*, 4570-4575.
2. Weimin, S., Qi, S., Yucheng, W., Lihong, L., and Jingchao, T. (2010) An alternative approach to amino porphyrins, *J. Heterocyclic chem. 47*, 1221-1224.
3. Karki, L., Vance, F. W., Hupp, J. T., LeCours, S. M., and Therien, M. J. (1998) Electronic Stark Effect Studies of a Porphyrin-Based Push−Pull Chromophore Displaying a Large First Hyperpolarizability: State-Specific Contributions to β, *J. Am. Chem. Soc. 120*, 2606-2611.
4. Suslick, K. S., Chen, C.-T., Meredith, G. R., and Cheng, L.-T. (1992) Push-Pull Porphyrins as nonlinear optical materials, *J. Am. Chem. Soc. 114*, 6928-6930.
5. Gust, D., Moore, T. A., Luttrull, D. K., Seely, G. R., Bittersmann, E., Bensasson, R. V., Rougée, M., Land, E. J., Schryver, F. C. D., and Auweraer, M. V. d. (1990)

Photophysical Properties of 2-Nitro-5,10,15,20-tetrap-tolylporphyrins, *Photochem. Photobiol. 51*, 419-426.

6. Barkigia, K. M., Renner, M. W., Senge, M. O., and Fajer, J. (2004) Interplay of Axial Ligation, Hydrogen Bonding, Self-Assembly, and Conformational Landscapes in High-Spin Ni(II) Porphyrins, *J. Phys. Chem. B 108*, 2173-2180.
7. Ono, N., Muratani, E., Fumoto, Y., Ogawa, T., and Tazima, K. (1998) Synthesis of 2,7,12,17-tetraaryl-3,8,13,18-tetranitroporphyrins; electronic effects on aggregation properties of porphyrins, *J. Chem. Soc., Perkin Trans. 1*, 3819-3824.
8. Drain, C. M., and Lehn, J.-M. (1994) Self-assembly of square multiporphyrin arrays by metal ion coordination, *J. Chem. Soc., Chem. Commun.*, 2313-2315.
9. Drain, C. M., Nifiatis, F., Vasenko, A., and Batteas, J. D. (1998) Ein Porphyrin-Mosaik nach Plan: metallvermittelte Selbstorganisation von großen Gittern und Bändern, *Angew. Chem. 110*, 2478-2481.
10. Hwang, I.-W., Kamada, T., Ahn, T. K., Ko, D. M., Nakamura, T., Tsuda, A., Osuka, A., and Kim, D. (2004) Porphyrin Boxes Constructed by Homochiral Self-Sorting Assembly: Optical Separation, Exciton Coupling, and Efficient Excitation Energy Migration, *J. Am. Chem. Soc. 126*, 16187-16198.
11. Ogawa, K., Zhang, T., Yoshihara, K., and Kobuke, Y. (2001) Large Third-Order Optical Nonlinearity of Self-Assembled Porphyrin Oligomers, *J. Am. Chem. Soc. 124*, 22-23.
12. Takahashi, R., and Kobuke, Y. (2003) Hexameric Macroring of Gable-Porphyrins as a Light-Harvesting Antenna Mimic, *J. Am. Chem. Soc. 125*, 2372-2373.
13. Shoji, O., Okada, S., Satake, A., and Kobuke, Y. (2005) Coordination Assembled Rings of Ferrocene-Bridged Trisporphyrin with Flexible Hinge-like Motion: Selective Dimer Ring Formation, Its Transformation to Larger Rings, and Vice Versa, *J. Am. Chem. Soc. 127*, 2201-2210.
14. Hunter, C. A., Sanders, J. K. M., Beddard, G. S., and Evans, S. (1989) A new approach to the assembly of electron donor-spacer-acceptor systems, *J. Chem. Soc., Chem. Commun.*, 1765-1767.
15. Maeda, C., Kim, P., Cho, S., Park, J. K., Lim, J. M., Kim, D., Vura-Weis, J., Wasielewski, M. R., Shinokubo, H., and Osuka, A. (2010) Large Porphyrin Squares from

the Self-Assembly of meso-Triazole-Appended L-Shaped meso–meso-Linked ZnII–Triporphyrins: Synthesis and Efficient Energy Transfer, *Chem. Eur. J. 16*, 5052-5061.

16. Drain, C. M., Varotto, A., and Radivojevic, I. (2009) Self-Organized Porphyrinic Materials, *Chem. Rev. 109*, 1630-1658.
17. Beletskaya, I., Tyurin, V. S., Tsivadze, A. Y., Guilard, R., and Stern, C. (2009) Supramolecular Chemistry of Metalloporphyrins, *Chem. Rev. 109* 1659-1713.
18. Chang, S. H., Chung, K.-B., Slone, R. V., and Hupp, J. T. (2001) Crown ether functionalization of a porphyrin-based "molecular square": induction of fluorescence sensitivity to alkali metal cations, *Synthetic Metals 117*, 215-217.
19. Lee, S. J., and Hupp, J. T. (2006) Porphyrin-containing molecular squares: Design and applications, *Coord. Chem. Rev. 250*, 1710-1723.
20. Drain, C. M., Hupp, J. T., Suslick, K. S., Wasielewski, M. R., and Chen, X. (2002) A perspective on four new porphyrin-based functional materials and devices, *J. Porphyrins Phthalocyanines 6*, 241-256.
21. Drain, C. M., Batteas, J. D., Flynn, G. W., Milic, T., Chi, N., Yablon, D. G., and Sommers, H. (2002) Designing supramolecular porphyrin arrays that self-organize into nanoscale optical and magnetic materials, *Proc. Natl. Acad. Sci. 99*, 6498-6502.
22. Milic, T. N., Chi, N., Yablon, D. G., Flynn, G. W., Batteas, J. D., and Drain, C. M. (2002) Controlled hierarchical self-assembly and deposition of nanoscale photonic materials, *Angew Chem. Int. Ed. 41*, 2117-2119.
23. Scandola, F., Chiorboli, C., Prodi, A., Iengo, E., and Alessio, E. (2006) Photophysical properties of metal-mediated assemblies of porphyrins, *Coord. Chem. Rev. 250*, 1471-1496.
24. Prodi, A., Chiorboli, C., Scandola, F., Iengo, E., Alessio, E., Dobrawa, R., and Würthner, F. (2005) Wavelength-Dependent Electron and Energy Transfer Pathways in a Side-to-Face Ruthenium Porphyrin/Perylene Bisimide Assembly, *J. Am. Chem. Soc. 127*, 1454-1462.
25. Drain, C. M. (2002) Supramolecular Chemistry And Self-assembly Special Feature: Self-organization of self-assembled photonic materials into functional devices: Photo-switched conductors, *Proc. Natl. Acad. Sci. 99*, 5178-5182.

26. Iengo, E., Zangrando, E., Minatel, R., and Alessio, E. (2002) Metallacycles of Porphyrins as Building Blocks in the Construction of Higher Order Assemblies through Axial Coordination of Bridging Ligands: Solution- and Solid-State Characterization of Molecular Sandwiches and Molecular Wires, *J. Am. Chem. Soc. 124*, 1003-1013.

27. Libera, J. A., Gurney, R. W., Schwartz, C., Jin, H., Lee, T.-L., Nguyen, S. T., Hupp, J. T., and Bedzyk, M. J. (2005) Comparative X-ray Standing Wave Analysis of Metal−Phosphonate Multilayer Films of Dodecane and Porphyrin Molecular Square, *J. Phys. Chem. B 109*, 1441-1450.

28. Splan, K. E., Massari, A. M., and Hupp, J. T. (2004) A Porous Multilayer Dye-Based Photoelectrochemical Cell That Unexpectedly Runs in Reverse, *J. Phys. Chem. B 108*, 4111-4115.

29. Massari, A. M., Gurney, R. W., Schwartz, C. P., Nguyen, S. T., and Hupp, J. T. (2004) Walljet Electrochemistry: Quantifying Molecular Transport through Metallopolymeric and Zirconium Phosphonate Assembled Porphyrin Square Thin Films, *Langmuir 20*, 4422-4429.

30. Jensen, R. A., Kelley, R. F., Joong Lee, S., Wasielewski, M. R., Hupp, J. T., and Tiede, D. M. (2008) Fast energy transfer within a self-assembled cyclic porphyrin tetramer, *Chem. Commun.*, 1886-1888.

31. Milic, T., Garno, J. C., Batteas, J. D., Smeureanu, G., and Drain, C. M. (2004) Self-Organization of Self-Assembled Tetrameric Porphyrin Arrays on Surfaces, *Langmuir 20*, 3974-3983.

32. Iengo, E., Zangrando, E., Bellini, M., Alessio, E., Prodi, A., Chiorboli, C., and Scandola, F. (2005) Pyridylporphyrin Metallacycles with a Slipped Cofacial Geometry: Spectroscopic, X-ray, and Photophysical Characterization, *Inorg. Chem. 44*, 9752-9762.

33. Nifiatis, F., Athas, J. C., Gunaratne, K. D. D., Gurung, Y., Monette, K. M., and Shivokevich, P. J. (2011) Substituent Effects of Porphyrin on Singlet Oxygen Generation Quantum Yields, *The open spectroscopy journal 5*, 1-12.

34. Harriman, A. (1981) Luminescence of porphyrins and metalloporphyrins. Part 3.-Heavy-atom effects, *J. Chem. Soc., Faraday Trans. 2: Mol. Chem. Phys. 77*, 1281-1291.

35. Tripathy, U., Kowalska, D., Liu, X., Velate, S., and Steer, R. P. (2008) Photophysics of Soret-Excited Tetrapyrroles in Solution. I. Metalloporphyrins: MgTPP, ZnTPP, and CdTPP, *J. Phys. Chem. A 112*, 5824-5833.

36. Drain, C. M., Kirmaier, C., Medforth, C. J., Nurco, D. J., Smith, K. M., and Holten, D. (1996) Dynamic Photophysical Properties of Conformationally Distorted Nickel Porphyrins. 1. Nickel(II) Dodecaphenylporphyrin, *J. Phys. Chem. 100*, 11984-11993.

37. Drain, C. M., Gentemann, S., Roberts, J. A., Nelson, N. Y., Medforth, C. J., Jia, S., Simpson, M. C., Smith, K. M., Fajer, J., Shelnutt, J. A., and Holten, D. (1998) Picosecond to Microsecond Photodynamics of a Nonplanar Nickel Porphyrin: Solvent Dielectric and Temperature Effects, *J. Am. Chem. Soc. 120*, 3781-3791.

38. Retsek, J. L., Drain, C. M., Kirmaier, C., Nurco, D. J., Medforth, C. J., Smith, K. M., Sazanovich, I. V., Chirvony, V. S., Fajer, J., and Holten, D. (2003) Photoinduced Axial Ligation and Deligation Dynamics of Nonplanar Nickel Dodecaarylporphyrins, *J. Am. Chem. Soc. 125*, 9787-9800.

39. Azenha, E. G., Serra, A. C., Pineiro, M., Pereira, M. M., Seixas de Melo, J., Arnaut, L. G., Formosinho, S. J., and Rocha Gonsalves, A. M. d. A. (2002) Heavy-atom effects on metalloporphyrins and polyhalogenated porphyrins, *Chem. Phys. 280*, 177-190.

40. António M.d'A. Rocha Gonsalves, Arménio C. Serra, and Pineiro, M. (2009) The small stones of Coimbra in the huge tetrapyrrolic chemistry building *J. Porphyrins Phthalocyanines 13*, 429-445.

41. Hartnell, R. D., and Arnold, D. P. (2004) Peripherally η1-Platinated Organometallic Porphyrins as Building Blocks for Multiporphyrin Arrays, *Organometallics 23*, 391-399.

42. Prodi, A., Kleverlaan, C. J., Indelli, M. T., Scandola, F., Alessio, E., and Iengo, E. (2001) Photophysics of Pyridylporphyrin Ru(II) Adducts: Heavy-Atom Effects and Intramolecular Decay Pathways, *Inorg. Chem. 40*, 3498-3504.

43. Prodi, A., Indelli, M. T., Kleverlaan, C. J., Alessio, E., and Scandola, F. (2002) Energy transfer pathways in pyridylporphyrin metal adducts and side-to-face arrays, *Coord. Chem. Rev. 229*, 51-58.

44. Seybold, P. G., and Gouterman, M. (1969) Porphyrins : XIII: Fluorescence spectra and quantum yields, *J. Mol. Spectroscopy 31*, 1-13.

45. Drain, C. M., Varotto, A., and Radivojevic, I. (2009) Self-Organized Porphyrinic Materials, *Chem. Rev. 109*, 1630-1658.

46. Hartnell, R. D., and Arnold, D. P. (2004) Peripherally Metallated Porphyrins: the First Examples of meso-η^1-Palladio(II) and -Platinio(II) Complexes with Chelating Diamine Ligands, *Eur. J. Inorg. Chem.*, 1262-1269.

47. Hartnell, R. D., Edwards, A. J., and Arnold, D. P. (2002) Peripherally-metallated porphyrins: meso-η^1-porphyrinyl-platinum(II) complexes of 5,15-diaryl- and 5,10,15-triarylporphyrins, *J. Porphyrins Phthalocyanines 6*, 695-707.

48. Dahal, S., and Krishnan, V. (1997) Excited singlet state intramolecular charge transfer in di and trinitrotetraphenylporphyrins, *Chem. Phys. Lett. 274*, 390-395.

49. Karelson, M., Pihlaja, K., Tamm, T., Uri, A., and Zerner, M. C. (1995) UV-visible spectra of some nitro-substituted porphyrins, *J. Photochem. Photobiol. A: Chem. 85*, 119-126.

50. Knyukshto, V., Sagun, E., Shul'ga, A., Bachilo, S., and Zen'kevich, É. (2000) Photoinduced electron transfer in meso-nitrophenyl-substituted porphyrins and their chemical dimers, *Opt. Spectroscopy 88*, 205-216.

51. Takahashi, K., Hase, S., Komura, T., Imanaga, H., and Ohno, O. (1992) The Fluorescence Properties of (2-Nitro-5,10,15,20- tetraphenylporphyrinato)zinc, *Bull. Chem. Soc. Jpn. 65*, 1475-1481.

52. Knyukshto, V., Zenkevich, E., Sagun, E., Shulga, A., and Bachilo, S. (1999) Pathways for photoinduced electron transfer in meso-nitro-phenyl-octaethylporphyrins and their chemical dimers, *Chem. Phys. Lett. 304*, 155-166.

53. Hirschfeld, T. (1976) Quantum efficiency independence of the time integrated emission from a fluorescent molecule, *Appl. Opt. 15*, 3135-3139.

54. Senge, M. O., Eigenbrot, C. W., Brennan, T. D., Shusta, J., Scheidt, W. R., and Smith, K. M. (1993) Aggregation properties of nitroporphyrins: comparisons between solid-state and solution structures, *Inorg. Chem. 32*, 3134-3142.

55. Serra, O. A., Neri, C. R., Iamamoto, Y., Nassar, E. J., Calefi, P. S., Cicillini, S. A., and Manso, C. M. C. P. (1999) Study of the Suppression of Porphyrin Emission upon Addition of Rare Earth Ions, *J. Incl. Phenom. Macro. Chem. 35*, 271-280.

56. Chirvony, V. S., van Hoek, A., Schaafsma, T. J., Pershukevich, P. P., Filatov, I. V., Avilov, I. V., Shishporenok, S. I., Terekhov, S. N., and Malinovskii, V. L. (1998) On the Nature of the Fluorescent State in β-Nitrotetraarylporphyrins, *J. Phys. Chem. B 102*, 9714-9724.

Chapter 6

1. Sternberg, E. D., Dolphin, D., and Brückner, C. (1998) Porphyrin-based photosensitizers for use in photodynamic therapy, *Tetrahedron 54*, 4151-4202.
2. Bonnett, R. (1995) Photosensitizers of the porphyrin the phthalocyanine series for phtodynamic therapy, *Chem. Soc. Rev. 24*, 19-33.
3. Pandey, R. K. (2000) Recent advances in photodynamic therapy, *J. Porphyrins Phthalocyanines 4*, 368-373.
4. Pandey, R. K., and Zheng, G. (2000) Porphyrins as photosensitizers in photodynamic therapy, In *The Porphyrin Handbook* (Kadish, K. M., Smith, K. M., and Guilard, R., Eds.), pp 157-230, Academic Press.
5. Pushpan, S. K., Venkatraman, S., Anand, V. G., Sankar, J., Parmeswaran, D., Ganesan, S., and Chandrashekar, T. K. (2002) Porphyrins in Photodynamic Therapy - A Search for Ideal Photosensitizers *Curr. Med. Chem. - Anti-Cancer Agents 2*, 187-207.
6. Spikes, J. D. (1990) New trends in photobiology: Chlorins as photosensitizers in biology and medicine, *J. Photochem. Photobiol. B: Biol. 6*, 259-274.
7. Kadish, K., Smith, K. M., and Guilard, R. (2000, 2003) *The Porphyrin Handbook*, Vol. 1-20, Academic Press, New York.
8. Drain, C. M., and Singh, S. (2010) Combinatorial Libraries of Porphyrins: Chemistry and Applications, In *The Handbook of Porphyrin Science with Applications to Chemistry, Physics, Materials Science, Engineering, Biology and Medicine* (Kadish, K., Smith, K. M., and Guilard, R., Eds.), pp 485-537, World Scientific Publisher, Singapore.
9. Smith, K. M. (1972) *Porphyrins and Metalloporphyrins*, Elsevier Amsterdam.
10. Dolphin, D. (1978) *The Porphyrins*, Academic Press.

11. Bonnett, R., Charlesworth, P., Djelal, B. D., Foley, S., McGarvey, D. J., and Truscott, T. G. (1999) Photophysical properties of 5,10,15,20-tetrakis(*m*-hydroxyphenyl)-porphyrin (m-THPP), 5,10,15.20-tetrakis(*m*-hydroxyphenyl)chlorin (m-THPC) and 5,10,15,20-tetrakis(*m*-hydroxyphenyl)bacteriochlorin (m-THPBC): a comparative study, *J. Chem. Soc., Perkin Trans. 2*, 325-328.

12. Nguyen, Q. T., Olson, E. S., Aguilera, T. A., Jiang, T., Scadeng, M., Ellies, L. G., and Tsien, R. Y. (2010) Surgery with molecular fluorescence imaging using activatable cell-penetrating peptides decreases residual cancer and improves survival, *Proc. Natl. Acad. Sci., USA 107*, 4317-4322.

13. Laville, I., Figueiredo, T., Loock, B., Pigaglio, S., Maillard, P., Grierson, D. S., Carrez, D., Croisy, A., and Blais, J. (2003) Synthesis, cellular internalization and photodynamic activity of glucoconjugated derivatives of tri and tetra(meta-hydroxyphenyl)chlorins, *Bioorg. Med. Chem. 11*, 1643-1652.

14. Chen, X., Hui, L., Foster, D. A., and Drain, C. M. (2004) Efficient synthesis and photodynamic activity of porphyrin-saccharide conjugates: targeting and incapacitating cancer cells, *Biochemistry 43*, 10918-10929.

15. Pasetto, P., Chen, X., Drain, C. M., and Franck, R. W. (2001) Synthesis of hydrolytically stable porphyrin C- and S-glycoconjugates in high yields, *Chem. Commun.*, 81-82.

16. Samaroo, D., Vinodu, M., Chen, X., and Drain, C. M. (2007) meso-Tetra(pentafluorophenyl)porphyrin as an Efficient Platform for Combinatorial Synthesis and the Selection of New Photodynamic Therapeutics using a Cancer Cell Line, *J. Comb. Chem. 9*, 998-1011.

17. Mauzerall, D. C. (1998) Evolution of Porphyrins, *Clin. Dermatol. 6*, 195–201.

18. Brückner, C., McCarthy, J. R., Daniell, H. W., Pendon, Z. D., Ilagan, R. P., Francis, T. M., Ren, L., Birge, R. R., and Frank, H. A. (2003) A spectroscopic and computational study of the singlet and triplet excited states of synthetic [beta]-functionalized chlorins, *Chem. Phys. 294*, 285-303.

19. Silva, A. M. G., Tomé, A. C., Neves, M. G. P. M. S., Silva, A. M. S., and Cavaleiro, J. A. S. (1999) meso-Tetraarylporphyrins as dipolarophiles in 1,3-dipolar cycloaddition reactions, *Chem. Commun.*, 1767-1768.

20. Silva, A. M. G., Tome´, A. C., Neves, M. G. P. M. S., Silva, A. M. S., and Cavaleiro, J. A. S. (2005) 1,3-Dipolar Cycloaddition Reactions of Porphyrins with Azomethine Ylides, *J. Org. Chem. 70*, 2306-2314.

21. Cavaleiro, J. A. S., Tomé, A. C., and Neves, M. G. P. M. S. (2010) meso-Tetraarylporphyrin Derivatives: New Synthetic Methodologies, In *The Handbook of Porphyrin Science with Applications to Chemistry, Physics, Materials Science, Engineering, Biology and Medicine* (Kadish, K., Smith, K. M., and Guilard, R., Eds.), pp 193-294, World Scientific Publisher, Singapore.

22. Jiménez-Osés, G., García, J. I., Silva, A. M. G., Santos, A. R. N., Tomé, A. C., Neves, M. G. P. M. S., and Cavaleiro, J. A. S. (2008) Mechanistic insights on the site selectivity in successive 1,3-dipolar cycloadditions to meso-tetraarylporphyrins, *Tetrahedron 64*, 7937-7943.

23. Maestrin, A. P. J., Ribeiro, A. O., Tedesco, A. C., Neri, C. R., Vinhado, F. S., Serra, O. A., Martins, P. R., Iamamoto, Y., Silva, A. M. G., Tomé, A. C., Neves, M. G. P. M. S., and Cavaleiro, J. A. S. (2004) A novel chlorin derivative of Meso-tris(pentafluorophenyl)-4-pyridylporphyrin: synthesis, photophysics and photochemical properties, *J. Braz. Chem. Soc. 15*, 923-930.

24. Hao, E., Friso, E., Miotto, G., Jori, G., Soncin, M., Fabris, C., Sibrian-Vazquez, M., and Vicente, M. G. H. (2008) Synthesis and biological investigations of tetrakis(p-carboranylthio-tetrafluorophenyl)chlorin (TPFC), *Org. Biomol. Chem. 6*, 3732-3740.

25. Hirohara, S., Obata, M., Alitomo, H., Sharyo, K., Ando, T., Tanihara, M., and Yano, S. (2009) Synthesis, photophysical properties and sugar-dependent in vitro photocytotoxicity of pyrrolidine-fused chlorins bearing S-glycosides, *J. Photochem. Photobiol. B: Biol. 97*, 22-33.

26. Hirohara, S., Obata, M., Alitomo, H., Sharyo, K., Ando, T., Yano, S., and Tanihara, M. (2009) Synthesis and Photocytotoxicity of S-Glucosylated 5,10,15,20-Tetrakis(tetrafluorophenyl)porphyrin Metal Complexes as Efficient $^1O_2$-Generating Glycoconjugates, *Bioconjugate Chem. 20*, 944-952.

27. Thompson, S., Chen, X., Hui, L., Toschi, A., Foster, D. A., and Drain, C. M. (2008) Low concentrations of a non-hydrolysable tetra-S-glycosylated porphyrin and low light

induces apoptosis in human breast cancer cells via stress of the endoplasmic reticulum, *Photochem. Photobiol. Sci. 7*, 1415-1421.

28. Drain, C. M., Singh, S., Samaroo, D., Thompson, S., Vinodu, M., and Tomé, J. P. C. (2009) New Porphyrin Glyco-conjugates, *Proc. Soc. Photo-Optical Instrumentation Engineers-SPIE 7380*.
29. Singh, S., Aggarwal, A., Thompson, S., Tomé, J. o. P. C., Zhu, X., Samaroo, D., Vinodu, M., Gao, R., and Drain, C. M. (2010) Synthesis and Photophysical Properties of Thioglycosylated Chlorins, Isobacteriochlorins, and Bacteriochlorins for Bioimaging and Diagnostics, *Bioconjugate Chem. 21*, 2136-2146.
30. Bonnett, R., and Martínez, G. (2001) Photobleaching of sensitisers used in photodynamic therapy, *Tetrahedron 57*, 9513-9547.
31. Seybold, P. G., and Gouterman, M. (1969) Porphyrins XIII: Fluorescence spectra and quantum yields, *J. Mol. Spectrosc. 31*, 1-13.
32. Tanielian, C., Wolff, C., and Esch, M. (1996) Singlet Oxygen Production in Water: Aggregation and Charge-Transfer Effects, *J. Phys. Chem. 100*, 6555-6560.
33. Mishra, P. P., Patel, S., and Datta, A. (2006) Effect of Increased Hydrophobicity on the Binding of Two Model Amphiphilic Chlorin Drugs for Photodynamic Therapy with Blood Plasma and Its Components, *J. Phys. Chem. B 110*, 21238-21244.
34. Drain, C. M., Gentemann, S., Roberts, J. A., Nelson, N. Y., Medforth, C. J., Jia, S., Simpson, M. C., Smith, K. M., Fajer, J., Shelnutt, J. A., and Holten, D. (1998) Picosecond to microsecond photodynamics of a nonplanar nickel porphyrin: solvent dielectric and temperature effects, *J. Am. Chem. Soc. 120*, 3781-3791.
35. Borbas, K. E., Chandrashaker, V., Muthiah, C., Kee, H. L., Holten, D., and Lindsey, J. S. (2008) Design, Synthesis, and Photophysical Characterization of Water-Soluble Chlorins, *J. Org. Chem. 73*, 3145-3158.
36. Obata, M., Hirohara, S., Tanaka, R., Kinoshita, I., Ohkubo, K., Fukuzumi, S., Tanihara, M., and Yano, S. (2009) In Vitro Heavy-Atom Effect of Palladium(II) and Platinum(II) Complexes of Pyrrolidine-Fused Chlorin in Photodynamic Therapy, *J. Med. Chem. 52*, 2747-2753.

37. Boisbrun, M., Vanderesse, R., Engrand, P., Olié, A., Hupont, S., Regnouf-de-Vains, J.-B., and Frochot, C. (2008) Design and photophysical properties of new RGD targeted tetraphenylchlorins and porphyrins, *Tetrahedron 64*, 3494-3504.

38. Gonsalves, A. M. d. A. R., Serra, A. C., and Pineiro, M. (2009) The small stones of Coimbra in the huge tetrapyrrolic chemistry building, *J. Porphyrins Phthalocyanines 13*, 429-445.

39. Chinnasamy Muthiah, Masahiko Taniguchi, Han-Je Kim, Izabela Schmidt, Hooi Ling Kee, Dewey Holten, David F. Bocian, and Lindsey, J. S. (2007) Synthesis and Photophysical Characterization of Porphyrin, Chlorin and Bacteriochlorin Molecules Bearing Tethers for Surface Attachment, *Photochem. Photobiol. 83*, 1513-1528.

40. Huang, Y.-Y., Mroz, P., Zhiyentayev, T., Sharma, S. K., Balasubramanian, T., Ruzié, C., Krayer, M., Fan, D., Borbas, K. E., Yang, E., Kee, H. L., Kirmaier, C., Diers, J. R., Bocian, D. F., Holten, D., Lindsey, J. S., and Hamblin, M. R. (2010) In Vitro Photodynamic Therapy and Quantitative Structure−Activity Relationship Studies with Stable Synthetic Near-Infrared-Absorbing Bacteriochlorin Photosensitizers, *J. Med. Chem. 53*, 4018-4027.

41. Kee, H. L., Bhaumik, J., Diers, J. R., Mroz, P., Hamblin, M. R., Bocian, D. F., Lindsey, J. S., and Holten, D. (2008) Photophysical characterization of imidazolium-substituted Pd(II), In(III), and Zn(II) porphyrins as photosensitizers for photodynamic therapy, *J. Photochem. Photobiol. A: Chem. 200*, 346-355.

42. Gentemann, S., Medforth, C. J., Forsyth, T. P., Nurco, D. J., Smith, K. M., Fajer, J., and Holten, D. (1994) Photophysical Properties of Conformationally Distorted Metal-Free Porphyrins. Investigation into the Deactivation Mechanisms of the Lowest Excited Singlet State, *J. Am. Chem. Soc. 116*, 7363-7368.

43. Csik, G., Balog, E., Voszka, I., Tölgyesi, F., Oulmi, D., Maillard, P., and Momenteau, M. (1998) Glycosylated derivatives of tetraphenyl porphyrin: photophysical characterization, self-aggregation and membrane binding, *J. Photochem. Photobiol. B: Biol. 44*, 216-224.

44. Thompson, S., Chen, X., Hui, L., Toschi, A., Foster, D. A., and Drain, C. M. (2008) Low Concentrations of a non-hydrolysable tetra-S-glycosylated porphyrin and low light induces apoptosis in human breast cancer cells via stress of the endoplasmic reticulum, *Photochem. Photobiol. Sci. 7*, 1415-1421.

45. Cselenyák, A., Pankotai, E., Csordás, A., Kiss, L., and Lacza, Z. (2010) Live-Cell Fluorescent Imaging of Membrane or Mitochondrion Transfer between Connected Cells in Culture, *MIicroscopy Book Series, 1*, 764-771.

46. Zhang, X.-a., Lovejoy, K. S., Jasanoff, A., and Lippard, S. J. (2007) Water-soluble porphyrins as a dual-function molecular imaging platform for MRI and fluorescence zinc sensing, *Proc. Natl. Acad. Sci., USA 104*, 10780-10785.

47. Morris, R. L., Azizuddin, K., Lam, M., Berlin, J., Nieminen, A.-L., Kenney, M. E., Samia, A. C. S., Burda, C., and Oleinick, N. L. (2003) Fluorescence Resonance Energy Transfer Reveals a Binding Site of a Photosensitizer for Photodynamic Therapy, *Cancer Res. 63*, 5194-5197.

48. Plaetzer, K., Kiesslich, T., Oberdanner, C. B., and Krammer, B. (2005) Apoptosis Following Photodynamic Tumor Therapy: Induction, Mechanisms and Detection, *Curr. Pharm. Des. 11*, 1151-1165.